STRUCTURAL BEHAVIOUR OF GLASS REINFORCED PLASTICS

BY

TARIG ABDUL RAHMAN BSc, MSc, MICE, CEng

A THESIS SUBMITTED FOR THE DEGREE

OF

DOCTOR OF PHILOSOPHY

DEPARTMENT OF CIVIL ENGINEERING
THE UNIVERSITY OF ASTON
IN BIRMINGHAM

MAY 1979

STRUCTURAL BEHAVIOUR OF GLASS REINFORCED PLASTICS

BY

TARIG ABDUL RAHMAN

THESIS SUBMITTED FOR

THE DEGREE OF DOCTOR OF PHILOSOPHY

The aim of this research is to promote the use of G.R.P. as a structural material. In the past the use of G.R.P. has been confined to non-load carrying applications. Such uses are still rapidly increasing but in addition significant changes have been made during the last decade in the development of semi-structural and now even fully structural applications.

Glass-reinforced plastic is characterized by a high strength but a relatively low modulus of elasticity. For this reason a G.R.P. structure can expect to show large deformations as a result of which the individual structural members will fail under load due to a loss of stability rather than approaching the ultimate strength of the material. For this reason the selection of the geometrical shapes of G.R.P. structural elements is considered to be an important factor in designing G.R.P. structures.

The first chapter of this thesis deals with a general review of the theoretical and experimental methods used to describe the structural properties of G.R.P. The research programme includes five stages dealing with the structural behaviour of G.R.P.

The first stage (Chapter 2) begins with selecting and designing an optimum box beam cross-section which gives the maximum flexural and torsional rigidity.

The second stage of investigation (Chapter 3) deals with beam to beam connections. A joint was designed and manufactured with different types of fasteners used to connect two beam units. A suitable fastener was selected and the research extended to cover the behaviour of long span beams using multiple joints.

The third part of the investigation includes a study of the behaviour of box beams subjected to combined bending, shear and torsion. A special torque rig was developed to perform the tests.

Creep deformation of 6 m span G.R.P. was investigated as the fourth stage under a range of loading conditions.

As a result of the phenomenon of post buckling behaviour exhibited in the compression flange during testing of box beams during earlier stages of the investigation it was decided to consider this phenomenon in more detail in the final stage of the investigation. G.R.P. plates with different fibre orientation were subjected to uniaxial compression and tested up to failure.

In all stages of the investigation theoretical predictions and experimental results were compared and generally good correlation between theory and experimental data was observed.

BEAMS, BUCKLING, CONNECTIONS, CREEP, PLASTICS.

ACKNOWLEDGEMENTS

The author would like to express his sincere gratitude to Professor M Holmes BSc, PhD, DSc, CEng, FICE, FIStructE, FIMunE, Head of the Department of Civil Engineering at the University of Aston in Birmingham for allowing this research to be carried out in the Departmental laboratories under his supervision, and for his continual help, encouragement and advice throughout this project.

The author is indebted to Mr W Parsons, the Department Superintendant and to the members of the staff of the Concrete and Structures Laboratories, for help during the experimental work. In particular the author would like to thank Mr J Hollins for the invaluable services provided during all of the tests carried out.

Thanks are due to Miss B M Ingram for typing the thesis neatly and efficiently and to Mrs P Taber for her preparation of the drawings.

THE AUTHOR

After graduating from the Department of Civil Engineering at Khartoum University in 1966, the author joined the Engineering Department of Sudan Railways for a period of four years after which he was awarded a scholarship to study for the degree of MSc. In 1972 the author graduated from the University of Strathclyde and jointed a firm of consulting civil engineers and was involved in the design and construction of a variety of civil engineering projects.

CONTENTS

Page No

CHAPTER 6 POSTBUCKLING BEHAVIOUR

CHAPTER 7

NOTATION

A	Area of cross section or a creep constant
A_{enc}	Enclosed area of a cross section = b x d
A_{ij}	In-plane stiffness matrix
B	Bimoment or a creep constant
B_{twr}	Torsional warping bimoment
$B_{twr}(Z)$	Bimoment of torsional warping at section Z
B_{ij}	Stiffness coupling matrix
b	Breadth of section
C	Creep constant
C_{ij}	Stiffness matrix
C_{cen}	Central torsional moment of inertia of cross section = $\int_A a_1^2 \, dA$
C_{svt}	Torsional moment of inertia of cross section in St Venant torsion = $\frac{4A^2}{\frac{dsper}{h}}$
C_{twr} or Iw	Torsional warping moment of inertia
D_{ij}	Flexural stiffness matrix or flexural rigidity
d	Depth of cross-section
E_1, E_2	Elastic moduli at an angle and to the principle fibre direction
E_L, E_T	Elastic moduli in the principal longitudinal and transverse directions.
E_f	Elastic modulus of glass fibres
E_m	Elastic modulus of the resin matrix
F_L	Axial strength of unidirectional composite
F_o	Axial strength of unvoided matrix
$F_{L(t)}$	Axial tensile strength of unidirectional composite
$F_{L(c)}$	Axial compressive strength of unidirectional composite

F_T	Transverse strength of unidirectional composite
F_y	Yield strength of the composite
f	Lateral deflection
G	Shear modulus
G_{LT} or G_{xy}	Longitudinal or principle shear modulus
G_{12}	Off-axis shear modulus
$\overline{G}_m$	Voided matrix shear modulus
G_f	Fibre shear modulus
h or t	Plate or element thickness
h_{top}	Thickness of compression flange of G.R.P. beam
h_{bot}	Thickness of tension flange of G.R.P. beam
h_{web}	Thickness of web of G.R.P. beam
I	Second moment of area
I_{NA}	Second moment of area about neutral axis
J	Torsional moment of area
L	Length of G.R.P. beam
M	Bending moment
m	cosα or number of buckling wavelength in the x or longitudinal compression or a creep constant
N_x, N_y	Normal stress resultant in the x or y direction respectively
N_{xy}	Shearing stress resultant
$N_x(cr)$ or P_{cr}	Critical compressive buckling load
N_{xy} (cr)	Critical buckling load in pure shear
n	Sin α or number of buckling wavelength in the y or transverse direction under uniaxial compression or a creep constant
P	Average radius of a section
p	Ratio of normal stress = $\frac{\sigma 2}{\sigma 1}$

q	Ratio of shear stress = $\frac{\tau 12}{\sigma 1}$
r	Ratio of axial to transverse strength
S	Shear strength of a composite or reduced length along section profile
S_{per}	Prepheral co-ordinate along the mid line of the corss-section
s	shearing strength ratio = $\frac{F_L}{S}$
T	Temperature
T_{ext}	Externally applied torque
$T_{svt(Z)}$	Torsional moment due to St Venant shear stresses at section Z
$T_{twr(Z)}$	Torsional moment due to the torsional warping shear stresses at section Z
V_f	Glass fibre volume fraction in the composite
V_m	Resin matrix volume fraction of reinforcement in the composite
Vv	Voids volume fraction in the composite
V_{twr}	Torsional shearing stress
W	Externally applied load
$\overline{W}'$	Reduced sectorial area
W_b	Sectorial area referred to a temporary pole
W_T	External vertical load producing torque
W_{twr}	Sectorial co-ordinate in torsional warping referring to the shear centre
Z	Section modulus
Z_T, Z_C	Section modulus in tension and compression
$\sigma 1$	Stress component Longitudinal stress

σ_2	Transverse stress component
$\sigma_1^{(k)}$	Stress component in the kth layer
σ_{cr}	Critical buckling stress
σ_{ui}	Ultimate stress in the principle axis
σ_{max}	Maximum edge stress
$\sigma_{x,\ y}$	Stress in the x, y directions
σ_{xb}	Average applied compression stress
τ	Shearing stress component
τ_{12}	Shearing stress in the principle direction
τ_{cr}	Critical shear stress
αx	Distance between shear centre and arbitrary pole
$\theta_Z(\bar{z})$	Twist about shear axis about section $\bar{z}$
	Deflection
ε	Total deformation or tensile compressive or
ε_o	shear strain at time t
	Initial deformation or tensile compressive or
	shear strain

Subscripts

f	Glass fibre
m	Resin matrix
v	Voids
L, X	Longitudinal associated with the principle direction
T, Y	Transverse associated with the principle direction
(t)	Tension
(c)	Compression

CHAPTER 1

STRUCTURAL PROPERTIES OF G.R.P.

1.1 INTRODUCTION

G.R.P. has an excellent strength/weight ratio and for this reason G.R.P. may be used as a structural material. Table (1.1) shows clearly the superiority of strength/weight ratio of G.R.P. in comparison to conventional building materials. However, G.R.P. which has a low modulus of elasticity (see Table (1.2) suffers from a poor stiffness/weight ratio , though this problem may be overcome by using suitable cross-sections.

Apart from the physical and mechanical properties, competitive installation costs and low maintenance costs, translucency, good resistance to weathering and versatility of fabrication methods, have led to wide application of G.R.P. in industry. In building construction G.R.P. is used in internal partitions, cladding window frames, pipe ducts and tanks etc.

In sectional buildings where lightness in weight combined with the ease of fabricating large components and simplicity of joining has meant that the design of sectional buildings is a logical application. Such structures are particularly suitable on sites where access is limited or where the ground cannot support traditional structures without excessive cost for foundations.

A recently completed secondary school roof in London, accommodating 1200 pupils was constructed in G.R.P. The largest span was 17 m long and 1.2 m. deep. All the spans were made of U shaped troughs joined by compression bolting through a foam layer at the ridges. The joints were covered from the outside by a specially moulded G.R.P. section to eliminate water penetration.

The spans were ribbed at reasonable spacings to increase stiffness and full load tests carried out confirmed calculations for deflections, but torsional rigidity caused concern.

G.R.P. is also used in boat hulls, chemical plants, rail transport, refrigerated containers and in aerospace structures.

G.R.P. has been used recently as both a temporary and permanent shutter in motor bridge decks and retaining walls replacing timber and steel.

1.2 PREVIOUS RESEARCH WORK

Various research workers have been engaged in the development of G.R.P. or plastic as a structural material and they obtained promising results. The main objective for research workers was to limit deflection and to increase the rigidity of the materials by using suitable geometric shapes in the form of hollow beams, double curvature shells, skeletal space frames, stressed skin and sandwich structures.

L H McCurrich[1.1] carried out research on single skin toroidel shells as a roof. M W Holloway[1.2] and N C MacDonald claimed that low density core materials used in sandwich construction have greater strength and stiffness for weight than could be attained by merely increasing the thickness of the skin material. Extensive cross-bracings in the form of tubular cells to stiffen the skins were used.

Benjamin[1.3] analysed folded plate structures with plastic and concluded that the design may be carried out on much the same principles as in normal structural design using their elastic and mechanical properties with special consideration to the factors affecting these properties e.g. creep, ageing and temperature. He also claimed that large deflections may be permitted, except in

places where they may lead to damage of other components or be unsightly.

H G Allen [1.4] carried out optimum design for sandwich struts and beams and concluded that the cost of materials in G.R.P. sandwich elements is relatively high and that while they may be feasible for roofs, and bearing walls, they would not be suitable for long span beams unless cheep cores can be developed.

Molyneux [1.5] investigated the feasibility of the design of 60 m span roof and concluded that long span lightly loaded G.R.P. structures are structurally and economically feasible.

1.3 G.R.P. MATERIALS

1.3.1 Resins

Polyester resins are by far the most commonly used resins for G.R.P. applications. Most applications involve hand lay up at room temperature, in which case the liquid polyester is accelerated prior to lay up of the moulded part, either with cobalt napthanate or manganese napthanate, so that the addition of a catalyst such as methyl ethyl ketone peroxide or cuemene hydroperoxide will initiate cure at room temperature. If cure is to be affected at higher temperature or under pressure (vacuum, autoclave or press moulding) modified catalyst systems can be used. The degree and rate of curing is controlled by catalysts. The function of a catalyst is to act as an initiator for the polymerisation process of the resin. By varying the catalyst curing times curing can be completed in times ranging from several days to minutes at temperatures from $70^{o}F$ to $300^{o}F$.

The high viscosity of polyester resin as received from suppliers can be modified by dissolving it in styrene to obtain the desired

viscosity. Most polyesters can be used satisfactorily at temperatures up to 482°F (250°C). A major disadvantage of polyester resins is that they shrink when cured up to 8% by volume. Polyester resins are often mixed with fillers such as silicone dioxide to improve the surface appearance, resistance to water and reduce shrinkage.

Epoxy resins of various types are often used with high performance composites, where their higher strength and greater stability are desirable. However they are seldom used in production of the more common lower strength G.R.P. composites due to the higher cost, greater personnel hazards and poorer workability in the hand lay-up process. Epoxes find their widest application in the fabrication of composites using boron, graphite carbon or high strength glass where breakdown of the fibre resin interface is more critical.

1.3.2 Glass Fibres

Glass fibres used in glass reinforced plastics are manufactured as continuous filaments. In this process, raw glass is fed into a furnace and melted. Then fibres are drawn from the molten glass at high speed. Commercially produced filaments have diameters ranging from (2.4×10^{-4} to 1.9×10^{-3} cm). These fibres after receiving a protective coating are gathered in the form of bundles called strands. The treatment of the glass fibres provides a suitable surface condition compatible with that of the resin matrix so that good adhesion can be achieved.

The variation of glass properties can be achieved by modifying the structure of silica with various additives. Among all the glass fibres used in composites, E glass is the type most widely used. Other types such as S-glass and D-glass have also been developed. S-glass possesses higher tensile strength and modulus of elasticity

than E-glass. The strength of D-glass is lower than those of E and S-glass.

D-glass is suitable for high performance electronic application due to its low dielectric constant. For more details concerning types and properties of glass fibres, Reference (1.6) may be consulted

The basic strands of glass filaments are used to make all of the different types of fibre glass reinforcements. Some examples of the types of reinforcement available are:-

(1) Chopped fibres

(2) Chopped mat

(3) Unidirectional mat

(4) Bidirectional (cross ply cloth mat)

(5) A combination of the above.

various commerical names exists amongst glass fibre suppliers for these types of reinforcement.

1.4 MATERIALS USED IN THE RESEARCH PROGRAMME

The materials used throughout the investigation were as follows.

(1) Reinforcements

E-glass in the form of unidirectional cloth type and bidirectional woven roving bearing the commercial names Y996 and Y023. Also chopped strand mat was used.

All glass reinforcement was supplied by Fothergill and Harvey Limited.

(2) Resin

BIP Beetle Polyester resin 836, accelerated by approximately 3%. BIP accelerator B and 1.5% of Methyl Ethyl Ketone peroxide as a catalyst. The exact amount of accelerator and catalyst were dependent upon the method of moulding and ambient temperature.

1.5 EFFECT OF MOULDING TECHNIQUES ON THE STRENGTH

Three things can happen to G.R.P. during the moulding process which will cause the material to have less than the desirable or optimum strength.

(1) Fibre breakage

(2) Fibre orientation

(3) Resin segregation

Fibre breakage occurs mostly as a function of the mechanical work put into the material during the preparation stages and is therefore a function of the processing equipment.

Fibre orientation is largely dependant upon the mould design and the part configuration. Location of size of gates, runner vents and core affect fibre orientation.

Resin segregation can occur in two areas. In the compound where resin is improperly formulated, mixed and wetted, G.R.P. will not mould properly. If the pressure, speed, and temperature of the injection process is not properly regulated, resin segregation can occur in the moulded parts, particularly in those parts with non-uniform cross-sections.

G.R.P. is a non-homogeneous material containing large volumes of reinforcing fibres. For this reason complex coring and over-dimensioning should be avoided where possible. G.R.P. compounds do not flow well around obstructions. If the reinforcing fibre is interferred with during its flow in the mould (by a core pin or a restricted area) a number of things may occur.

1 - The fibre can flow around the obstructions and this is desirable.

2 - The fibre can break upon contact with the obstruction, which is less desirable.

3 - The fibre can stop flowing and the resin can continue to flow

(particularly under high pressure injection) causing a fibre rich area at the core section and a resin rich area elsewhere in the part.

Control in moulding reinforced thermoset material stems largely from the initial considerations in the part design, material selection and process equipment.

1.6 MOULDING TECHNIQUES

G.R.P. can be manufactured by various methods [1.7] some of which are mentioned below.

1.6.1 Hand Lay-up

Hand lay-up is the simplest of all methods and suitable for large components with a small number of mouldings and therefore versatile in civil engineering construction. Major advantages are that a minimum of equipment is required and the mould can be made at relatively low cost using wood, plaster, sheet metal or even reinforced plastics. Besides the advantages of minimal restriction of size and relatively easy design changes.

The disadvantages are that the labour content is quite high and the quality of moulding depends to a large extent on the skill of the operators and also under most conditions only one good surface is produced.

In this method a layer of fibre mat or woven cloth is first laid on a form.

Thermosetting plastics are then brushed onto the reinforcing materials and this process is repeated until the desired thickness of the composite is reached. Air trapped in the resin is squeezed out by a roller. The resin, which is catalysed, is then allowed to cure at room temperature. Polyester and epoxy are the two most

common resins used in hand lay-up method. Very often organic or inorganic fillers such as wood-flour, saw dust, clay or sandstone are added to the resin for the purpose of reducing inflammability, providing extra weight and decoration. The content of reinforcement achieved by this method is relatively low about 30% by weight. Mould releases, for example polyvinyl alcohol silicone and mineral oils, are often used for facilitating release of the final product from the mould.

Although every method has its advantages and disadvantages, the actual method will be determined by the number of components which are needed, their dimensions, the properties required and the cost of manufacture.

In this research programme, the hand lay-up method was used extensively for all structural elements, whilst a controlled compression mould was used to produce flat plated elements.

1.6.2 Spray up

In this method of spray-up of fibres are first fed through a chopper and cut into desired lengths. A mixture of fibre, resin and catalyst is sprayed on to a mould. A roller is then used to smooth the surface and remove entrapped air.

1.6.3 Bag-Moulding

Bag moulding is used to improve the quality of hand lay-up products by further removing the entrapped air. The three basic bag moulding methods are vacuum bag, autoclave and pressure bag fig (1.1).

In applying the vacuum bag method, the lay-up of resin and reinforcing materials is first covered with a perforated parting film and a layer of jute bleeder material. This combination allows the

bleeding of air and excess resin. Then the lay-up is covered with a flexible film diaphragm such as cellophane or nylon which is sealed to the mould. The vacuum is then drawn upon the whole system with a pressure of about 12 psi (8.28×10^4 N/m^2). The bagging process should immediately follow the lay-up in order to avoid the hardening of resins. The entire bagged systems can be cured either in an oven or an autoclave system.

In the case of autoclave curing a large metal pressure vessel is used and is pressurised with a gas-typically nitrogen. The pressure applied is in the range of 50 to 100 psi (345×10^5 to 6.89×10^5 N/m^2). The autoclave system is heated and the hot gas is circulated to provide a uniform temperature within the vessel. Sophisticated autoclave systems provide electronic controls which produce programmed temperature/pressure time cycles.

1.6.4 Filament Winding

The method of filament winding employs continuous filaments which are wound onto a mandrel in predetermined orientations. Since it is possible to align the reinforcements along the direction of high stress, the strength of filaments can be utilised in an efficient manner.

Structural applications of filament winding have been used in the aerospace industry as well as in commerical applications such as storage tanks, pipes and pressure vessels. The weight percentage of glass fibres attainable in filament winding is the highest of all fabrication methods.

Two types of fabrication, wet-winding and dry-winding are often employed. In wet-winding the fibres are impregnated with resin just before winding while in dry winding filaments are preimpregnated.

Continuous fibre glass strands are usually wound over mandrels in two different patterns, planor winding where the mandrel is stationary and the helical winding in which the mandrel rotates. The tension exerted in the filaments can be controlled during winding which can affect the void content, resin content and hence the thickness of laminate.

1.6.5 Continuous Extrusion Process

If glass fibres are saturated with a particular resin and then pulled through a simple dye, it is possible to construct shapes such as rods, bars, piping etc. Also possible are more complex items such as ductwork, angles I beams, channels etc. Such standard cross-sections are important for designers. Glass content as high as 60 to 80% by weight can be achieved.

1.6.6 Closed Moulding Methods

These include matched-die moulding, pre mix moulding and injection moulding. They are employed when detail is important and when a two sided finish is desired. Two piece male and female moulds are used in these methods.

Matched-die moulding is usually employed in the fabrication of structural parts where the contour is complex and the tolerence is close. Reinforcing materials in the form of glass mats chopped glass preforms or fabrics are used. Plastic resins are then applied onto the reinforcements and curing is achieved through heating and pressing the moulds at pressures which are in the order of 1000 psi (6.89×10^6 N/m^2). Chopped glass preforms are used when moulding articles with considerable contours. The preform is manufactured by depositing chopped glass fibres onto a screen which has the desired contour. The content of reinforcement material achieved by this

method is higher than that of bag-moulding. Pre-mix moulding differs from matched die moulding in that it employs a ready for use moulding compound. This compound is a mixture of chopped glass fibres, resin, catalyst and filler.

The main attraction of this method is the comparatively low cost and the ease with which it can be moulded. It is particularly suitable for moulding objects with variable wall thickness and sharp contour changes. The injection moulding process also utilises a moulding compound which is injected into the cavity of the mould. However, unlike pre-mix moulding, the moulding compound used in injection moulding consists of thermo plastic resins. The injection moulding process offers the moulder advantages in many areas, for example faster curing cycles and greater machine-mould part, minimized part finishings and uniform preheating and feeding.

However, the general disadvantage is that the factors of fibre breakage, fibre orientation and resin segregation and not just a function of flow distance within a mould, but also a function of the velocity and pressure of the material being injected into the mould.

1.6.7 Compression Moulds [1.8]

In the majority of cases the compression mould is found to be the most suitable. In view of fibre orientation this method yields the highest quality. In the compression process the only flow distance required of the material is that necessary to properly displace it into the cavity extremities. Since the material must flow a relatively short distance within the mould, there is little chance of resin segregation. The desired fibre orientation of the bulk material is maintained, also since the fibres in compression moulding need travel only a short distance, the probability of them being broken or damaged is minimized.

Another consideration in favour of compression moulding is the wear of the tool itself. Compression moulding however has some disadvantages. The material is difficult to feed and it must be pre-measured or pre-weighed before being placed into the compression mould. Another problem which must be contended with, is flash cut-off and part finishing. As a compression mould closes it is normal for some flow of the material from the moulds to occur. This flow or flash can be minimized but it cannot be eliminated. Generally the flash is removed by hand or machine trimmed. The major disadvantage of compression moulding is the extended cure time necessary to achieve properly moulded parts. Fig (1.2) shows a typical arrangement of a compression mould with a vertical flash.

1.7 QUALITY CONTROL

The possible adverse effect of human variations in the fabrication process of G.R.P. undermines confidence in its structural use. This leads to the importance of both quality control and the techniques used to assure quality.

Kies [1.9] has observed that lay-up and moulding quality affect the failure of G.R.P. Many other investigators have observed that thorough wetting of the reinforcement and low void content of the product are required for good strength.

The validity of these observations are well established. The ability to measure the strength of the composite without cutting a coupon is unfortunately not presently available. Nor is there a device or technique, except the human eye, to determine the void content in the laminate non destructively.

Quality control procedure may involve testing samples of each lot of glass reinforcement before impregnation. Similarly it is

important to test not only each batch of resin constituents before use, but also the resin after mixing the constituents. It is also recommended that the resin should be sampled and tested frequently during the laminating process to assure that all its properties are within the tolerances allowed.

The seriousness of the lack of a non destructive test technique for G.R.P. laminates has long been appreciated. Radiography has been tried without marked success [1.10]. When glass with a modest amount of lead present was used in a filament winding process radiography was successful. However, in determining whether or not the winding pattern was as specified, ultrasonic scanning of laminates for void content has shown better promise than radiography [1.11]. The reward for the development of a successful non destructive test technique is well worth the effort involved and without it the expansion of the use of G.R.P. will proceed with caution and hesitancy.

Lastly, the level of quality control and inspection applicable to the G.R.P. components is primarily determined by the customer. For example, G.R.P. built to military or aerospace standards are subject to relatively stricter control and inspection requirements than G.R.P. used for ship building.

1.8 COST

On a cost-performance basis, by generally accepted standards, a typical G.R.P. sheet may cost more than a sheet of steel. In order to justify G.R.P. use on a cost basis other savings may be considered, careful attention to the mechanical requirements of a part offers potential savings in part thickness and weight. In complex parts, trim waste may be substantially less than sheet steel.

The processing cost for G.R.P. is largely a function of the tooling and equipment provided for the job which in turn is influenced by the quantities of parts required. Time cycles for moulding G.R.P. laminates are greater than for stamping forming and drawing operations for sheet metal, but total processing costs include many other factors. For example, elimination of assembly and painting operations may make G.R.P. more economical.

The cost of tooling for press moulding of G.R.P. parts may be as little as 10% of the tooling cost may be entirely different in other parts of the world. Low-cost G.R.P. moulds can be used for the hand lay-up production of parts where labour costs are low.

1.9 ENGINEERING PROPERTIES REQUIRED FOR STRUCTURAL DESIGN

Engineering properties of G.R.P. laminates depend on the type and orientation of fibre and the resin/glass/void volume ratio. The data on structural properties of G.R.P. that are required for structural design may be summarized as:-

(1) Young's modulus

(2) Shear modulus

(3) Poisson's ratio

(4) Tensile strength

(5) Compressive strength

(6) Shear strength

(7) Strength degradation over 30 years

(8) Equivalent modulus over 30 years

(9) Impact strength

(10) Fatigue strength

(11) Fire resistance

(12) Thermal expansion.

Several investigators [1.12-16] have worked on most of the above properties of G.R.P. laminates and discussion of their results is beyond the scope of this research. In determining the elastic and the strength properties theoretical and experimental methods may be used. In this section some of these properties will be briefly discussed.

1.10 ELASTIC AND STRENGTH PROPERTIES OF G.R.P.

The elastic and strength properties of G.R.P. are influenced by a number of factors. These include the anisotropic and non-homogeneous nature of the material, the mechanical incompatibility of the constituent phases, the effect of interfacial bonding, the elastic and plastic behaviour of the matrices and the reinforcing materials, the volume fractions of the component materials and the directions of applied load.

In view of the complexity of the deformation process it is not surprising that there is a lack of comprehensive knowledge of failure mechanisms in composite materials. However, due to the intense efforts made by researchers it is now possible to describe some typical fracture modes in G.R.P. Relative theories used to predict the elastic and strength properties of G.R.P. are discussed in the following sections.

1.11 DETERMINATION OF ELASTIC CONSTANTS

The elastic constants for the basic monolayer may be determined by three methods. [1.16]

(a) Boundary methods utilizing variational principles [1.17-20]

(b) Elasticity approaches involving computerized solutions [1.21-24]

(c) Simplified models involving micromechanic approach [1.25-27]

Using method (c), Reference[1.15] indicated that micromechanic approach could be used for predicting elastic properties of the monolayer from the basic constituent materials e.g.

The longitudinal modulus

$$E_L = K(V_f E_f + V_m E_m) \quad \text{(law of mixtures)} \tag{1.1}$$

The transverse modulus

$$E_T = 2[(1-\nu_f + (\nu_f - \nu_m)V_m]$$

$$\frac{(1-C)\, k_f\, (2K_m + G_m) - G_m\, (K_f - K_m)\, V_m}{(2K_m + G_m) + 2\,(K_m - K_f)\, V_m} +$$

$$C\ \frac{K_f\, (2K_m + G_f) + G_l\, (K_m - K_f)\, V_m}{(2K_m + G_f) - 2\,(K_m - K_f)\, V_m} \quad \text{(Tasia approach)} \tag{1.2}$$

The longitudinal Poisson's ratio

$$\nu_{LT} = V_f \nu_f + V_m \nu_m \quad \text{(law of mixtures)} \tag{1.3}$$

The transverse Poisson's ratio

$$\nu_{TL} = \frac{E_T}{E_L} \cdot \nu_{LT} \tag{1.4}$$

and the longitudinal shear modulus

$$G_{TL} = \frac{G_f G_m}{V_m G_f + V_f G_m} \quad \text{(Ekv all approach)}$$

$$= (1-C)Gm \cdot \frac{2G_f - (G_f - G_m)\, V_m}{2G_m + (G_f - G_m)\, V_m}$$

$$+ CG_f \frac{G_f + G_m) - (G_f - G_m)\, V_m}{(G_f + G_m) + (G_f - G_m)\, V_m} \tag{1.6}$$

where

k = a misalignment factor ranging from 0.9 to 1.00

E_f = Elastic modulus of glass fibre

E_m = Elastic modulus of the resin matrix

ν_f = Poisson's ratio of fibre

ν_m = Poisson's ratio of resin matrix

$$K_f = \frac{E_f}{2(1-\nu_f)}$$

$$K_m = \frac{E_m}{2(1-\nu_m)}$$

$$G_f = \frac{E_f}{2(1+\nu_m)}$$

$$G_m = \frac{E_m}{2(1+\nu_m)}$$

If the fibre is oriented at angle α to the longitudinal direction of the laminate it is possible to calculate the longitudinal and transverse elastic constants in terms of the elastic properties. E_L, V_{LT}, V_{TL} and G_{LT} of the basic unidirectional lamina. Considering a lamina loaded in its plane with stresses that make angle α with the principle fibre direction fig (1.3), the following formulae may be used for determining the elastic properties of the lamina corresponding to its longitudinal and transverse directions. The derivation of these formulae is found in reference [1.28]

$$\frac{1}{E_1} = \frac{\cos^4\alpha}{E_L} + \left(\frac{1}{G_{LT}} - 2\frac{\nu_{LT}}{E_L}\right)\sin^2\alpha\cos^2\alpha + \frac{\sin^4\alpha}{E_T} \qquad (1.7)$$

$$\frac{1}{E_2} = \frac{\sin^4\alpha}{E_L} + \left(\frac{1}{G_{LT}} - 2\frac{\nu_{LT}}{E_L}\right)\sin^2\alpha\cos^2\alpha + \frac{\cos^4\alpha}{E_T} \qquad (1.8)$$

$$\frac{1}{G_{12}} = \frac{\cos^2 2\alpha}{G_{LT}} + \left(\frac{1-\nu_{LT}}{E_L} + \frac{1+\nu_{TL}}{E_T}\right) \sin^2 2\alpha \qquad (1.9)$$

$$\frac{\nu_{12}}{E_1} = \frac{\nu_{21}}{E_2} = \frac{\nu_{LT}}{EL} = \frac{1}{4}\left(\frac{1+\nu_{LT}}{E_L} + \frac{1+\nu_{LT}}{E_T} - \frac{1}{G_{LT}}\right) \sin^2 2\alpha \qquad (1.10)$$

The stress strain equations may be written as:-

$$\sigma_1 = \bar{C}_{11}\varepsilon_1 + \bar{C}_{12}\varepsilon_2 + \bar{C}_{16}\gamma_{12} \qquad (1.11)$$

$$\sigma_2 = \bar{C}_{12}\varepsilon_1 + \bar{C}_{22}\varepsilon_2 + \bar{C}_{26}\gamma_{12} \qquad (1.12)$$

$$\tau_{12} = \bar{C}_{16}\varepsilon_1 + \bar{C}_{26}\varepsilon_2 + \bar{C}_{66}\gamma_{12} \qquad (1.13)$$

or in the matrix form

$$\begin{bmatrix} \sigma_1 \\ \sigma_2 \\ \tau_{12} \end{bmatrix} = [\bar{C}] \begin{bmatrix} \varepsilon_1 \\ \varepsilon_2 \\ \frac{1}{2}\gamma_{12} \end{bmatrix} \qquad (1.14)$$

and

$$[\bar{C}] = [T]^{-1} [C] [T] \qquad (1.15)$$

where [T] is the transformation matrix

$$\begin{bmatrix} \cos^2\alpha & \sin^2\alpha & 2\sin\alpha\cos\alpha \\ \sin^2\alpha & \cos^2\alpha & -2\sin\alpha\cos\alpha \\ -\sin\alpha\cos\alpha & \sin\alpha\cos\alpha & \cos^2\alpha - \sin^2\alpha \end{bmatrix} \qquad (1.16)$$

and $$[C] = \begin{bmatrix} C_{11} & C_{12} & 0 \\ C_{12} & C_{22} & 0 \\ 0 & 0 & C_{66} \end{bmatrix} \quad (1.17)$$

which defines stress strain relationship in the unidirection mono-layer i.e. $\alpha = 0$.

Performing the matrix multiplication in equation (1.15) yields

$$\bar{C}_{11} = C_{11} \cos^4\alpha + 2(12 + 2C_{66}) \sin^2\alpha \cos^2\alpha + C_{22} \sin^4\alpha$$

$$\bar{C}_{12} = (12 + C_{22} - 4C_{66}) \sin^2\alpha \cos^2\alpha + C_{12}(\sin^4\alpha + \cos^4\alpha)$$

$$\bar{C}_{16} = (C_{11} - C_{12} - 2C_{66}) \sin\alpha \cos^3\alpha + (12 - C_{33} + 2C_{66}) \sin^3\alpha \cos\alpha$$

$$\bar{C}_{22} = C_{11} \sin^4\alpha + 2(C_{12} + 2C_{66}) \sin\alpha \cos^2\alpha + C_{22} \cos^4\alpha$$

$$\bar{C}_{26} = (C_1 - C_{12} - 2C_{66}) \sin^3\alpha \cos\alpha + (C_{12} - C_{22} + C_{66}) \sin\alpha \cos^3\alpha$$

$$+ C_{66} (\sin^4\alpha + \cos^6\alpha) \quad (1.18)$$

where

$$C_{11} = \frac{E_L}{1 - \nu_{LT}\nu_{TL}}$$

$$C_{12} = \frac{E_T \nu_{LT}}{1 - \nu_{LT}\nu_{TL}} = \frac{E_L \nu_{TL}}{1 - \nu_{LT}\nu_{TL}}$$

$$C_{22} = \frac{E_T}{1 - \nu_{LT}\nu_{TL}} \qquad C_{66} = G_{LT}$$

Uneven fibre spacing, voids and residual stresses in the resin implies that certain reservations should be made if an analysis of a G.R.P. structure is based on the foregoing analysis.

1.12 DETERMINATION OF THE STRENGTH OF UNIDIRECTIONAL MONO-LAYER

Unlike elastic constants, strength properties cannot be predicted reliably from theory. This is due to the complexities introduced by

(a) Number, size shape and position of voids

(b) Variation of interface bonding strength

(c) Statistical variation of fibre spacing

(d) Variation of material properties at micro and macro level.

(e) Influence of residual stresses

(f) Strain rate

(g) Time-dependant effects

Despite these complexities some research workers suggested empirical approaches. An expression was introduced by Rosen [1.29] for the longitudinal tensile strength

$$FL(t) = V_f (d\beta\delta e)^{\frac{1}{B}} \qquad (1.20)$$

where V_f is the volume fraction of fibre α, β are constants defining the link strength of fibres.

δ = is the ineffective fibre length

e = the base of natural logarithms

Greszezuk [1.25] suggested a formulae for the transverse strength

$$FL_{(t)} = \frac{F_o}{e^{v.f}} \left[1 - \frac{A_p}{1 + (A-1)p}\right] \qquad (1.21)$$

where F_o = strength of matrix unvoided

$P = V_u (1-V)$

V_f = volume fraction of fibre

A = constant

longitudinal compressive strength prediction is based on two failure modes [1.30]

(a) For shear mode the compressive stress is given by

$$FL_{(c)} = \frac{G_m}{1-V_f} \qquad (1.22)$$

(b) For the extensional mode

$$FL_{(c)} = V_f \left[\frac{2E_f E_m V_f}{3(1-V_f)}\right]^{\frac{1}{2}}$$

Transverse compressive strength FC(t) may be computed using upper and lower bounds detailed in Reference [1.31]

1.13 DETERMINATION OF THE ELASTIC AND STRENGTH PROPERTIES OF THE MULTIDIRECTIONAL LAMINATE

An element parallelopiped cut from a laminate is shown in fig (1.4). The element is considered in the plane stress state having stresses σx and σy. In order to find a system of forces and moments acting at the geometric midplane.

The stress resultants are defined which are equal to the sum or the integral of these stresses in the z direction.

i.e.

$$Nx = \int_{-\frac{h}{2}}^{\frac{h}{2}} \sigma x \, dz$$

$$Ny = \int_{-\frac{h}{2}}^{\frac{h}{2}} \sigma y \, dz \qquad (1.24)$$

$$Nxy = \int_{-\frac{h}{2}}^{\frac{h}{2}} \tau xy \, dz$$

similarly the moment resultants are given as the sum of the stresses times the area over which they act multiplied by the moment are with respect to the mid plane.

$$Mx = \int_{-\frac{h}{2}}^{\frac{h}{2}} \sigma x z \, dz$$

$$My = \int_{-\frac{h}{2}}^{\frac{h}{2}} \sigma x z \, dz \qquad (1.25)$$

$$Mxy = \int_{-\frac{h}{2}}^{\frac{h}{2}} \tau xy z \, dz$$

For a lamina with n plies using the notation in fig (1.5). the stress state in the k th ply can be written in terms of the mid-plane strains e_x, e_y, e_z, the plate curvatures k_x, k_y, k_{xy}, the z co-ordinate, and the lamina stiffness properties Cij

i.e.
$$\begin{bmatrix} \sigma x \\ \sigma y \\ \tau xy \end{bmatrix} = \begin{bmatrix} C_{11} & C_{12} & C_{16} \\ C_{12} & C_{22} & C_{26} \\ C_{16} & C_{26} & C_{66} \end{bmatrix} \begin{bmatrix} e_x \\ e_y \\ \gamma xy \end{bmatrix} + z \begin{bmatrix} C_{11} & C_{12} & C_{16} \\ C_{12} & C_{22} & C_{26} \\ C_{16} & C_{26} & C_{66} \end{bmatrix} \begin{bmatrix} k_x \\ k_y \\ k_{xy} \end{bmatrix} \qquad (1.26)$$

or

$$[\sigma]_k = [Cij]_k [e] + z [C_{cj}] [k] \qquad (1.27)$$

for n layers the stress resultants are expressed as the sum of n simple integrals.

$$\begin{bmatrix} N_x \\ N_y \\ N_{xy} \end{bmatrix} = \sum_{k=1}^{n} \begin{bmatrix} \sigma_x \\ \sigma_y \\ \tau_{xy} \end{bmatrix} dz \qquad (1.28)$$

$$= \sum \left\{ \int_{h_{k-1}}^{h_x} \begin{bmatrix} C_{11} & C_{12} & C_{16} \\ C_{12} & C_{22} & C_{26} \\ C_{16} & C_{26} & C_{66} \end{bmatrix} \begin{bmatrix} e_x \\ e_y \\ \gamma_{xy} \end{bmatrix} dz \right. \qquad (1.29)$$

The previous equation can be reduced to the following relatively simple form

$$\begin{bmatrix} N_x \\ N_y \\ N_{xy} \end{bmatrix} = \begin{bmatrix} A_{11} & A_{12} & A_{16} \\ A_{12} & A_{22} & A_{26} \\ A_{16} & A_{26} & A_{66} \end{bmatrix} \begin{bmatrix} B_{11} & B_{12} & B_{16} \\ B_{12} & B_{22} & B_{26} \\ B_{16} & B_{26} & B_{66} \end{bmatrix} \begin{bmatrix} k_x \\ k_y \\ k_{xy} \end{bmatrix}$$

or

$$[N] = [A]\,[e] + [B]\,[k] \qquad (1.31)$$

where

$$Aij = \sum_{k=1}^{n} (Cij)_k \, (h_k - h_{k-1}) \qquad (1.32)$$

$$Bij = \frac{1}{2} \sum_{n=1}^{n} (Cij)_k \, (h^2_k - h^2_{k-1}) \qquad (1.33)$$

similarly the moment resultants may be written in the following matrix form

$$M_x = \begin{bmatrix} B_{11} & B_{12} & B_{16} \\ B_{12} & B_{22} & B_{26} \\ B_{16} & B_{26} & B_{66} \end{bmatrix} \begin{bmatrix} e_x \\ e_x \\ e_{xy} \end{bmatrix} \begin{bmatrix} D_{11} & D_{12} & D_{16} \\ D_{12} & D_{22} & D_{26} \\ D_{16} & D_{26} & D_{66} \end{bmatrix} \begin{bmatrix} k_z \\ k_y \\ k_{xy} \end{bmatrix} \qquad (1.34)$$

or

$$[M] = [B]\,[e] + [D]\,[K] \tag{1.35}$$

where

$$Bij = \frac{1}{2} \sum_{k=1}^{n} (Cij)_k \,(h^2_k - h^2_{k-1}) \tag{1.36}$$

$$Dij = \frac{1}{3} \Sigma\, (Cij)_k \,(h_k^3 - h^3_{k-1}) \tag{1.37}$$

combining equations 1.30 and 1.34 the total laminate constitutive equation may be written as follows

$$\begin{bmatrix} N \\ M \end{bmatrix} = \begin{bmatrix} A & B \\ B & D \end{bmatrix} \begin{bmatrix} e \\ k \end{bmatrix} \tag{1.38}$$

or as

$$\begin{bmatrix} N_x \\ N_y \\ N_{xy} \\ M_r \\ M_y \\ M_{xy} \end{bmatrix} = \begin{bmatrix} A_{11} & A_{12} & A_{16} & B_{11} & B_{12} & B_{16} \\ A_{12} & A_{22} & A_{26} & B_{12} & B_{22} & B_{26} \\ A_{16} & A_{26} & A_{66} & B_{16} & B_{26} & B_{66} \\ B_{11} & B_{26} & B_{16} & D_{11} & D_{12} & D_{16} \\ B_{12} & B_{22} & B_{26} & D_{12} & D_{22} & D_{26} \\ B_{16} & B_{26} & B_{66} & D_{16} & D_{26} & D_{66} \end{bmatrix} \begin{bmatrix} e_x \\ e_y \\ \gamma_{xy} \\ k_x \\ k_y \\ k_2 \end{bmatrix}$$

where Aij is the inplane stiffness matrix

Bij is the coupling stiffness matrix

Dij is the flexural stiffness matrix

For laminates reinforced with symmetrical layers with respect to the midplane the term Bij = 0, the equation is further simplified by making the terms $A_{16} = A_{26} = D_{16} = D_{26} = 0$. This is achieved only in a laminate where every layer of a plus orientation corresponds to another layer of the same orthotropic properties and thickness

with a negative orientation, i.e. the stacking sequence should in the following manner $+\theta/-\theta/-\theta/+\theta$. The general constitutive equation may be put in the inverse form [1.13].

$$\begin{bmatrix} e \\ k \end{bmatrix} = \begin{bmatrix} A' & B' \\ C' & D' \end{bmatrix} \begin{bmatrix} N \\ M \end{bmatrix} \tag{1.40}$$

where

$$[A'] = [A^*] - [B^*]\,[D^{*-1}]\,[C^*] \tag{1.41}$$

$$[B'] = [b^*]\,[D^{*-1}]$$

and

$$[C'] = -[D^{*-1}]\,[C^*];\quad [D'] = [D^{*-1}]$$

$$[A^*] = [A^{-1}]$$

$$[B^*] = -[A^{-1}]\,[B]$$

$$[C^*] = [B]\,[A^{-1}];\quad D^* = [D] - [B]\,[A^{-1}]\,[B] \tag{1.42}$$

To predict the elastic constants of a laminate in which the coupling matrix Bij = O, the inplane matrix, Aij is inversed.

i.e.

$$[A'ij] = [Aij]^{-1} \tag{1.43}$$

where

$$A'_{11} = \frac{1}{\bar{A}}\,(A_{22}\,A_{66} - A_{26}^2)$$

$$A'_{12} = \frac{1}{\bar{A}}\,(A_{26}\,A_{16} - A_{12}\,A_{66})$$

$$A'_{16} = \frac{1}{\bar{A}}\,(A_{12}\,A_{16} - A_{22}\,A_{16})$$

$$A'_{22} = \frac{1}{\bar{A}}\,(A_{11}\,A_{66} - A'_{16})$$

$$A'26 = \frac{1}{\bar{A}}\,(A_{12}\,A_{16} - A_{11}\,A_{26})$$

$$A'_{16} = \frac{1}{\bar{A}}\,(A_{11}\,A_{22} - A^2_{12})$$

$$\bar{A} = A_{11}\,(A_{22}\,A_{66} - A_{26}^2)\,(A_{12}\,A_{66} - A_{26}\,A_{16}) + A_{16}\,(A_{12}\,A_{66} - A_{26}\,A_{16}) \tag{1.44}$$

From which it follows

$$E_L = \frac{1}{A_{11}'}$$

$$E_T = \frac{1}{A_{22}'}$$

$$G_{LT} = \frac{1}{A_{66}'}$$

$$\nu_{LT} = \frac{A'_{12}}{A_{11}'}$$

$$\nu_{TL} = \frac{A_{12}'}{A_{22}'}$$

The terms Aij and Aij' are defined in equations (1.32 and (1.43). For the prediction of the stress components for the kth layer are

$$\sigma i^{(k)} = Cij^{(k)} \left[Ajk + 2B_{jk}\right] \bar{N}k + (Bjk + 2D_{jk}) \bar{M}_k - \alpha_j^{(k)} T \qquad (1.45)$$

This is the general expression of stresses as functions of stress resultants, bending moments and temperatures.

where α = thermal expansion matrix

T = temperature degree (F^o)

A^1, B^1, D^1, and z as defined before.

The yield condition in a combined state in a laminate can be expressed in the form of

$$\left[(1-P)P^2 r^2 + q^2 S^2\right] m^4 + 2q \left[3 - P - 2pr^3 + (P-1)s^2\right] m^3 n + 8q^2 + 2(P + 2q^2)r^2 + (P - 1)^2 (S^2 - 1) - 2q^2 S^2\right] m^2 n^2 + 2q \left[3P - 1 - 2r^2 - (P - 1)S^2\right] mn^3 + \left[P^2 - P + r^2 + q^2 S^2\right] n^4 = \frac{F_L}{\sigma 1} = \left(\frac{rF_T}{\sigma 1}\right) = \left(\frac{sS}{\sigma 1}\right)^2 \qquad (1.46)$$

where $m = \cos \alpha$

$n = \sin \alpha$

$p = \frac{\sigma 2}{\sigma 1}$ ratio of normal stress

$q = \frac{\sigma 6}{\sigma 1}$ ratio of shear stress

$r = \frac{F_1}{F_T}$ ratio of normal strength

$s = \frac{F_L}{s}$ shear strength ratio

F_L = Axial strength

F_T = transverse strength

S = shear strength

Thus for a uniaxial tension or compression p = q = 0, in eqn. (1.46) the failure condition reduces to

$$m^4 + (s^2-1)\, m^2 n^2 + r^2 n^4 = (F_L/\sigma 1)^2 \qquad (1.47)$$

$$\text{or} \quad \sigma 1 = F_L/[m^4+(s^2-1)\, m^2 n^2 + r^2 n^4]^{\frac{1}{2}} \qquad (1.48)$$

For pure shear case $\sigma 1 = \sigma 2 = 0$ is substituted in equation (1.46) which results in

$$4m^2 n^2 (r^2+2)/[s^2 + (m^2-n^2)^2] = (s/\sigma 6)^2 \qquad (1.49)$$

$$\text{or} \quad \sigma 6 = s/[4m^2 n^2 (r^2+2)/s^2 + (m^2 + n^2)^2]^{\frac{1}{2}} \qquad (1.50)$$

1.14 EXPERIMENTAL DETERMINATION OF ELASTIC AND STRENGTH PROPERTIES OF MULTIDIRECTIONAL LAMINATE

The elastic and strength properties of G.R.P. laminates may be determined experimentally. Al Khayat [1.15] gave comprehensive data for various experimental methods used to determine elastic and strength properties. He found a disagreement between experimental and theoretical results predicted from the micro and macros

approach. However elastic properties showed better agreement with theoretical predictions than strength properties.

In this research investigation elastic and strength properties for various G.R.P. elements were determined experimentally by testing specimens cut from the G.R.P. elements.

The short term structural properties were obtained from selected specimens, among the specimens used by Alkhayat [1.15] were the following:-

Tensile specimen

A uniform cross-section specimen was used. The advantage of this specimen fig (1.6a) is that it can be used to determine the tensile strength, modulus, the stress-strain behaviour up to failure and the Poisson's ratio at different stress levels. This type of specimen reduces the shear stresses compared with other specimens [1.15]

Compression specimen

The straight edged specimen fig (1.6b) was adopted to obtain compressive properties. This specimen was designed according to ASTD6 95, Pt 27 1973 for G.R.P. sheets of thickness greater than 32 mm. Aluminium end blocks were bonded to both ends of the specimens to prevent end crushing or brushing and to transmit load by shear from the test machine to the specimen as suggested by several authors [1.32-34]

The advantages of this specimen are

(i) It provides adequate space for fixing electrical strain gauges in the longitudinal and transverse directions in order to measure the stress-strain relationship, Young's modulus and Poisson's ratio.

(ii) It is easier and more economical to produce accurately than other types of specimen.

(iii) Full strength and stiffness characteristics can be obtained from one specimen.

Both types of specimens were tested in a Dennison testing machine using wedge grips. The load was applied at suitable rates.

1.15 IMPACT STRENGTH

One of the important parameters that should be considered in designing G.R.P. structures is the rate of loading since many applications of such structures involve severe impact loading. A very common way to define impact properties is to determine material toughness by measuring the energy required to break a specimen of a particular geometry. Many Izod, Charpy and other impact tests have been conducted by various investigators [1.35-39]. Limitations to these methods are in the inability to provide data of basic physical significance. The geometry of the specimen and test arrangement influence the results thus leading to serious difficulties in applying the results to structures under consideration.

Impact strength (rather than energy) has been measured by a number of people using either an instrumented Izod impact apparatus or a drop weight testing machine [2.40-43]. Stress was measured by a load cell and strain was obtained from strain gauges bonded to the specimen.

1.16 CREEP

Creep deformation of G.R.P. under constant stress is dependant on type of loading, time and temperature. G.R.P. laminates of different fibre orientation and resins will exhibit different creep

characteristics [1.44]. The creep of G.R.P. is naturally greatly dependent upon the creep characteristics of constitutent materials. The resin which serves to distribute the stresses amongst the reinforcement is itself subject to creep. The creep in the fibres and the resin therefore influence each other leading to a redistribution of stress and a transfer of load to other fibres which in turn is accompanied by further creep. This leads to a gradual rupture of the bond between resin and fibres with attendant slip leading to eventual failure of the laminate.

Boller [1.45] carried out tests on the long term properties of laminates under both dry and wet conditions indicating that the percentage reduction of ultimate strength with time of laminates in the wet condition is more severe than in the dry condition.

Other tests have been carried by Ainsworth [1.46] who suggested that 50% of the ultimate short term load will be sustained over a period of 30 years.

Reference [1.47] claimed that the results of short term creep tests may be extrapolated over longer periods. Finally, the phenomenon of creep will be dealt with in greater detail in chapter 5.

1.17 FATIGUE

When G.R.P. is subjected to load, the material tends to suffer progressive and irreversible damage. The detailed nature of the damage depends on several factors including the type of loading, fibre orientation, the properties of the matrix and the properties of the interfacial region. With increasing load the damage is intensified until complete separation of the specimen occurs. It has been shown that the damage processes are both time dependent

(stress rupture) and cycle dependent (fatigue).

Owen and Dukes [1.48] examined laminates made from E-glass mat and a general purpose polyester resin. They showed that it was possible to follow the process of damage microscopically by repeated loading (non-destructive load). They observed that individual strands lying perpendicular to the line of loading showed the first signs of damage taking the form of a separation between the fibres and the resin matrix, a phenomenon called "debonding". They concluded that in a tensile test, debonding occurred at about 30% of the ultimate tensile strength and that resin cracking commenced at about 70%.

Owen [1.49] followed the progress of fatigue damage and found that it was possible to produce conventional stress cycles to failure (S-N) curves fig (1.7) for debonding and resin cracking as well as for final separation of the specimen.

The detailed progress of damage in cross-piled prepreg epoxy resin laminates has been described by Broutman and Sohu [1.50] and again debonding of transverse fibres under static and fatigue loading was observed.

Tanimato and Amijima [1.51] concluded from test results of tensile specimens that the progression process of fatigue damage in composite materials can be divided into three stages as follows.

(1) There is no significant decrease in static strength in the first stage in spite of many cracks in the specimen.

(2) In the second stage cracks propogate in the specimen and the residual strength of the G.R.P. decreases continuously with an increase of cycle ratio.

(3) In the third stage, the rate of decrease in static strength

is reduced until the fatigue life is reached and then the specimen fails suddenly.

Fuwa et al [1.52] have shown that in uniaxial G.R.P. composites, a coustic emissions signalling fibre damage occur at stresses as low as 25% of the static failure stress.

Owen and Smith [1.53] found that debonding in fatigue began at between 25 to 30% of the failure stress amplitudes for any given life. Howe and Owen [1.54] considered that the accumulation of damage is independant of the stress level and is non-linear. Owen [1.53] observed that fatigue damage is progressive and occurs throughout the stressed region even after the first cycle although the composite may still survive for 10^4 to 10^5 cycles after the first visible signs of damage.

1.18 DURABILITY

Although G.R.P. suffers from reduction in strength when subjected to water or ultra-violet light [1.55] several advantages may be claimed for the durability of G.R.P. as compared with other materials.

In the fields of boat hulls, Alfers and Bushey [1.56] claimed that G.R.P. has a superiority over wood in dimensional stability, distortion, deterioration including dry rot. Alfers and Graner [1.57] also reported low maintenance costs. Beurman and Dell Rocca quoted the advantages of resistance to corrosion, dry rot, reduced maintenance and resistance to most acids, oils and solvents at normal temperatures.

1.19 EFFECTS OF IMMERSION AND WEATHERING

Extensive test data on specimens subjected to water immersion and accelerated weathering under laboratory conditions [1.59] and

on specimens cut from boat hulls [1.60] and submarine casings [1.61] after prolonged service indicate losses of strength and stiffness in E-glass/polyester laminates of up to about 20%.

1.20 EFFECTS OF TEMPERATURE ON MATERIAL PROPERTIES

Tests on typical marine type laminates [1.59-62] indicate losses of up to 35% in modulus and 40% in strength at temperatures of 70°C relative to properties at 20°C.

1.21 FIRE RESISTANCE

Flame-retardant resins have been used to a limited extent in boat construction but have been rejected for naval applications [1.62-63] because of higher cost, lower strength, inferior weathering properties and greater fume toxicity. Fire retardant coatings applied to laminate surfaces have however been adopted in mine-sweeper designs [1.64].

Schmidt [1.65] considered the problem of flame retardancy including the mechanism of burning and the possible functions of flame retardants. He pointed out that over the previous years some 250 patents had been granted in the field of flame-retardant additives but no new basic approaches were discovered. The general trend appeared to be towards using a combination of phosphorous and halogen compounds.

Material	Density $N/mm^3 \times 10^{-5}$	Yield strength N/mm^2	$\frac{\text{Strength}}{\text{Density}} \times 10^{-5}$	Normalized value
Medium steel Grade M	7.675	227.5	29.641	1
High tensile steel Grade HT	7.675	324	42.215	1.42
High yield steel Grade HY 80	7.675	552	71.922	2.43
Aluminium	2.644	227.5	86.043	2.90
High yield steel Grade HY 100	7.675	689.5	89.837	3.03
Oak wood	0.613	57.9	94.453	3.19
Pine wood	0.564	64.1	113.65	3.83
G.R.P.	1.643	310	188.68	6.37

TABLE (1.1)

WEIGHT AND STRENGTH OF TYPICAL STRUCTURAL MATERIALS

Nominal Material Properties	G.R.P.		E Glass	Polyester resin	Wood (oak)	Mild Steel	Aluminium
	chopped strand mat	woven rovings					
Resin weight fraction	0.7	0.5	-	1.00	-	-	-
Tensile strength (N/mm^2)	110	240	3500	50	90	240 (yield)	140
Compressive strength (N/mm^2)	130	180	-	140	50	240	140
Shear strength (N/mm^2)	85	120	-	-	13	140	85
Inter laminar shear strength (N/mm^2)	20	15	-	-	-	140	85
Young's Modulus (kN/mm^2)	10	14	70	3.5	9.5	207	70
Shear Modulus (kN/mm^2)	4	3.5	28	1.30	0.75	83	26
Poisson's Ratio	0.18	0.13	0.22	0.33	0.50	0.3	0.32
Coeff. of Expansion (c) -1 x 10^{-6}	30	14	5	90	5	12	22
Specific gravity	1.5	1.7	2.5	1.2	0.60	7.8	2.7

TABLE (1.2)

COMPARISON OF MATERIAL PROPERTIES

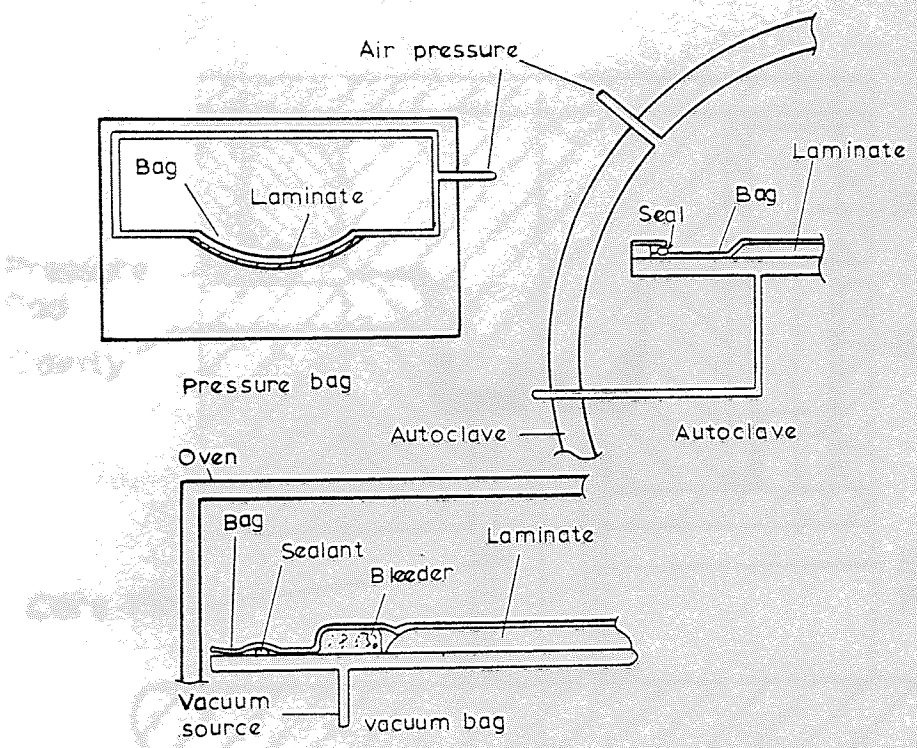

Fig 1.1. Schematic views of bag moulding

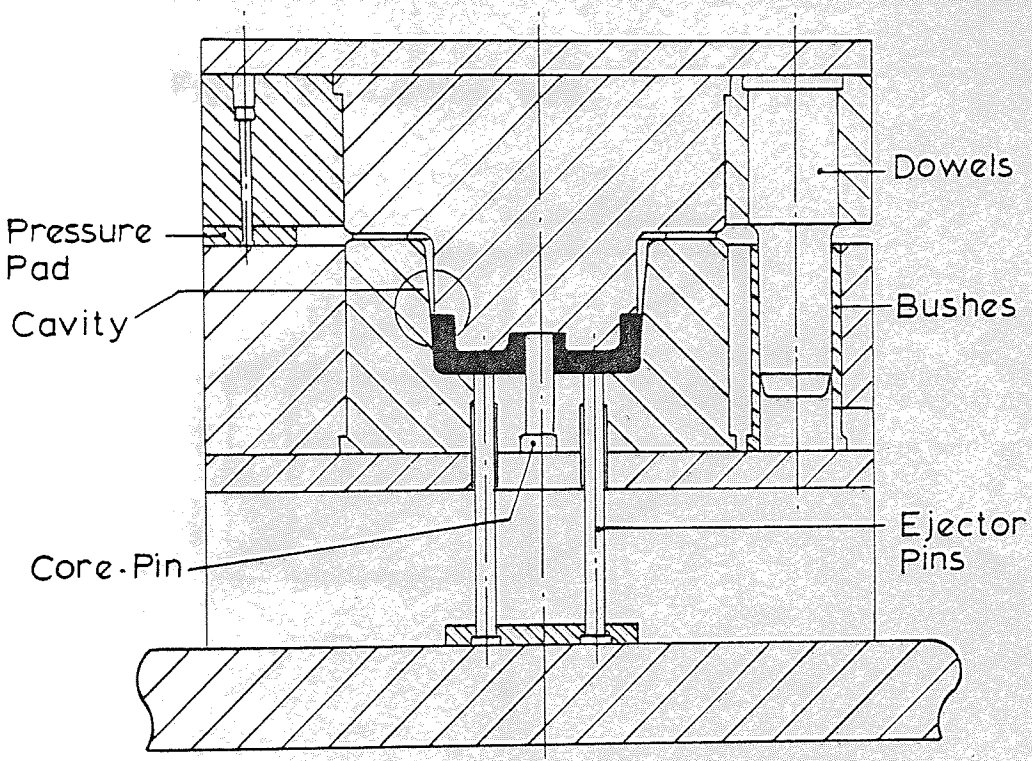

Fig. 1.2 General arrangement of a compression mould - vertical flash.

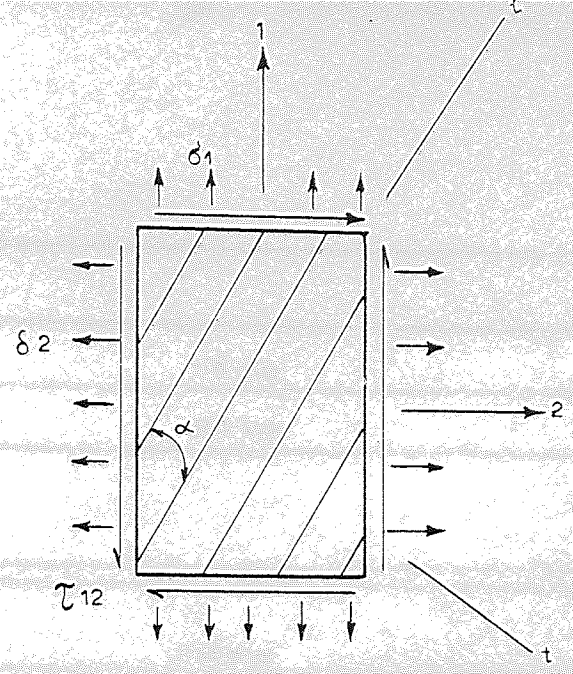

Fig. 1.3 Lamina axis

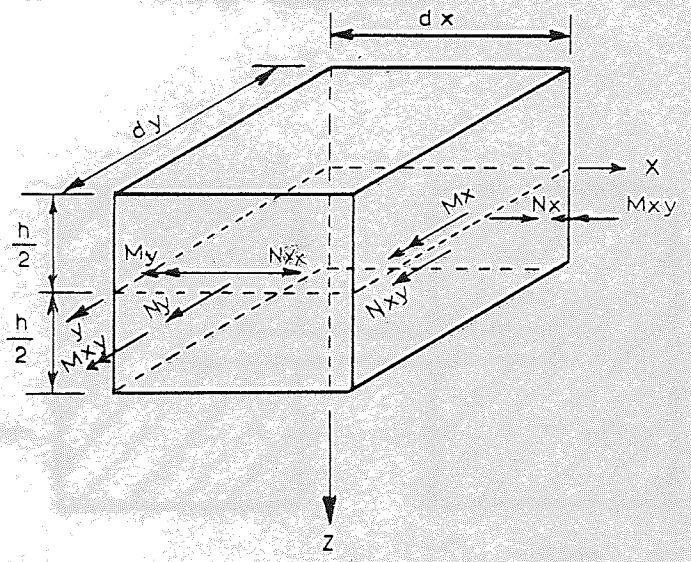

Fig. 1.4. Stress and moment resultants on elemental parallopiped.

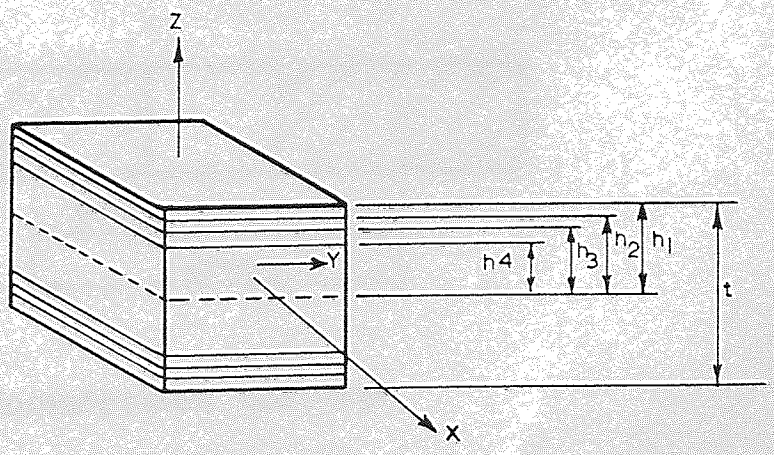

Fig 1.5. Notation for lamina co-ordinate within a lamina

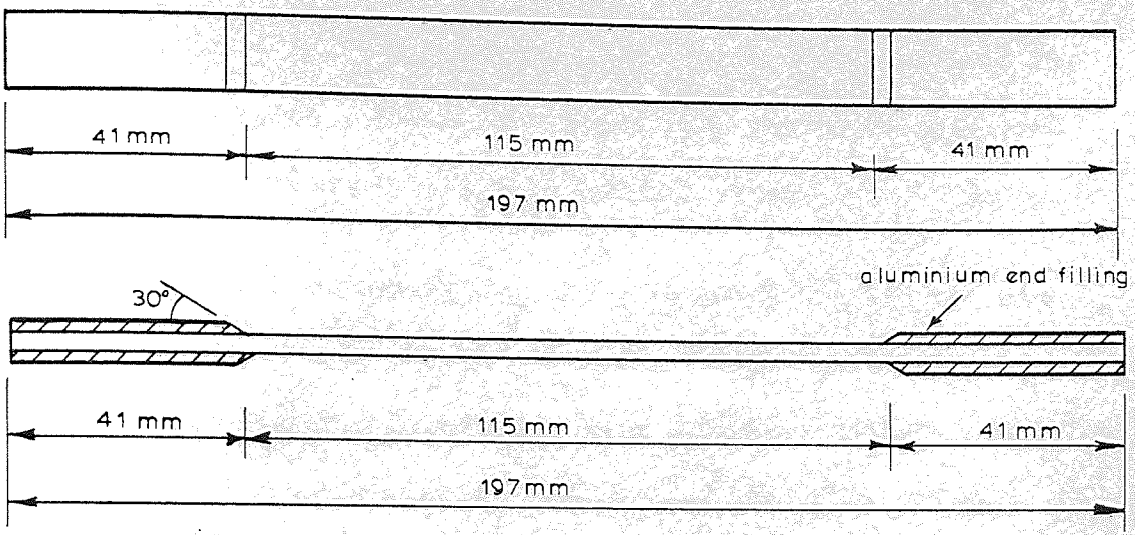

a. Tensile specimen

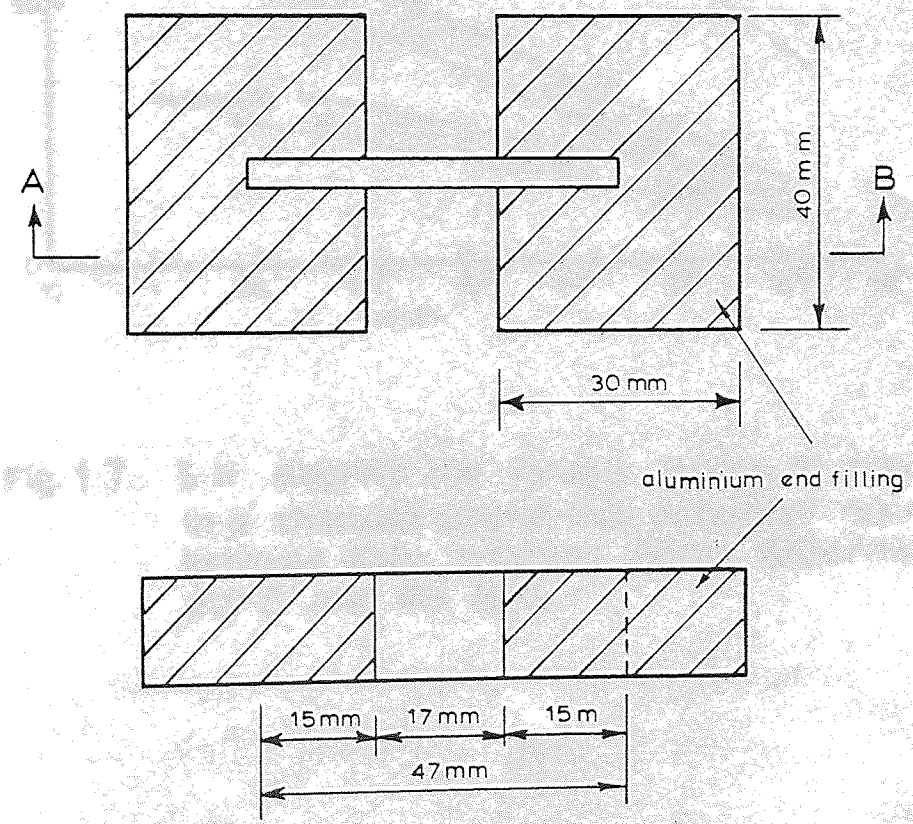

b. Compression specimen

Fig. 16. Tensile and compression specimens

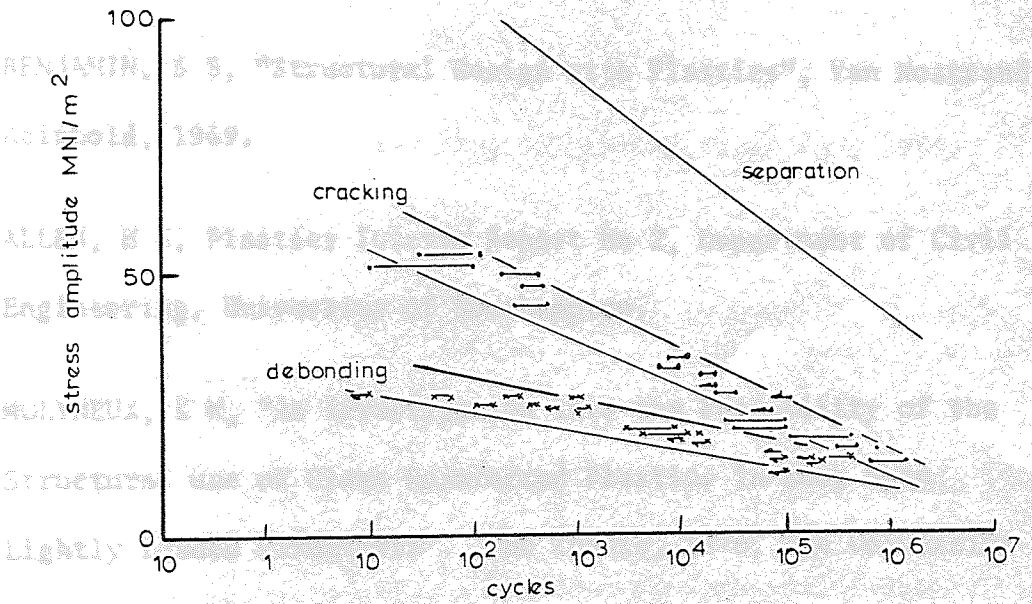

Fig. 1.7. S.N diagram the various stages of failure in a chopped strand mat polyester resin laminate fully reversed stress, 100 c/min 20°C and 40 42%.

REFERENCES

1.1 McCURRICH, L H, "A Glass Reinforced Plastic Roof Designed for Mass Production", 5th International Plastics Conference 1966 pp 21, The British Plastics Federation Group.

1.2 HOLLOWAY, N W and MacDONALD, N C, "Composite Structures as High Strength Light Weight Fillers', Fourth International Reinforced Plastic Conference. The British Plastics Federation Reinforced Plastics Group, London, 25-27 November 1964.

1.3 BENJAMIN, B S, "Structural Design with Plastics", Van Nostrand Reinhold, 1969.

1.4 ALLEN, H G, Plastics Interim Report No 2, Department of Civil Engineering, University of Southampton.

1.5 MOLYNEUX, K W, "An Investigation into the Feasibility of the Structural use of Glass Reinforced Plastics in Long Span Lightly Loaded Structures". PhD Thesis, 1976, The University of Aston in Birmingham.

1.6 METTES, D G, "Handbook of Fibreglass and Advanced Plastics Composites. Glubin ed. Van Nostrand Reinhold Co, New York (1969) p 143.

1.7 "Handbood of Fibreglass and Advanced Plastic Composites". Glubin ed. Van Nostrand Reinhold Co, New York (1969).

1.8 STEPHEN H BAUER, "Injected Moulding, Reinforced Thermoset Materials", 27th Annual Technical Conference, 1972, Reinforced Plastics/Composites Institute, The Society of Plastics Industry Inc.

1.9 KIES, J A, "Filaments for Reinforcement and the Applicability of Filament - Wound Laminates for Deep-Submergence Vehicles, Marine Technology No 3, January 1966, pp 52-59.

1.10 WENDT, FW, LIEBOWITZ, H, PERRONE, N, "Mechanics of Composite Materials". Proceedings of the fifth symposium on Naval Structural Mechanics, Pergamon.

1.11 HAFERKAMP, H, "Non-Destructuve Testing of Glass Fibre Reinforced Plastics", Fourth International Reinforced Plastics Conference, London, 25-27 November, 1964, page 31.

1.12 KABELKA, J, "5th International Reinforced Plastics", 1966. The British Plastic Federation.

1.13 TSIA, "Structural Behaviour of Composite Materials", N.A.S.A. CR71, July 1969.

1.14 PARKYN, B, "Glass Reinforced Plastics" Hiffe Books, London 1970.

1.15 ALKHAYAT, Q C, "Structural Properties of Glass Reinforced Plastics". PhD Thesis, The University of Aston in Birmingham.

1.16 JONES, B H, "Predicting the Stiffness and the Strength of Fibrementary Composites for Design Application". Plastics and Polymers, April, 1968.

1.17 PAUL, B, Trans. Am. Soc. Mech. Engineers, 219 (1960)

1.18 HASHIN, Z and SHTRIKMAN, S, J Franklin Inst. 271 (1961) 336.

1.19 HASHIN, Z and ROZEN, B W, J. Appl. Mech. 31 (1961) 336.

1.20 TSAI, S W, SPRINGER, A S and SCHOLTZ A B, Proc. XIVth Int. Astronautical Congress 11 (1963) 387.

1.21 PICKETT, G, Tech. Doc. Report AFML, TR-65-220 (1965).

1.22 FOYE, R L, Ist Quart. Prog. Report Contract AF 33 (615)-5150 (1966).

1.23 ADAMS, D F, and DONER, D R, J. Comp. Maths. 1 (1) (1967) 4.

1.24 ADAMS, D F, and DONER, D R, J. Comp. Maths. 1 (2) (1967) 152.

1.25 GRESZCZUK, L, Douglas Aircraft Co. Report DAC 33347 (1966).

1.26 JONES, B H, Douglas Aircraft Co. Report DAC 3347 (1966).

1.27 EKVALL, J, ASME Paper No 6, 1-AV-56 (1961).

1.28 CALCOTE, L R, "Analysis of Laminated Composite Structures" V.N.R. Publisher, July 1969.

1.29 ROSEN, B W and JONES, B H, Z.N.A.S.A. Report CR 31 (1964).

1.30 SCHUERCH, H, "Prediction of Composite Strength in Uniaxial Boron Fibre-Metal Matrix Composite Material". AIAA Journal Volume 4, January 1966.

1.31 SHU, L S, Int. Conf. on Mechs, of Composite Materials, Philadelphia.

1.32 STURGEON, J B, "Specimens and Test Methods for Carbon Fibres Reinforced Plastics", R.A.E. Technical Report, 71026, 1971.

1.33 PURSLOW, D, and COLLINGS, T A, "A Test Specimen for the Compressive Strength and Modulus of Unidirectional Carbon Fibres Reinforced Plastic Laminate". R.A.E. Technical Report, 72096, 1972.

1.34 EWINS, P D, "Techniques for Measuring the Mechanical Properties of Composite Materials". Composite - Standard Testing and Design, N.P.L. Conference, April, 1974.

1.35 MORRIS, A W H and SMITH, R S, "Some Aspects of the evaluation of the Impact Behaviour of Low Temperature Fibre Composites", Fibre Science and Technology, Vol 3. (1971), page 219.

1.36 MORRIS, A W H, "The Fabrication and Evaluation of Carbon Fibre - Reinforced Aluminum Composites". Ist Int. Conf. on Carbon Fibres, Paper 17, London (1971).

1.37 SIMON, R A and BARNET, F R, "The Mechanical Properties of Carbon Fibre Composites". 1st.Int. Conference on Carbon Fibres, Paper 26, London (1971).

1.38 WINSA, E A and PETRASEK, D W, "Pendulum Impact Resistance of Tungsten Fibre/Metal Matrix Composites". Comp. Materials, Testing and Design (2nd Conf.), ASTM, STP, 497 (1972), P 350.

1.39 BROUTMAN, L H and MALLICK, P K, "Impact Behaviour of Hybrid Composites", Grant AFOSR 72-2214, Tech. Report No 3, November (1974).

1.40 ROTEM, A and LIFSHTIZ, "Longitudinal Strength of Unidirectional Fibrous Composite Under High Rate of Loading", 26th Annual SPI Conf. 10-G (1971).

1.41 BROUTMAN, L H and MALLICK, "Impact Strength and Toughness of Fibre Composite Materials", Grant AFOSR 72-2214, Tech Report No 2, September (1974).

1.42 BROUTMAN, L H and ROTEM, A, "Impact Strength and Fracture of Carbon Fibre Composite Beams". 28th Annual SPI Conf. 17-B (1973).

1.43 ROTEM, A and BROUTMAN, L H, "Impact Strength and Toughness of Fibre Composite Materials". ASTM STP 568, (1973).

1.44 BOLLER, K H, "Effect of Long Term Loading on Glass Fibre Reinforced Plastic Laminates 11th Annual Reinforced Plastic Division Society of the Plastics Industry Inc. 1956.

1.45 BOLLER, K H, "The Effect of Long Term Loading on Glass Reinforced Plastic Laminates" Proc. 14th Technical and Management Conference. Reinforced Plastic Division SPI (Feb 1959).

1.46 AINSWORTH, L, "Properties of Glass for Plastic Reinforcement" 2nd International Reinforced Plastics Conference. London November 1960. British Plastics Federation.

1.47 McLOUGHLIN, T R, Modern Plastics, Volume 45, February 1968.

1.48 OWEN, M J and DUKES, R, J. Strain Anal. 2. P. 272-279 (1967).

1.49 OWEN et. al. 1969.

1.50 BROUTMAN and SAHU, S (1969) Ann. Tech. Conf. SPI 24th Washington DC Sect 11-D.

1.51 TOSHIO TANIMOTO and SADAO AMIJIMA, Journal of Composite Material Vol 9, 1975, pp 382.

1.52 FUWA, M, BRUNSELL, A R and HARRIES, B, (1974) Composite Materials, Standard Testing and Design Proceedings of Conference at the N.P.L. (UK) IPC Press pp 77-79.

1.53 OWEN, M J and SMITH T R (1968), Plastics and Polymers, 36, 33 see also Proc. 6th International Reinforced Plastics Conference, British Plastics Federation, Paper 27.

1.54 HOWE R J and OWEN M J, (1972), Proceedings of the 8th International Reinforced Plastics Conference, British Plastics Federation pp 137-148.

1.55 MATTHON, J et al, "Ageing and Weathering of Glass Fibre Reinforced Polyester Resins". A review of the literature on the ageing and weathering of plastics. Part 4, R.A.P.R.A. 1970.

1.56 ALFERS, J B, and BUSHEY, A C, Reinforced Down to Sea in Plastics, Buships, Journal 1, No 6, October 1952, pp 5-10.

1.57 ALFERS, J B and GRANER, W R, "Reinforced Plastics - A Structural Material for Marine Applications". Trans. Soc. Nav. and Mar. Eng. 68, 1960, pp 138-192.

1.58 BUERMAN, T M and DELLA ROCCA, R J, "Fibreglass Reinforced Plastics for Marine Structures". Trans. Soc. Nav. and Mar. Eng. 68m 1960, pp 130-192.

1.59 GIBBS and COX INC. "Marine Design Manual for Fibreglass Reinforced Plastics" McGraw-Hill Book Company Inc.

1.60 COBB, B, "Long-Term Durability of Resin Glass Boats" Ship and Boat Builder, February, 1963.

1.61 FRIED, N, GRANGER, W R, "Durability of Reinforced Plastic Materials in Marine Service", Marine Technology, July 1966.

1.62 DIXON, R H, RAMSEY, B W, USHER, P J " Design and Building of HMS WILTON", Proc. of Symposium on G.R.P. Ship Construction, RINA, London, October 1972.

1.63 HENTON, D, "Glass Reinforced Plastics in the Royal Navy." Trans. RINA, Vol 109, October 1967.

1.64 SMITH, C S, "Application of Fibre Reinforced Composites in Marine Technology". Composites - standard Testing and Desing, National Physical Laboratory Conference 8-9 April, 1974.

1.65 SCHMIDT, W G, "Flame-Retardant Additions in Plastics and Recent Patents". Trans. of Plastics Inst. 1965. 33, No 108, pp 247-255.

CHAPTER 2

BOX BEAMS UNDER COMBINED BENDING AND SHEAR

2.1 INTRODUCTION

Beams form main members in a complete structure and therefore the research programme was directed initially for the design of a G.R.P. beam to sustain suitable loads compared to those adopted in ordinary buildings. The manner of loading shown in Fig (2.1) was adopted thus subjecting the beams to the effect of combined bending and shear.

2.2 SECTION SELECTION

In selecting a G.R.P. beam section, several requirements need to be satisfied chiefly:-

(1) The section should be economical as G.R.P. in an expensive material.

(2) The section should have a reasonable stiffness to resist deflection buckling and torsion.

To satisfy the first requirement the section should be a thin walled section. Several types of thin walled section were considered of which a closed box section emerged as the most suitable one. The main advantage of a closed box section is its high torsional rigidity compared to open section. Also a closed section has its elements fixed to each others which ensures a reasonable local and overall buckling and warping resistance. The only disadvantage of a close box section beam is that its manufacture is not as simple as an open section especially when considering hand lay up techniques. Box beams have also been used extensively and successfully in bridge decks and in many aspects of civil engineering.

2.3 SECTION DESIGN

To achieve the maximum possible flexural and torsional stiffnesses (EI and GJ) for a section so as to control flexural and torsional deflection and buckling a box section of gross-sectional area of 900 t mm^2 fig (2.2) was considered as a case for study.

Using the notation below for the section:-

E = Young's modulus

I = 2nd moment of area

G = Shear modulus

J = Torsional moment of area

t = Thickness of the section

b = Breadth of the section

d = depth of the section

As the section is symmetrical the neutral axis bisects d and the 2nd moment of area I may be written as

$$I_{NA} = (b+t)t\left(\frac{d-t}{2}\right)^2 + \frac{2bt^3}{12} + \frac{2t(d-t)^3}{12} \qquad (2.1)$$

As the section is a thin walled one, t is small compared to the dimensions d and b hence rewriting equation (2.1) ignoring terms which include higher orders of t we have

$$I_{NA} = 2b\left(\frac{d}{2}\right)^2 + \frac{2td^3}{12} \qquad (2.2)$$

i.e.

$$I_{NA} = \frac{td^2(3b+d)}{6} \qquad (2.3)$$

The torsional 2nd moment of area of the section J is equal to

$$J = \frac{4A^2 enc}{\frac{dsper}{t}} \qquad (2.4)$$

Where Aenc = Area enclosed by mid-line of wall of closed portion of cross section = bd and $\frac{dsper}{t}$ = $\frac{\text{total perimeter of the section}}{\text{thickness of the section}}$

$$= \frac{2(b+d)}{t}$$

Hence substituting for Aenc and dsper in equation (2.4)

$$J = \frac{4tb^2d^2}{2(b+d)} \qquad (2.5)$$

i.e.

$$J = \frac{2tb^2d^2}{b+d} \qquad (2.6)$$

The total area of the section is $2(b+d)t$ mm^2 and since this is equal to 900 t mm^2 (see initial assumption) it follows that

$$b+d = 450 \text{ mm} \qquad (2.7)$$

Values of I_{NA} and J in equations (2.4) and (2.6) can be varied by substituting b and d according to the relation b+d = 450 of equation (2.7). Graphs if I_{NA} and J were plotted agains b and d fig (2.2) and three cases arose for the same cross-sectional area (900 t mm^2) and these were

(a) either $d << b$

(b) $d = b$

(c) or $d >> b$

Case (a) produced the minimum I_{NA} and minimum J.

Case (b) produced a higher value of I_{NA} compared with case (a) with the maximum J. Case (c) where d is much higher than b producing the maximum I_{NA} and minimum J

None of these cases is the most suitable solution and an acceptable solution lies between case b and c. From fig (2.2) a suitable solution was selected where $b = \frac{d}{2}$ resulting in the following

section properties

$b = 150$ mm

$d = 300$ mm

$I_{NA} = 11.25 \times 10^6 t \text{ mm}^4$

$J = 9 \times 10^6 t \text{ mm}^4$

Sharp corners of the box section were slightly rounded fig (2.3) to reduce stress concentrations. A nominal thickness of 4 mm was adopted for the webs and tension flange, whilst a nominal thickness of 6 mm was adopted later for the compression flange after a pilot beam test, to reduce the tendency for local buckling.

2.4 DIAPHRAGM DESIGN

Diaphragms in box beams are needed for two main reasons.

(i) To prevent beam warping and distortion.

(ii) To decrease the tendency of buckling of individual elements of the beam by restraining the beam element at suitable spacings.

Many papers have appeared on box girder beams [2.1] [2.2] [2.3] [2.4] [2.5] and [2.6] yet very few [2.5] and [2.6] of them deal with the spacing of diaphragms. However guided by an equation introduced by Kristeck [2.5] which gives the critical spacing between diaphragms as

$$Cr = 0.844 \sqrt[4]{b^2 d^2 (dt + bt)\left(\frac{d}{t^3} + \frac{b}{t^3}\right)} \qquad (2.8)$$

where b, d are the dimensions of the box section and t the section thickness.

Assuming a nominal thickness of 4 mm and substituting for the section dimensions, Kristeck's equation gives Cr = 1.898 m which indicates that only one diaphragm is sufficient. However a spacing

of 500 mm between diaphragms was considered to be adequate for two reasons.

Firstly the Kristeckformula was mainly introduced for concrete box beams which are more rigid than G.R.P. box beams and secondly, even distribution of diaphragms along the beam is necessary to prevent wrapping at beam ends and at points of applications of loads to prevent local buckling. A diaphragm thickness of 6 mm was considered suitable.

2.5 BEAM REINFORCEMENT

Based on the theoretical analysis A Rothwell [2.7] claimed that the optimum fibre orientation for buckling in compression is 45^{o} and in shear is 60^{o}. Q C Alkhayat [2.8] on experimental evidence found that a multidirectional laminate of 0 ± 45 gave the optimum orientation to resist buckling in compression and -45 to resist buckling in shear. Richard [2.9] also considered a similar fibre orientation adopted by Rothwell [2.7]

In the light of the above divergence of views it was decided to design five box beams with different fibre orientation after a pilot beam had been tested.

To reduce the number of parameters involved webs and diaphragms were reinforced with equal fibre orientation and compression and tension flanges were also reinforced with equal fibre orientation. Symmetrical layering of fibre layers was also maintained in all components of the beams to ensure orthotropic conditions in each element by eliminating the coupling matrix B_{ij}.

Table (2.1) shown the type, number and fibre orientation in each beam element with respect to the axis defined in fig (2.4). Chopped strands were used at the corners of the box beam to reduce stress concentrations, and local reinforcement of chopped strand

mats were also used to bond diaphragms to the beam elements fig (2.1).

2.6 SUPPORT AND BEARING DESIGN

Special details were incorporated in the box beam (see fig (2.5) at the supports and where the loads were applied for the following reasons:-

(a) The additional diaphragms and stiffener assemblies carry most of the shear thus reducing the tendency of the web to buckle in shear.

(b) To prevent local deformation in the tension and compression flange.

(c) According to Vlasov [2.10,11] thin walled members are subjected to bimoment stresses and the special details which created closed square sections (50 x 50 mm) reduces these stresses to zero (see Appendix A).

2.7 BEAM INSTRUMENTATION

Fig (2.6) shows a general schematic layout of the strain and deflection gauges adopted for the box beam.

2.8 BEAM CASTING

With the difficulty of casting a box beam with diaphragms in one stage mould it was necessary to develop a method which involved a sequence of steps which led eventually to the desired box beam. The procedure was as follows:-

(1) Using a suitable mould fig (2.3) cast two layers of fibre for the tension, compression flange and one web forming a U shape.

(2) Cast the diaphragms to the required thickness from a separate mould.

(3) Now insert the diaphragms support and bearing assemblies and bond them to the sides of the U shape using chopped mat.

(4) Cast the other web separately from the mould and place it on the top of the diaphragms and bond with chopped mat along the corners of the beam.

(5) Lay up the rest of fibre layers and allow to cure.

2.9 BEAM ANALYSIS

Generally the following methods are used for analysis of box beams:-

(1) Simple beam theory based on transformed section

(2) Folded plate theory [2.12]

(3) Finite element method [2.13]

(4) Finite strip method [2.14]

Due to the complexity of the last three methods which would require complicated computer programmes, it was decided to check the validity of the first method which is more convenient to the designer and only requires the use of a programmable desk calculator. The method is detailed below.

2.10 THEORETICAL ANALYSIS

The analysis of the beam is carried out in the following manner:-

(1) The elastic properties for the beam elements were found from experimental methods using specimens cut from the middle portion of each beam. Longitudinal and transverse modulii and Poisson's ratio corresponding to each beam element are shown in Tables (2.2-2.7). Uniform cross-section specimens fig (1.6) as described in the previous chapter were used.

The testing of tensile and compressive specimens was carried out using the Denison testing machine with a suitable rate of loading and an average of three specimens results was considered suitable.

To determine the shear modulus for the web elements in the

beam additional specimens at 45^{o} to the reference axis (see fig 2.4), were cut and the shear modulus was determined from the following equation.

$$\frac{1}{G_{LT}} = \frac{4}{E_1} - \frac{1}{E_L} - \frac{1}{E_T} + \frac{2\nu LT}{E_L} \qquad (2.9)$$

where

E_1 = modulus at 45^{o} to the reference axis

E_L = longitudinal modulus

E_T = transverse modulus

G_{LT} = shear modulus

νLT = longitudinal Poisson's ratio.

(2) The average thickness of each beam element i.e. web compression flange, diaphragms etc. was measured by a suitable micrometer. As for each element the elastic modulus is different along the longitudinal direction and equivalent thickness was introduced for each beam element (see Tables 2.2-2.6) which was based on the element longitudinal modulus relative to the longitude of the compressive flange, for example the equivalent thickness of the web = Average thickness of web x $\frac{\text{E web}}{\text{E comp. flange}}$. Thus an equivalent (or transformed section is found from which the equivalent section properties Z_T, Z_C are obtained Table (2.8 and used to compute the stresses in the analysis. Diaphragms and local reinforcements are represented by a strip in the equivalent section. Appendix B shows a typical method of analysis worked for beam type B1.

(3) The theoretical compressive and tensile stresses were computed from the simple bending theory equation

$$f_{CT} = \frac{M y}{I_{NA\ equivalent}} \qquad (2.10)$$

(4) For the box section, the maximum shear stress occurs at the neutral axis and is computed from the equation,

$$\tau = \frac{VAY}{Ib} \qquad (2.11)$$

where V = the total shearing force at the section

A = area of the equivalent cross-sectional area above N.A.

Y = the distance from centroid of area A to N.A.

b = breadth at N.A.

(5) The maximum deflection which occurs at the centre of the beam fig (2.1) may be calculated from the equation readily obtained by the area moment method.

$$\delta = \frac{Wa(3L^2-4a^2)}{48E_L I_{NA}} \qquad (2.12)$$

where

W = total load applied

L = span length

a = distance from load to ℄ of support

E_L = Equivalent longitudinal modulus

I_{NA} = the 2nd moment of area about N.A. based on equivalent section.

(6) Theoretical stresses in the diaphragms are calculated from the equation

$$\sigma = \frac{V}{A} \qquad (2.13)$$

where V is the shearing force at any section of the beam, and A is the area of diaphragms under the effect of shear force.

The maximum compressive stress will occur for diaphragms between the support and applied load. This method is based on two assumptions. Firstly, the effects of webs and flanges are neglected, and secondly, the shear force along the beam is assumed to produce an axial compressive force on the diaphragms.

2.11 CRITICAL STRESSES

As the box beam is composed of thin walled elements local buckling of elements is liable to occur during loading. Design considerations for buckling in such case becomes a necessity. Methods for predicting critical stresses which produce local buckling in various elements of the beam are described below.

2.11.1 Diaphragms

The boundary conditions of each diaphragm were considered to be fixed along all edges. Each diaphragm was therefore treated as a built in plate subject to end compression caused by the shearing force. The theoretical critical compressive stress may be computed using Bulson [2.15] equation

$$\sigma_{cr} = \frac{K_{min}\,\pi^2\sqrt{D_L\,D_T}}{b^2 t} \qquad (2.14)$$

where $$K_{min} = \frac{8}{3}\left(3 + \frac{0.88H}{D_L D_T}\right) \qquad (2.15)$$

$$H = \frac{1}{2}\left(\nu_L D_T + \nu_T D_L\right) + \frac{2Gt^3}{12} \qquad (2.16)$$

$$D_L = \frac{E_L t^3}{12(1-\nu_L^2)} \qquad (2.17)$$

$$D_T = \frac{Et^3}{12(1-\nu_T^2)} \qquad (2.18)$$

t = thickness of diaphragm

b = width of diaphragm

ν_L ν_T = longitudinal and transverse Poisson's ratio respectively

2.11.2 Webs

To predict the critical shear stress which will produce buckling of the webs, the webs were treated as long plates with clamped edges. An equation given by Timoshenko [2.16] for the critical buckling shear stress for orthotropic long plates with the same boundary conditions was used as follows:-

$$\tau_{cr} = \frac{4K\,4\sqrt{D_L D_T^3}}{b^2 t} \quad \text{for} \quad \theta > 1 \qquad (2.19a)$$

and

$$\tau_{cr} = \frac{4K\sqrt{D_L}H}{b^2 t} \quad \text{for} \quad \theta < 1 \qquad (2.19b)$$

where $\theta = \frac{\sqrt{D_L D_T}}{H}$ and K value dependant on θ obtained from table (2.9).

D_L, D_T, H, b and as defined before.

2.11.3 Compression Flange

The local buckling stress in the compression flange was obtained from a modified form of the equation given by Bulson [2.15] for box sections constructed from isotropic materials.

$$\sigma_{cr} = \frac{Kt^2E}{12(1-\nu^2)} \left(\frac{t}{b}\right)^2 \qquad (2.20)$$

where K is a factor depending on the restraint offered to the compression flange which in this case is equal to 4.

E = the modulus of elasticity

t = thickness

b = width of compression flange

ν = Poisson's ratio

As the compression flange is in reality of orthotropic nature E was replaced by $\sqrt{E_L E_T}$ and ν^2 was replaced by $\nu_L \nu_T$ and thus the basic Bulson equation becomes:-

$$\sigma_{cr} = \frac{Kt^2\sqrt{E_L E_T}}{12(1-\nu_L \nu_T)} \left(\frac{t}{b}\right)^2 \qquad (2.21)$$

where E_L, E_T is the longitudinal and transverse modulu for the flange.

ν_L ν_L is the longitudinal and transverse Poisson's ratio for the flange.

t, b is the thickness and the width of the flange.

2.12 EXPERIMENTAL PROGRAMME

The programme started with testing the pilot beam B_p and upon satisfactory results it was decided to proceed with casting and testing five beams series B1-B5. A suitable testing rig was employed and loading was applied at a steady rate of 2.5 kN increments up to failure.

2.13 DISCUSSION

2.13.1 Mode of Failure

The mode of failure of the pilot beam B_p and the rest of the beams B1-B5 was similar fig (2.7). The failure took place in the

compression flange with a sudden crack propagation and was accompanied by an explosive sound. It was observed that signs of local buckling were shown generally after the beams sustained $\frac{2}{3}$ of their failure load. As the applied load increased the number of buckle waves in the compression flange tended to increase and it was apparent that midspan diaphragms formed nodal lines which initiated failure to occur between diaphragms at mid span. Fig (2.8) shows typical abrupt changes of the pattern of the wave form as the load increased.

No buckling was observed in the tension flange or at the support assembly diaphragms but slight buckling of the web was exhibited.

In designing structural members composed of flat plate it is common to proportion the member so that overall failure occurs prior to local buckling. Thus in the compression flange if local buckling is not to occur at a stress smaller than the ultimate compressive stress.

i.e. $f_{cr} > f_{comp}$ (2.22)

where f_{cr} is the critical local buckling and f_{comp} is the ultimate compressive stress.

Substituting for f_{cr} in equation (2.21)

$$\frac{K\pi^2\sqrt{E_L E_T}}{12(1-\nu_L \nu_T)} \left(\frac{t}{b}\right)^2 > f_{comp} \qquad (2.23)$$

considering for example beam type B1 for the compression flange where

$K = 4$

$\nu_L = 0.27$

$\nu_T = 0.08$

$f_{comp} = 198.41\ N/mm^2$

$$E_L = 17.81 \text{ kN/mm}^2$$

$$E_T = 4.95 \text{ kN/mm}^2$$

and equation (2.23) results in $t > 11.89$ mm which means that failure of the beam compression flange in local buckling cannot be avoided unless the compression flange thickness is at least 2¼ its adopted thickness (5.30 mm). For economic considerations the increased thickness could be limited to the middle third zone of the compression flange. The use of external or internal stiffening ribs may provide an alternative solution.

Predicted local buckling stress Table (2.10) for beam series B1-B5 were in general 60% of the maximum compressive stress which agreed well with visual observations. Table (2.11) shows that the maximum exhibited shear stress in the web exceeded the predicted critical shear buckling stress whereas in Table (2.12) the maximum stresses exhibited in the diaphragms were considerably lower than the critical buckling stress range.

2.13.2 Fibre Orientation

Beam type B1 attained the maximum failure load 65.00 (kN) followed by beam type B5 (62.5 kN). The multidirectional fibre orientation (0, +45, -60, -60, +45, 0), did not seem to have a great significance on the failure load as the failure was governed by local buckling in the compression flange. The laying of fibre with the designed fibre orientation in the case of beam B4 required more time compared with beam B5 (bidirectional fibre 0/90). In view of the number of reinforcing layers beam type B4 is the most expensive in the series. In civil engineering construction sites where the accuracy, time and cost are important factors, it is advisable that complicated multidirectional orientations in structural members should be avoided wherever possible. In this respect the use of

bi-directional reinforcement (0/90) is more favoured than multi-directional reinforcement.

2.13.3 Prediction of Stresses

Close agreement between the test data and theoretical compressive and tensile stresses at mid span computed from simple beam theory based on the equivalent section was observed figs (2.15-2.20) and figs (2.21-2.26). However, in the case of compressive stresses, the good correlation only applied up to the limit where local buckling began after this point stresses tended to decrease figs (2.15 and 2.18). Computed shear stresses were generally lower than the test data figs (2.27-2.32).

2.13.4 Deformations

Predicted deflections were lower than the actual deflections figs (2.9-2.14) and a correction factor was introduced Table (2.13). The deviation from theory may be due to the interaction of diaphragms and the irregulatives of beam element thickness. The maximum deflections at failure for the beam series B_p, B1-B5 are excessive compared to the allowable deflections set codes of practise and this is due to the low modulus of G.R.P.

In the case of G.R.P. beams it is possible to exceed allowable deflections specified for other materials provided that they are not observable and do not affect the safety of the beam.

2.13.5 Lateral Stability

All beams experienced between 0 and 3 mm lateral deflection fig (2.34) which indicated that the beams were reasonably stable laterally up to failure.

2.13.6 Safety Factors

Safety factors introduced for beam series B_p, B1-B5 Table (2.14) resulted in theoretical failure loads comparable to the experimental failure loads with the exception of beam type B1 and B5. Factors of safety ranged from 1.57 to 3.57.

Safety factors based on the theoretical critical buckling stress in the compression flange were also introduced (see Table (2.15). The theoretical failure loads are lower than the experimental loads and the corresponding factors of safety ranging from 2.51 to 4.72. As the failure by local buckling was dominant in all the beam series, it is recommended that a factor of safety based on the theoretical local buckling stress should be used in G.R.P. box beams.

Factors of safety depend also on the type of load. Gibbs and Cox (2.17) suggested the following safety factors.

Static short term loads	= 2
Static long term loads	= 4
Variable or changing load	= 4
Cyclic load	= 6
Fatigue loads	= 6
Impact loads	= 10

These safety factors are based on the allowable working stress. Makowski [2.18] suggested similar values of factors of safety.

2.14 CONCLUSION

The following conclusions may be drawn from the foregoing discussion.

(1) Although a G.R.P. box beam may be designed initially on the basis of its section capacity the beam must be checked against local buckling in the compression flange. In practise the

compression flange is usually hidden, and therefore failure may occur suddenly without warning which implies that an adequate factor of safety must be used based on the critical buckling stress.

(2) G.R.P. box beams may exhibit large deformations without failure.

(3) Additional stresses in the form of bimoment stresses due to Vlascv [2.10] theory must be catered for in designing thin walled G.R.P. structural elements and wherever possible, attempts should be made to reduce them.

(4) A design which eliminates the failure of G.R.P. box beams by a local buckling mode may prove to be expensive.

(5) The use of chopped mat reinforcement around the corners of the box beams was effective in controlling stress concentrations. Also a minimum lapping length of 100 mm in reinforcing layers was satisfactory.

Beam Series	No, type and orientation of reinforcing layers with reference to the axis shown in fig (2.4)			
	Webs	Compression Flange	Tension Flange	Diaphragm
B_p	4B 4(0/90)	4B 4(0/90)	4U 4(0)	4B 4(0/90)
B1	4U 0,+45,+45,0	6U 6(0)	U,B,B,U 0,0/90,90/0,0	4U 0,+45,+45,0
B2	4U 60,-45,-45,60	6U 6(0)	4U 4(0)	4U 60,-45,-45,60
B3	4U +45,-45,-45,+45	6U 6(0)	4U 4(0)	4U +45,-45,-45,+45
B4	6U 0,+45,-60, -60,+45,0	6U 6(0)	4U 4(0)	6U 0,+45,-60, -60,+45,0
B5	4B 4(0/90)	6B 6(0/90)	4B 4(0/90)	4B 4(0/90)

B = Bidirectional

U = Unidirectional

C = Chopped mat

TABLE (2.1)

DETAILS OF REINFORCEMENT BEAMS BP, B1-B5

Structural property	Webs	Compression flange	Tension flange	Diaphragms	Local reinforcement
Average thickness mm	4.03	4.30	4.02	6	5
Longitudinal modulus E_L kN/mm^2	15.60 Tensile	15.60 Compressive	15.80 Tensile	12.25 Tensile	10 Tensile
Transverse modulus E_T kN/mm^2	9.09 Tensile	13.21 Compressive	*	8.43 Tensile	*
Shear modulus G kN/mm^2	4.02	*	*	3.89	*
Longitudinal Poisson's ratio ν_{LT}	0.13	0.17	*	0.13	*
Transverse Poisson's ratio ν_{TL}	0.11	0.12	*	0.09	*
Modulus at 45^o E_{45} kN/mm^2	10.73 Tensile	*	*	9.17	*
Equivalent longitudinal modulus kN/mm^2	15.60	15.60	15.60	15.60	15.60
Equivalent thickness mm	4.03	4.03	4.07	4.65	3.2

* not required in the analysis

TABLE (2.2)

STRUCTURAL PROPERTIES FOR BEAM (B_P) ELEMENTS

Structural property	Webs	Compression flange	Tension flange	Diaphragms	Local reinforcement
Average thickness mm	4.27	5.30	3.99	6.00	5.00
Longitudinal modulus E_L kN/mm^2	16.80 Tensile	17.81 Compressive	17.70 Tensile	12.53 Tensile	10 Tensile
Transverse modulus E_T kN/mm^2	9.65 Tensile	4.95 Compressive	*	8.50 Tensile	*
Shear modulus G kN/mm^2	5.34	*	*	4.25	*
Longitudinal Poisson's ratio ν_{LT}	0.32	0.27	*	0.28	*
Transverse Poisson's ratio ν_{TL}	0.18	0.081	*	0.17	*
Modulus at 45^o E_{45} kN/mm^2	12.81 Tensile	*	*	10.31	*
Equivalent longitudinal modulus kN/mm^2	17.81	17.81	17.81	17.81	17.81
Equivalent thickness mm	4.03	5.30	3.97	4.22	2.81

* not required in the analysis

TABLE (2.3)

STRUCTURAL PROPERTIES FOR BEAM (B1) ELEMENTS

Structural property	Webs	Compression flange	Tension flange	Diaphragms	Local reinforcement
Average thickness mm	4.12	5.23	4.09	6.00	5.00
Longitudinal modulus E_L kN/mm^2	8.10 Tensile	18.06 Compressive	18.62 Tensile	6.30 Tensile	10.00 Tensile
Transverse modulus E_T kN/mm^2	7.20	5.54 Compressive	*	6.2 Tensile	*
Shear modulus G kN/mm^2	9.13	*	*	2.1	*
Longitudinal Poisson's ratio ν_{LT}	0.45	0.25	*	0.43	*
Transverse Poisson's ratio ν_{TL}	0.42	0.11	*	0.43	*
Modulus at 45^o E_{45} kN/mm^2	15.34	*	*	6.28	*
Equivalent longitudinal modulus kN/mm^2	18.06	18.06	18.06	18.06	18.06
Equivalent thickness mm	1.84	5.23	4.21	2.09	2.68

* Not required in the analysis

TABLE (2.4)

STRUCTURAL PROPERTIES FOR BEAM (B2) ELEMENTS

Structural property	Webs	Compression flange	Tension flange	Diaphragms	Local reinforcement
Average thickness mm	4.10	5.26	4.14	6.00	5.00
Longitudinal modulus E_L kN/mm^2	8.20 Tensile	17.81 Compressive	17.80 Tensile	7.5 Tensile	10.00
Transverse modulus E_T kN/mm^2	8.20 Tensile	5.93 Compressive	*	7.50 Tensile	*
Shear modulus G kN/mm^2	5.77	*	*	5.15	*
Longitudinal Poisson's ratio ν_{LT}	0.41	0.26	*	0.39	*
Transverse Poisson's ratio ν_{TL}	0.36	0.093	*	0.39	*
Modulus at 45^o E_{45} kN/mm^2	12.61	*	*	11.21	*
Equivalent longitudinal modulus kN/mm^2	17.81	17.81	17.81	17.81	17.81
Equivalent thickness mm	1.89	5.26	4.14	2.53	2.81

* Not required in the analysis

TABLE (2.5)

STRUCTURAL PROPERTIES FOR BEAM (B3) ELEMENTS

Structural property	Webs	Compression flange	Tension flange	Diaphragms	Local reinforcement
Average thickness mm	5.10	5.28	3.98	6.00	5
Longitudinal modulus E_L kN/mm^2	15.1 Tensile	17.85 Compressive	17.85 Tensile	13.31 Tensile	10 Tensile
Transverse modulus E_T kN/mm^2	7.34 Tensile	5.01 Compressive	*	6.40 Tensile	*
Shear modulus G kN/mm^2	6.49	*	*	4.62	*
Longitudinal Poisson's ratio ν_{LT}	0.25	0.25	*	0.22	*
Transverse Poisson's ratio ν_{TL}	0.12	0.91	*	0.13	*
Modulus at 45^o E_{45} kN/mm^2	12.37	*	*	9.64	*
Equivalent longitudinal modulus kN/mm^2	17.85	17.84	17.85	17.85	17.85
Equivalent thickness mm	4.31	5.28	3.98	4.47	2.80

* Not required in the analysis

TABLE (2.6)

STRUCTURAL PROPERTIES FOR BEAM (B4) ELEMENT

Structural property	Webs	Compression flange	Tension flange	Diaphragms	Local reinforcement
Average thickness mm	4.12	5.29	4.18	6	5
Longitudinal modulus E_L kN/mm^2	14.10 Tensile	13.45 Compressive	13.93 Tensile	11.94 Tensile	10 Tensile
Transverse modulus E_T kN/mm^2	13.98 Tensile	13.45 Compressive	*	11.90 Tensile	*
Shear modulus G kN/mm^2	3.46	*	*	3.34	*
Longitudinal Poisson's ratio ν_{LT}	0.13	0.16	*	0.12	*
Transverse Poisson's ratio ν_{TL}	0.13	0.16	*	0.12	*
Modulus at 45^o E_{45} kN/mm^2	9.68	*	*	8.95	*
Equivalent longitudinal modulus kN/mm^2	13.45	13.45	13.45	13.45	13.45
Equivalent thickness mm	4.32	5.29	4.33	5.33	3.72

* Not required in the analysis

TABLE (2.7)

STRUCTURAL PROPERTIES FOR BEAM (B5) ELEMENT

Beam Series	Equivalent Inertia INA x 10^{-6} mm^4	N.A. Distance from Tension flange y mm	Equivalent Section Modulus ZT x 10^{-3} mm^3	Equivalent Section Modulus ZC x 10^{-3} mm^3
B_p	60.033578	152.43	397.836	393.843
B1	61.828860	157.06	420.004	393.663
B2	46.938942	158.15	320.862	296.800
B3	48.147560	158.35	337.475	304.057
B4	63.290029	155.45	428.968	403.841
B5	67.609963	155.45	453.241	434.930

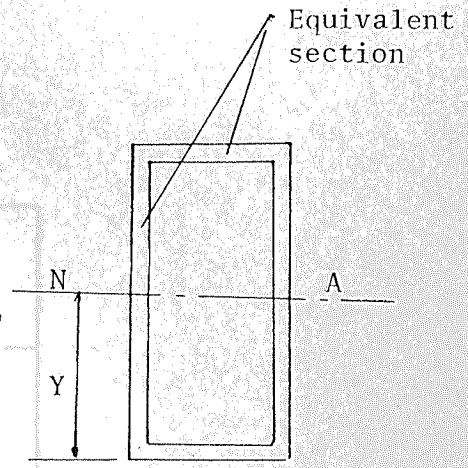

TABLE (2.8)

EQUIVALENT SECTION PROPERTIES FOR BEAMS BP, B1-B5

Θ	K
0	18.6
0.2	18.9
0.5	19.9
1	22.15
2	18.8
3	17.6
5	16.6
10	15.9
20	15.5
40	15.3
	15.1

TABLE (2.9)

VALUES OF THE FACTOR K IN EQUATION 2.19.A AND 2.19.B FOR A LONG PLATE WITH CLAMPED EDGES

Beam type	Critical local buckling stress (n/mm^2)	Maximum compressive stress exhibited N/mm^2	$\frac{\text{Critical stress}}{\text{Maximum stress}}$
B_p	39.62	35.00	1.132
B1	39.42	92.00	0.428
B2	41.14	82.00	0.501
B3	42.60	72.00	0.592
B4	39.68	68.00	0.584
B5	56.48	90.00	0.627

TABLE (2.10)

COMPARISON OF PREDICTED CRITICAL LOCAL BUCKLING STRESS AND MAXIMUM STRESS EXHIBITED IN THE COMPRESSION FLANGE BEAM SERIES B_p, B1-B5

Beam type	Critical local buckling stress (N/mm^2)	Maximum compressive stress exhibited N/mm^2	$\frac{\text{Critical stress}}{\text{Maximum stress}}$
B_p	14.11	9.20	1.517
B1	17.572	6.20	2.834
B2	17.26	27.50	0.627
B3	19.88	30.40	0.6539
B4	21.26	37.70	0.650
B5	17.96	27.50	0.653

TABLE (2.11)

COMPARISON OF PREDICTED CRITICAL SHEAR BUCKLING STRESS AND MAXIMUM SHEAR STRESS EXHIBITED IN THE WEBS, BEAM SERIES Bp, B1-B5

Beam type	Critical local buckling stress (N/mm^2)	Maximum compressive stress exhibited N/mm^2	$\frac{\text{Critical stress}}{\text{Maximum stress}}$
B_p	67.09	8.45	7.939
B1	71.10	5.78	12.30
B2	50.04	2.15	23.27
B3	57.82	2.95	19.60
B4	62.27	0.90	69.19
B5	78.79	7.00	11.25

TABLE (2.12)

COMPARISON OF PREDICTED CRITICAL COMPRESSIVE BUCKLING STRESS AND MAXIMUM COMPRESSIVE STRESS EXHIBITED IN THE DIAPHRAGMS, BEAM SERIES B_p, B1-B5

Beam type	Limit state deflection C.P. 110 $\frac{L}{250}$ (mm)	Maximum deflection at failure (mm)	Theoretical Maximum deflection at failure (mm)	Correction factor
B_p	11.60	28.5	18.48	0.648
B1	11.60	35	23.75	0.678
B2	11.60	30.00	22.29	0.743
B3	11.60	34.00	25.20	0.741
B4	11.60	32.00	22.86	0.714
B5	11.60	46.9	28.45	0.607

TABLE (2.13)

COMPARISON OF ALLOWABLE MAXIMUM AND THEORETICAL DEFLECTIONS
BEAM SERIES B_p, B1-B5

$$\text{Correction factor} = \frac{\text{theoretical deflection}}{\text{Max. deflection at failure}}$$

Beam type	Ultimate compressive strength N/mm^2	Maximum stress in compression flange at failure fw (N/mm^2) Eqn 2.10	Factor of safety	Theoretical failure load (kN)	Experimental failure load (kN)
B_p	125.00	35.00	3.57	29.31	42.5
B1	198.41	92.00	2.16	81.35	60.00
B2	191.20	82.00	2.33	55.39	50.00
B3	201.30	72.00	2.79	51.15	52.25
B4	187.25	68.00	2.75	61.41	65.00
B5	141.60	90.00	1.57	42.94	62.00

Note:-

Theoretical failure load obtained from the equation

$M = fwZc$

Factor of safety = $\frac{\text{ultimate stress}}{\text{maximum stress}}$

TABLE (2.14)

FACTORS OF SAFETY
BEAM SERIES B_p, B1-B5

Beam type	Ultimate compressive strength N/mm^2	Critical local buckling stress in compression flange f_{cr} N/mm^2 Eqn 2.2	Critical factor of safety	Theoretical critical failure load (kN)	Experimental failure load
B_p	125.00	39.62	3.15	33.18	42.50
B1	198.41	39.42	5.03	34.86	60.00
B2	191.20	41.14	4.65	27.79	50.00
B3	201.30	42.60	4.72	30.27	52.25
B4	187.25	39.68	4.72	35.83	65.00
B5	141.60	56.48	2.51	53.89	62.50

Note:-

Theoretical critical failure load obtained from the equation

$M = f_{cr} \cdot Z_c$

Critical factor of safety = $\frac{\text{ultimate stress}}{\text{critical stress}}$

TABLE (2.15)

CRITICAL FACTORS OF SAFETY
BEAM SERIES B_p, B1-B5

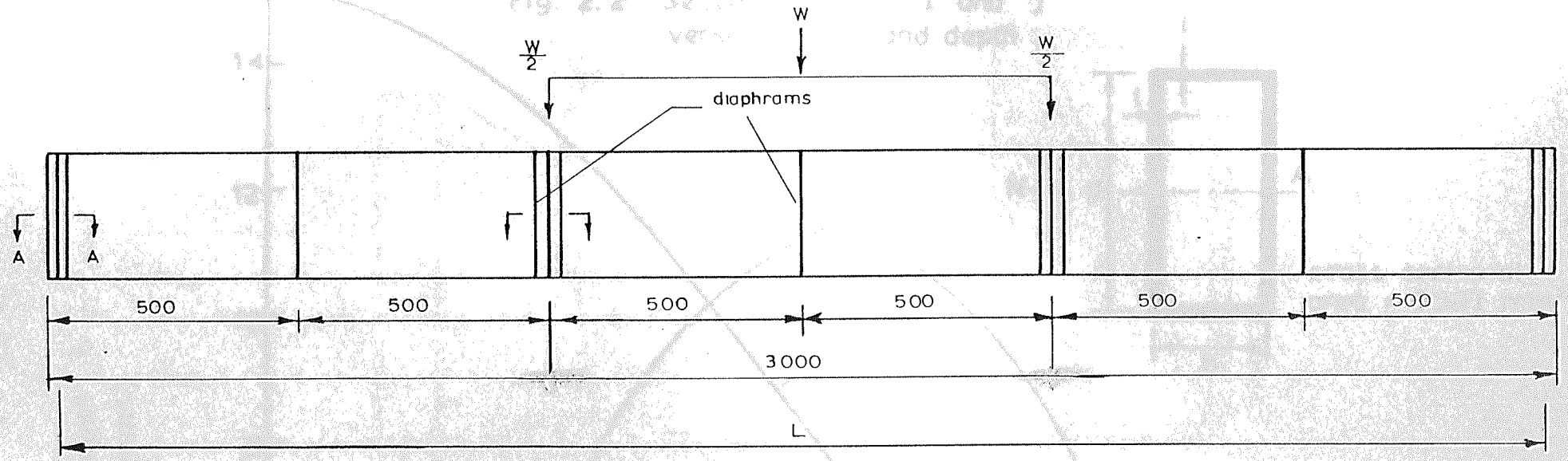

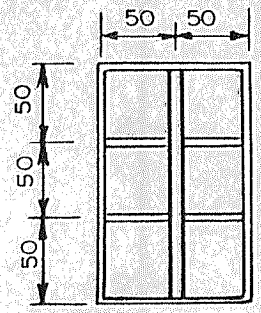

SECTION A A

local reinforcement 10 layers of chopped mat width 25

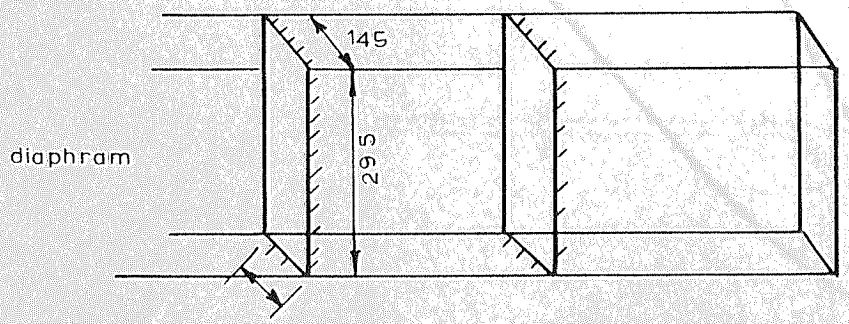

Dimensions in mm

Fig. 2.1. General arrangement of box beam.

Fig. 2.2 Section design I and J versus width and depth

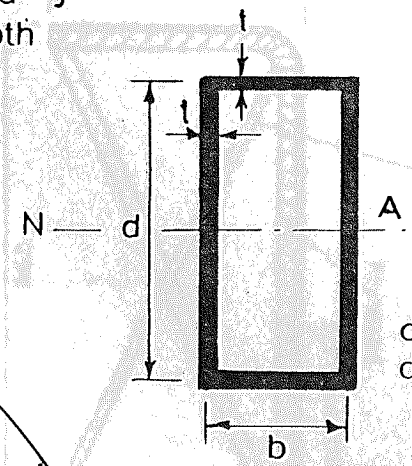

cross sectional area = 900 t mm²

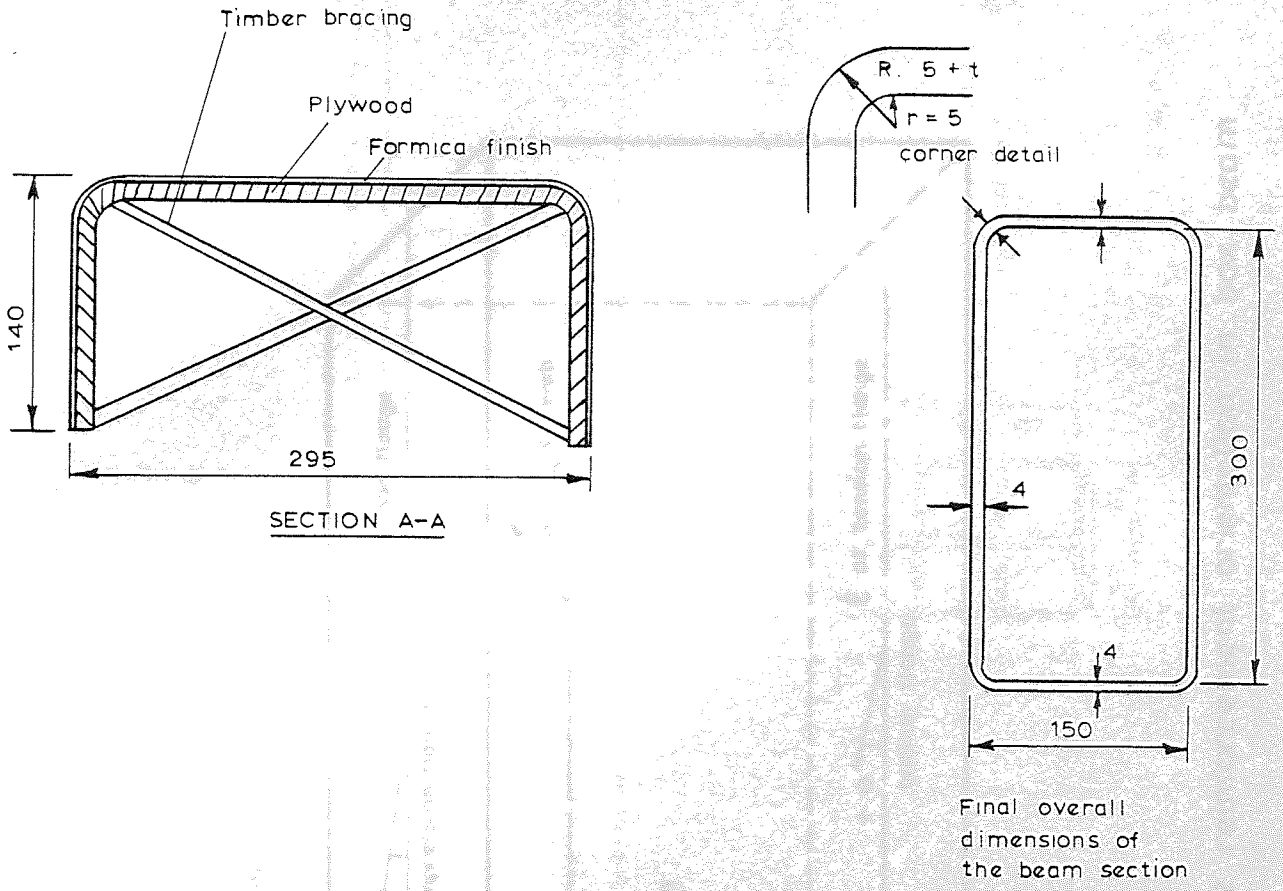

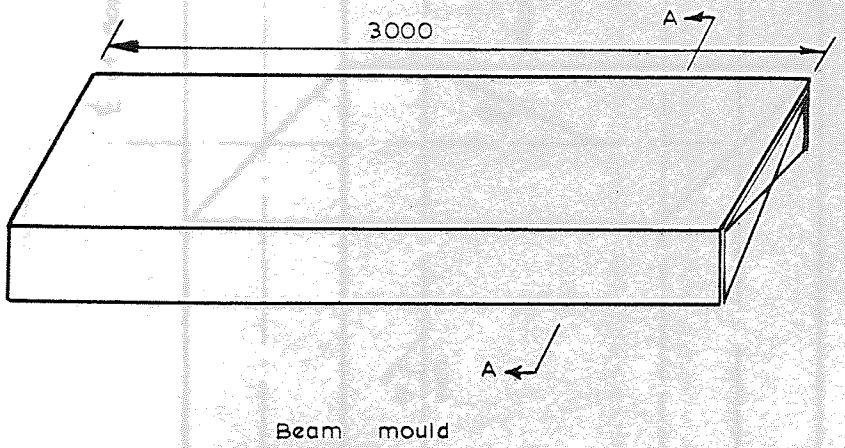

dimensions in mm

Fig. 23 Details of beam mould.

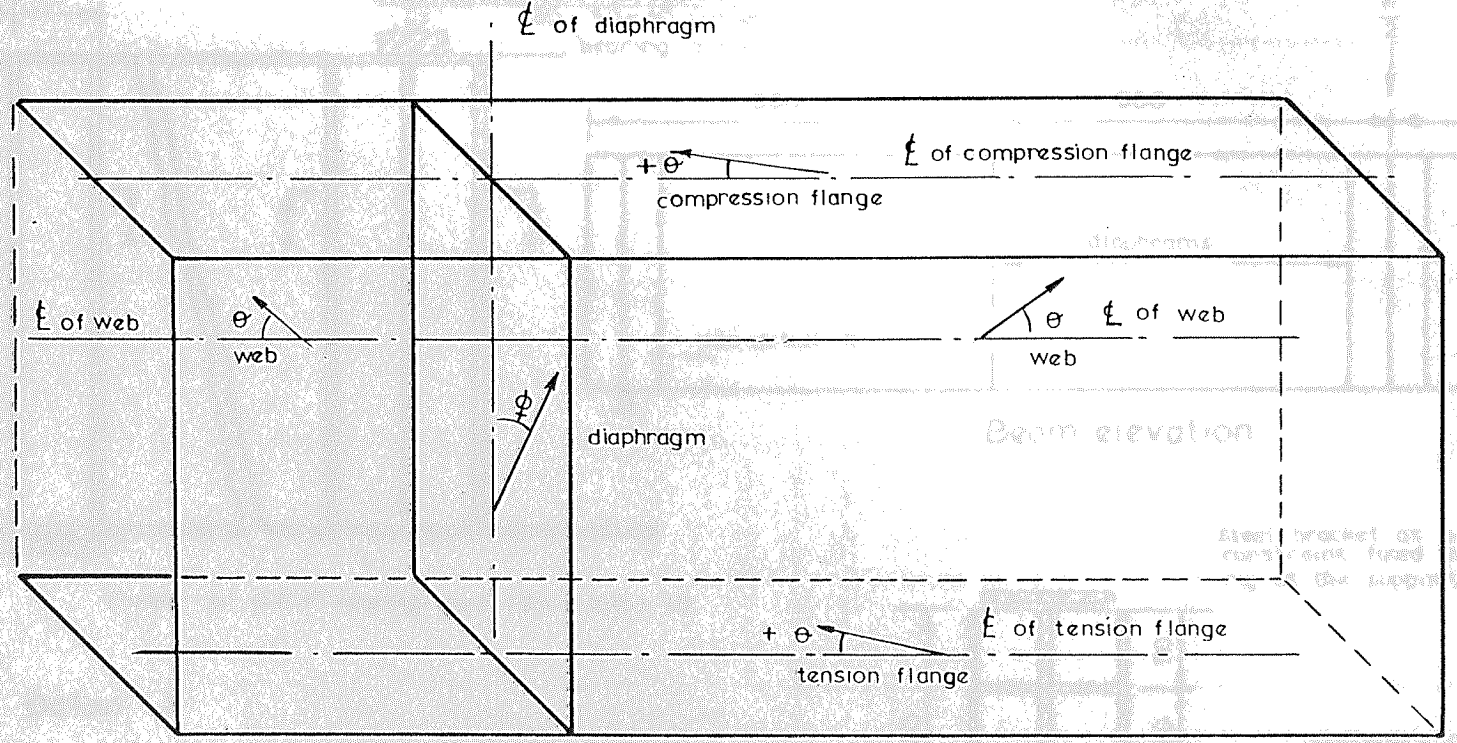

Fig. 2.4. Axis relative to fibre reinforcement orientation in box beam

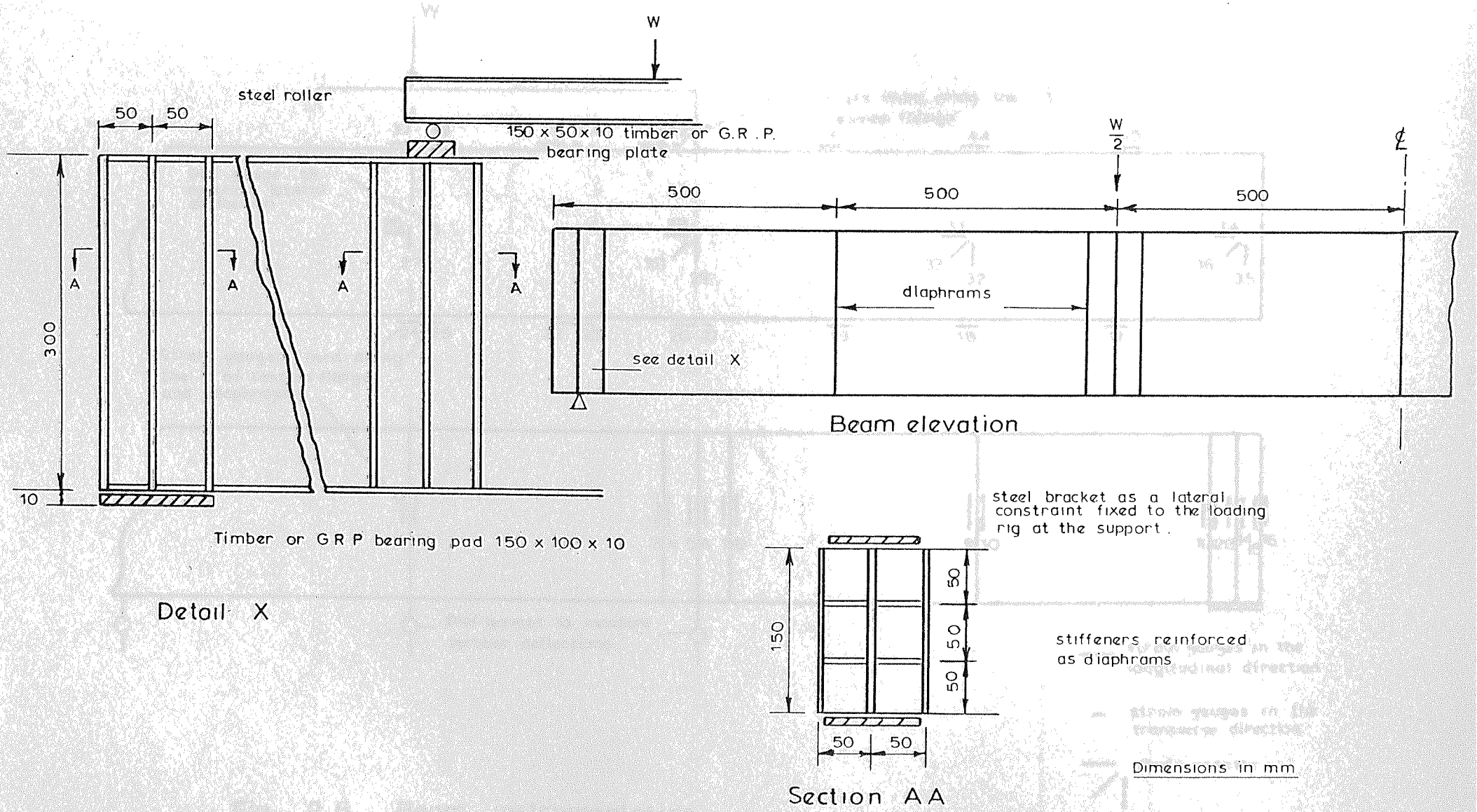

Fig. 2.5 Location and details of diaphrams special assembly

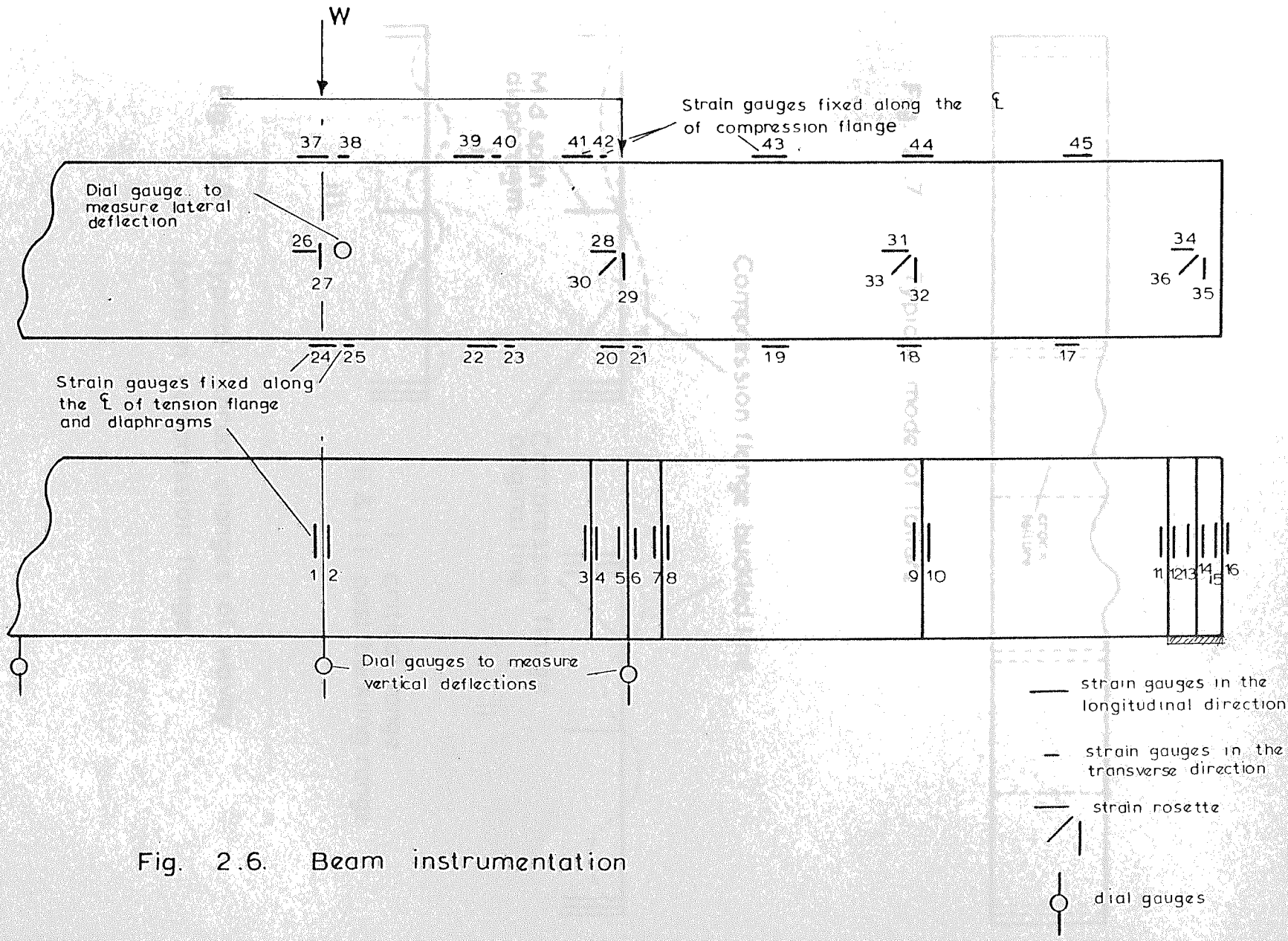

Fig. 2.6. Beam instrumentation

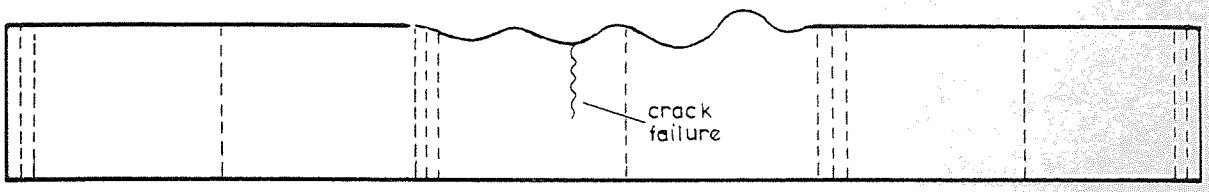

Fig. 2.7. Typical mode of failure

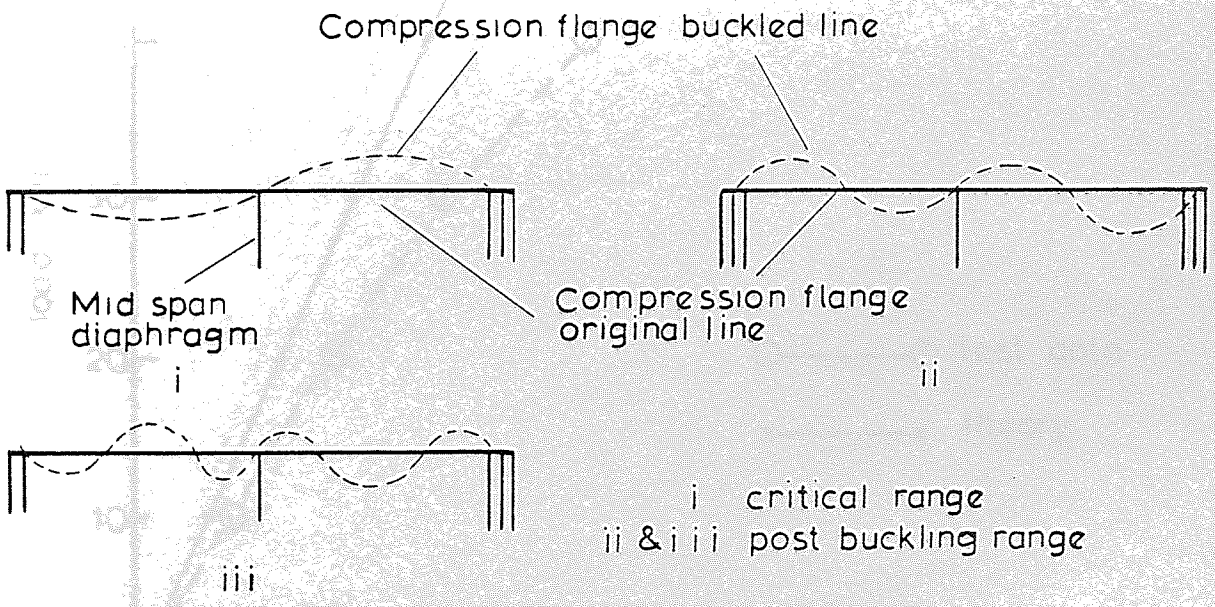

Fig. 2.8. Typical abrupt changes of wavey form in compression flange

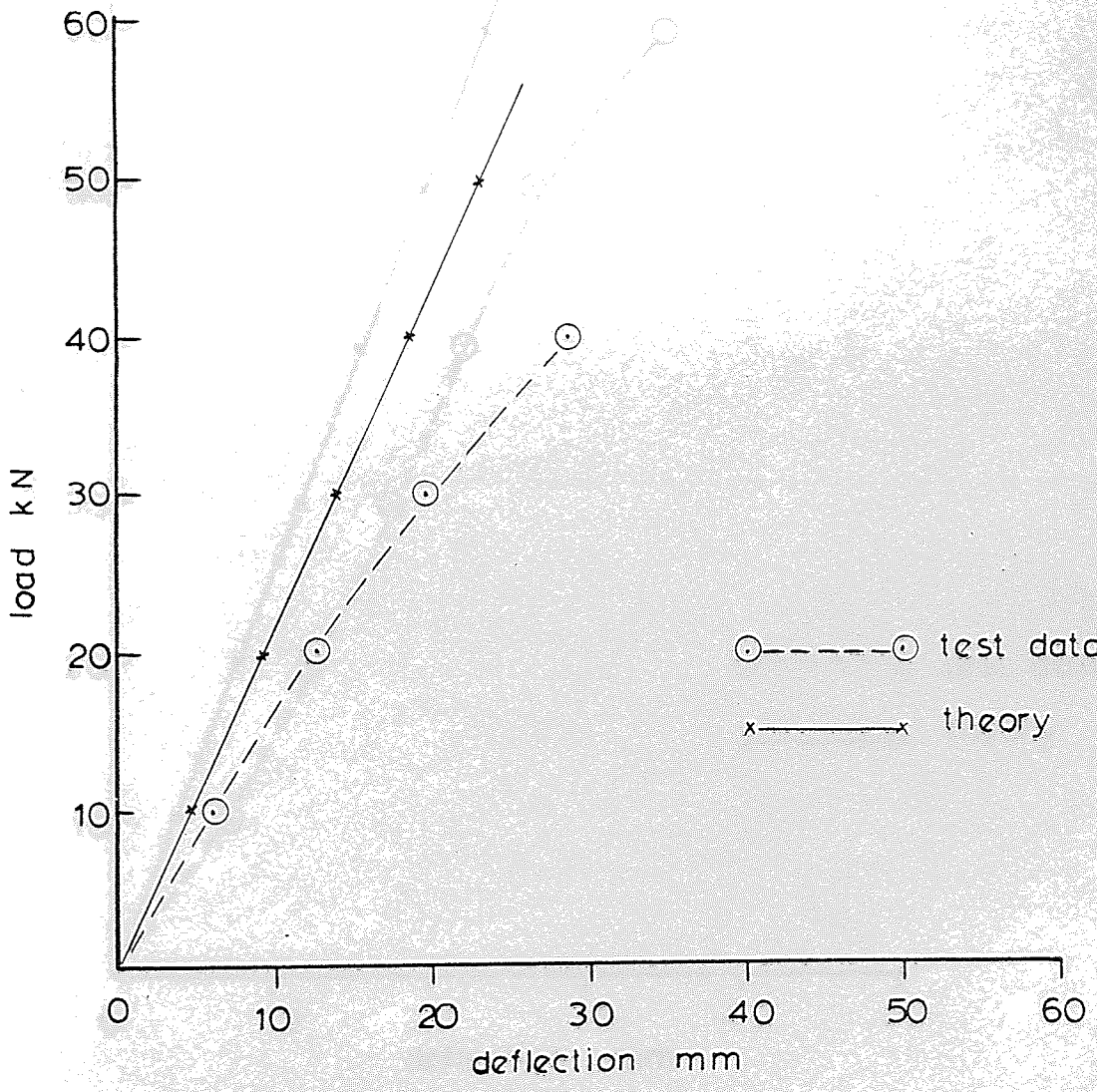

Fig. 2.9 Experimental and theoretical plots of load versus mid-span deflection pilot beam

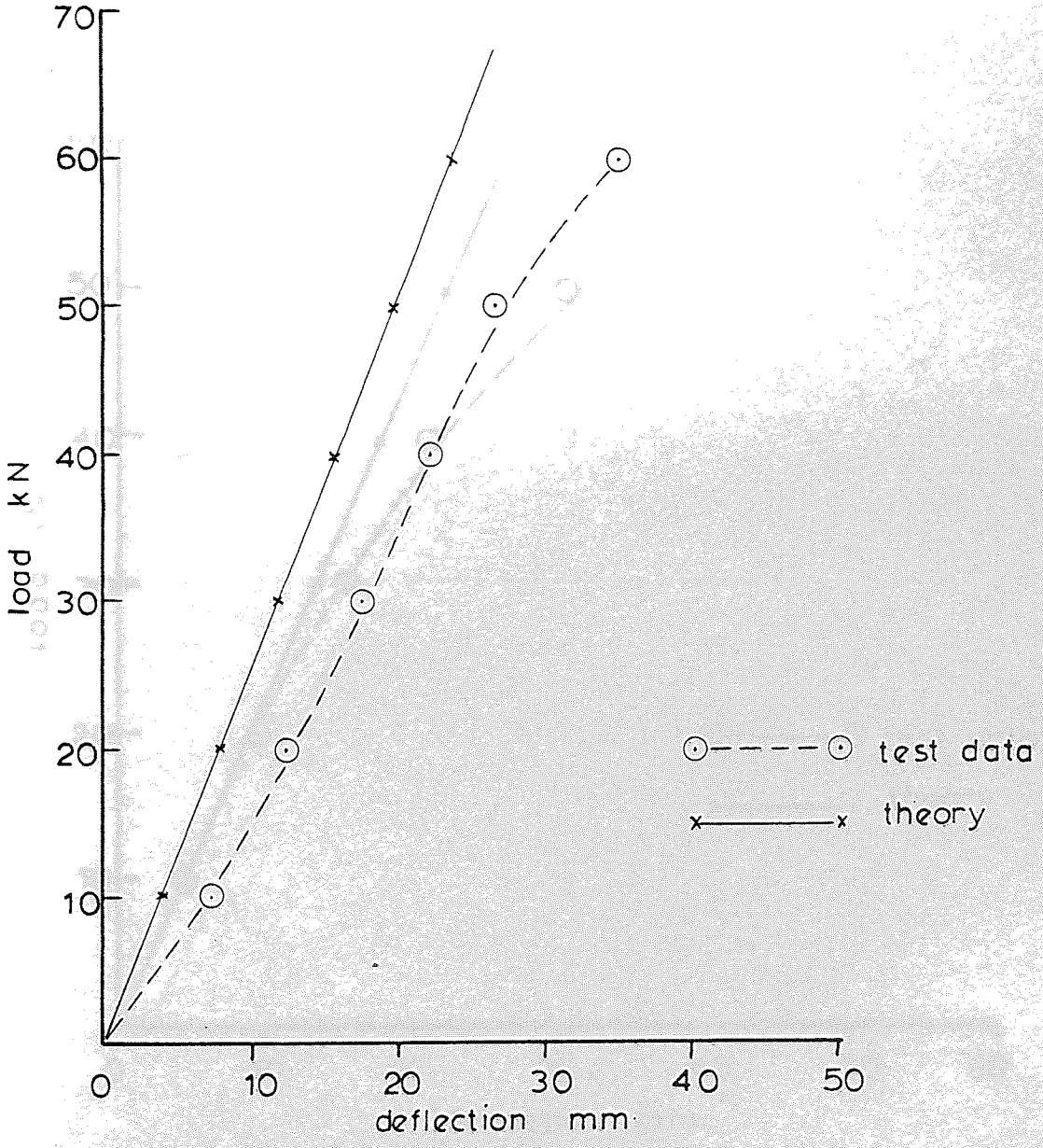

Fig. 2.10 Experimental and theoretical plot of load versus mid-span deflection beam type B1

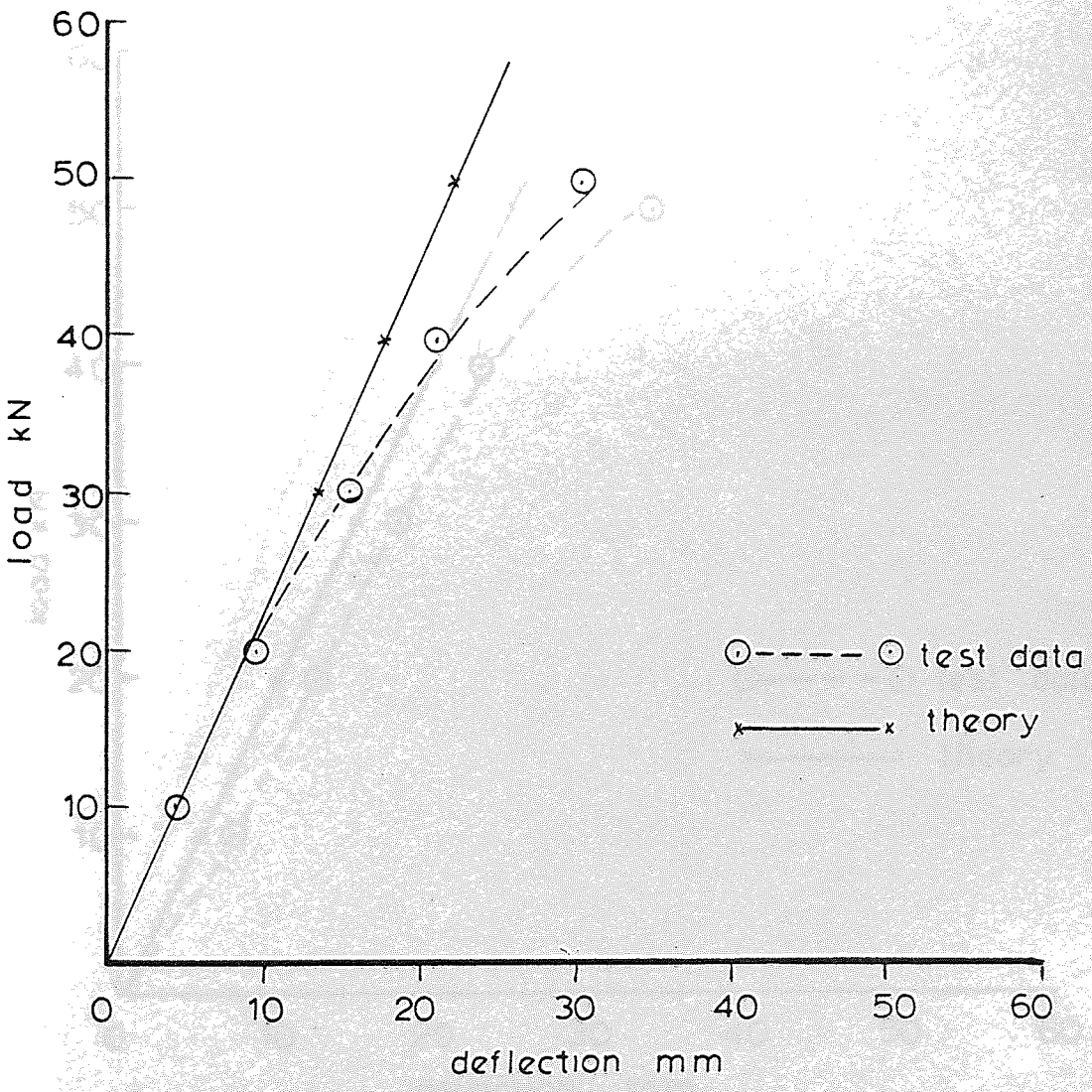

Fig. 2.11. Experimental and theoretical plots of load versus. mid span deflection. beam type B2

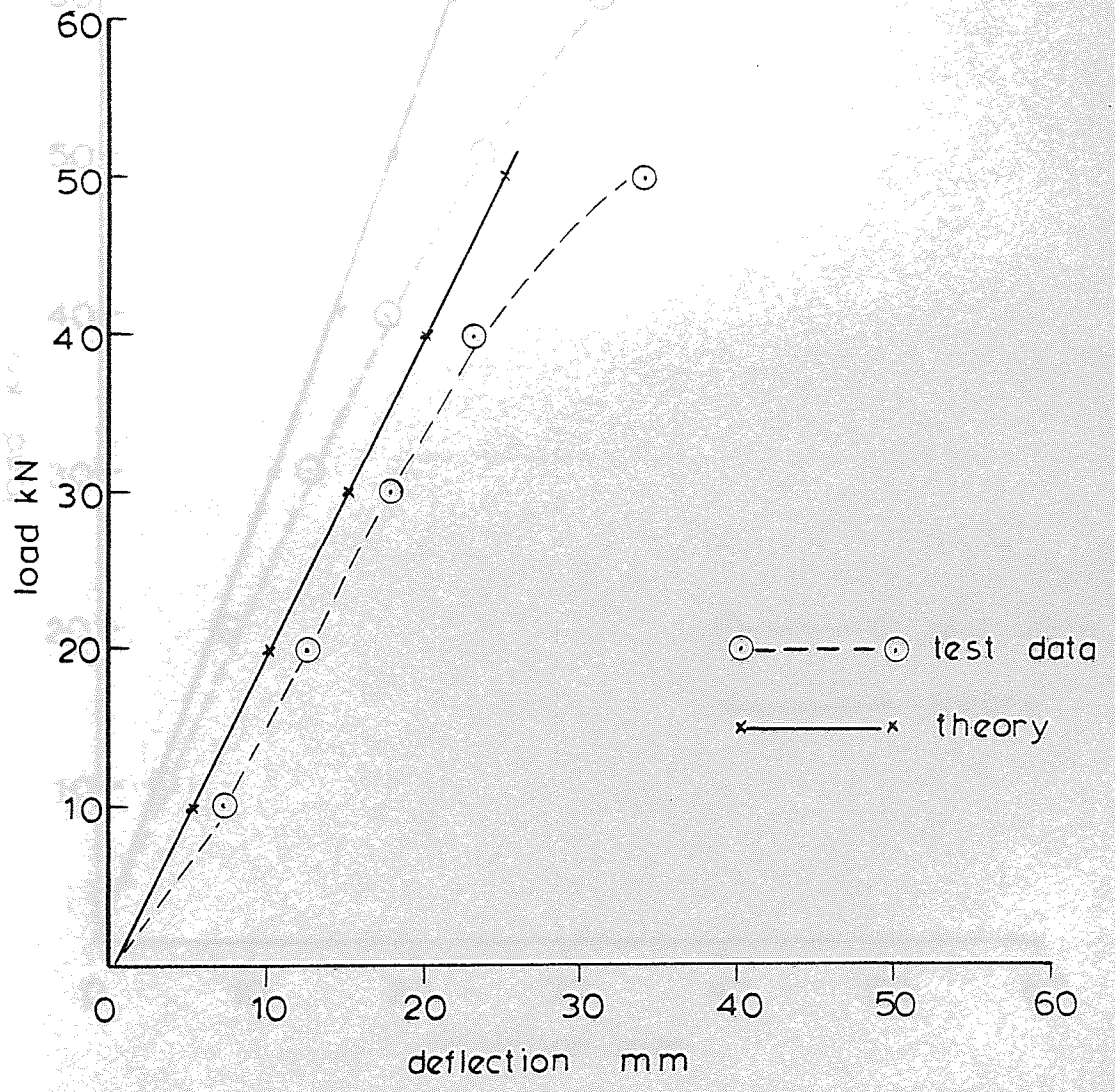

Fig. 2.12 Experimental and theoretical plots of load versus mid-span deflection. beam type B3

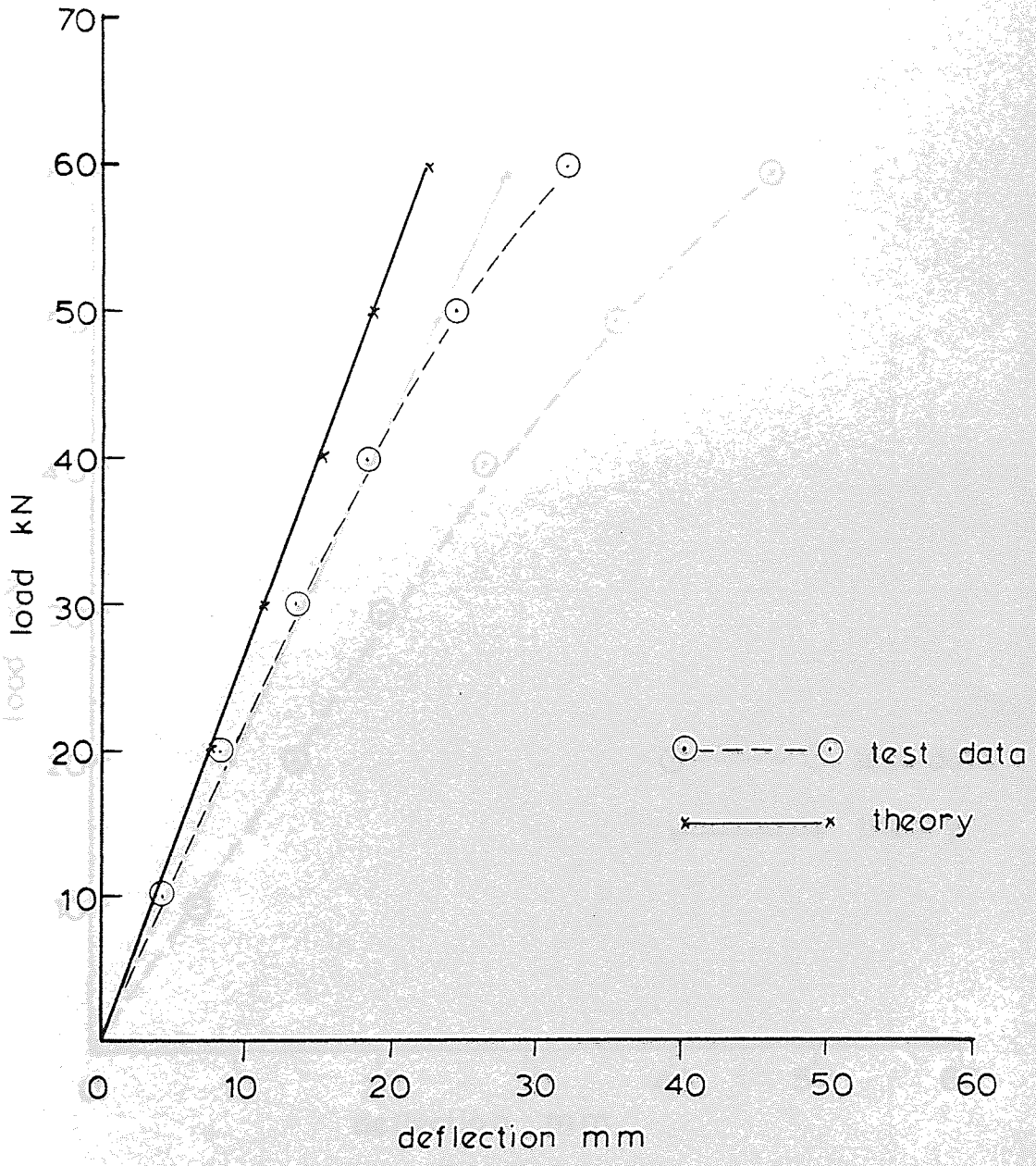

Fig. 2.13 Experimental and theoretical plots of load versus mid span deflection. beam type B4

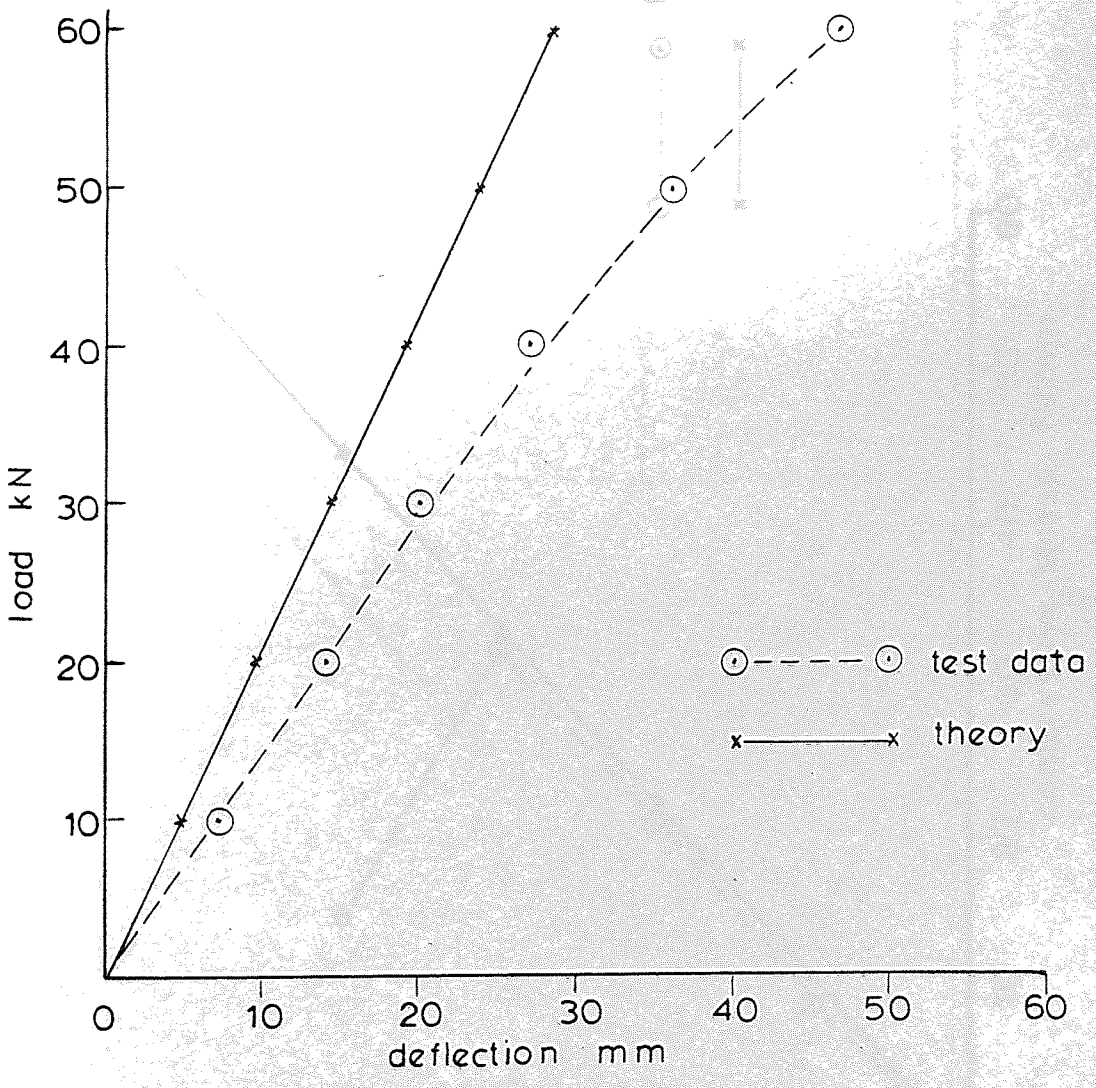

Fig. 2.14 Experimental and theoretical plots of load versus mid-span deflection. beam type B5

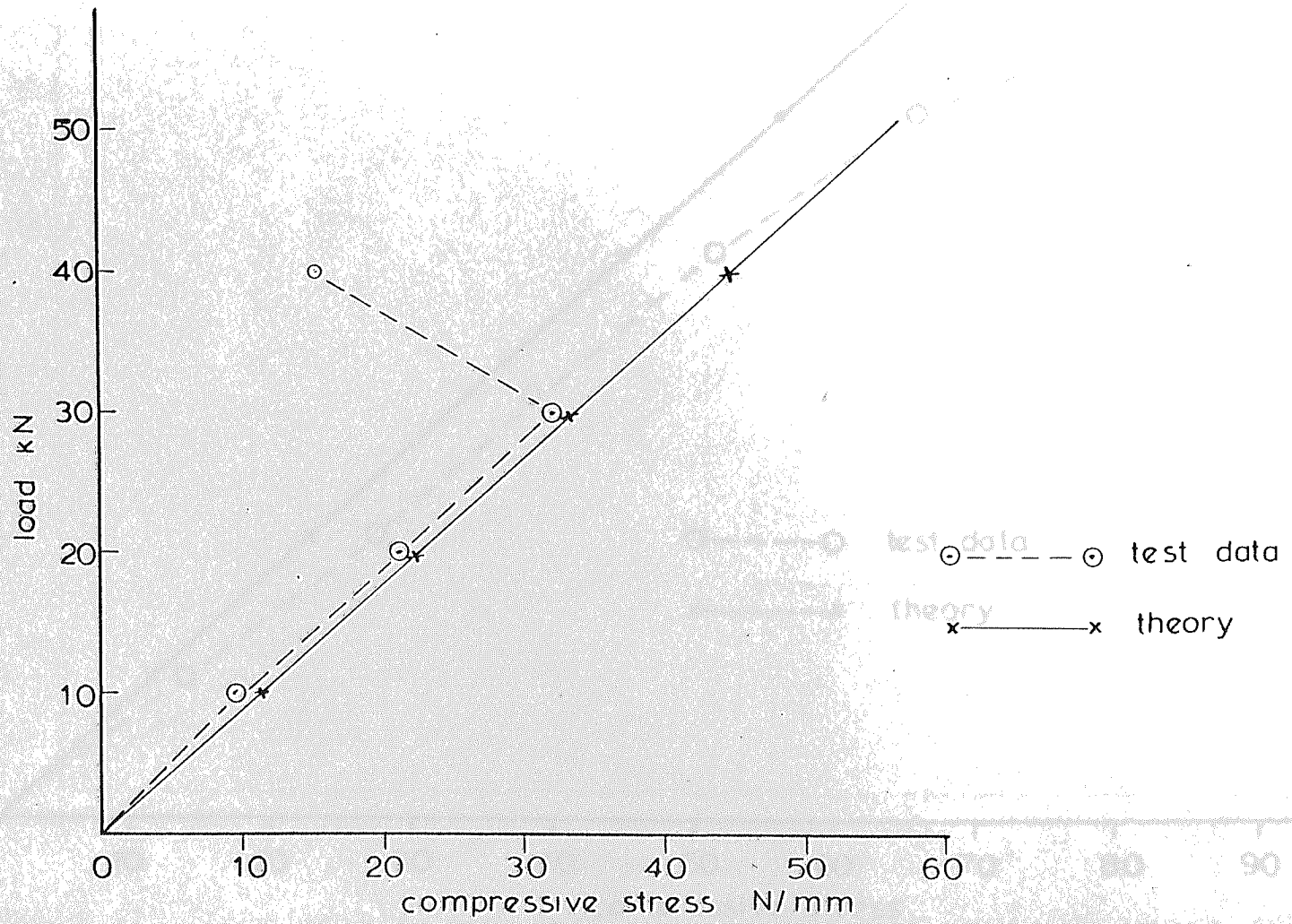

Fig. 2.15 Experimental and theoretical plots of load versus mid span stress at compression flange . pilot beam Bp

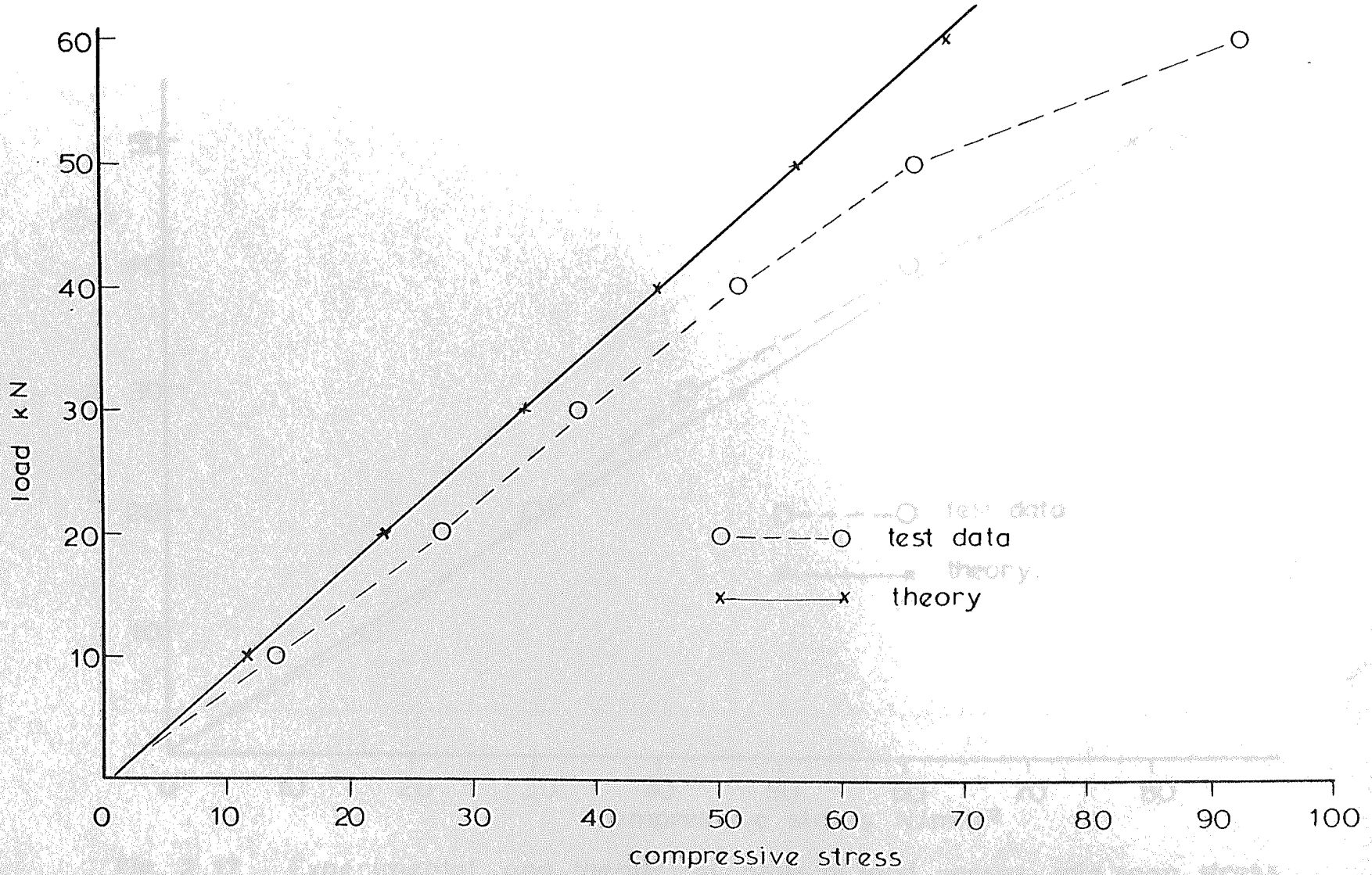

Fig. 2.16. Experimental and theoretical plots of load versus mid-span stress at compression flange. beam type B1.

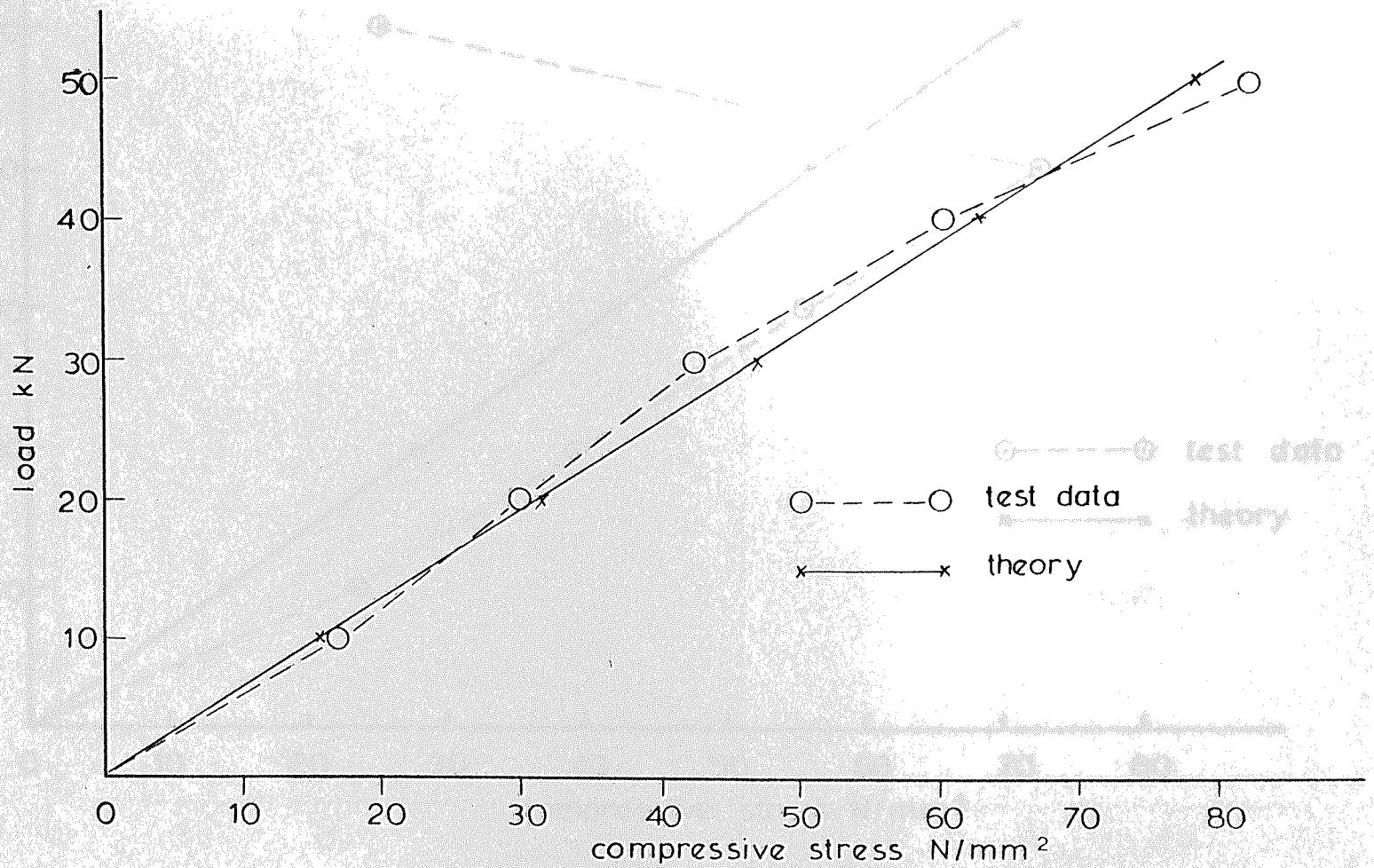

Fig. 2.17. Experimental and theoretical plots of load versus mid span stress at compression flange . beam type B2

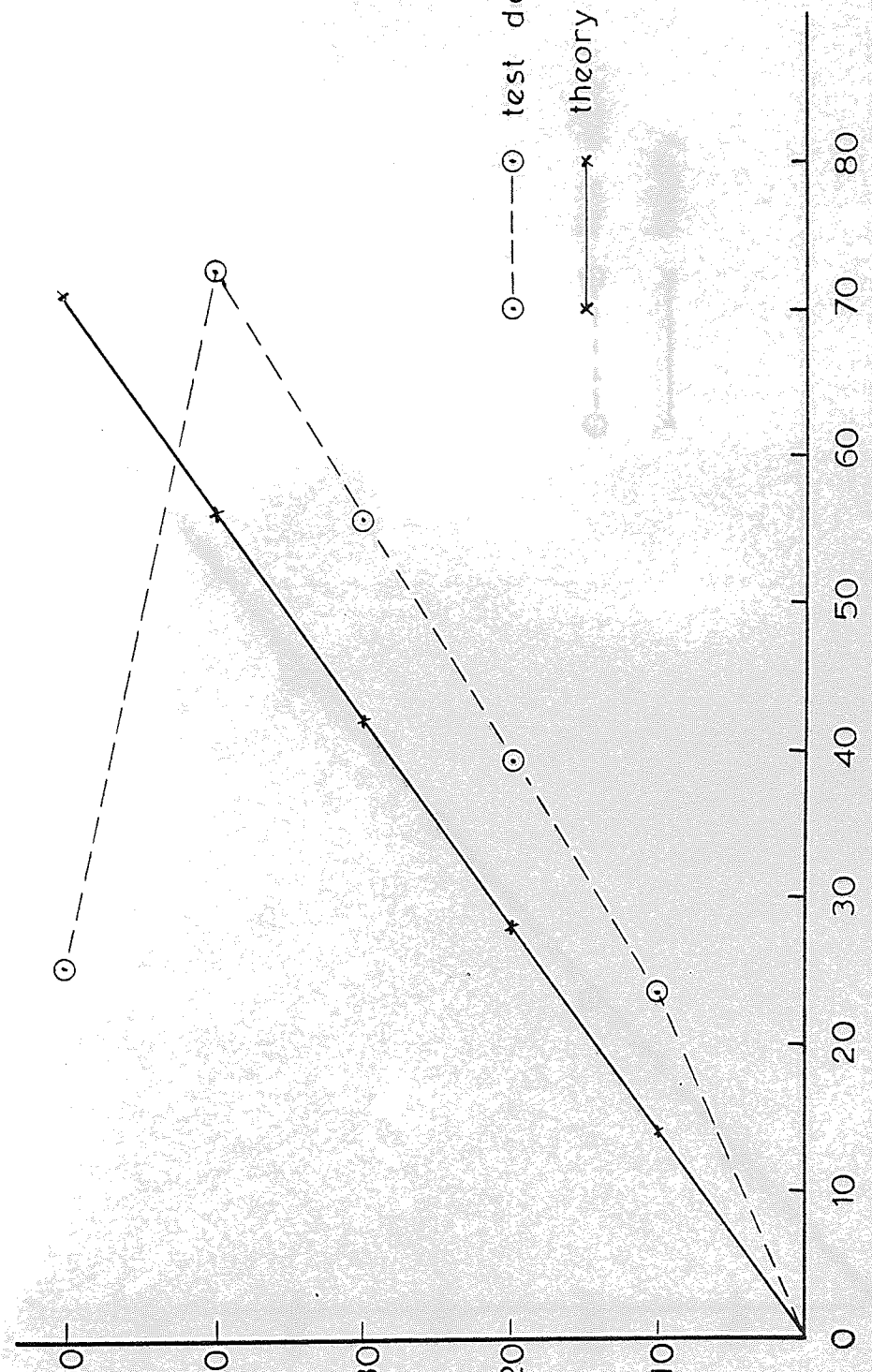

Fig. 2.18 Experimental and theoretical plots of load versus mid span stress at compression flange. beam B3

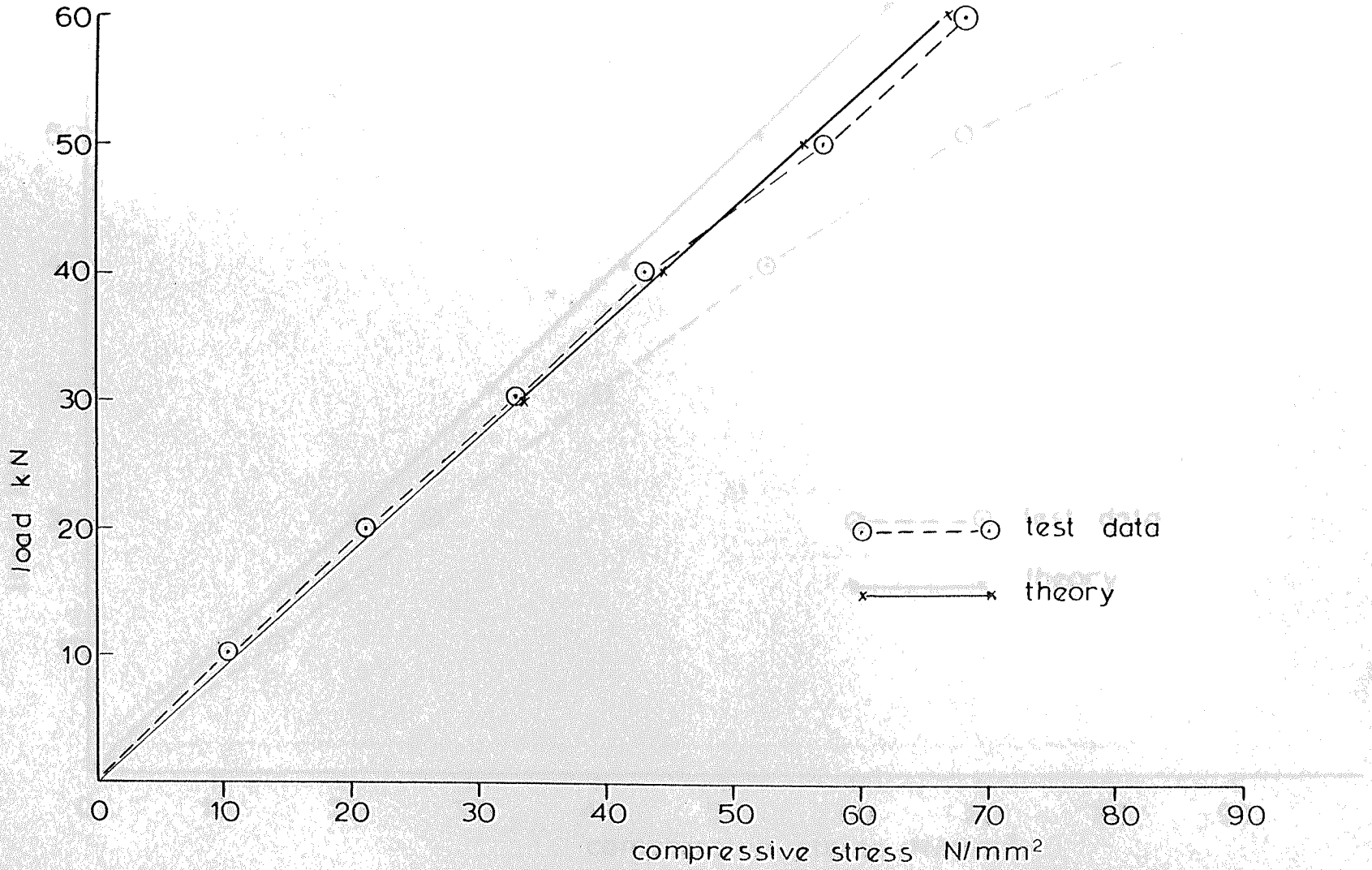

Fig. 2.19 Experimental and theoretical plots of load versus mid-span stress at compression flange . beam type B4

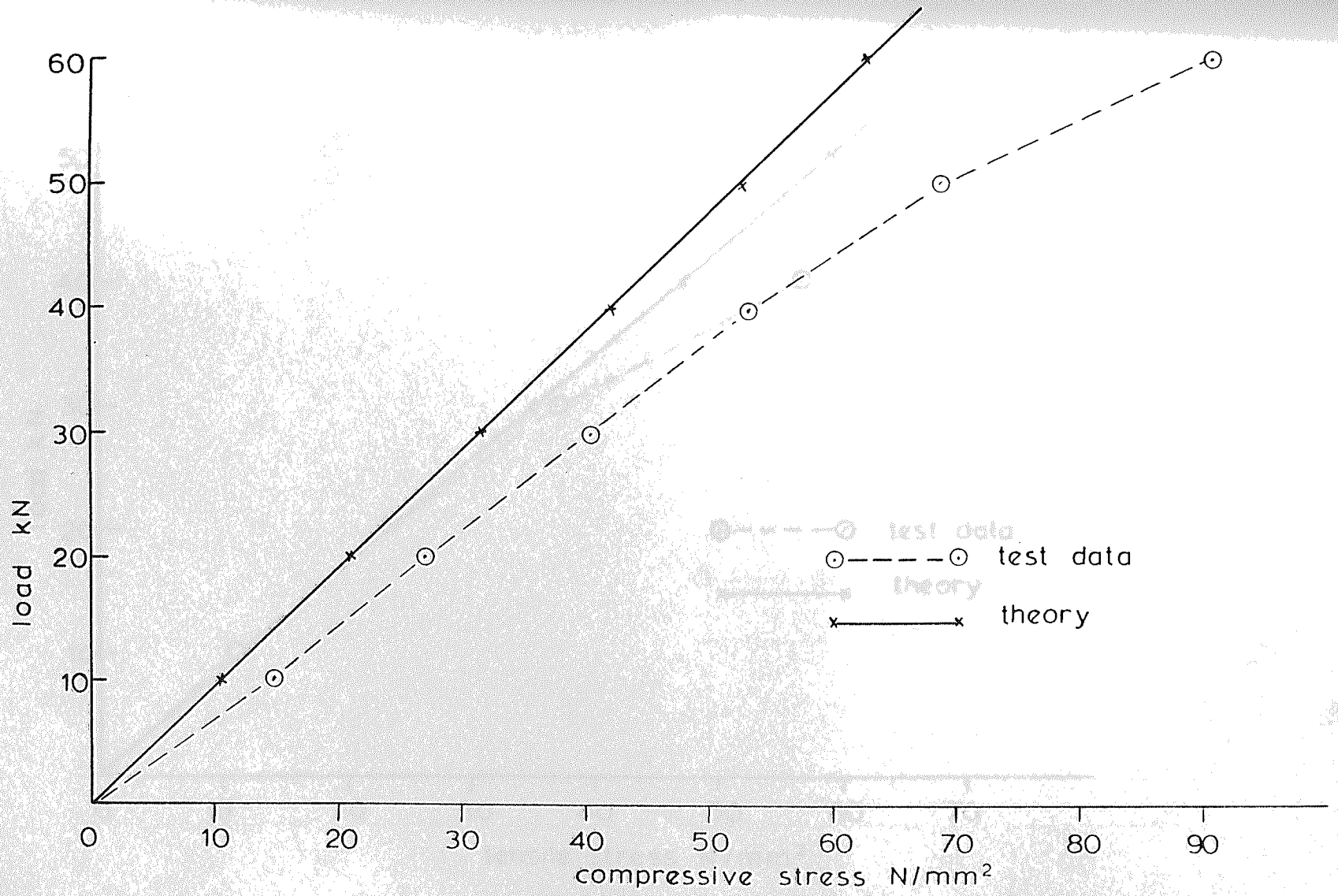

Fig.2.20. Experimental and theoretical plots of load versus mid span stress at compression flange. beam type B5.

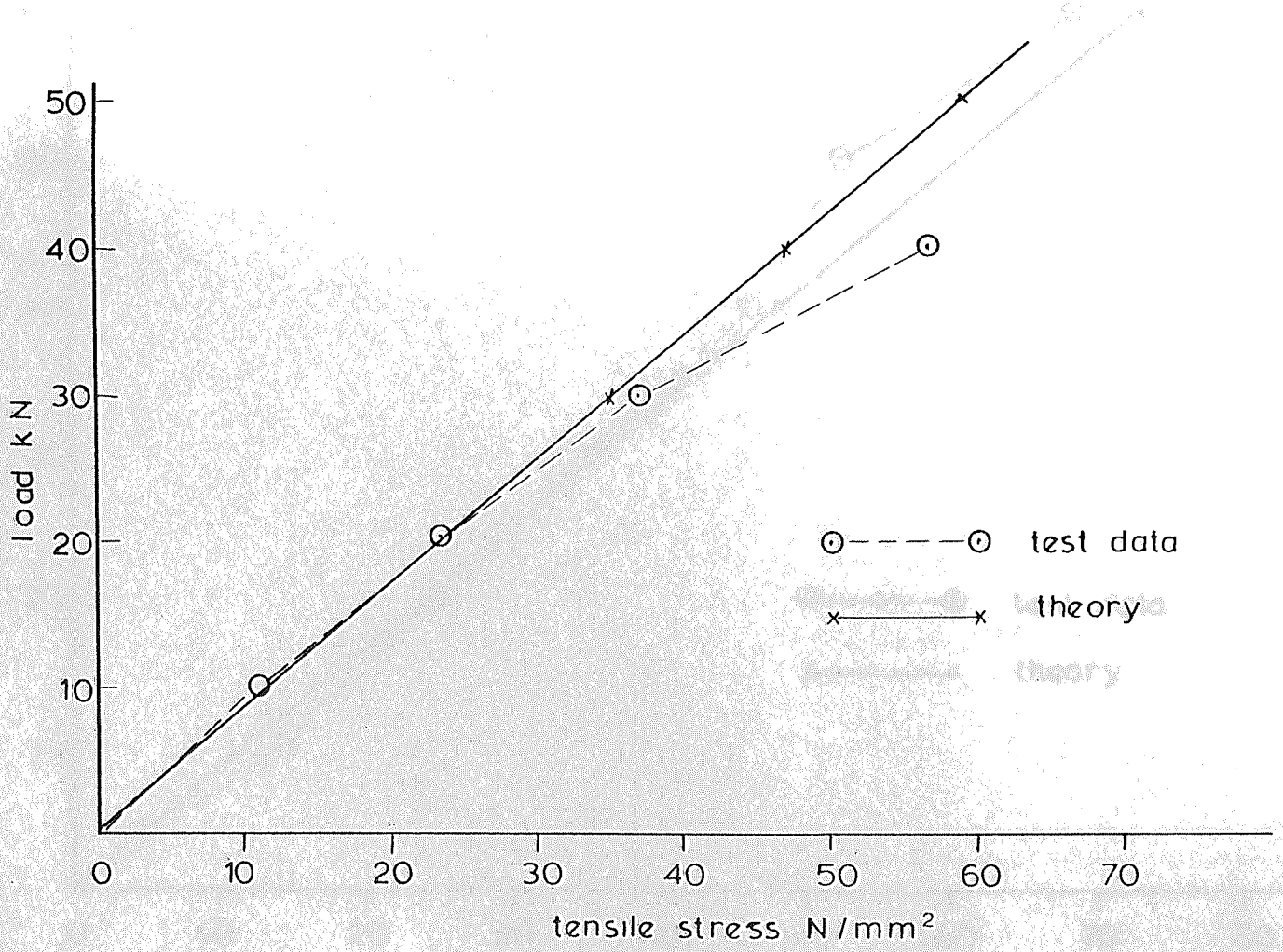

Fig. 2.21 Experimental and theoretical plots of load versus mid span stress at tension flange. pilot beam Bp

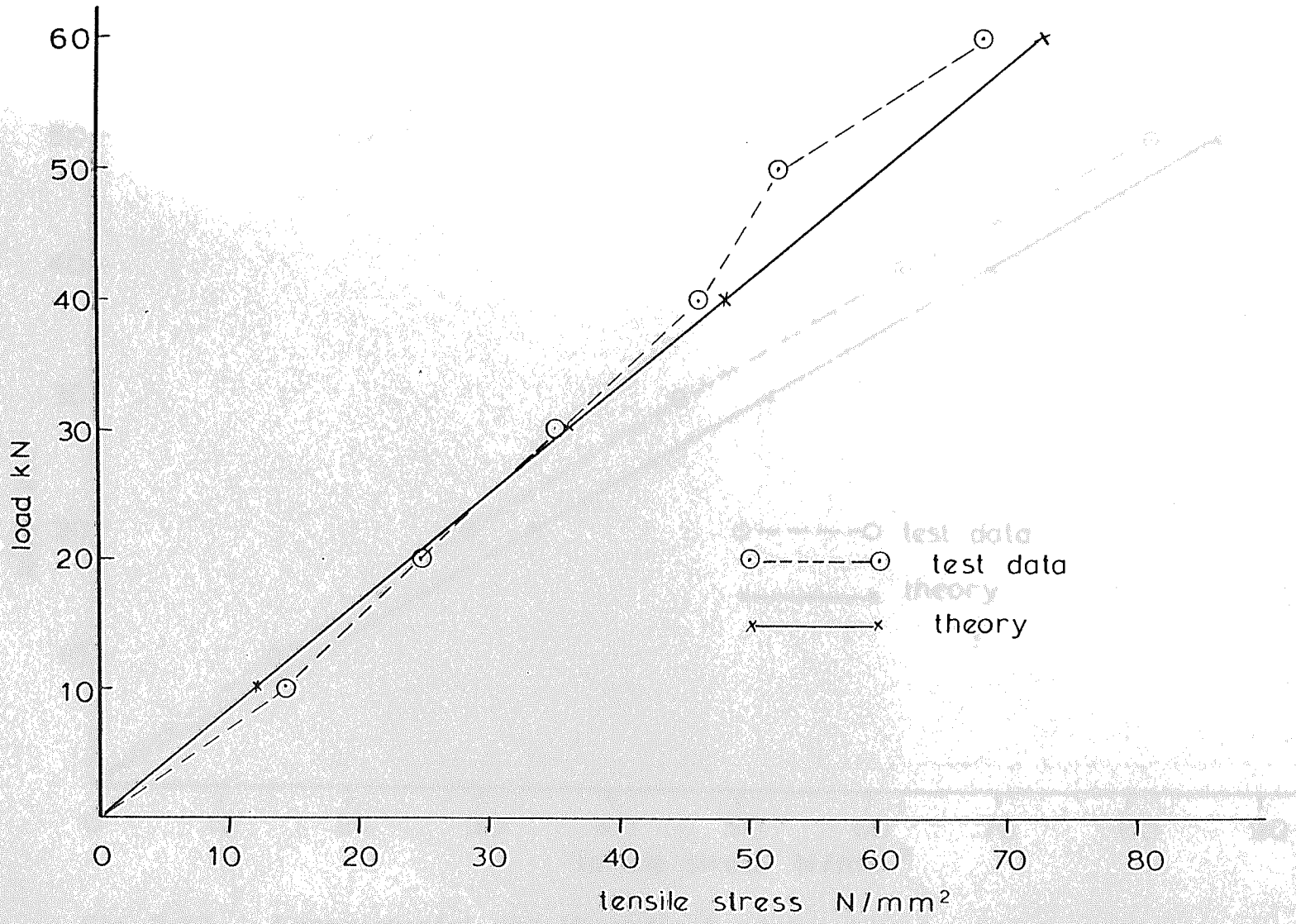

Fig. 2.22 Experimental and theoretical plots of load versus mid-span stress at tension flange . beam type BI

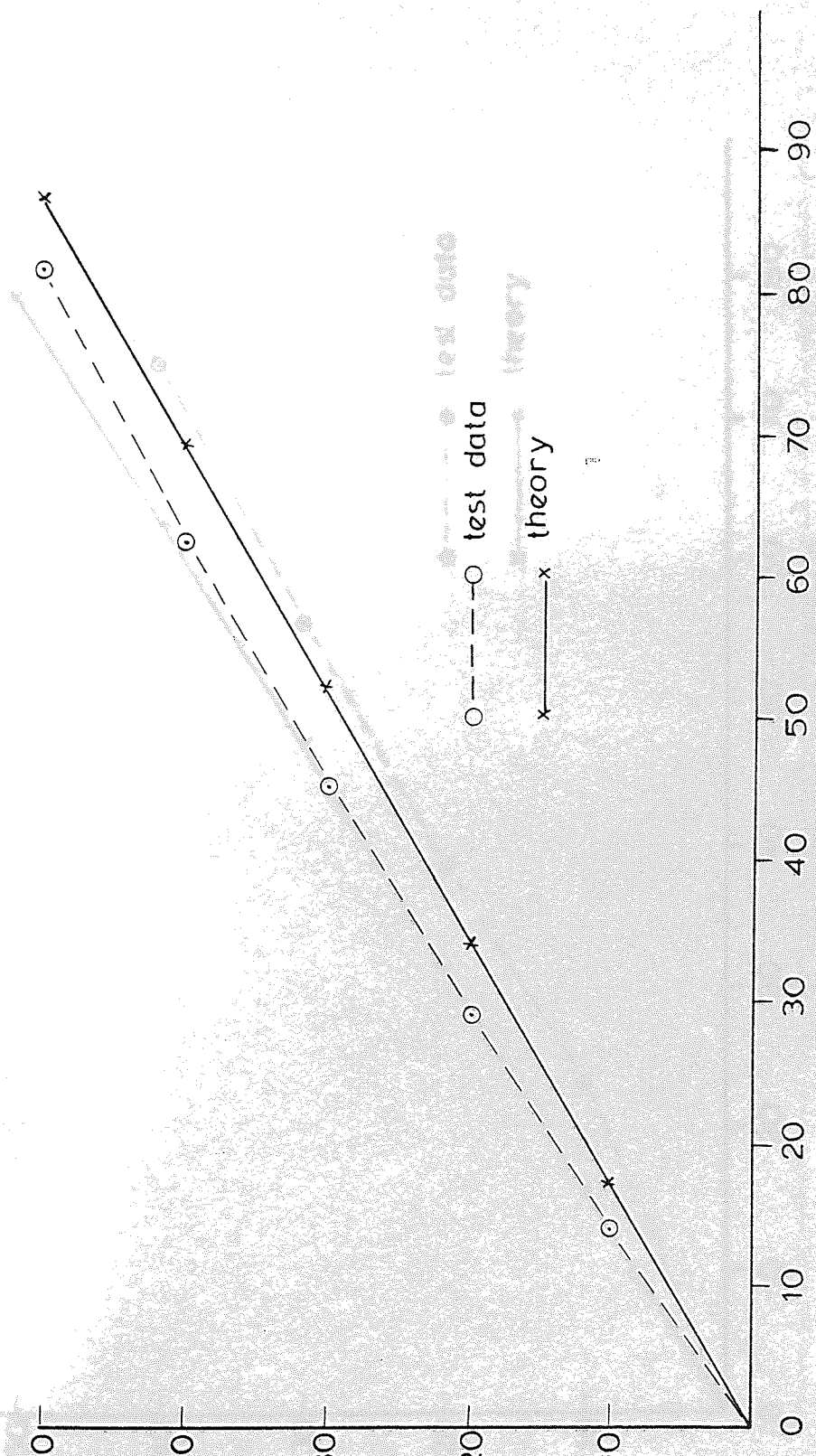

Fig. 2.23. Experimental and theoretical plots of load versus mid span stress at tension flanges. beam type B2

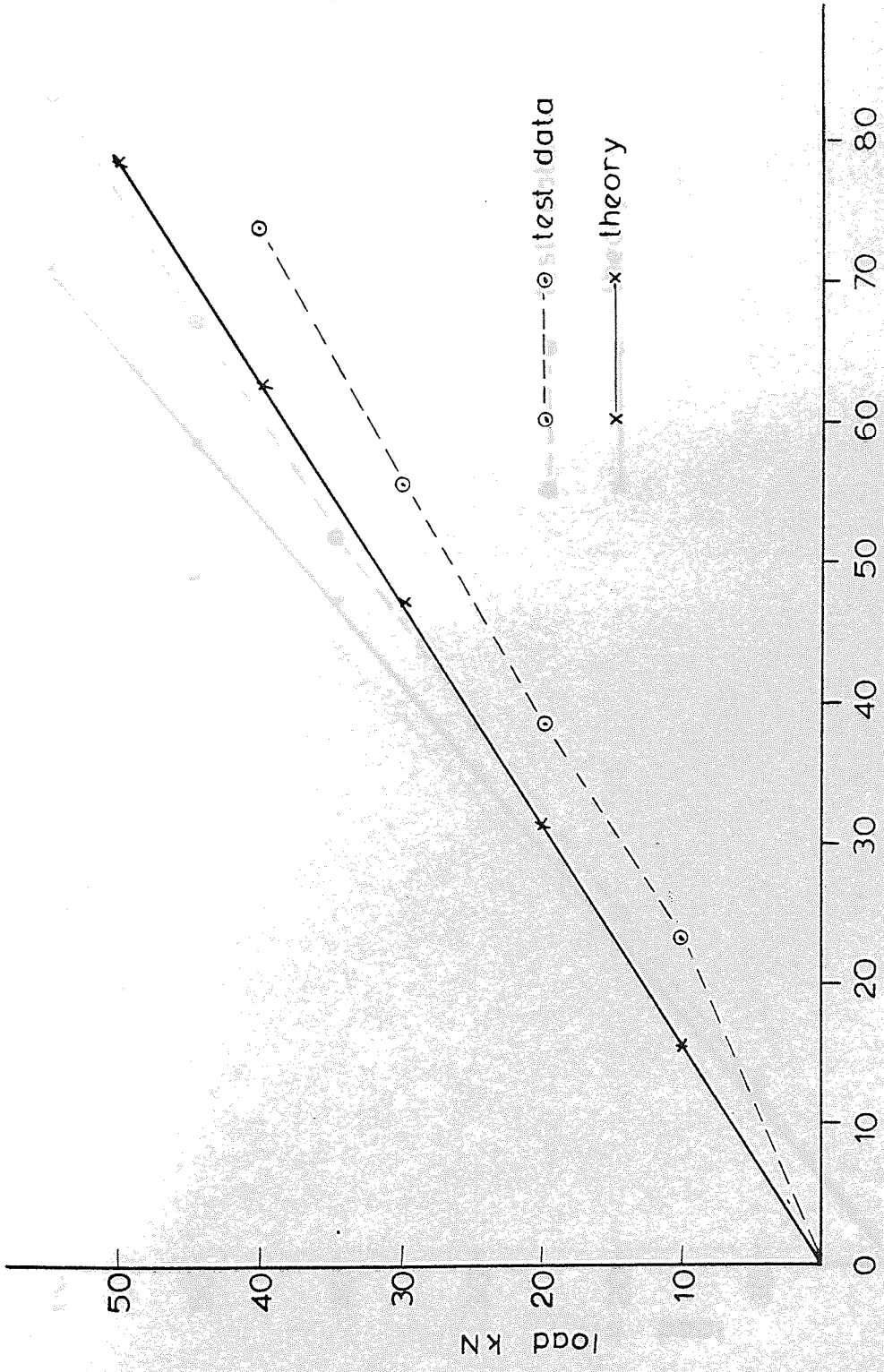

Fig. 2.24. Experimental and theoretical plots of load versus mid span stress at tension flange. beam type B3

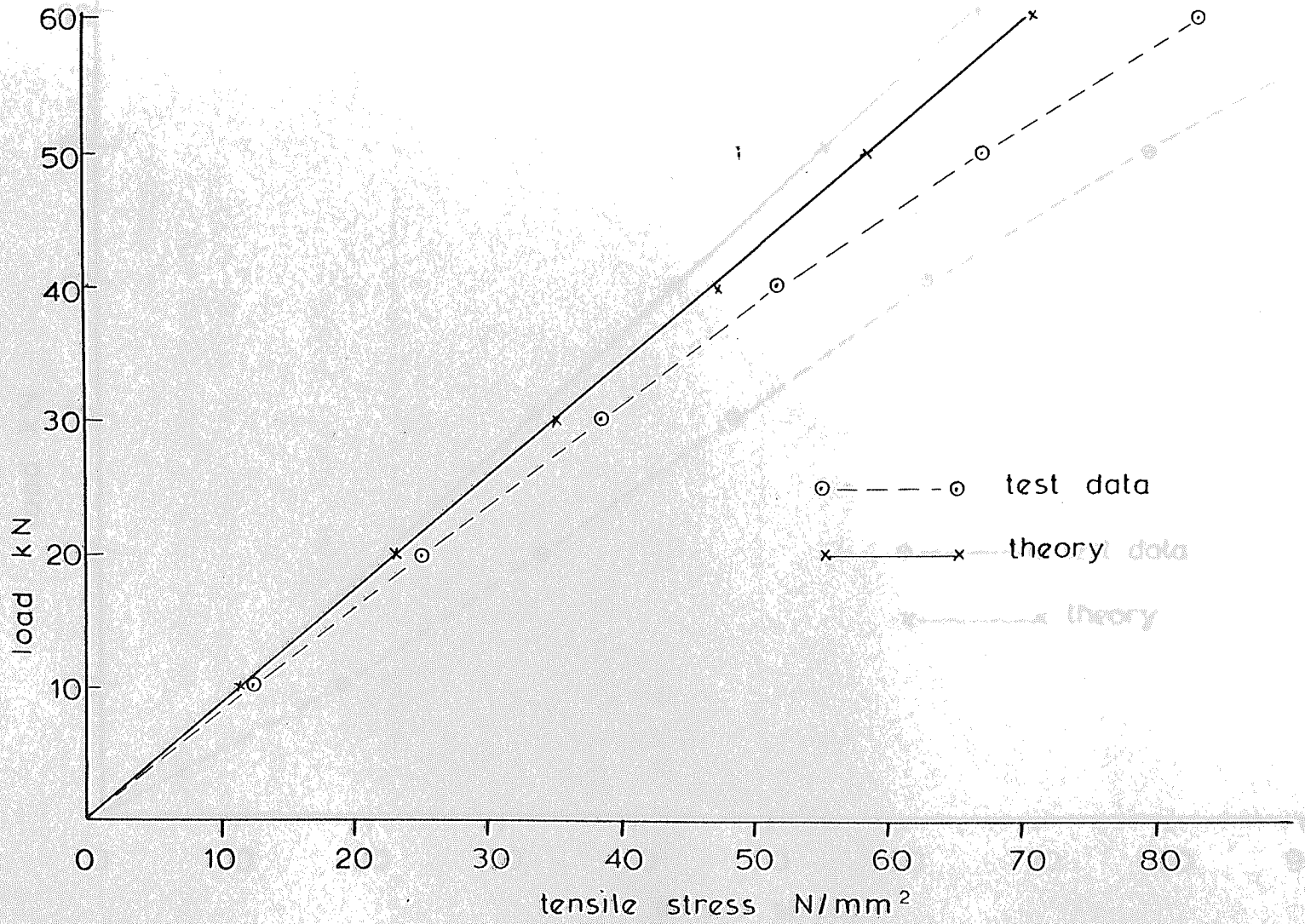

Fig. 2.25 Experimental and theoretical plots of load versus mid span stress at tension flange. beam type B4

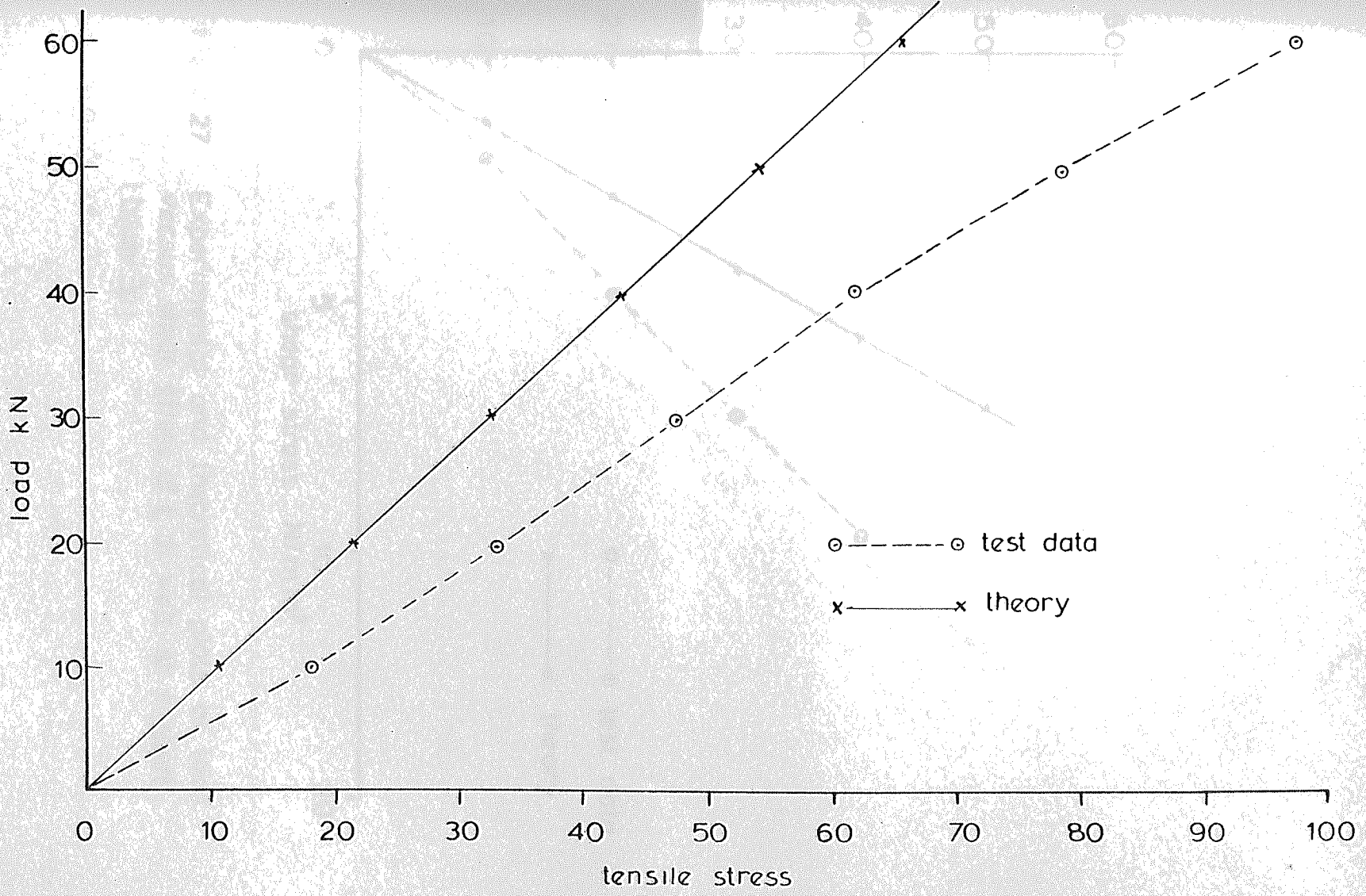

Fig. 2.26 Experimental and theoretical plots of load versus mid span stress at tension flange. beam type B5

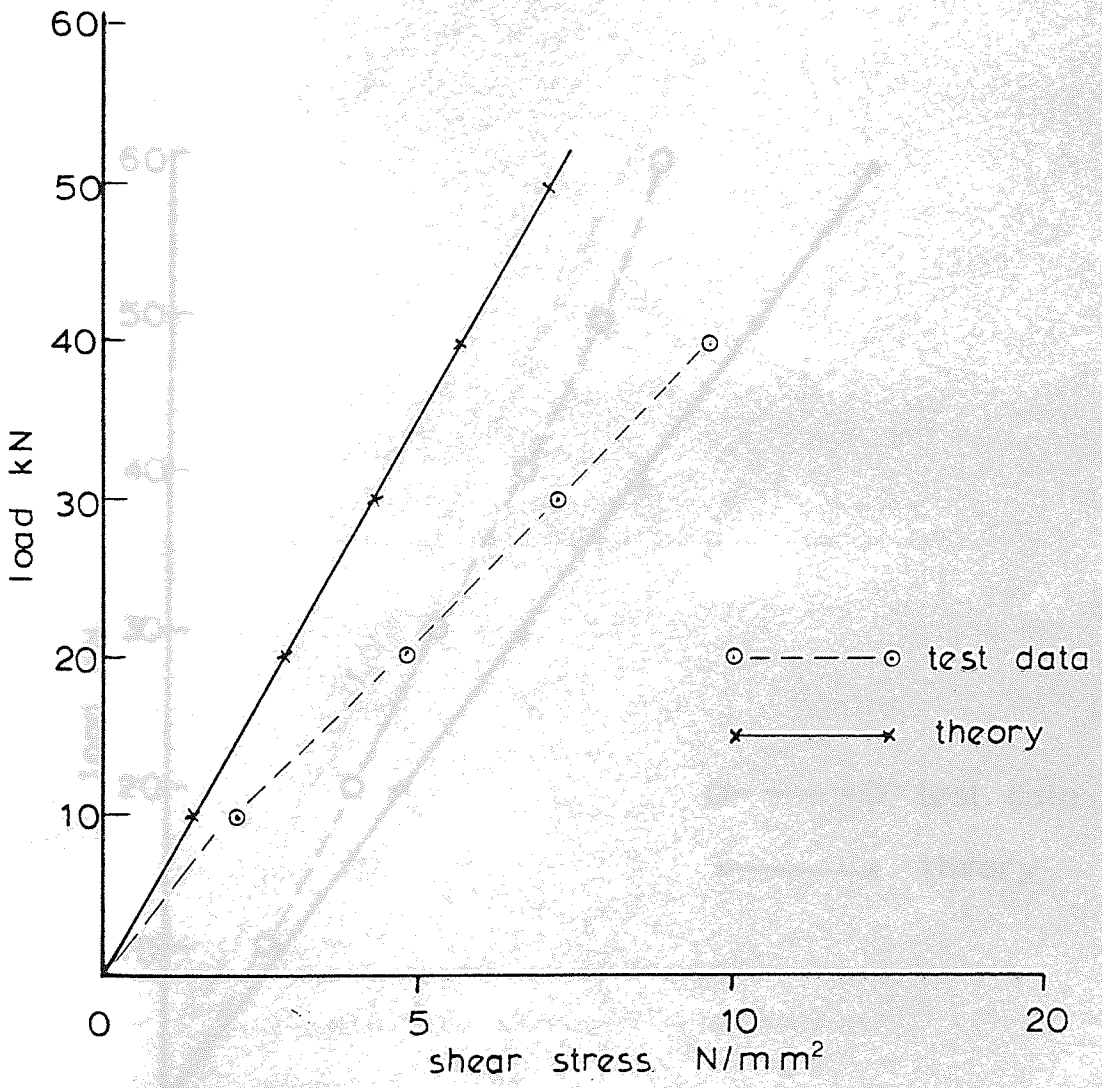

Fig. 2.27 Experimental and theoretical plots of load versus shear stress at ℄ of web at support (beam 3p)

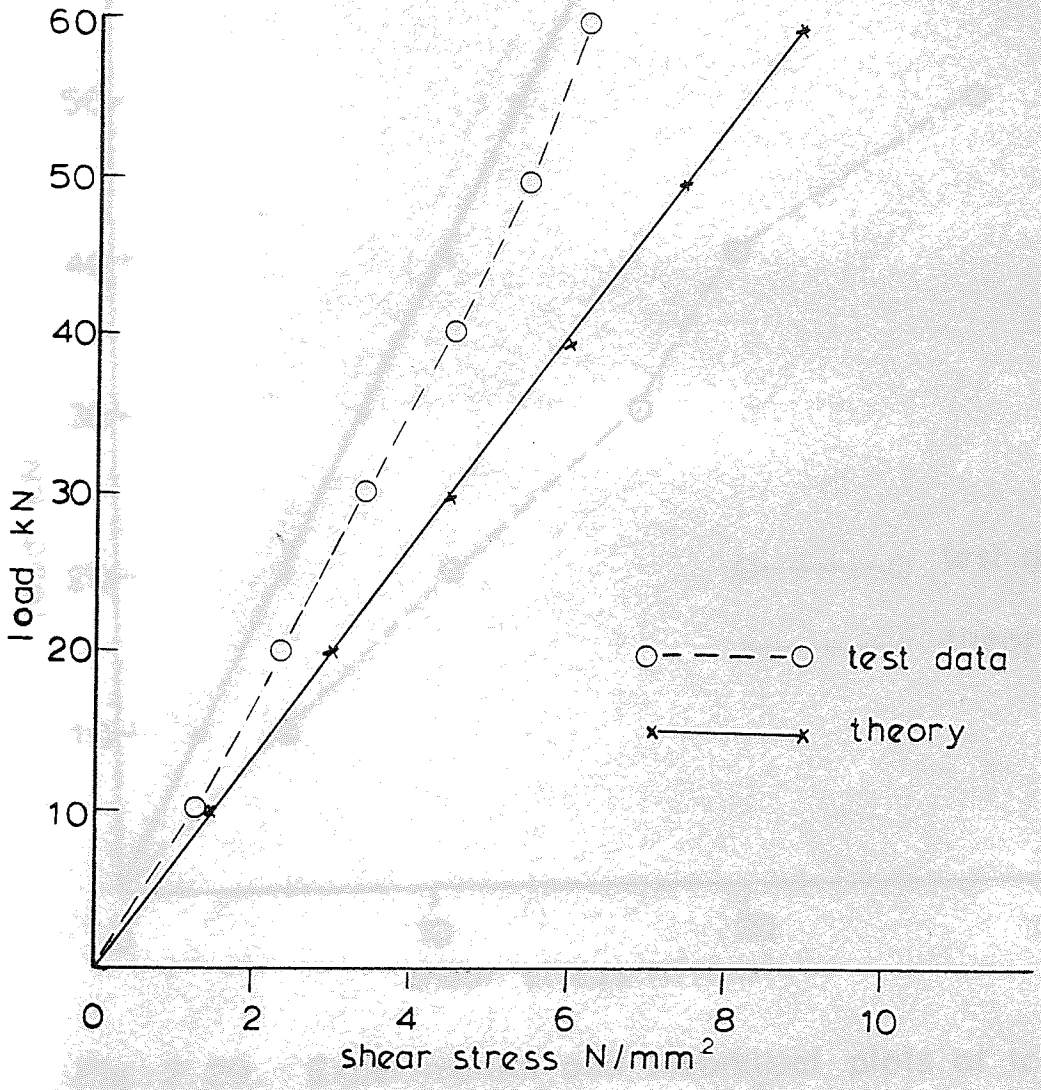

Fig. 2.28 Experimental and theoretical plots of load versus shear stress at ℄ of web at support (beam 1)

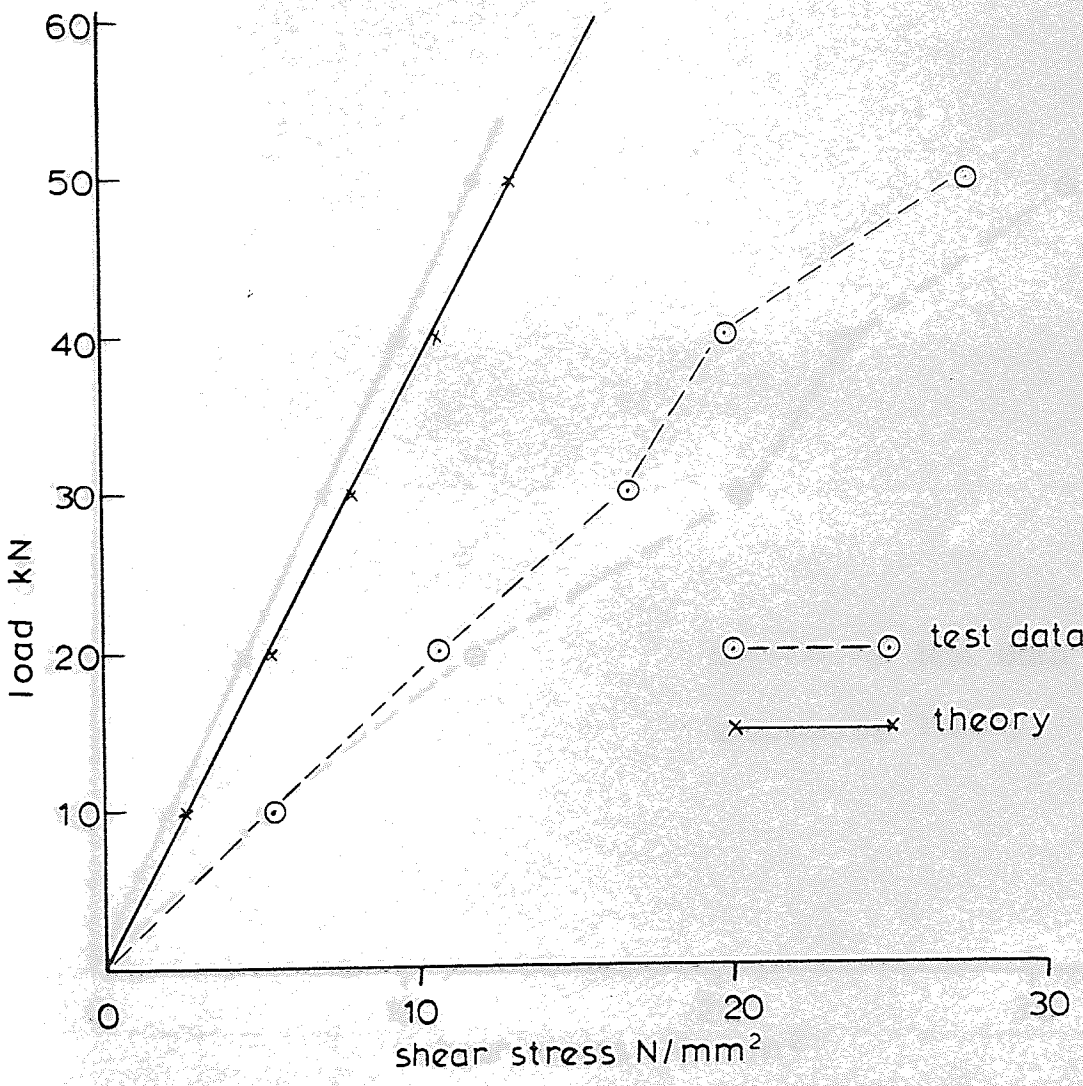

Fig. 2.29. Experimental and theoretical plots of load versus shear stress at ℄ of web at support (beam 2)

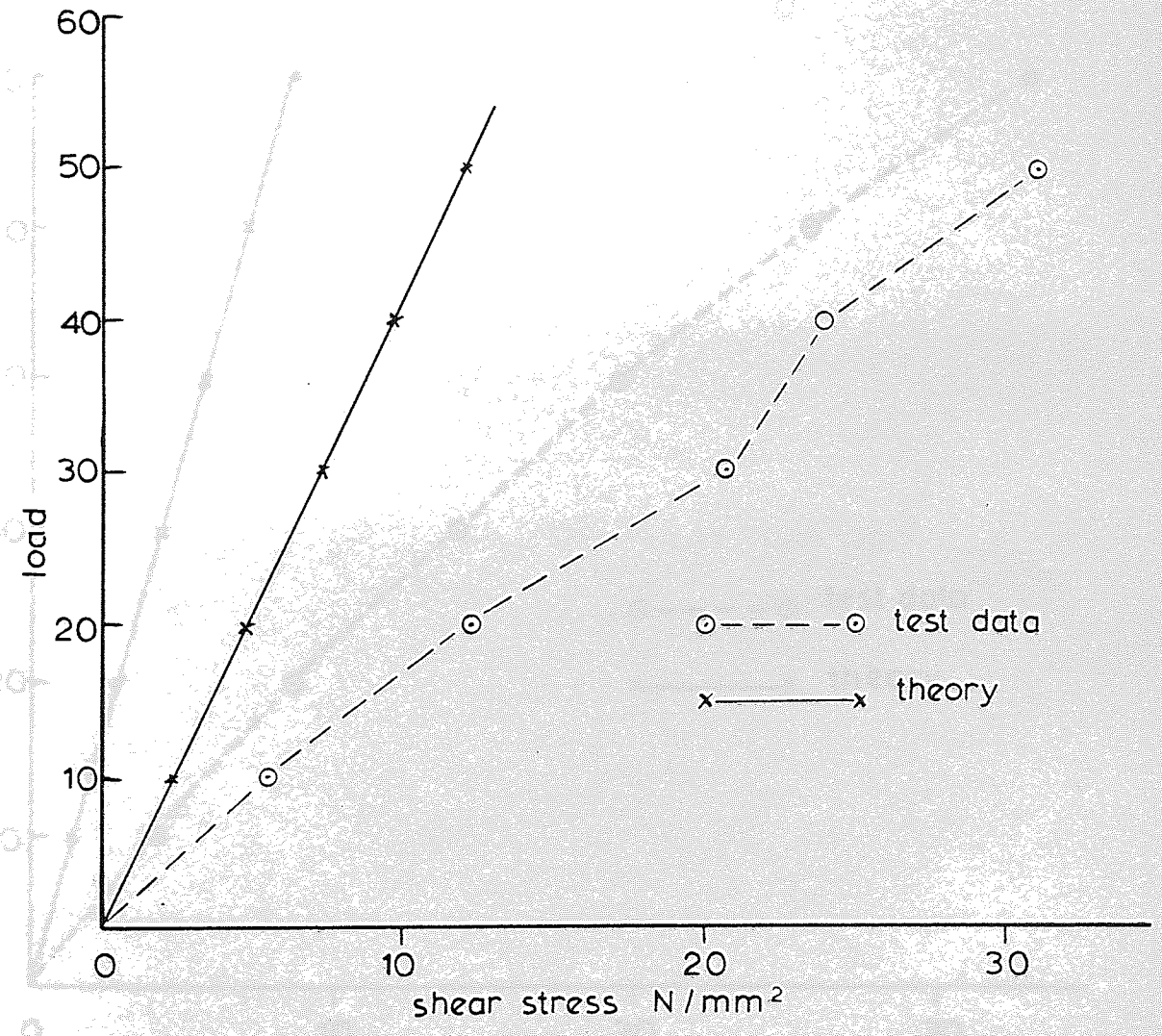

Fig. 2.30. Experimental and theoretical plots of load versus shear stress at ℄ of web at support (beam type B3)

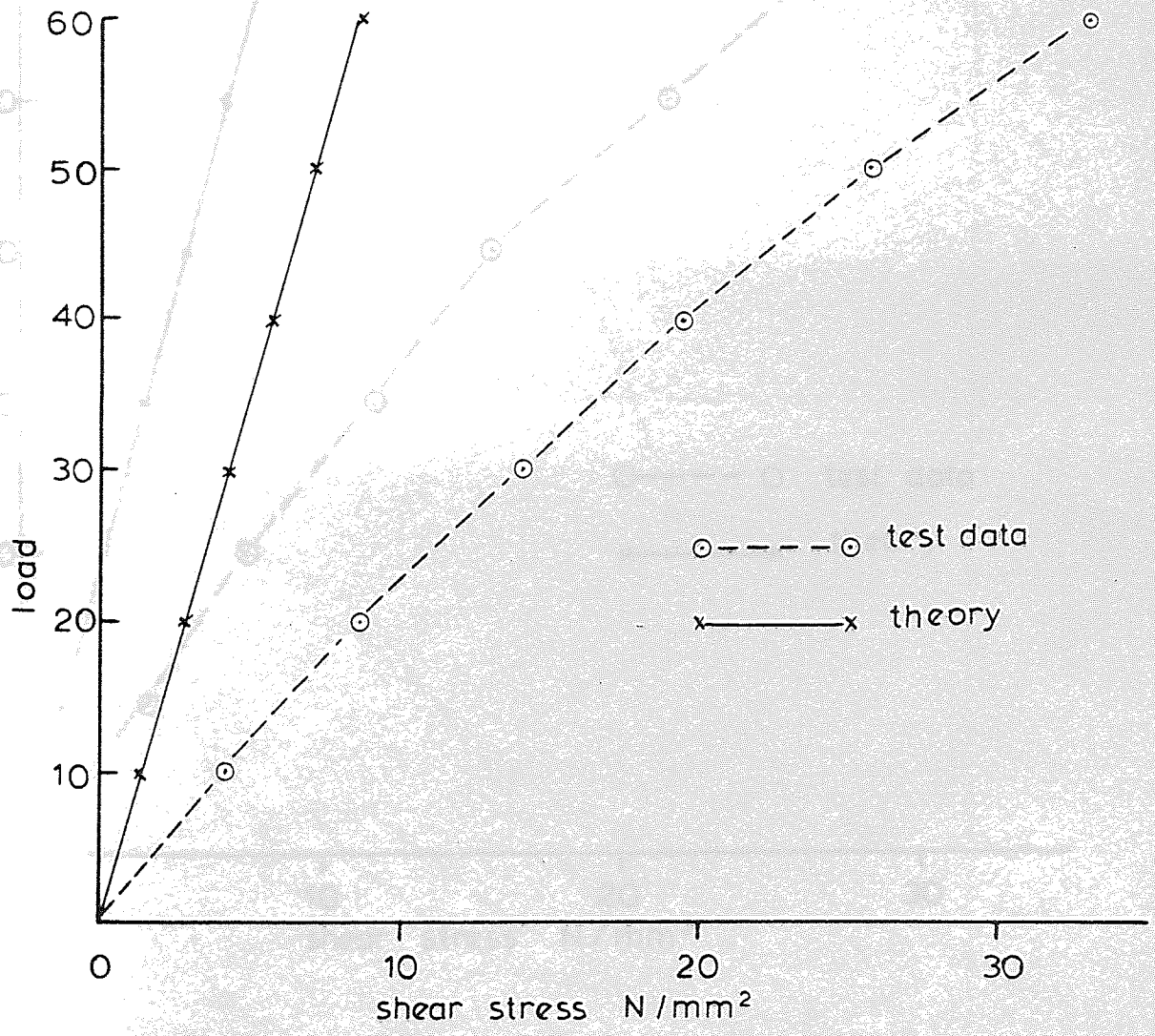

Fig. 2.31. Experimental and theoretical plots of load versus shear stress at ℄ of web at support (beam type B4)

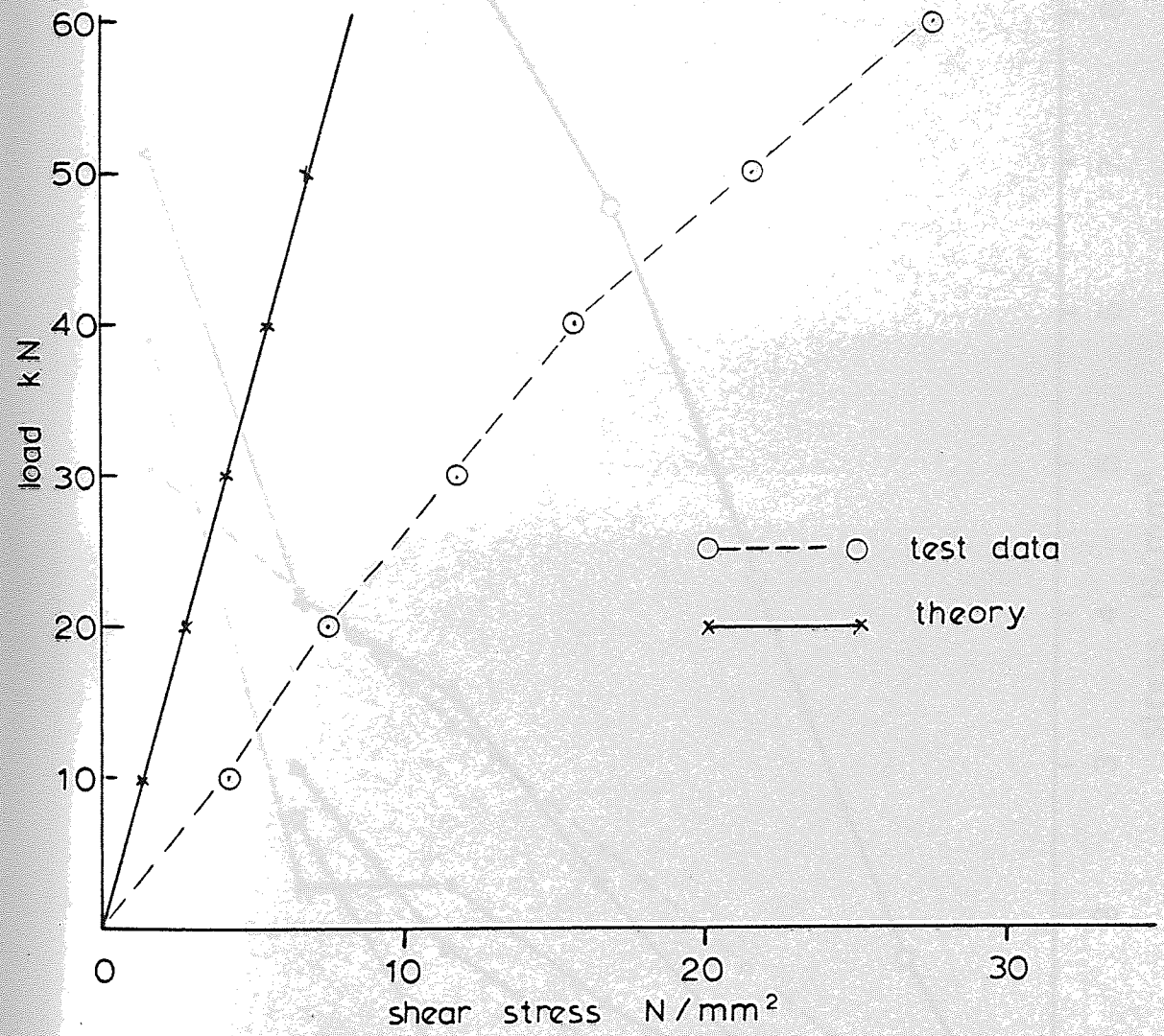

Fig. 2.32 Experimental and theoretical plots of load versus shear stress at ℄ of web at support (beam type B5)

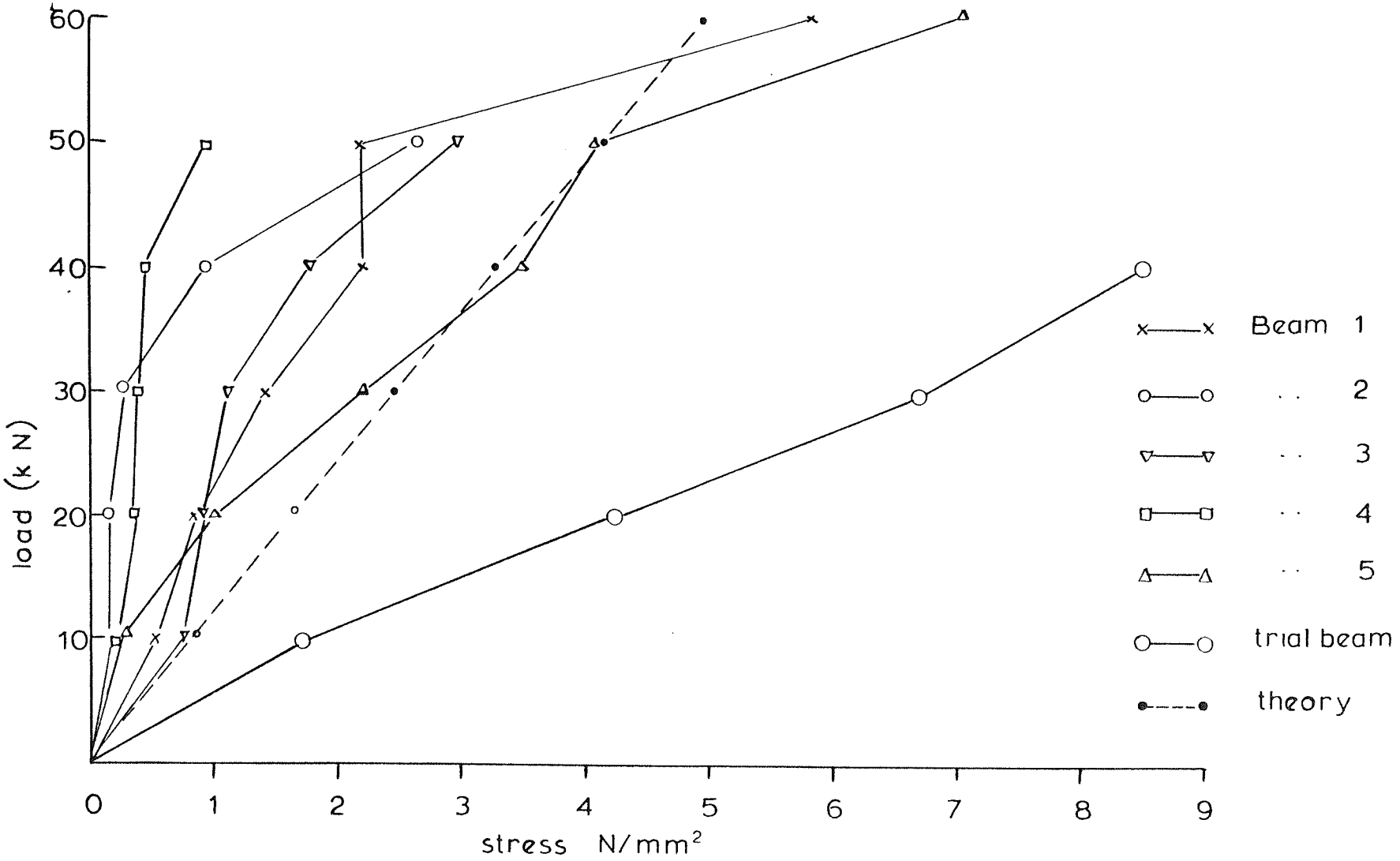

Fig. 2.33 Typical load versus stress in diaphragm for beams B1 - B5 BT

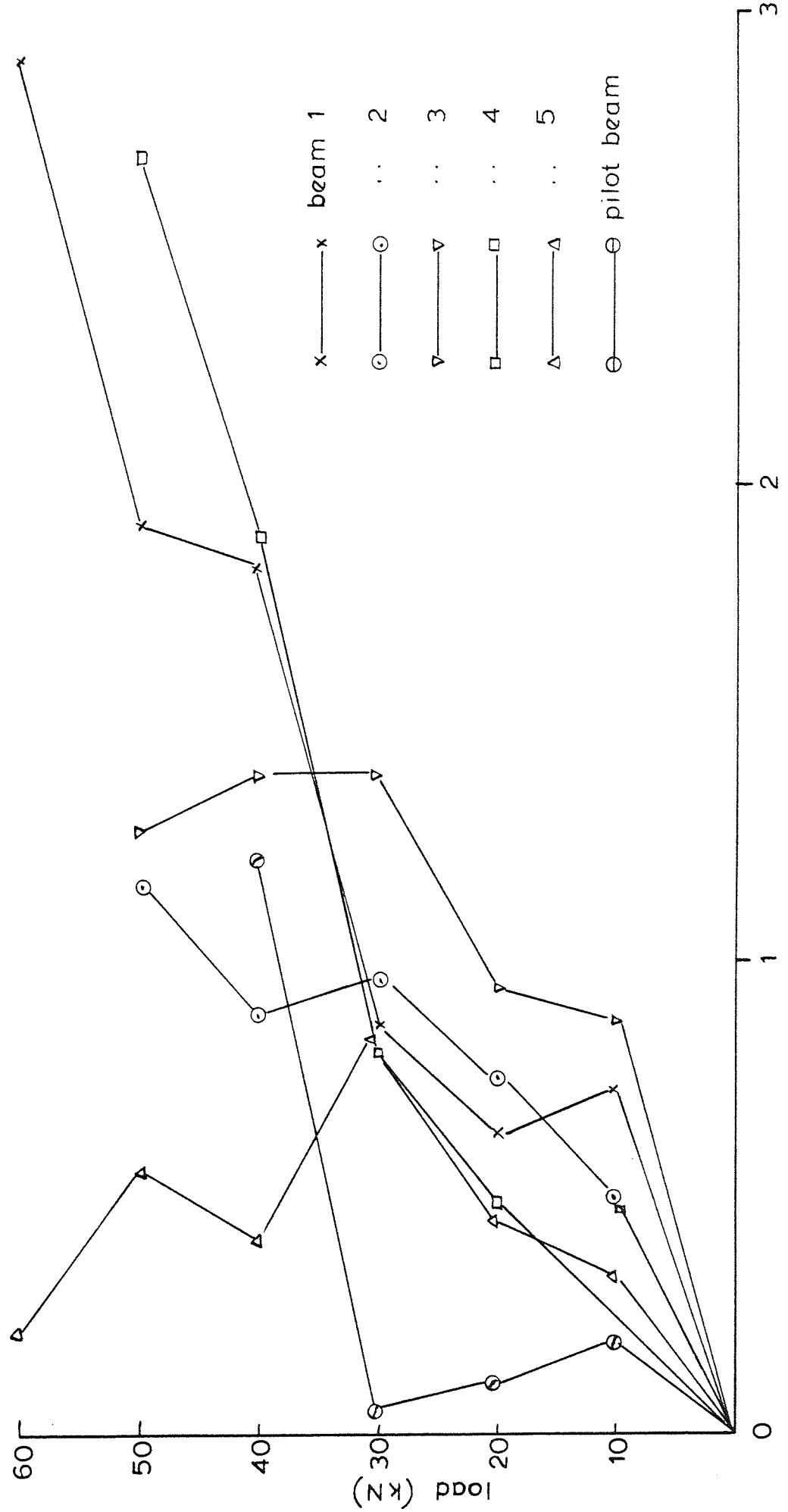

Fig. 2.34. Load versus lateral buckling for beams B1 - B5 Bp

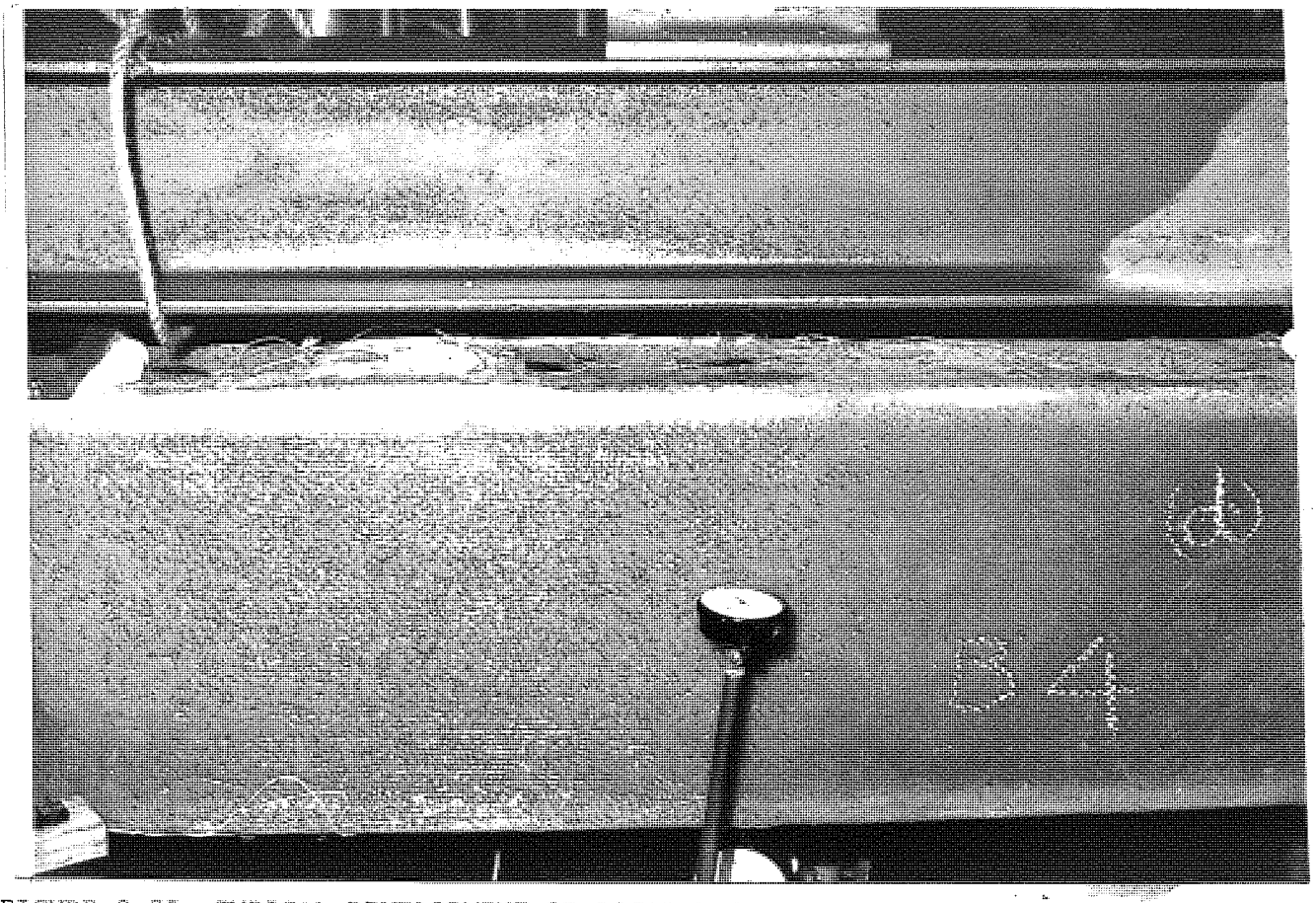

FIGURE 2.35 TYPICAL DEVELOPMENT OF LOCAL BUCKLING IN COMPRESSION FLANGE DURING LOADING

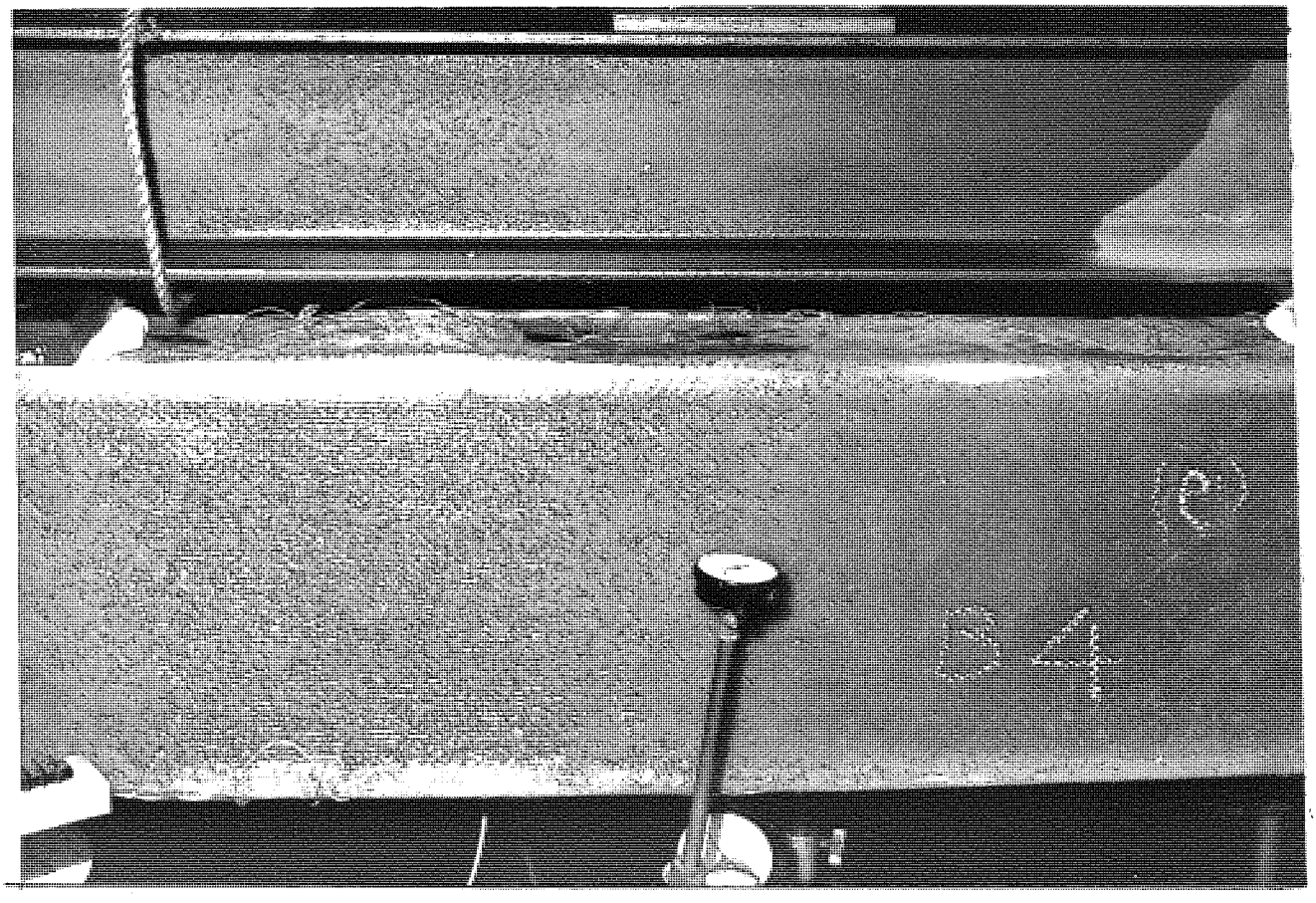

FIGURE 2.36 LOCAL BUCKLING IN COMPRESSION FLANGE IN PROGRESS

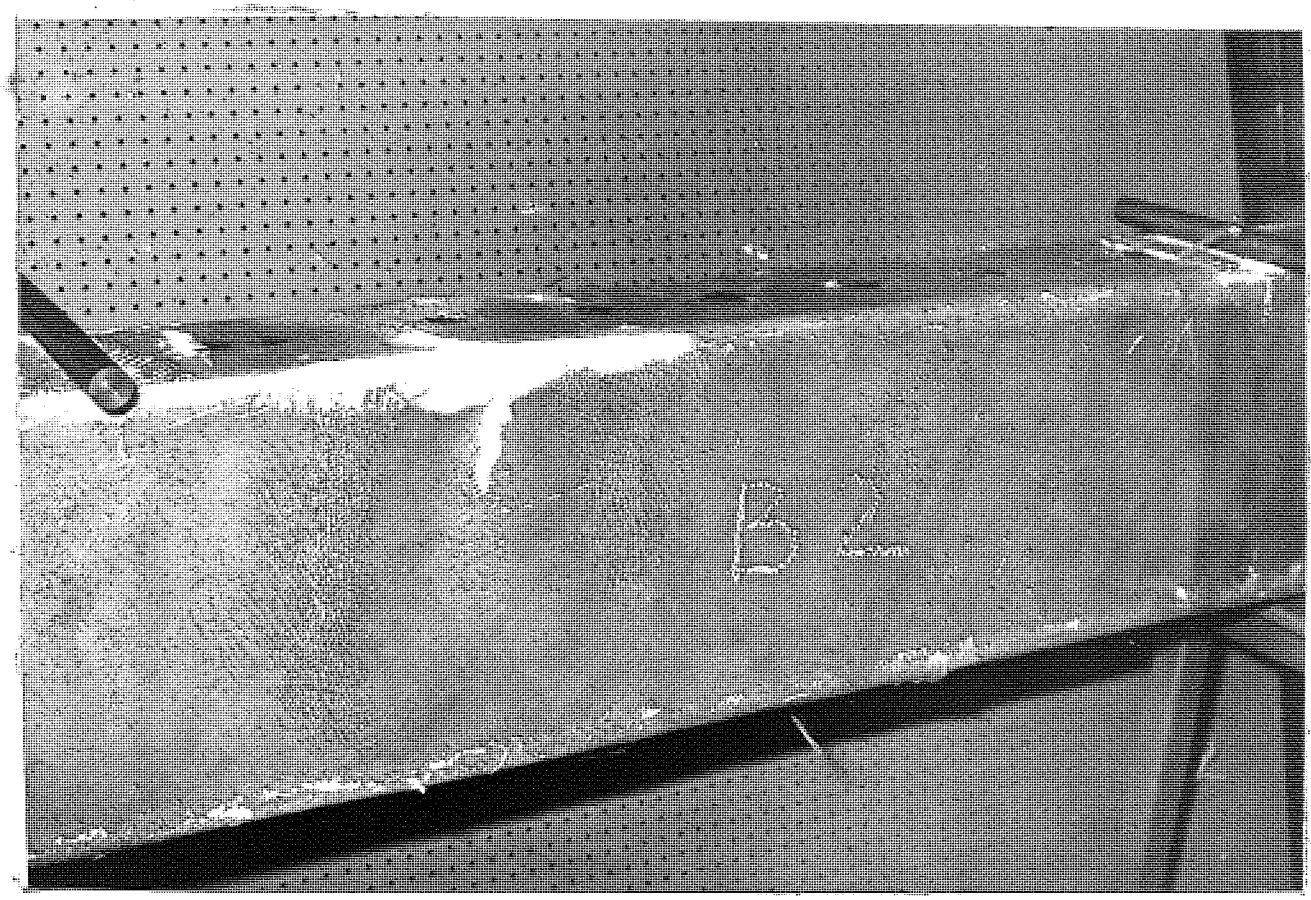

FIGURE 2.37 MODE OF FAILURE BEAM TYPE B2

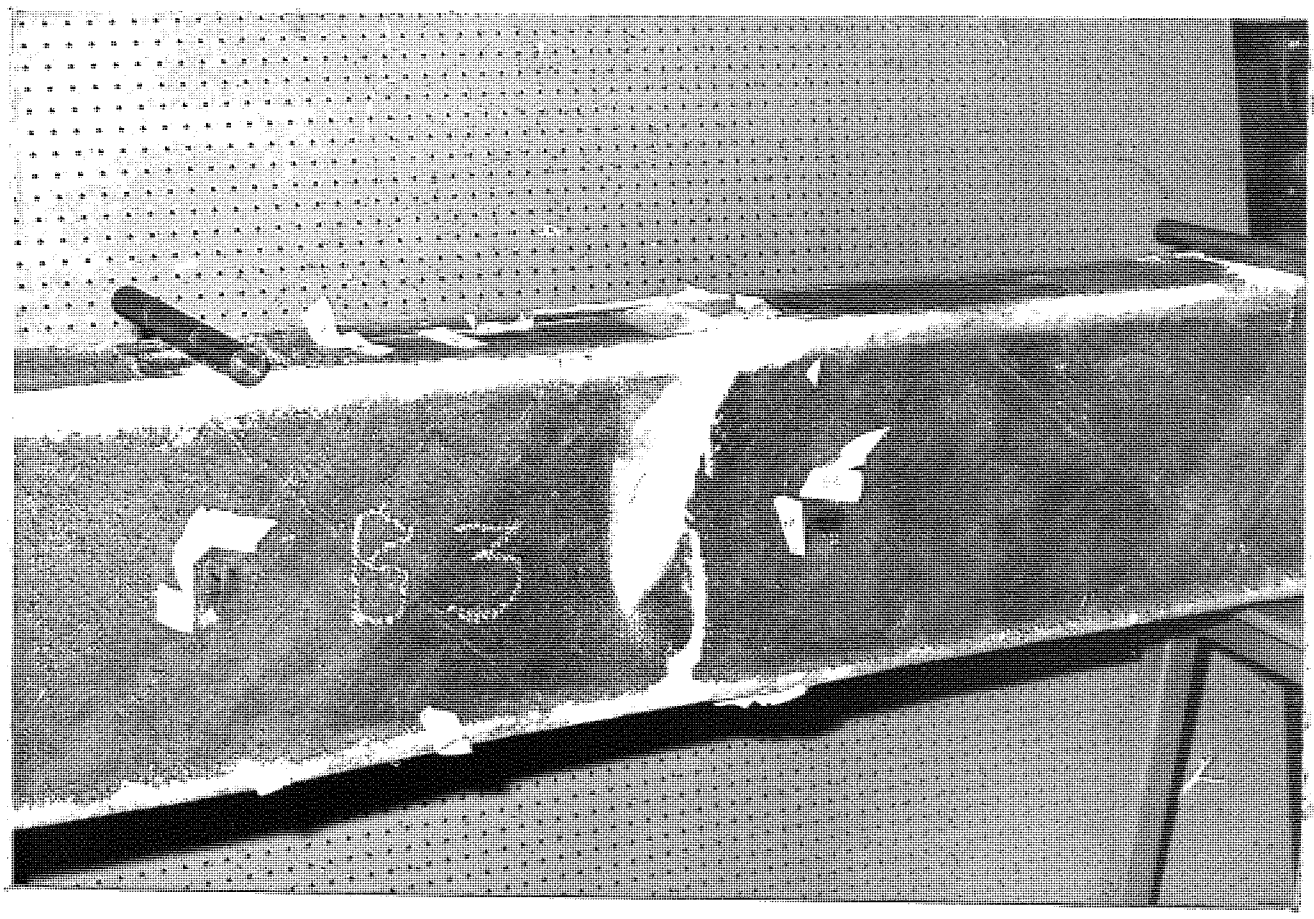

FIGURE 2.38 MODE OF FAILURE BEAM TYPE B3

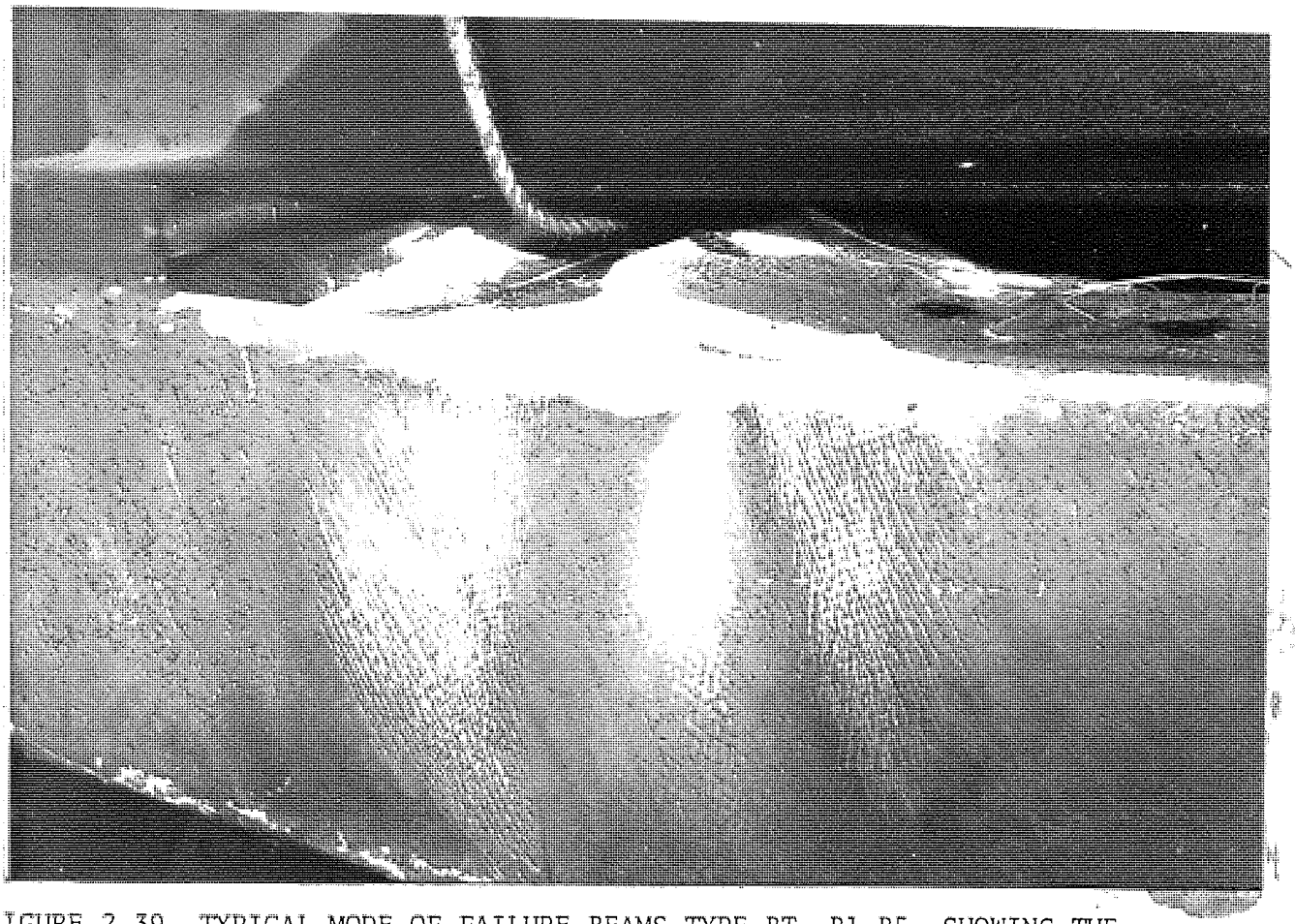

FIGURE 2.39 TYPICAL MODE OF FAILURE BEAMS TYPE BT, B1-B5, SHOWING THE EXHAUSTION OF MATERIAL IN THE WEBS AROUND THE COMPRESSION FLANGE FAILURE REGION

REFERENCES

2.1 "Developments in Bridge Design and Construction" Crosby Lockwood and Son Ltd., London 1971.

2.2 CHAPMAN J C, DOWLING, P J, LIM P T L and BILLINGTON C J, "The Structural Behaviour of Steel and Concrete Box Girder Bridges". The Structural Engineer, March 1971, pp 111-120, January 1972, pp 21-28.

2.3 CHU, K H and PINJAR, S G, "Analysis of Horizontally Curved Box Girder Bridges". Proceedings of the ASCE Vol 97, No ST 10, October 1971, pp 2481-2501.

2.4 DAS, D C, "Analysis of Box-type Structures". Proceedings of the Institution of Civil Engineers, Part 2, June 1972 pp 19-40, December 1972, pp 629-30.

2.5 KRISTEK, V, Box Girders of Deformable Cross-sections" Proceedings of the Institution of Civil Engineers, October 1970 pp 239-253.

2.6 LEE, D J, The Selection of Box Beam Arrangements in Bridge Design "Developments in Bridge Design and Construction". Crosby Lockwood and Son Ltd, 1971, pp 400-426.

2.7 ROTHWELL, A, "Optimum Fibre Orientation Plastics and Polymers" Fibre Science Technology, Vol 2, 1969.

2.8 ALKHAYAT, Q C, "Structural Properties of Glass Reinforced Plastic", PhD Thesis, 1974, The University of Aston in Birmingham.

2.9 RICHARD, D M, "Optimum Design of Fibre Reinforced Corrugated Compression Panels". College of Aeronautics Report, Aero 20, 1969.

2.10 VLASOV, V Z, "Thin Walled Elastic Beams", National Science Foundation, 1961.

2.11 K ZBIROHOWSKI-KOSCIA, "Thin Walled Beams", Crobsy Lockwood.

2.12 EVANS, H R and ROCKEY, K C, "A Folded Plate Approach to the Analysis of Box Girders". Developments in Bridge Design and Construction, Crosby Lockwood and Son Ltd., London 1971, pp 246-263.

2.13 CRISFIELD M A, "Finite Element Methods for the Analysis of Multicellular Structures." Proceedings of the Institute of Civil Engineers, March 1971, pp 413-437.

2.14 CHEUNG, M S and CHEUNG Y K, "Analysis of Curved Box Girder Bridges by Finite Strip Method. IABSE Publications, Vol 31-I, 1971, 1-19.

2.15 BULSON, P S, "The Stability of Flat Plates", Chat.o and Windus, London 1970.

2.16 TIMOSHENKO, S P and GERE, J M, "Theory of Elastic Stability"

2.17 GIBBS and COX INC. "Marine Design Manual for Fibre Glass reinforced plastics', McGraw Hill, 1960.

2.18 MAKOWSKI, Z S, EFTA Association Symposium on Plastics in Buildings 1972.

2.19 M A H KHAN and B STAFFORD SMITH, "Restraining Action of Bracing in Thin Walled Open Section Beams", Proceeding of the Institution of Civil Engineers, Part 2, Vol 59, 1975, pp 67.

CHAPTER 3

BEAM TO BEAM CONNECTIONS

3.1 INTRODUCTION

One of the major advantages of G.R.P. is that in many cases the basic material may be used to form the connection between two parts in a manner analogous to the construction of connections in steel. However, G.R.P. being brittle and generally anistropic cannot relieve stress concentrations in the manner of steel. The joining devices in G.R.P. connections include adhesives and metal fasteners such as steel screws bolts and rivets. Each joining device is appropriate for a particular structural consideration. For example adhesives are used for static loads and when the failure of the joint is not critical to total structural failure whilst screws and bolts are used for static or dynamic load [3.1]. Jointing devices will now be discussed in some detail.

3.2 ADHESIVE BONDED JOINTS - INTRODUCTION

The main purpose of adhesive - bonded joints is to provide a mechanical connection between two structural components. In those joints the stress distribution should be uniform over the entire surfaces and adhesive bonding effectively satisfies this requirement whereas it cannot be fulfilled by metal fasteners owing to the limited contact surface. The use of an appropriate adhesive frequently enables joints to be produced at equal or reduced cost and often with a saving in weight as compared with conventional fastening methods. Adhesive bonding can be employed to advantage for instance in cases where a thin, flat structural component must be connected to a thicker flat component, as it ensures that the strength of the thinner component is fully utilized. By contrast,

if conventional methods of fastening with screws or bolts is used, the joint obtained will have a strength which is limited by the area of contact of the thinner component. Adhesives frequently contribute important properties that are not provided by mechanical fasteners. For example because an adhesive extends over the entire area of the joint, it can act as a sealant preventing the passage of liquids provided that they do not attack the adhesive chemically. Adhesives also provide thermal and electrical insulation. An important advantage of an adhesive - bonded joint is that the external shape of the bonded parts is not altered, i.e. there is no visual indication of the actual joint as in the case of mechanical fasteners.

However, adhesive bonded joints suffer from the following disadvantages.

(1) Surface of adherends require cleaning prior to bonding.

(2) Relatively long curing times are required and this can add to the cost of the operation when considering tightly scheduled construction periods in civil engineering.

(3) Adhesives tend to creep more than the adherend material.

(4) Low peel strength.

3.2.1 Design considerations for adhesive - bonded joints

Although adhesive bonding makes it possible to produce joints which may be reliable, considerable care must be taken in designing the joint. It is hardly feasible to produce a bonded joint which can permenently withstand all types of loads arising from external forces.

It is essential to follow strictly the instructions of the

adhesive manufacturers which normally indicate the limits of applicability with reference to the type and magnitude of loads or to external effects such as temperature and humidity. The main types of stresses encountered in adhesive bonded joints are shown in fig (3.1). In general the joints should be designed so that they are mainly stressed in shear and tension. Peeling stresses should be avoided as much as possible. In addition bonded joints should be designed to eliminate the occurrance of high local stress peaks such as those in rivetted joint shown in fig (3.2a).

3.2.2 Design Applications for Adhesive-Bonded Joints

Butt joints of the type illustrated in fig (3.3a) are the easiest to produce, but are hardly suitable for the transmission of forces as the bonded area is small and the strength of the adherends is many times greater than those of the adhesives so that their ability to transmit tensile, compressive or torsional loads is limited to the strength of the adhesive. The right angle butt joints illustrated in figs (3.3b-d) are also simple to produce but the type in fig (3.3b) is suitable only for lightly loaded constructions. A better solution is a combination of butt and lap joints fig (3.3e).

Lap joints are the more commonly used than other types of joints. Fig (3.4) shows various types of adhesive bonded lap joints. A simple type of lap joint such as fig (3.4a), when subjected to shear by a tensile force will produce a non-uniform stress distribution fig (3.5c). The non-uniformity of stress distribution is caused by two factors i.e. by the stress differential between the joint surface and the adhesive layer and by the deflection of the overlap surface due to the parallel offset of the positions of force application resulting from the respective thickness of the

adherends and the adhesive layer. The stress differential arises because under a given load, the adhesive stretches to a greater extent than the adherends. Offset loads, which are typical of lap-joint designs, result in bending stresses in lap bonded joints. Deflection of the joint under a given load can be reduced by stiffening the adherends or by reducing their thickness. It is possible also to reduce the overlap length by the use of rivets or screws at the ends of the overlap portion. Changes in the design of the simple lap joint fig (3.4a) makes it possible to eliminate or compensate for the effects of parallel offset in load application and of differential stresses. For example the strap joint in fig (3.4g) can provide a satisfactory solution to many problems but is fairly expensive to produce and is feasible only with comparatively thick components. The same advantages of good stress distribution and also the same disadvantage are obtained with the bevelled lap joint fig (3.4b), while the rebated lap joint fig (3.4c) has somewhat more favourable strength properties. The double lap joint in fig (3.4f) provides a reliable joint at a low cost. Of the strap joints figs (3.4h-k) which can be regarded as a combination of lap and butt joints, the double strap joint fig (3.4j) which has good strength properties but is expensive to produce. The bevelled double strap joint has a good stress-distribution pattern but is appropriate only if strips of the appropriate profile are used otherwise machining costs will be excessive.

Detailed analysis of internal stress distributions within a structural joint using approximate analytical [3.2] or finite element [3.3] methods have been carried out by several research workers.

Erdogan and Ratwani [3.4] developed a model for the calculation

of stresses on bonded overlapped joints in plates and tubes. The model was based on the assumption of generalized plane stress.

Sinha and Reddy [3.5] analysed the bond stress in joints between orthotropic adherends taking into account the variation between the curing temperature and the operation temperature which was found to be an important criterion.

Hart and Smith [3.6] also investigated the problem of thermal mismatch effects in bonded joints in some detail, and they observed that temperature variation in the joint had a considerable effect on the shear strength of the joint. The lap length was also found to influence the stress significantly. Rather complicated approximate theories were developed by some investigators [3.7, 3.9] for predicting the shear strength of a lapped bonded joint, but the simpliest was that attributed to Volkersen [3.7] which is expressed in the following form, considering fig (3.5a).

$$\tau_c = \frac{T_o \delta}{2c} \frac{\cos h\ \delta\ (x/c)}{\sin h\ \delta} \qquad (3.1)$$

where

$$\delta = \frac{2\ G_c}{Eth}\ xc$$

and

E = Young's modulus of the adherends

G_c = Young's modulus of the adhesive

$\ell = 2c$ = Length of joint overlap

t = Adherend thickness

h = Adhesive thickness

τ_c = Shear stress in the adhesive (τxy)

T_o = Tensile load per unit width applied to joint.

Goland and Reissner [3.10] presented a theory which predicts the shear stresses at the joint which are largely dependant upon the strain in the adherend at the interface. They pointed out that the maximum tearing and shear stresses reach asymptotic values for large overlap lengths. Hence, provided the system remain linearly elastic the joint strength reaches a limiting value with increasing length of overlap.

The long term behaviour of bonded joints, which is an important factor, has not received much attention from research workers. Recently Fairbairn [3.11] carried out an experimental investigation of the effects of acceleration age testing on adhesives in an attempt to study the long term behaviour of bonded joints subjected to creep, fatigue, elevated temperature and environmental conditions.

3.3 METAL FASTENER JOINTS - INTRODUCTION

In designing connections utilizing metal fasteners it is necessary to provide adequate strength to prevent failure of the fastener or the laminate retaining the fasteners. Bolts and threaded fasteners, sometimes used with a bonding adhesive, are the most commonly used with G.R.P. The selection of the type of fastener to be used depends on the load, laminate strength and thickness and ease of disassembly when necessary.

At connections in which high tensile stresses act across bonded interfaces, use of metal fasteners is likely to be necessary. Bolts, rivets and screws of many types may be used for this purpose.

In counteracting bond tension, metal fasteners act by carrying a proportion of tensile load and in some cases by imposing an initial compression across the bond, thus raising its apparent

tensile strength. Fasteners also act as "peel arrestors" inhibiting the propagation of local debonding. Metal fasteners introduced with the primary object of preserving the resin bond should where possible be designed with the secondary fail-safe capability of transmitting all or most of the designed loads in the event of bond failure. Due to the many types of fasteners in G.R.P. laminates, the use of only two types of fasteners namely threaded fasteners and bolts will be discussed in detail.

3.3.1 Threaded Fasteners Joints

Whenever threaded type fasteners are to be used in G.R.P. laminates, the fastener should always be perpendicular to the laminate, reinforcement. Edge fastening should be avoided since this tends to delaminate the laminate and has very little strength.

The strength of threaded fasteners in G.R.P. laminates depends on a number of factors including the type of laminate, type of fastener, depth of penetration, diameter of fastener, size of the pilot hole and direction of loading.

Rufolo [3.1] carried out tests on two basic directions of loading, axial which tends to pull the fastener directly out of the laminate and transverse which pull the fastener sideways. According to Gibbs and Cox [3.12] threaded fasteners should have edge and side distances equal to two and a half times the fastener diameter and a spacing of three times the fastener diameter. Tables were also provided by the same authors for the ultimate strengths for axial and transverse loading of three types of fasteners.

3.3.2 Bolted Joints

For bolted joints several types of laminate failure may occur

before the full strength of the bolt is attained. These failures are tearing from the bolt hole to the edge of the laminate, tearing the laminate along the line of the bolt holes and shearing a plug between the bolt hole and the edge of the laminate. Typical modes of failure in bolted joint connections are shown in fig (3.6).

Gibbs and Cox [3.12] recommended that the minimum edge distances for bolts should be 2.5 the diameter of the bolt in case of bidirectional reinforcement and twice the diameter in the case of chopped mat. Also the spacing between the bolts were restricted to a minimum of three times the diameter of the bolt.

Wood and Hall [3.13] investigated bolted joints and concluded that the crushing stress of a G.R.P. connection varies with

(1) The percentage of reinforcement

(2) The diameter of the bolt

(3) Ratio of hole size to bolt size

(4) The method of forming the hole

(5) The type of reinforcement

(6) Whether the crushing is enclosed or not.

Waszczak and Cruse [3.14] analysed the strength of a bolted joint of composite with reference to the failure modes shown in fig (3.6). They predicted the failure load based on the distortional energy criterion which exhibited good agreement with experimentally failed specimens. The distortional energy may be written in the form.

$$\text{DIST. ENERGY} = \left(\frac{\sigma_1}{\sigma_{1u}}\right)^2 + \left(\frac{\sigma_2}{\sigma_{2u}}\right)^2 + \left(\frac{\tau_{12}}{\tau_{12u}}\right)^2 - \left(\frac{\sigma_{2u}}{\sigma_{1u}}\right)\left(\frac{\sigma_1}{\sigma_{1u}}\right)\left(\frac{\sigma_2}{\sigma_{2u}}\right) \qquad (3.2)$$

where σ_1, σ_2, σ_1 are the principle stresses and σ_{1u}, σ_{2u}, σ_{1u} their corresponding ultimate stresses. The maximum stress (or strain) failure criterion requires that the ratio of principle stresses (or strains) to their respective ultimate stresses (or strains) be greater than or equal to unity for failure to occur.

3.4 OTHER TYPES OF JOINTS

Many other types of joints are available. For example a combination of fasteners or bolts with adhesive has the advantages of both types. In addition fasteners assist in fixing the alignment of the joint during curing of the adhesive.

A recent type of joint was designed by Arbed - F and G [3.15] which essentially consists of two sheet - metal washers to which a number of metal wires are fastened by a stud-welding process. The arrangement of the wires depends on the direction of the applied force and the number and diameter of the wires can be made to suit the stresses. The metal washers can have through holes or be fitted with tapped welded nuts. Fig (3.7a) shows one type of these units which have the following advantages.

(1) A relatively small sheet-metal part for the fixing of bolts or nuts disturbs the homogeneity of the material only.

(2) Through the spider-like arrangement of the wires forces are distributed over a wider area and thus stress concentrations are reduced.

(3) The wires prevent a sudden discontinuity in the force field at the circumference of the metal fasteners.

Big Head Bonding Fasteners Limited produced a type of fastener (fig (3.7b) which can be bonded and screwed or bolted on to G.R.P. components.

3.5 AIM OF INVESTIGATION

The remainder of this chapter will be concerned mainly with the development of a suitable mechanical joint for G.R.P. box beams having the same cross-sectional area as beams series B1-B5. This investigation programme was carried out in three stages.

The first stage was concerned with the design of a joint configuration and the selection of a suitable type of fastener. In the second stage the behaviour of the selected joint in fibre oriented beams was investigated. In the third stage a study was made of the behaviour of long span box beams with multiple joints.

3.6 JOINT DESIGN

The trial 3 m span beam series B1 was cut into three parts fig (3.8) and the damaged portion was removed leaving parts A and B, to be joined, by a suitable G.R.P. joint. Three alternatives were considered for joining these parts and these are shown in fig (3.9).

(1) A closed G.R.P. box unit which may be inserted into the two parts to be joined fig (3.9a)

(2) A joint consisting of two external G.R.P. channels and two internal plates fig (3.9b).

(3) Two overlapping channel sections used externally fig (3.9c).

After careful consideration the first alternative was eliminated (though it looks attractive) due to irregularities resulting from hand lay up techniques.

The second alternative was also eliminated due to problems in fixing the internal plates and due to the fact that the two channel sections provide continuity along the webs only. The

The third alternative was adopted due to its simplicity and also because it provides continuity for the box beam elements along both webs and flanges. In addition the compression and tension flanges are strengthened at the joint cross-section by two thicknesses of the overlapping material.

The length of the overlapping channels was chosen to be 450 mm for the provision of a suitable lap length between parts of the beam to be joined the reinforcement for the channels was four layers of bidirectional and four layers of chopped mat laid in alternating layers. The reason for chosing this type of reinforcement was that both longitudinal and transverse stiffeness of the member is needed to provide for the various stresses to which the joint is subjected. The chopped mat also helps in relieving stress concentrations around the fastener. Fig (3.10) shows the detailed dimensions and reinforcement of the overlapping channels. The position of the fasteners in the channels is shown in Fig (3.11) these locations were chosen to comply with the following requirements:-

(1) The spacing between fasteners and the edge distance to the nearest fastener not be be less than three times the diameter of the fastener.

(2) A staggered arrangement of holes in the web was adopted to minimize the effect of weakening the channels components.

(3) The orientation of holes in the compression and tension flanges was such as to allow long fasteners or tie bars which would not foul fasteners or tie bars used in the web.

(4) The optimum number of holes were adopted in order to minimise the weakening of the beam units at the joint.

3.7 STAGE 1 INVESTIGATION

As there are a wide variety of types of mechanical fasteners used in G.R.P. laminates, the investigation was limited for four types of mechanical fasteners namely:-

(1) long tie bars

(2) self tapping screws

(3) rawl plug bolts

(4) high tensile bolts.

The details of these fasteners are shown in fig (3.12). Each type of fastener was used to connect two 1 m beam units fig (3.13), except that for the long tie bars the beam units were obtained by cutting the trial beam B1 into two 1.250 m beam units. In all beam units the reinforcement type and orientation was identical - see Table (3.1). In addition an end diaphragm was fixed in the beam unit at the joint to prevent the connected beams from warping and buckling at the joint.

Where long tie bars were used the procedure of joining the beam units was complicated and included the following steps. Referring to fig (3.14):-

(1) After casting the two overlapping channel components the two beam units A and B were brought together enclosed by the two channels and the whole correctly aligned and drilled

(2) The two channels and beam units A and B were then dismantled.

(3) The threaded tie bars were inserted through the specially provided access holes. Internal nuts and washers were then screwed flush against the inside walls of the units

(4) The additional diaphragms were then added at each joint end.

(5) Units A and B were then brought together and enclosed by the lapping channels and after correcting aligning them, they were drilled.

External nuts and washers were then applied to complete the joint.

In the case of self tapping screws self rawl plug bolts and high tensile bolts the procedure was much simpler and faster. It essentially comprised of enclosing the beam units in the overlapping channels, correcting the alignment and marking out for drilling. However, in the case of the high tensile bolts it was necessary to form a 110 mm diameter access hole fig (3.13) in the webs along the neutral axis to allow for inserting and fixing nuts and bolts from inside the beam.

The jointed beam units resulted in the following series of beams.

Beam type C1 (included long tie bars joint)

Beam type C2 (included self tapping screws joint)

Beam type C3 (included self rawl plug bolts joint)

Beam type C4 (included high tensile bolts joint)

A four point load test was applied to each beam thus subjecting the joint to constant bending moment.

Additional external ribs fig (3.13) were cast into the box beam units at the supports and load points to prevent local buckling due to high bearing stresses. The ribs were reinforced by 10 layers of chopped strand mat. Fig (3.15) shows a typical beam assembly and instrumentation for beams series C1-C4.

3.8 TEST RESULTS

Load versus deflection strains in the compression and tension

flange were plotted for selected gauges at and near the joint fig (3.17-3.21). In order to compare the behaviour of each type of fastener used in the joint, load versus shear strain at centre of the web was also plotted for beams C1-C4 fig (3.22).

3.9 EFFECIENCY OF THE CONNECTION

The effeciency of the beam connection is expressed as a percentage of its failing load relative to the failing load of a non-jointed beam having the same cross-sectional area, span, and fibre orientation etc.

As the jointed and unjointed beams did not have the same span the results were normalised in the following way:-

Let new span of the jointed beam be L_1 m and original span of the unjointed beam be L_m. Let the failure load of the unjointed beam be W kN and failure load of the jointed beam be W_1 kN.

Assuming the same cross-sectional area and fibre orientation in both cases by simple bending theory we obtain.

$$f = \frac{M}{Z} = \frac{WL}{Z} \quad \text{(For unjointed beam)} \tag{3.3}$$

and

$$f = \frac{M}{Z} = \frac{W_1 L_1}{Z} \quad \text{(For the jointed beam)} \tag{3.4}$$

on the assumption that the same mode of failure will occur, from equation (3.3) and (3.4) we obtain

$$\frac{W_1}{W} = \frac{L}{L_1} \tag{3.5}$$

or

$$W_1 = \frac{WL}{L_1}$$

Beam series C1-C4 have the same cross-sectional area and reinforcement orientation as beam B1.

3.10 DISCUSSION - STAGE 1 INVESTIGATION

From Table (3.2) and the graphical plot of load versus strains fig (3.18-3.22), it was possible to compare the performance of each type of fastener. Beam types C1, C2 and C4 achieved the maximum efficiencies and the failure took place away from the joint while beam type C3 resulted in a joint failure failure and achieved the least effeciency. Beam series C1, C2 and C3 attained a greater deflection and failure than beam C4 and their load deflection behaviour was non-linear fig (3.17) stress concentrations were observed around the fasteners in the case of beam types C2 and C3 while this phenomenon was not observed in beam type C4. The rate of recovery from the deflected form when the applied load removed was noticed to be highest for beam type C4, followed by beam types C2 and C1. Further more, in the case of beam type C3 the beam only recovered partially. This was due to the fact that some rawl plug bolts retained their original non-buckled form. Some of the tie bars were buckled in the case of beam type C1 and in the case of beam type C3, the joint failed by the pulling out of the joint - self tapping screws. Despite the 110 mm diameter access holes in the beam unit webs in the case of beam type C4 which meant weakening the beam units near the joint, this beam achieved the maximum ultimate load.

The load-strain graphical plots fig (3.18-3.22) showed that beam type C4 attained the maximum elastic range in comparison with the other beams. The non-linear behaviours which was exhibited by beam types C1-C2 and C3 figs (3.18-3.22) corresponded to the behaviour of their fasteners which suffered from buckling (beam types C1 and C2 and pulling out (beam type C3). In all beams the

strains in the beams near the joint were larger than those at the joint itself fig (3.18-3.21), which may be due to the stress concentrations around the fasteners.

Although rawl plug bolts have the advantage of being easy for fixing they suffer from two main problems. Firstly, the tolerence of these bolts are fixed fig (3.12b) whilst the thickness of the joint (considering the irregularities of the surface using hand lay methods) is variable and secondly the buckling of the outer frame of the bolt which controls the tightness of the joint depends to a great extent on personal judgement.

From consideration of the above discussion it is clear that the high tensile bolts were the most effecient type of fasteners from amongst those used in the investigation.

3.11 STAGE 2 INVESTIGATION

Beam series B1-B5 of the tests on which were described in the previous chapter, were reused in this investigation in the form of beam series C5-C9. The damaged portions of beam series B1-B5 were cut out resulting small beam units of 1 m lengths with different fibre orientation fig (3.23). The beam units were then assembled fig (3.24) and the two G.R.P. lapping channel jointing system was used with high tensile bolts as fasteners. In this case the joint details were kept identical in beam series C5-C9 except that the fibre orientation was different and corresponded to the original beam series B1-B5 Table (3.1).

Beam series C5-C9 were tested in the same manner as beam series C1-C4. Fig (3.24) shows the assembly and instrumentation for beam series C5-C9.

Load versus deflections, strains in the flanges and shear strains in the webs were plotted at and near the joint fig (3.25-

3.40), in order to study the effect of fibre orientation in G.R.P. box beams.

3.12 DISCUSSION

The modes of failures in beam series C5-C9 were similar in all cases, a crack propagated in the compression flange near the joint after a visual local buckling occurred in the compression flange near the joint. It was possible to trace the local buckling in the compression flange from the load versus strain plots figs (3.26, 29, 32, 35 and 38). The strains in the compression flange near the joint were initially compressive but at a later stage in the loading became tensile. With local buckling occurring in the compression flange it is well understood that failure should occur at the weakest section which is near the joint.

Another feature shown in the failed beams, was the presence of a highly localized region of delamination at the bolt-joint interface. The effecieny of the connection based on the same calculation described in section 3.9 is shown in Table (3.3) for the beam series C5-C9.

Load versus deflection plots figs (3.25, 28, 31, 34 and 37) showed good linear behaviour at and away from the joint.

The maximum deflections at failure ranged from 24.95 mm to 36.79 mm in the beam series C5-C9. Beam type C7 and C9 achieved the maximum efficiency but the second largest deflection in the series, while beam type C6 attained the least deflection and the maximum ultimate load. In terms of least deflection it was considered that beam types C6 and C4 were better than others. In view of the test results Table (3.3) and various graphical representations fig (3.25-40), it may be concluded that fibre orientation in the beams had little effect on the behaviour of the connection

for two reasons. Firstly the mode of failure of the beams was identical and secondly apart from beam type C1 the ultimate loads reached were comparable. Deflection at the joint depends to a greater extent on the type and the thightness of the beam units with the jointing channels. However, it is advisable that at joints, the lapped region of the beam sections should be reinforced with bidirectional material to resist the various stress directions to which the joint may be subjected.

3.13 STAGE 3 INVESTIGATION

The first two stages of investigation dealt with the behaviour of joints in short span box beams in which the joint were subjected to the effect of pure bending. Since in practise the need for longer beams with multiple joints may arise and in this case the joints are subjected to bending and shear, it was decided to investigate the behaviour of a long span box beam assembled from small beam units with multiple joints. It was also decided to test the beam with a central load thus subjecting the mid span joint to the effect of maximum shear and bending.

A 6 m span beam type C10 was assembled for 1 m beam units with five joints typical of those used in beam series C4-C9. Fig (3.42) shows the beam assembly and instrumentation. Details of the beam unit and reinforcement are shown in fig (3.41).

For each beam unit it was necessary to cut two 110 mm access holes to allow for fixing the bolts and nuts from the inside. Carefull alignment was made before jointing each beam unit, to ensure the straightness of the span.

Load versus mid span deflections and strains at and near the joint were plotted for selected gauges figs (3.43-46).

3.14 DISCUSSION

The failure of the beam took place in the compression flange of one of the beam units adjacent to mid span and occurred near a joint at a load of 20 kN and accompanied by large deformations. Dual gauges were not useful during the application of the first increment of load and were quickly replaced by meter scales fixed to a datum level and readings were then recorded. Load versus mid span deflection fig (3.43) indicates that an overall linear behaviour was exhibited, up to 62% of the failure load. The maximum deflection at failure of 130 mm represents $\frac{1}{46}^{th}$ of the span is considered to be large compared with the allowable deflection in codes of practise for concrete and steel beams. Strains in the compression flange and mid span, fig (3.45), shows a non-linear tensile strain developed at mid span indicating that local buckling near the joint in the compression flange developed at an early stage of loading.

From Table (3.4) and the corresponding vertical profile at the joints fig (3.47), it may be concluded that a reasonable profile of deformation of the beam along the span was exhibited, during various stages of loading. However, theoretically the deflection at the joints 1 and 2 should be identically the same as at the joint 4 and 5 (Table 3.4) but due to the interaction of the joints, a slight variation was recorded.

3.15 CONCLUSION

The following conclusions may be drawn out from the 3 stage investigation on joints:-

(1) G.R.P. jointing components can be formed in various shapes analogous to those in steel or other metals.

(2) The selection of a suitable fastener in a G.R.P. joint is extremely important as each fastener serves a special type of structural action.

(3) The tightness and gripping of bolts in a G.R.P. jointing component is largely responsible for its effeciency, but on the other hand excessive torque applied to the bolts should be avoided since this can lead to crushing of the material under the nut or bolt head.

(4) Long G.R.P. span beams can be assembled using multiple joints provided that the problem of large deformations is overcome.

(6) In joining G.R.P. beams using bolts an optimum number of fasteners should be used since using a greater number of bolts can lead to weakening the connected beam at the joint.

Beam Series	No type and orientation of reinforcing layers with reference to the axis shown in fig (3.16)				
	Web	Compression flange	Tension flange	Diaphragm	External rib
C1	4B 4(0/90)	4B 4(0/90)	4B 4(0/90)	4B 4(0/90)	10C
C2	4B 4(0/90)	6B 6(0/90)	4B 4(0/90)	4B 4(0/90)	10C
C3	4B 4(0/90)	6B 6(0/90)	4B 4(0/90)	4B 4(0/90)	10C
C4	4B 4(0/90)	6B 6(0/90)	4B 4(0/90)	4B 4(0/90)	10C
C5	4U 0,+45,+45,+0	4U 0,+45,+45,0	U,B,B,U 0,0/90,90/0,0	4U 0,+45,+45,0	10C
C6	4B 4(0/90)	4B 4(0/90)	U,B,B,U 0,0/90,90/0,0	4B 4(0/90)	10C
C7	4U +60,-45,-45,+60	4U +60,-45,-45,+60	U,B,B,U 0,0/90,90/0,0	4U +60,-45,-45,+60	10C
C8	4U +45,-45,-45,+45	4U +45,-45,-45,+45	U,B,B,U 0,0/90,90/0,0	4U +45,-45,-45,+45	10C
C9	6U 0,+45,-60 -60,+45,0	6U 0,+45,-60 -60,+45,0	U,B,B,U 0,0/90,90/0,0	6U 0,+45,-60 -60,+45,0	10C
C10	4B 4(0/90)	4B 4(0/90)	4B 4(0/90)	4B 4(0/90)	10C

note:-

B = Bidirectional
U = Unidirectiona
C = Chopped mat

TABLE 3.1 DETAILS OF REINFORCEMENT BEAMS TYPE C1-C10

Beam Series	?Joint type	Fastener type	Span	Failure load	Expected ultimate load	Joint efficiency %	Maximum deflection at failure	Mode of failure	General Remarks
C1	Two over-lapping channels	6 mm	2.500	57.5	75	76.6	48.86	shear failure	Excessive non-linear deflection due to buckling of ties.
C2	" "	6 mm rawl plug bolt	2000	85	120	70.8	50.65	compression failure	Generally non-linear deflection behaviour stress concentration around bolts.
C3	" "	6 mm self tapping screws	2000	70	120	58.3	49.93	joint failure	Generally linear deflection behaviour prior to failure. Screws pulled out of the joint.
C4	As above + two 110 mm dia holes in beam.	9 mm H.T. black bolts	2000	92.5	120	77	26.43	compression failure	Linear deflection behaviour up to failure

TABLE (3.2)

DETAILS OF BEAM SERIES C1-C4

Beam Series	Joint type	Fastner type	Span (mm)	Failure load (kN)	Expected ultimate load	Joint effeciency %	Maximum deflection at failure	Mode of failure	General Remarks
C5	Two overlapping channels	9 mm H black bolts	2000	100	90	111	33.2	compression	Development of Local buckling in the compression flange near the joint leading to a crack at failure
C6	" "	" "	2000	80	78.75	101	24.95	Compression	
C7	" "	" "	2000	95	78.75	120	36.79	Compression	
C8	" "	" "	2000	95	97.5	97.4	27.5	Compression	
C9	" "	" "	2000	105	90	116	34.65	Compression	

TABLE (3.3)

DETAILS OF BEAM SERIES C5-C9

Load increment (kN)	Deflect at ℄ of Joints (mm)				
	Joint 1	Joint 2	Joint 3	Joint 4	Joint 5
0	0	0	0	0	0
2.5	6	12	13	12	6
5	12	25	28	24	11
7.5	20	37	44	36	20
10	30	50	60	53	34
12.5	40	68	73	68	44
15.00	60	86	95	84	52
17.5	82	104	130	101	86

TABLE (3.4)

DEFLECTION AT ℄ OF FOINTS AT LOADING INCREMENTS

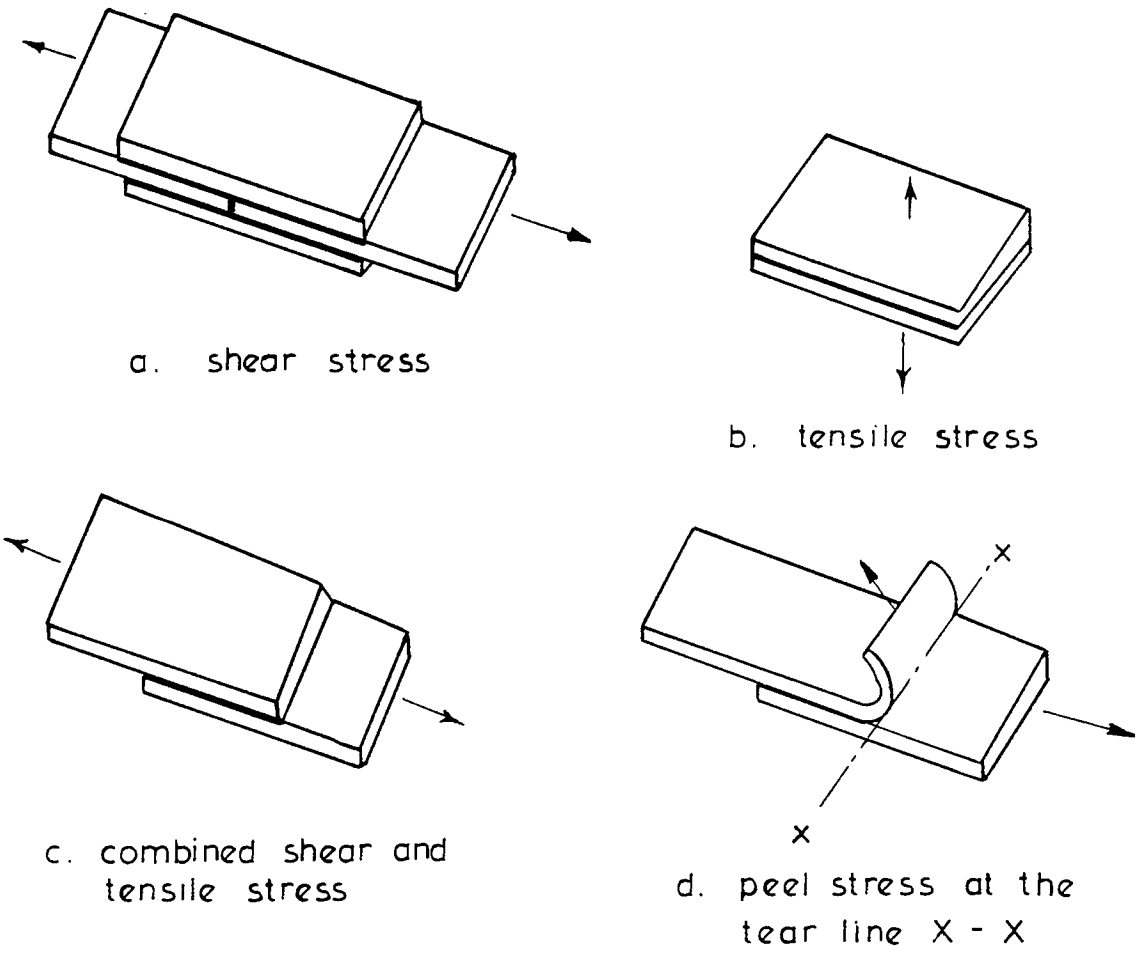

Fig. 3.1. Main types of stress encountered in adhesive bonded joints.

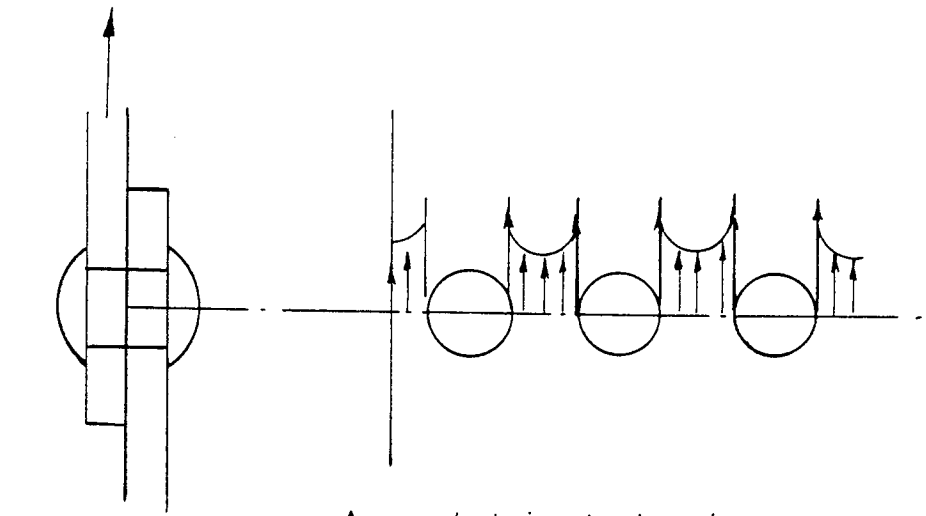

a. A riveted joint showing stress peaks at the rivet edges.

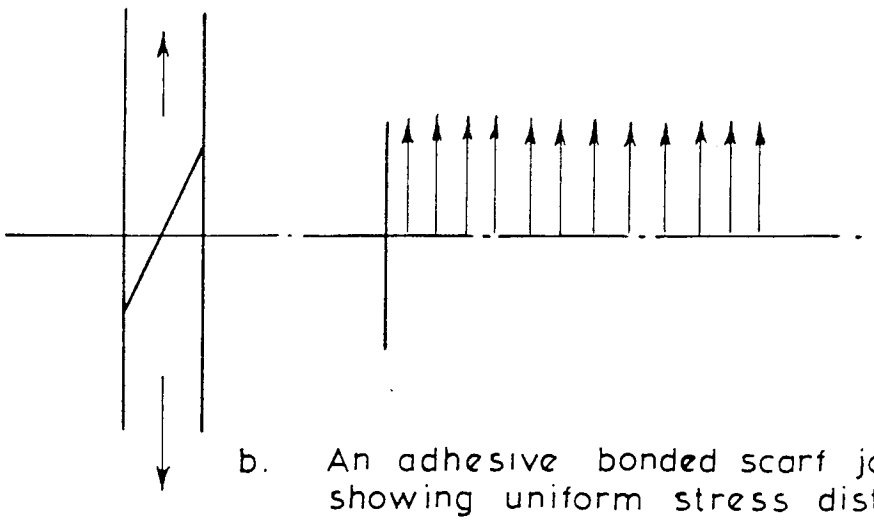

b. An adhesive bonded scarf joint showing uniform stress distribution

Fig. 3.2. Typical stress patterns in joints produced by riveting and adhesive bonding

a. Simple butt

b. Simple right angle.

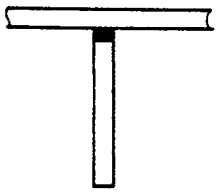

c. Right angle

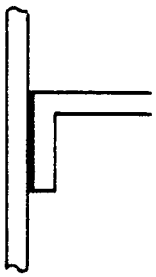

d. Right angle

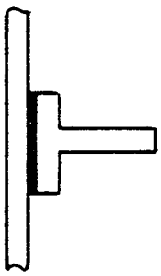

e. Combination of butt and lap joint

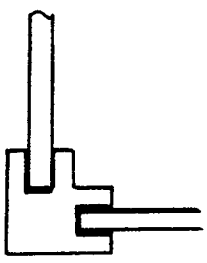

Fig. 3.3. Examples of butt joints

a. Simple lap

b. Bevelled lap

c. Rebated lap

d. Stepped lap

e Double stepped lap

f. Double lap

g. Scarf

h. Simple strap

i. Double strap

j. Bevelled bouble strap

k. Stepped double strap

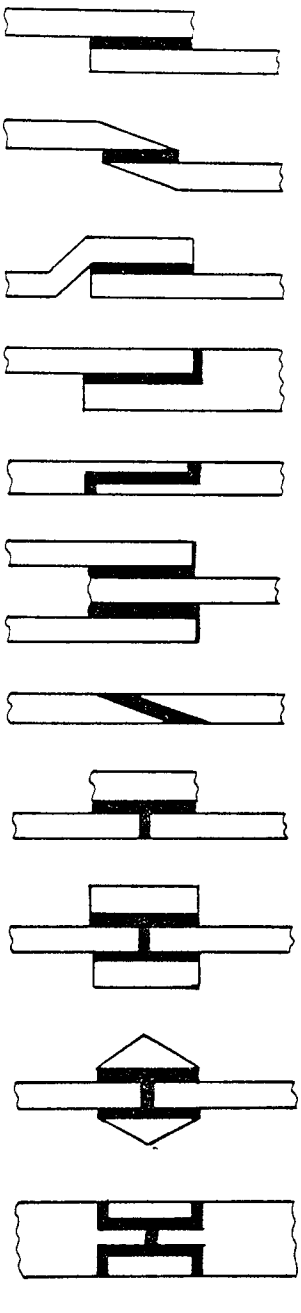

Fig. 3.4. Example of lap joints

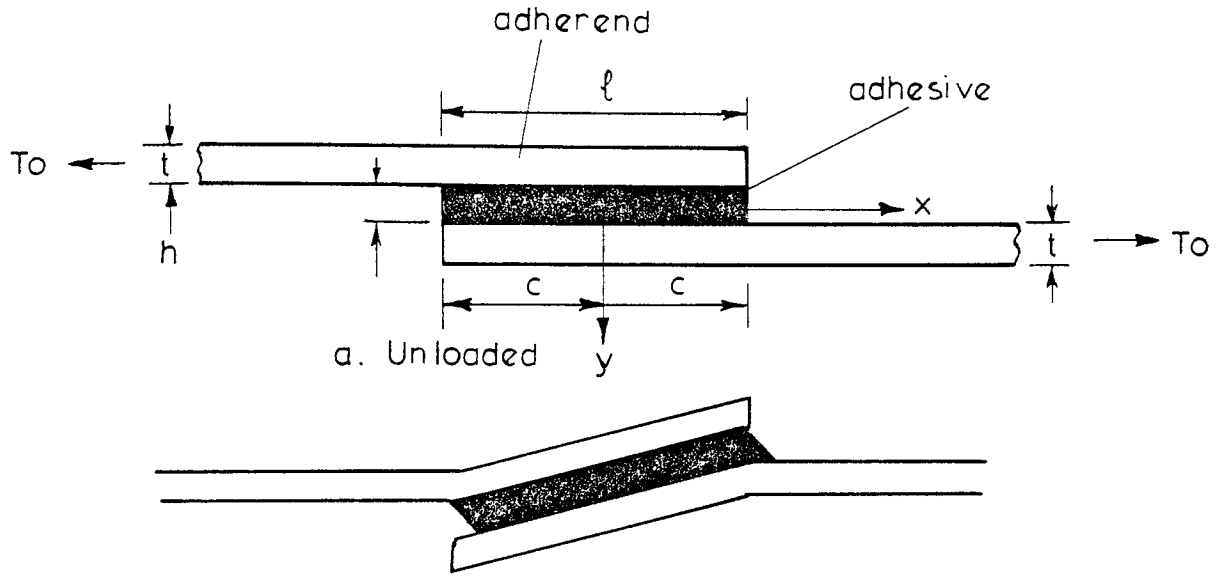

b. Loaded

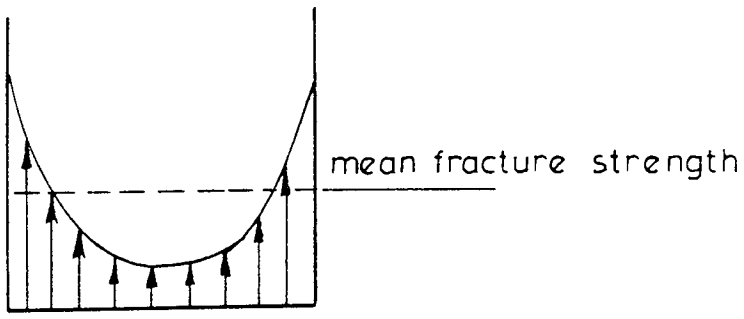

c. Stress distribution in adhesive

Fig. 3.5. Effect of load on a lap joint.

a. Net tension

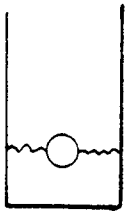

b. Shear out

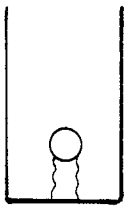

c. Bending tear out

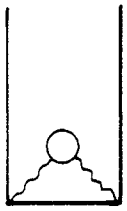

d. Bearing

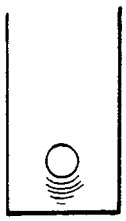

e. Combination

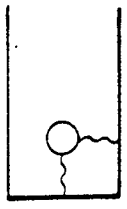

Fig. 3.6. Failure modes in bolted joints

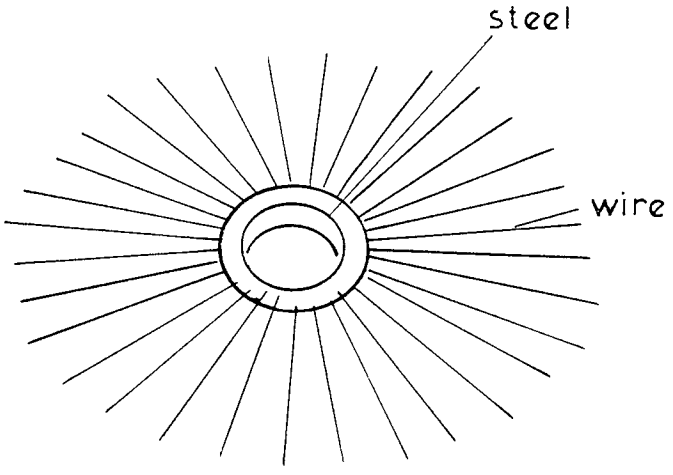

a. Arbed F & F fostener type

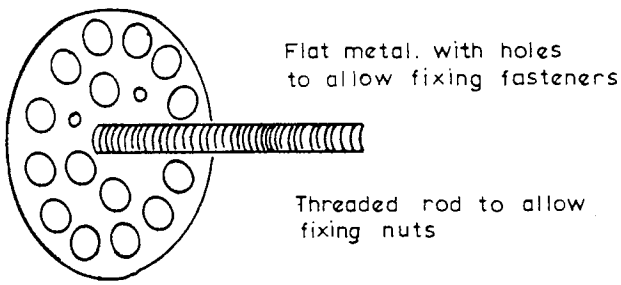

b. Big headed bond fastener type

Fig.37 Example of bonded fasteners

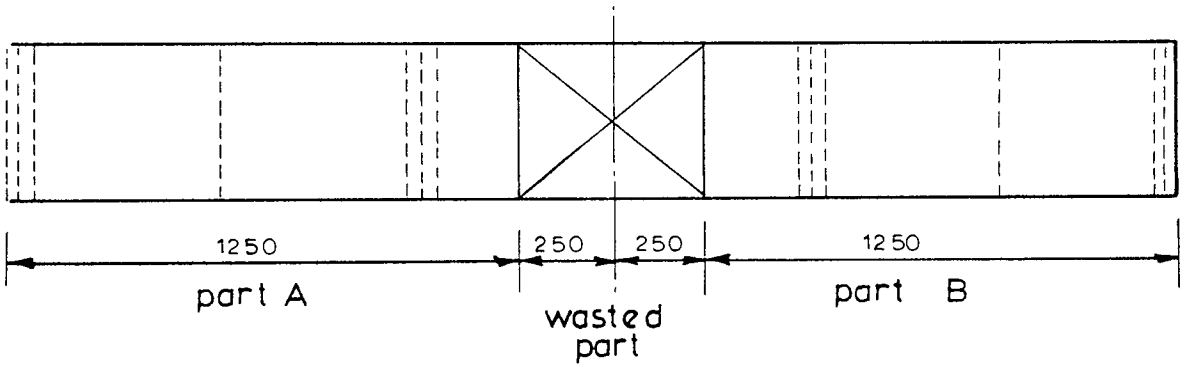

Fig. 3.8 Trial beam type B_1 portioning

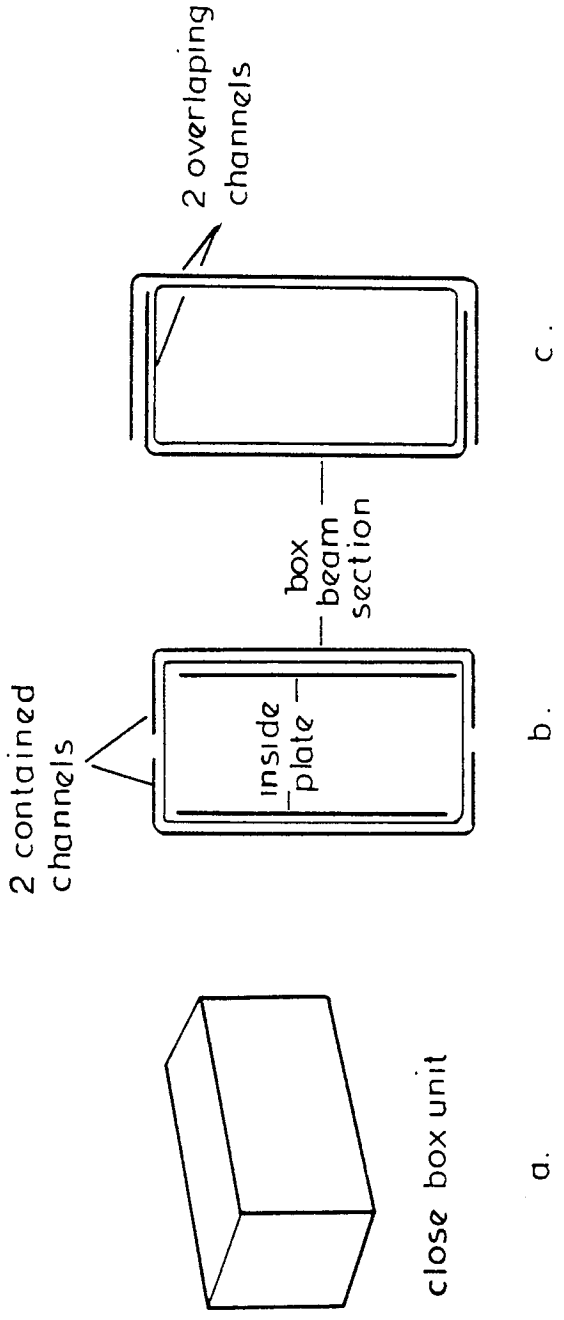

Fig. 3.9 Connection elements considered

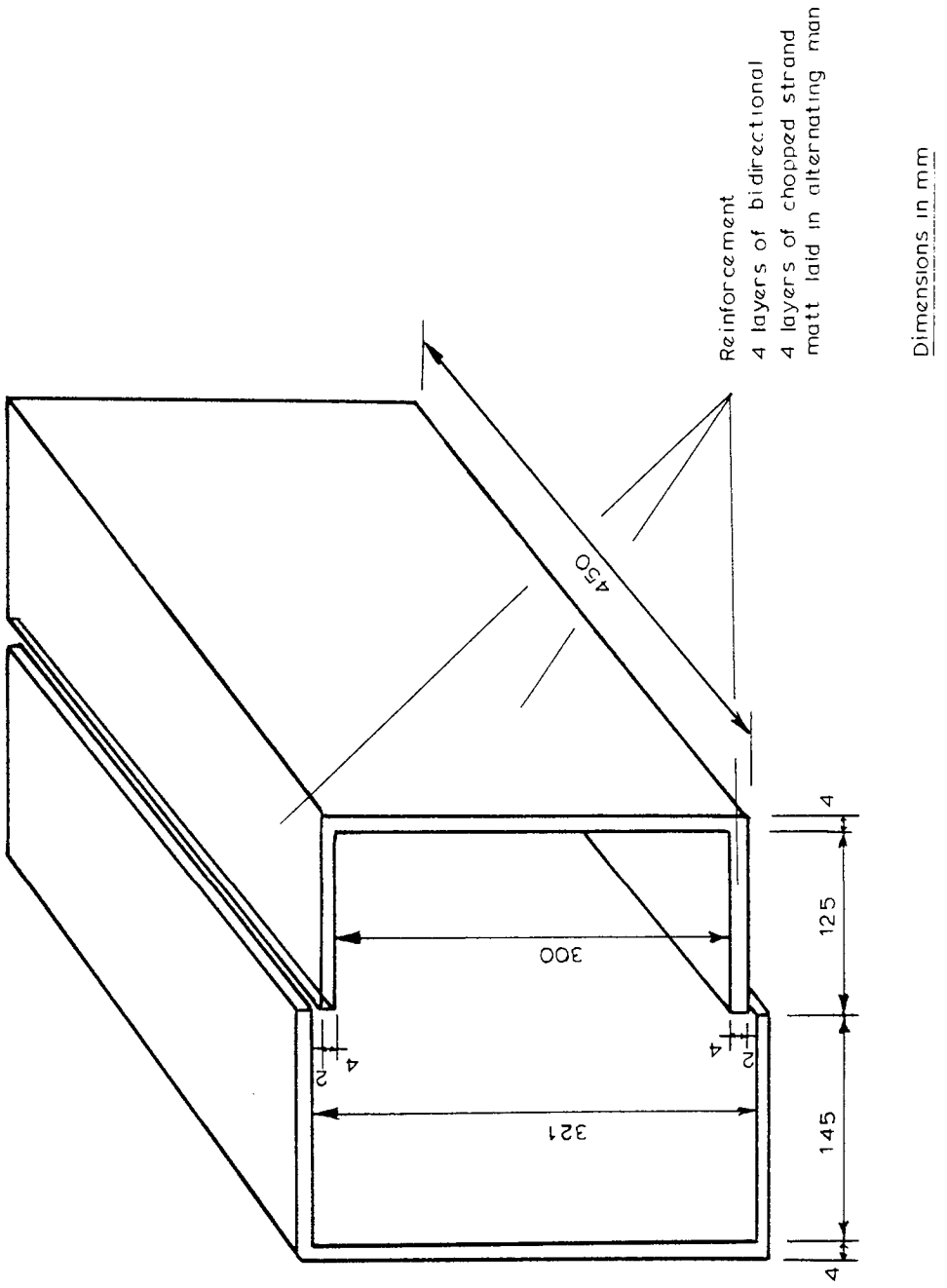

Fig. 3.10. Detail of overlapping channels joint

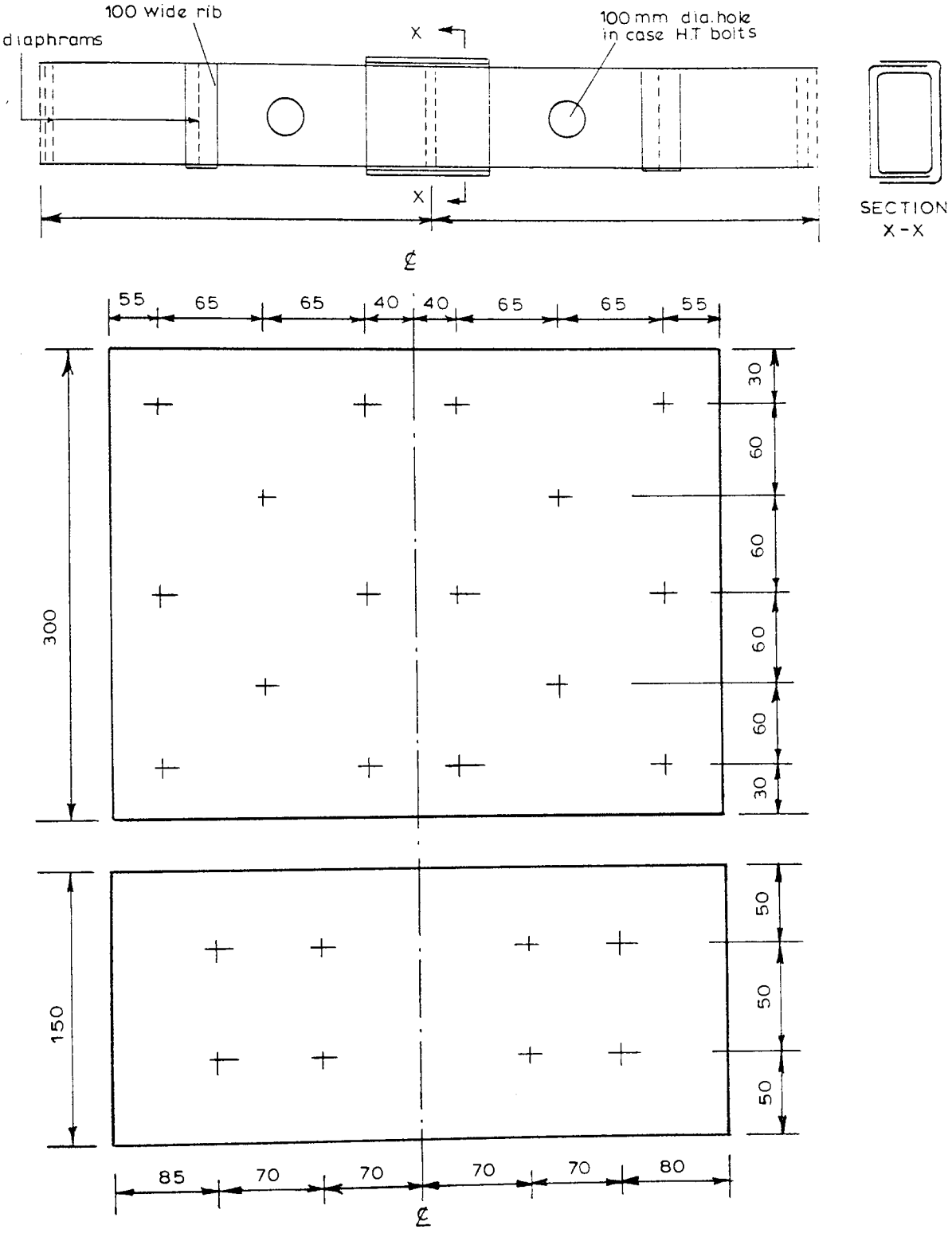

Fig. 3.11 Detail of connection

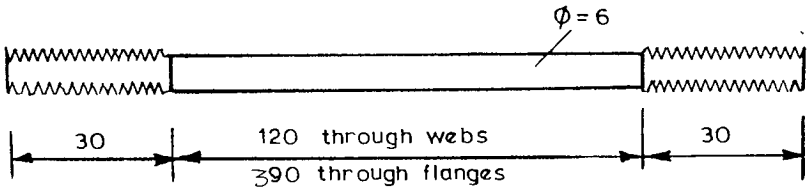

a. Tie bar

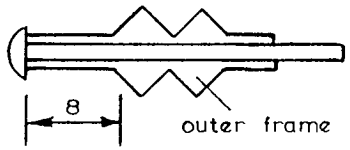

b. Rawl plug bolt

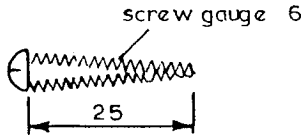

self tapping screw

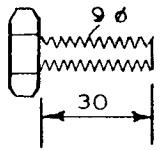

High tensile bolt

Dimensions in mm

Fig. 3.12 Detail of mechanical joint systems used in beams C1 – C4

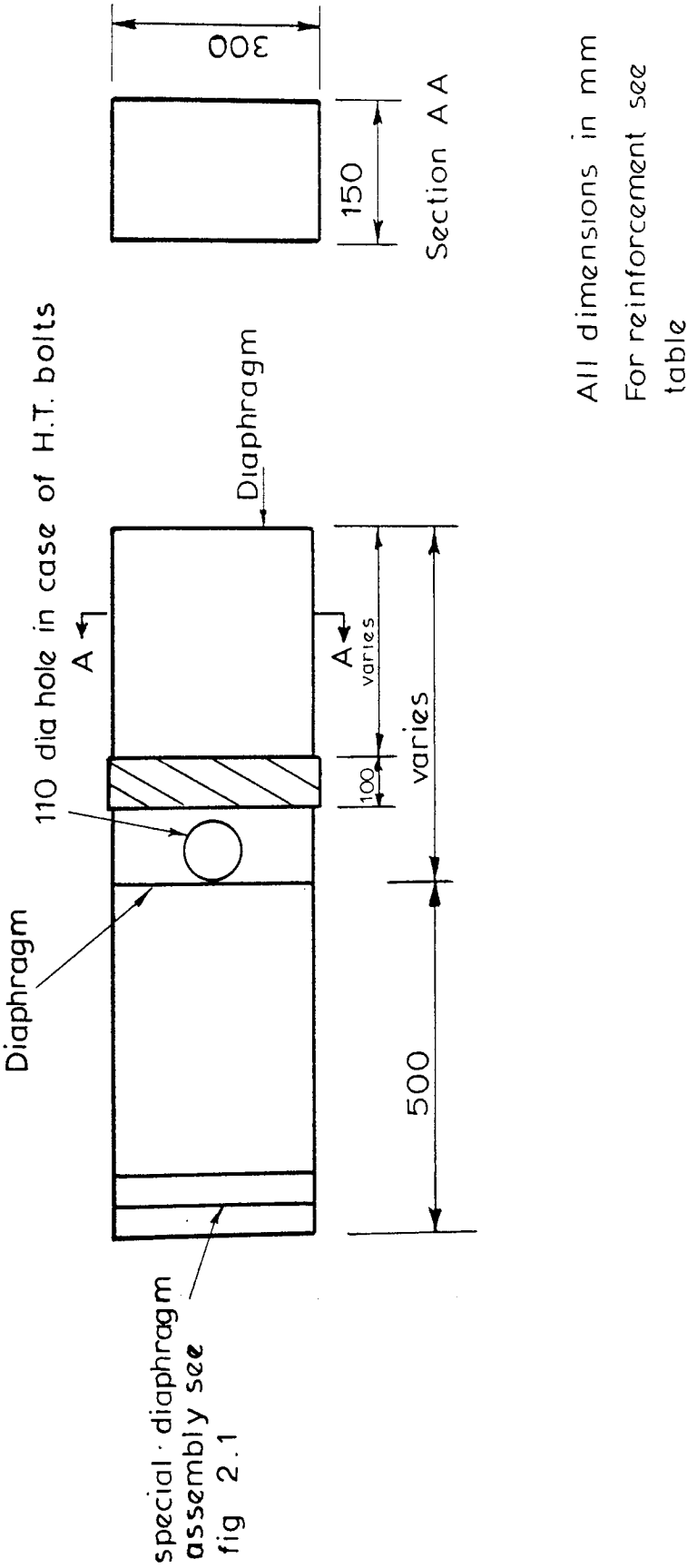

Fig. 3.13 Details of beam unit refrence beams $C_1 - C_4$

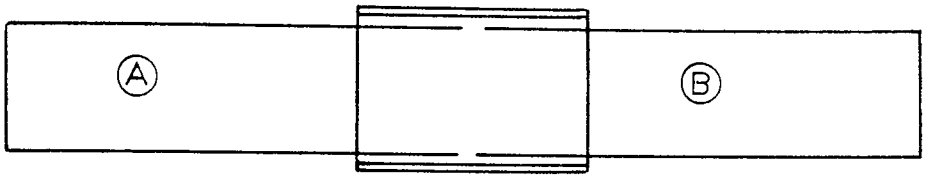

1. Correct alignment and drill holes

2. Separate both parts

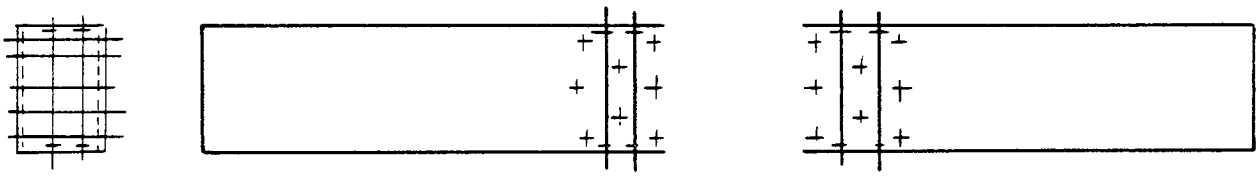

3. Insert tie bars and fix internal nuts

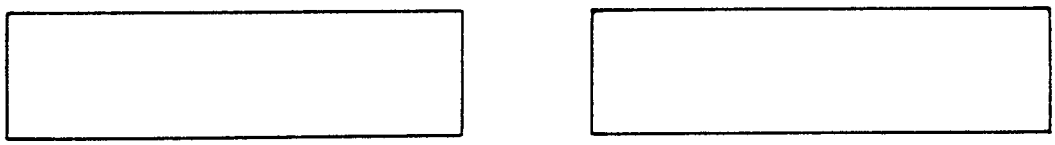

4. Fix end diaphragm

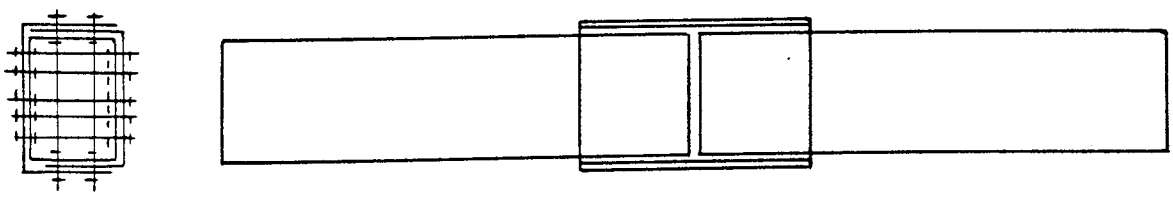

5. Enclose channel and fix outer nuts

Fig. 3. 14. Steps for connecting beam C_1 with tie bars.

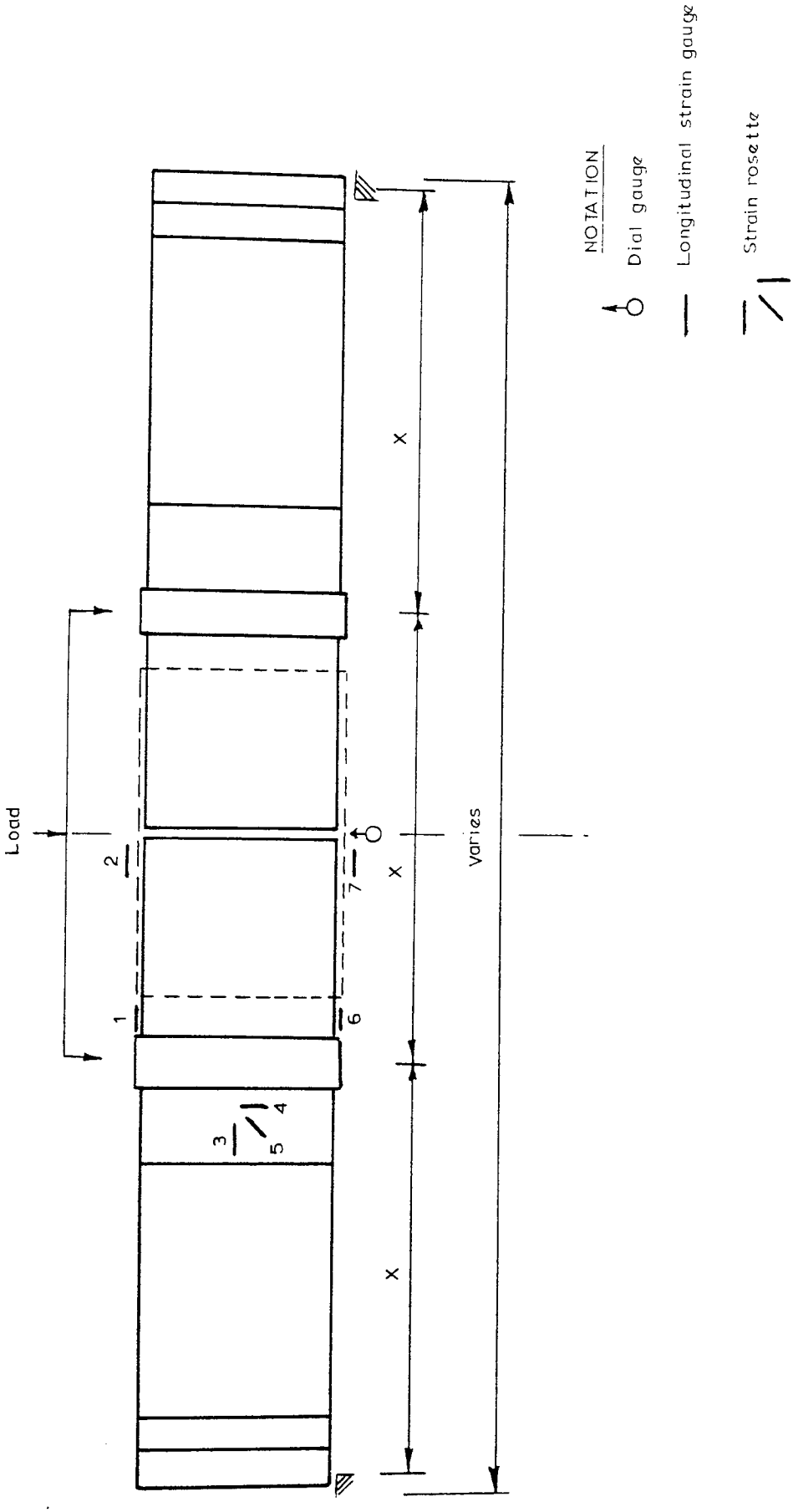

Fig. 3.15. Beams C_1 – C_4 assembly and instrumentation

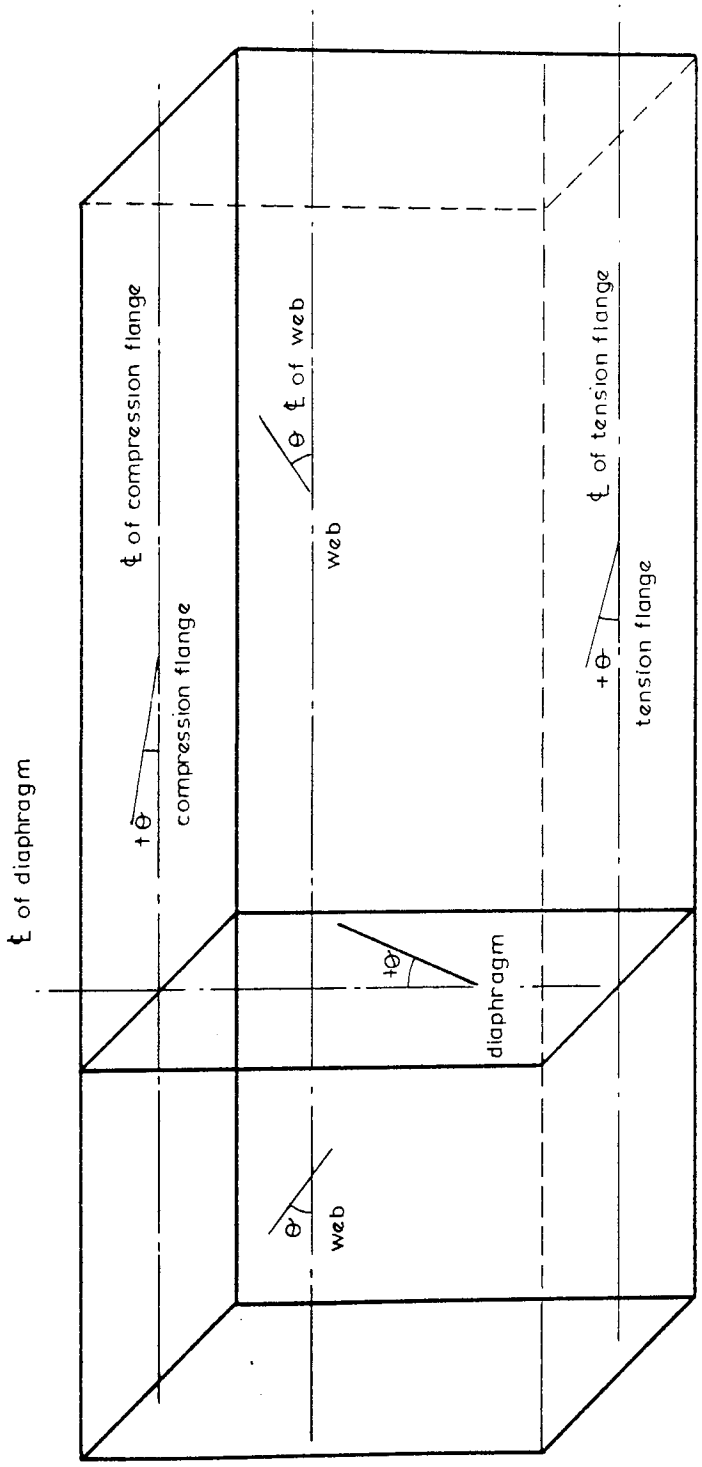

Fig. 3.16. Axis relative to fibre reinforcement orientation in box beam unit elements

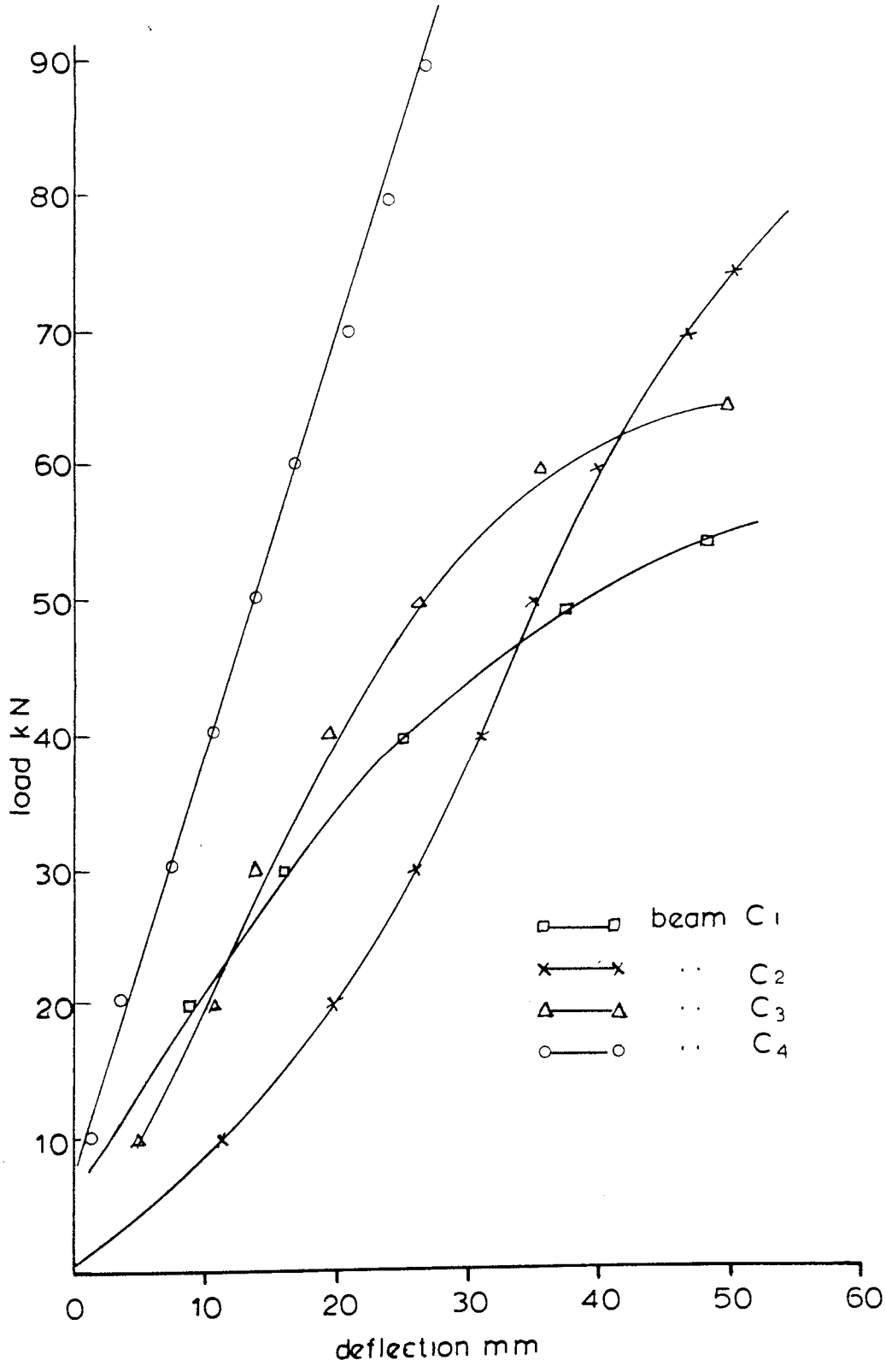

Fig .3.17 Load versus deflection beams C_1- C_4

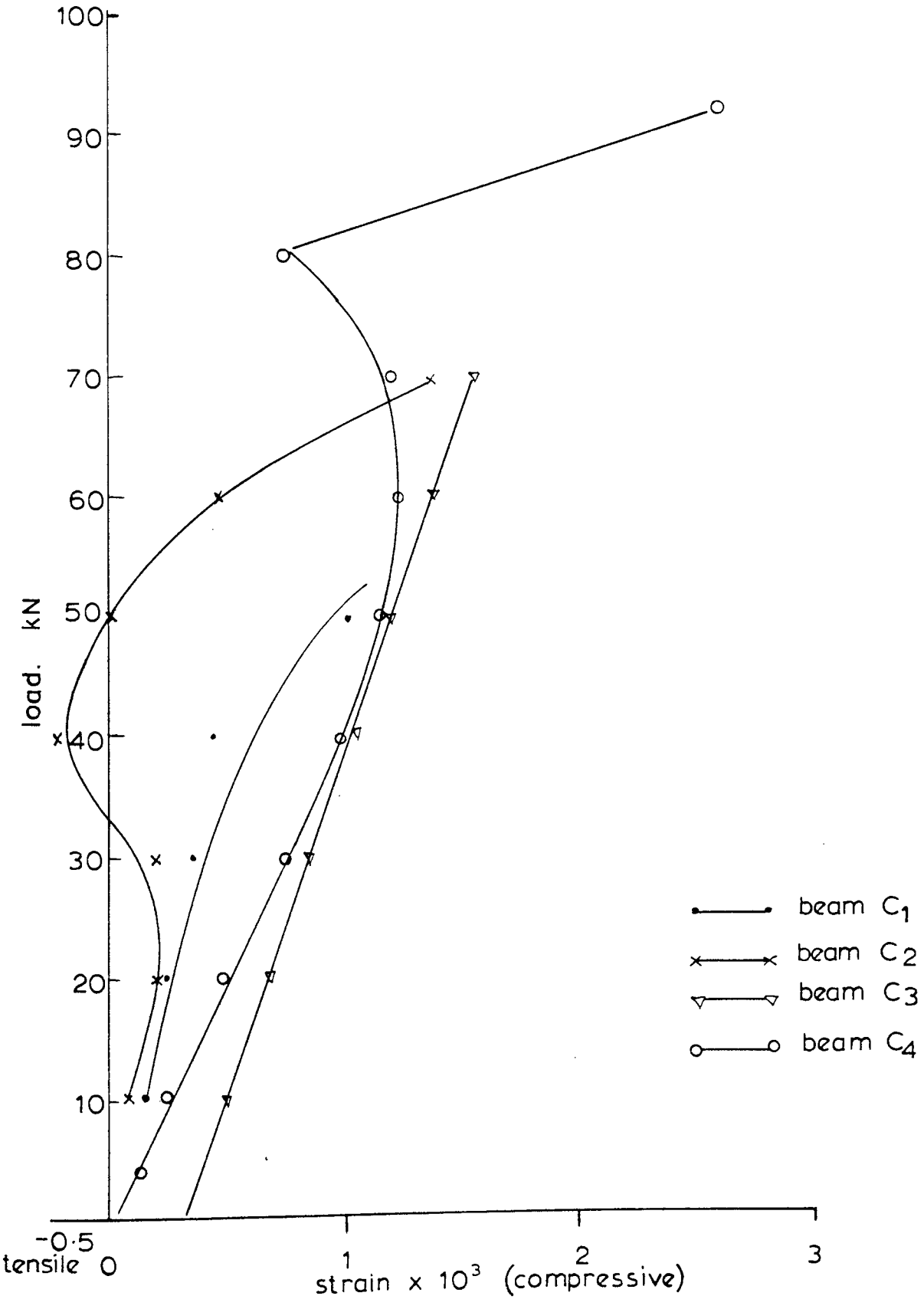

Fig . 3.18 Strain in comp. flange near joint (gauge 1)

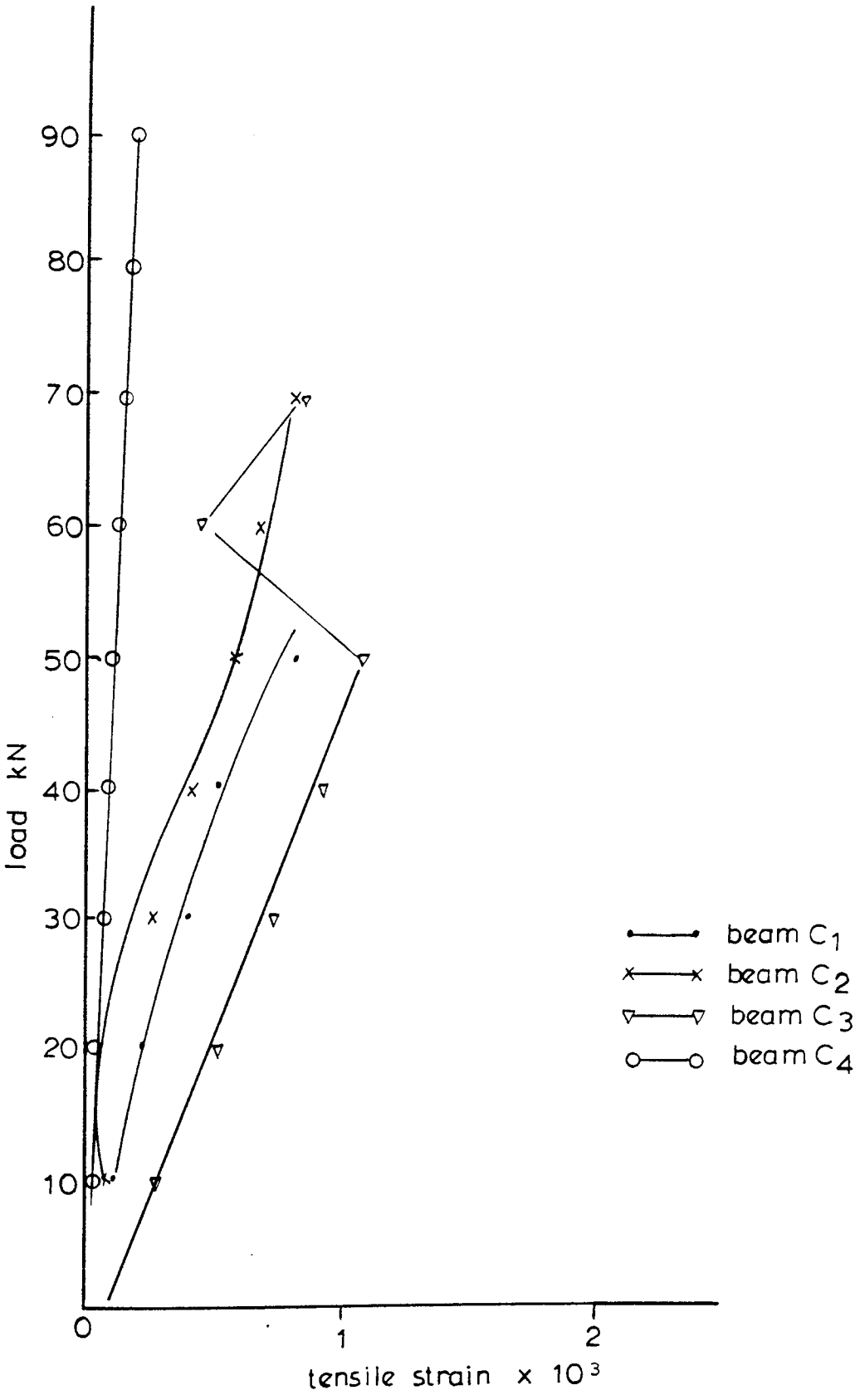

Fig. 3.19 Strain at the joint (gauge 7)

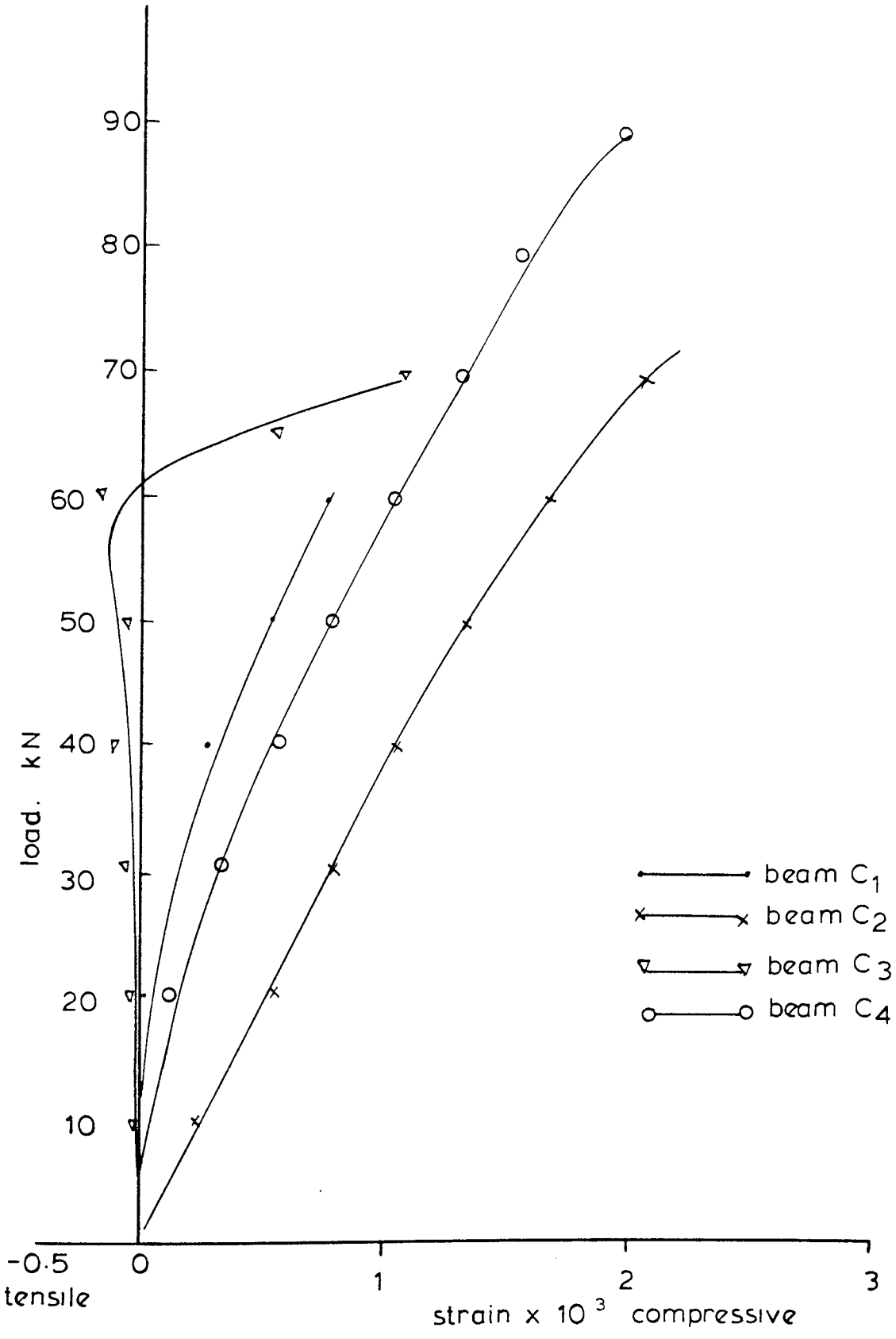

Fig. 3.20 Strain at the joint (gauge 2)

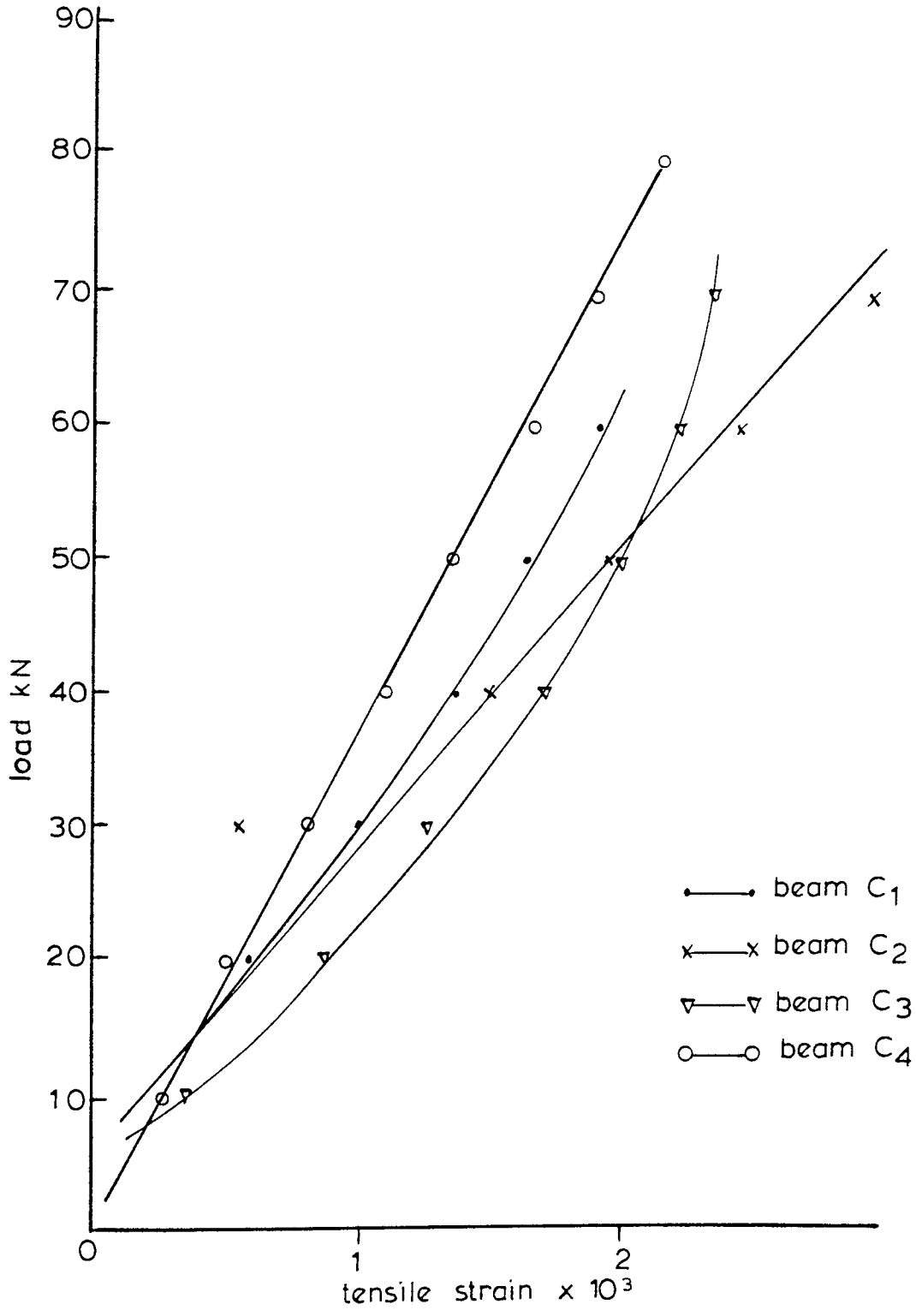

Fig. 3.21. Strain on the tension flange near joint (gauge 6)

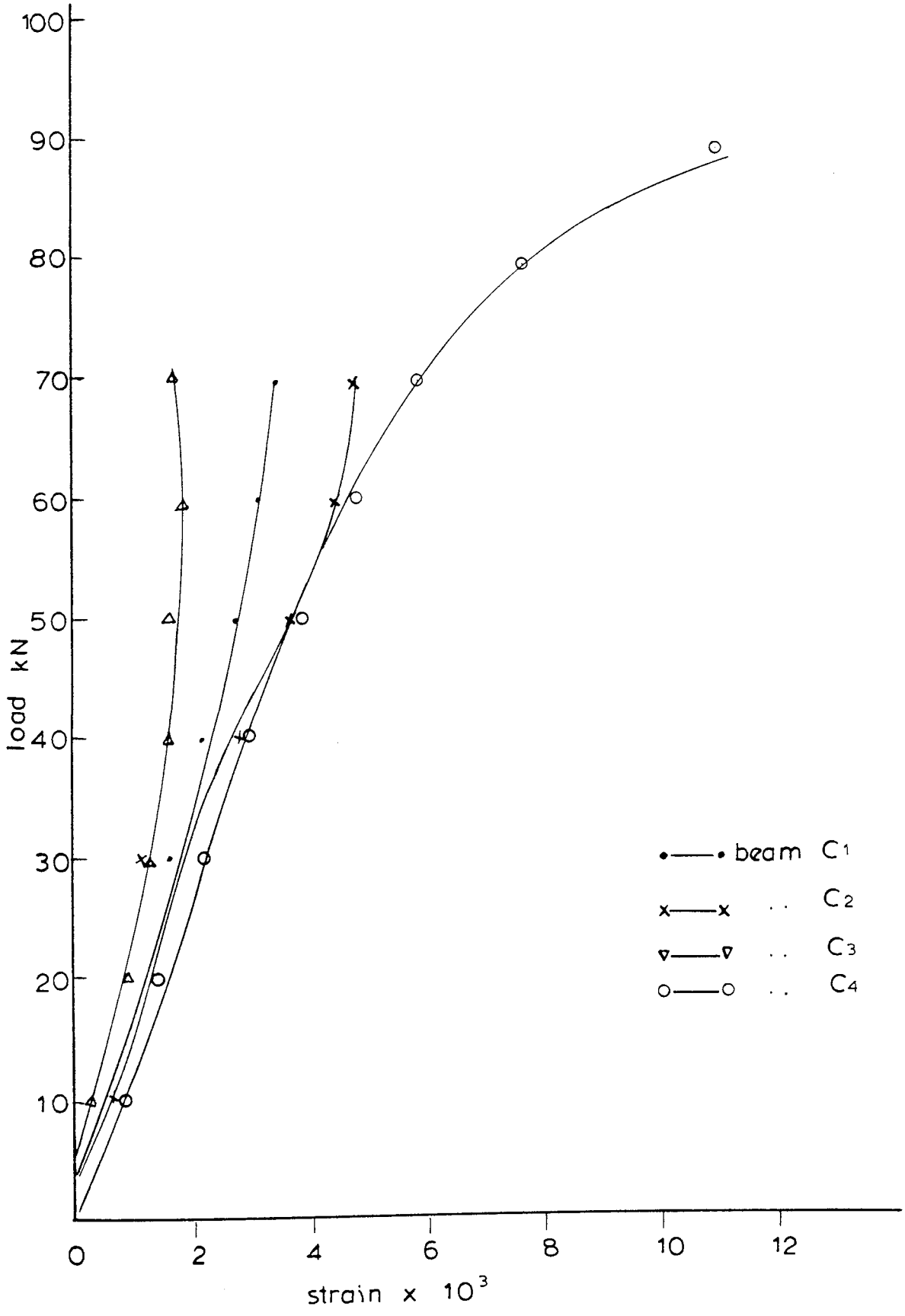

Fig. 3.22. Shear strain at centre of web near rib gauges (3.4.5)

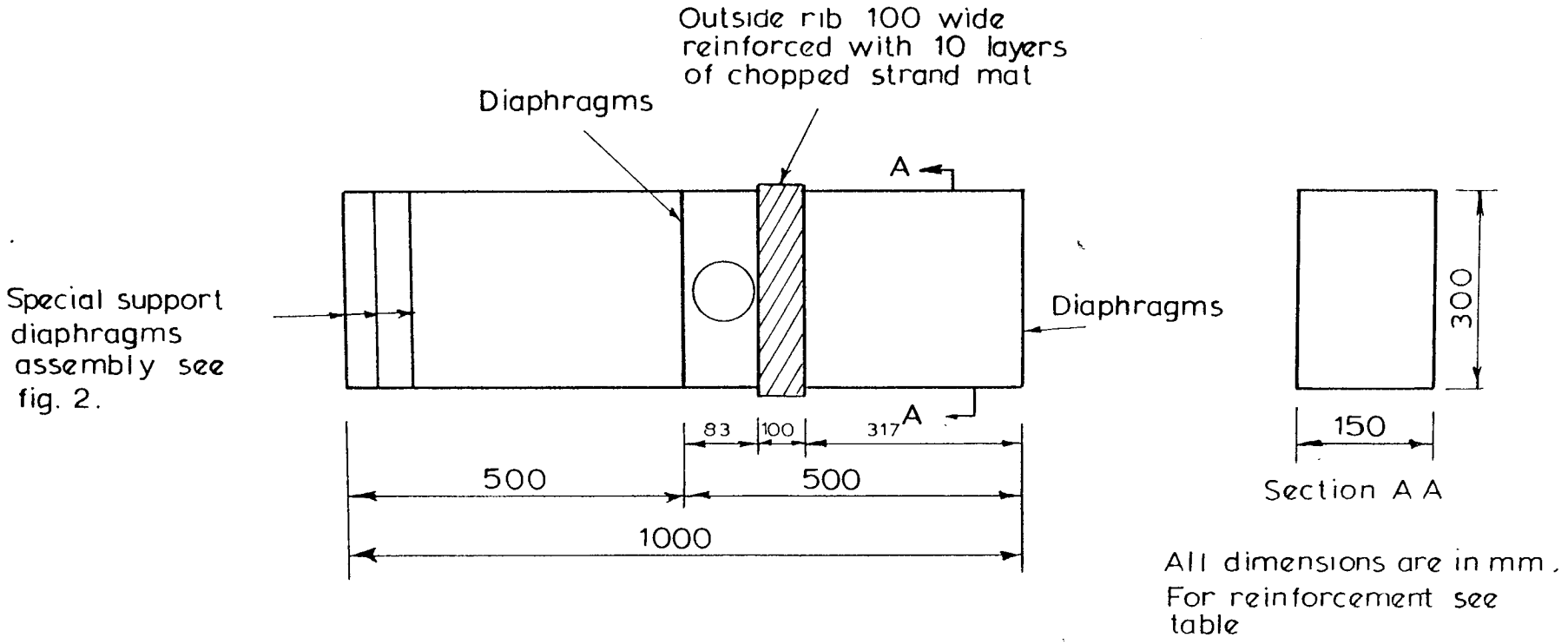

Fig. 3.23. Detail of beam unit reference beams $C_5 - C_9$

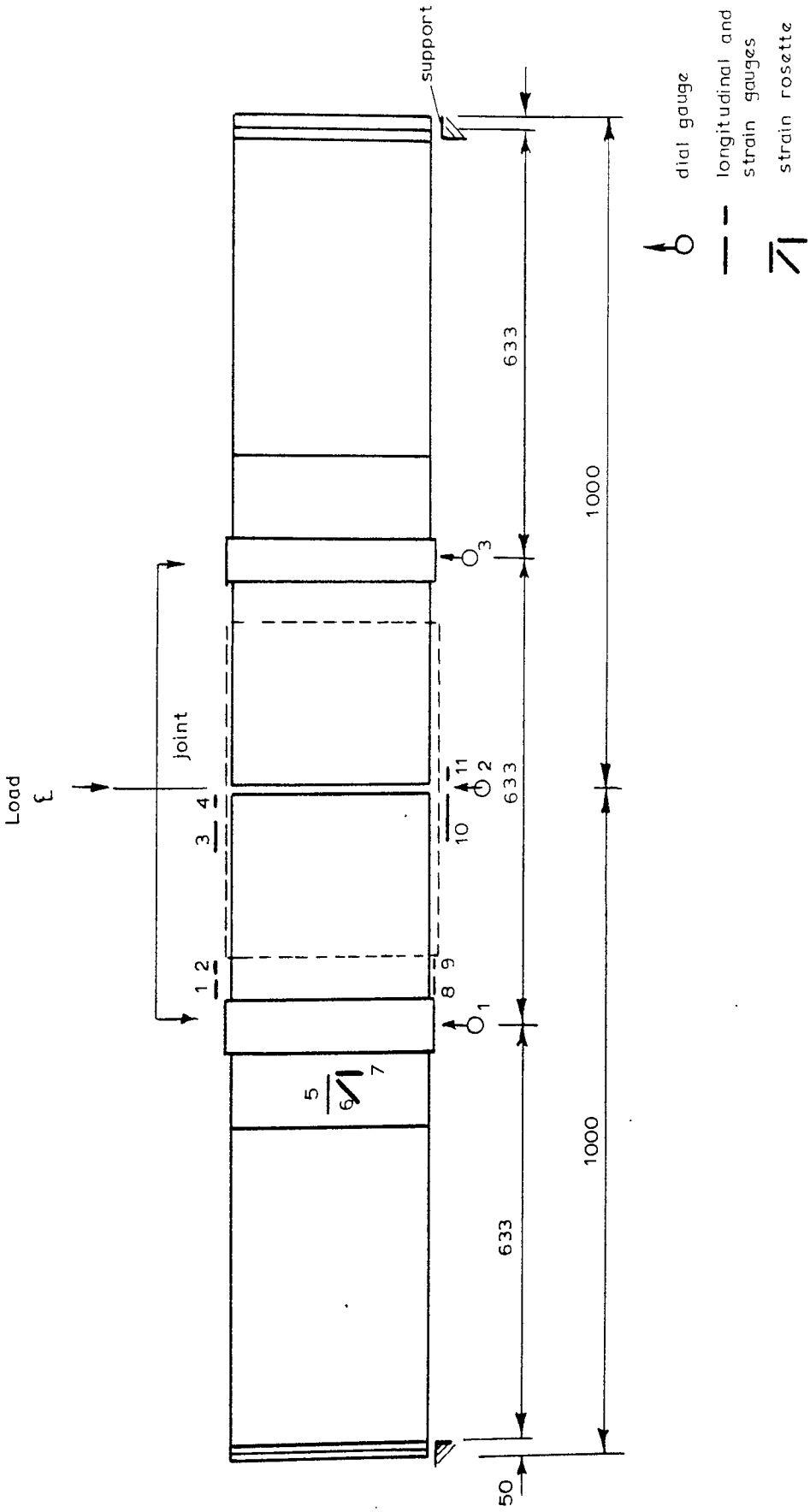

Fig .3.24. Beams $C_4 - C_9$ assembly and instrumentation

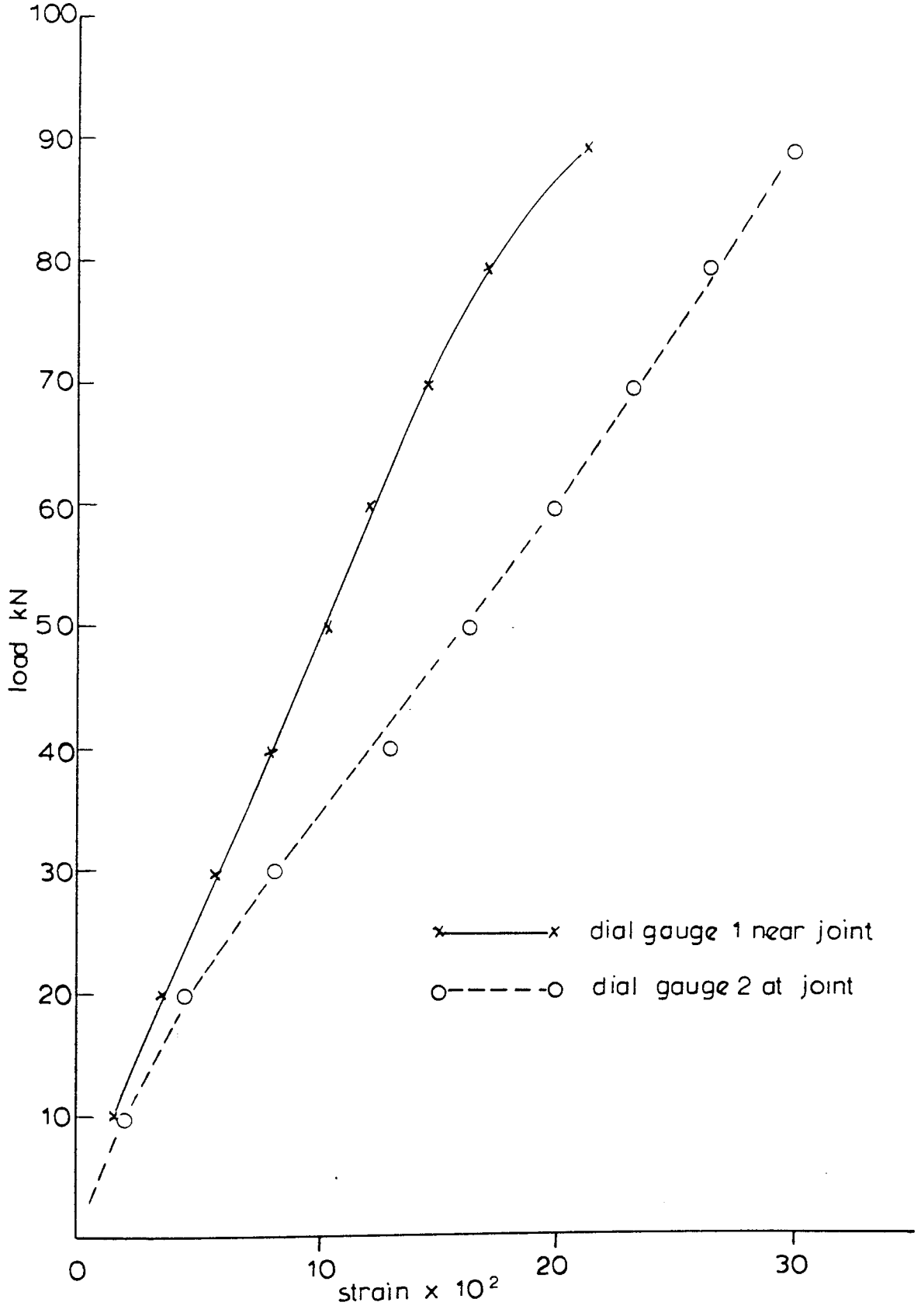

Fig. 3.25. Load versus deflection at and near joint beam C5

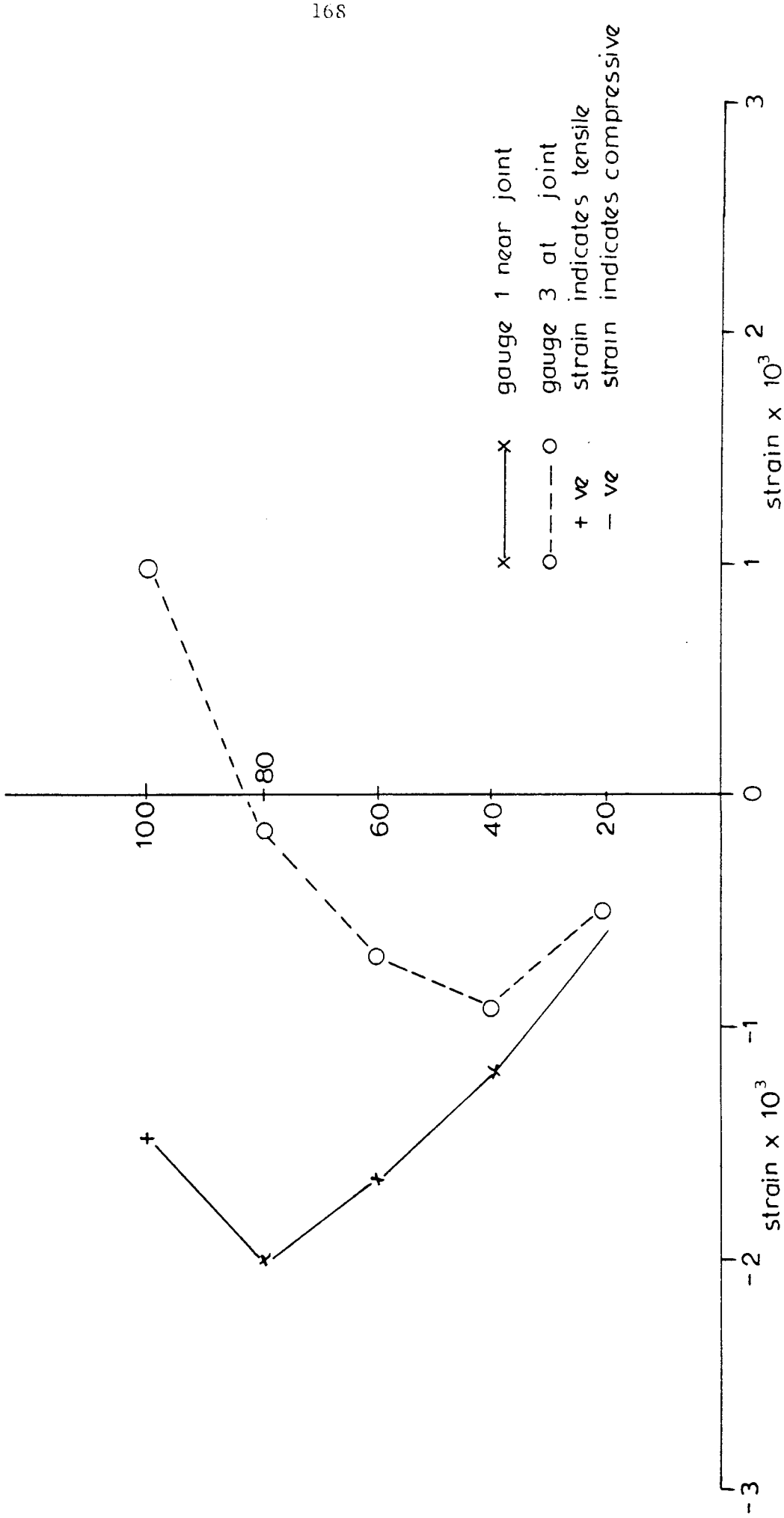

Fig. 3.26. Load versus strains at the compression flange at and near joint beam C_5

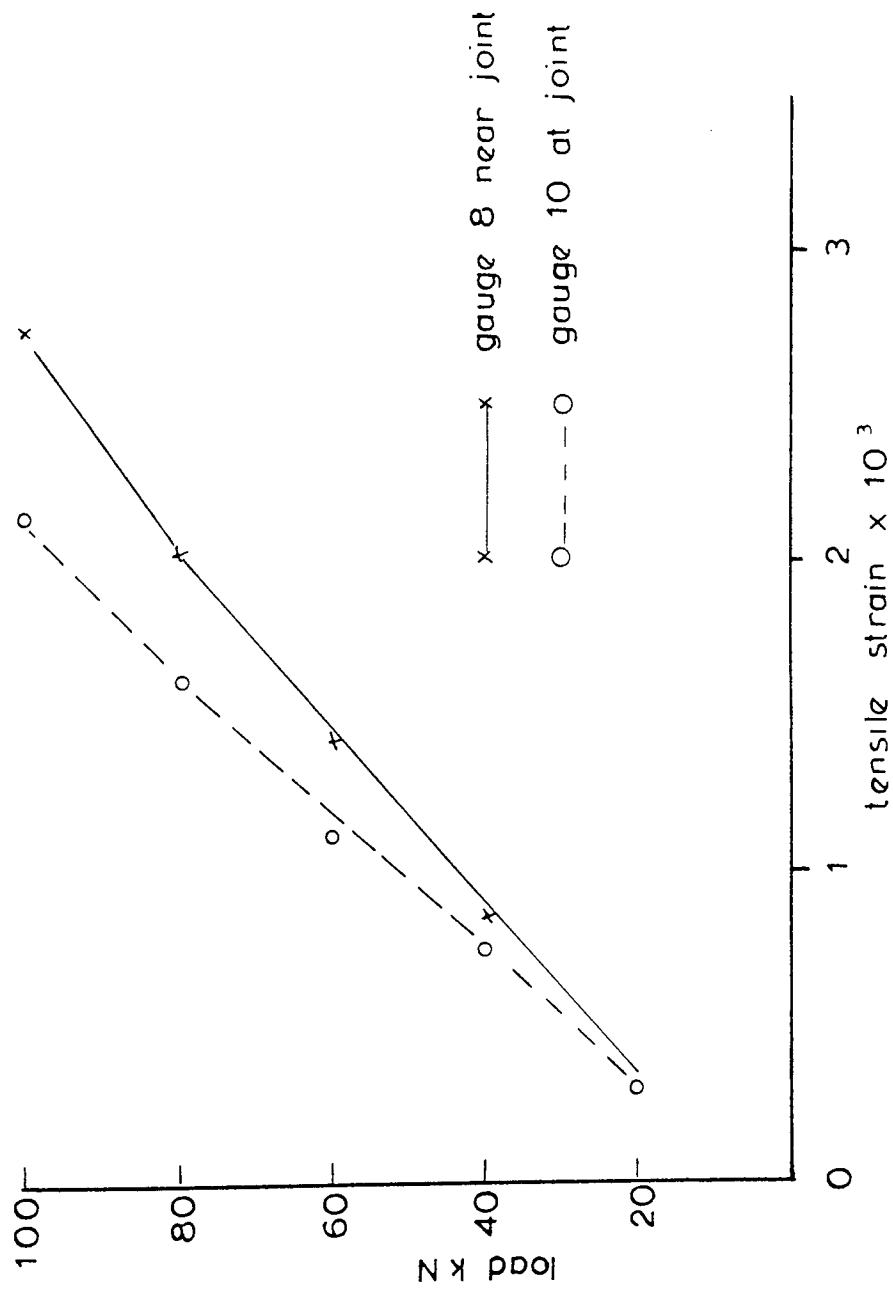

Fig. 3.27. Load versus strains on the tension flange at and near joint beam C_5

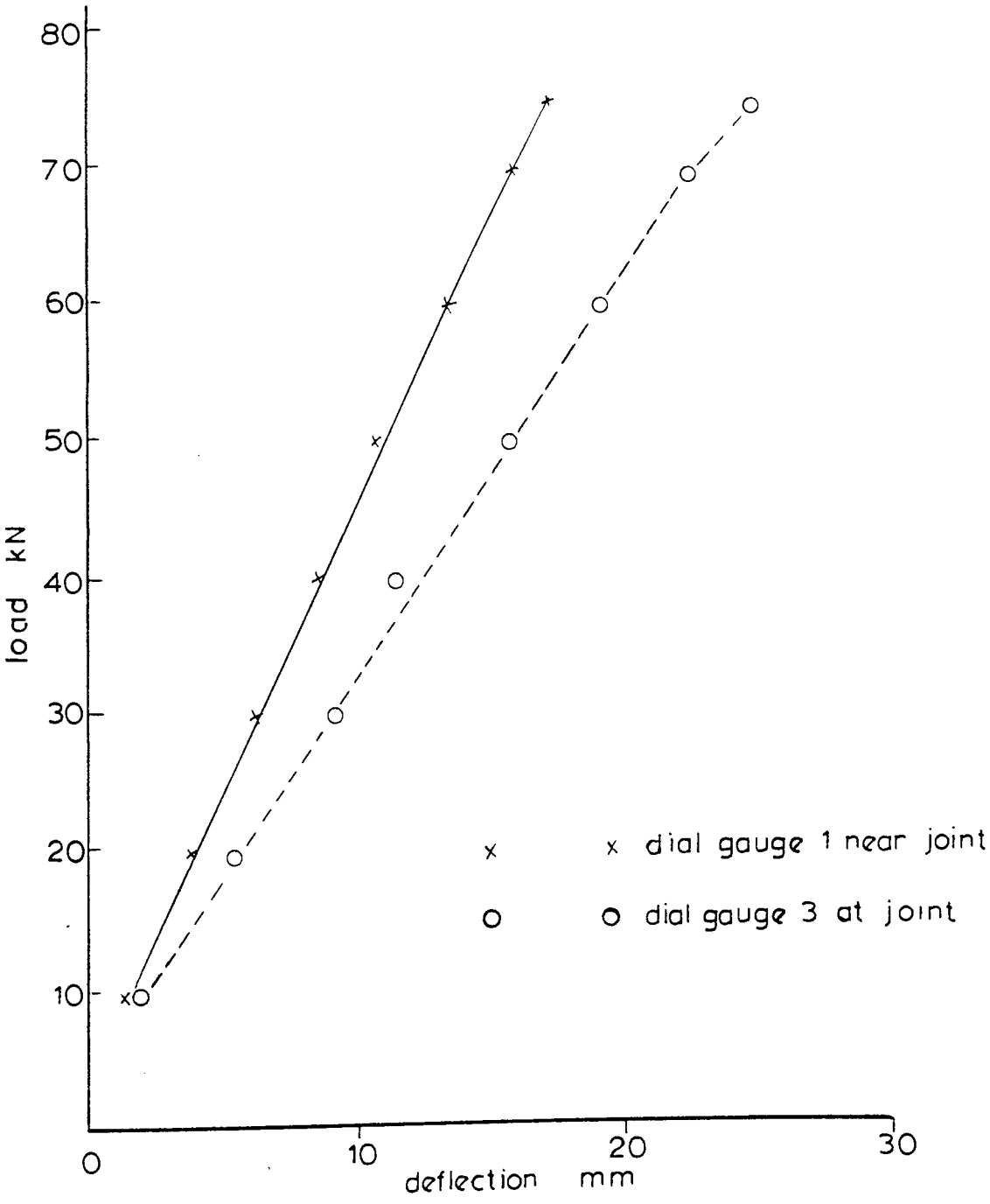

Fig. 3.28. Load versus deflection at and near joint beam C_6

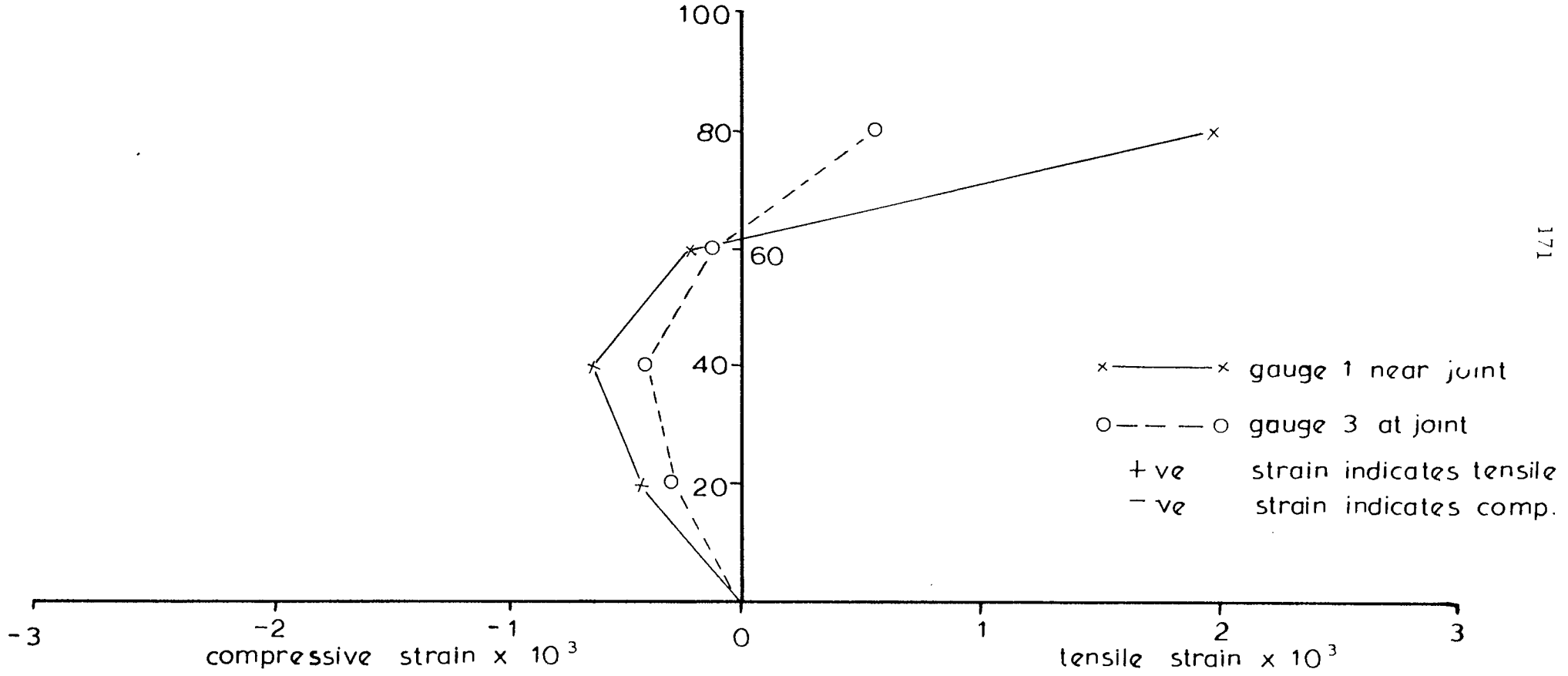

Fig. 3.29. Load versus strain on the compression flange at and near joint beam C_6

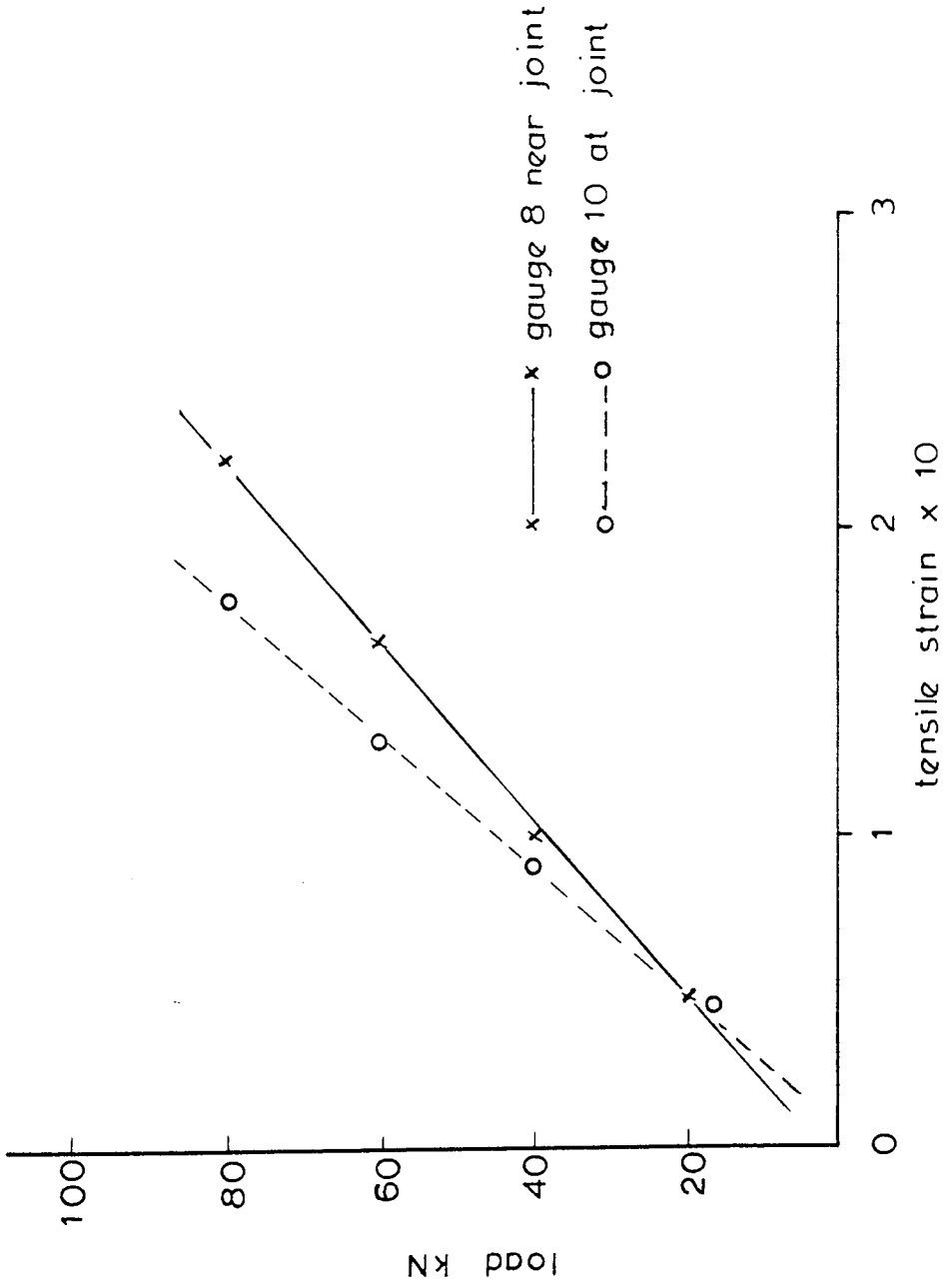

Fig. 3.30. Load versus strains on the flange at and near joint beam C_6

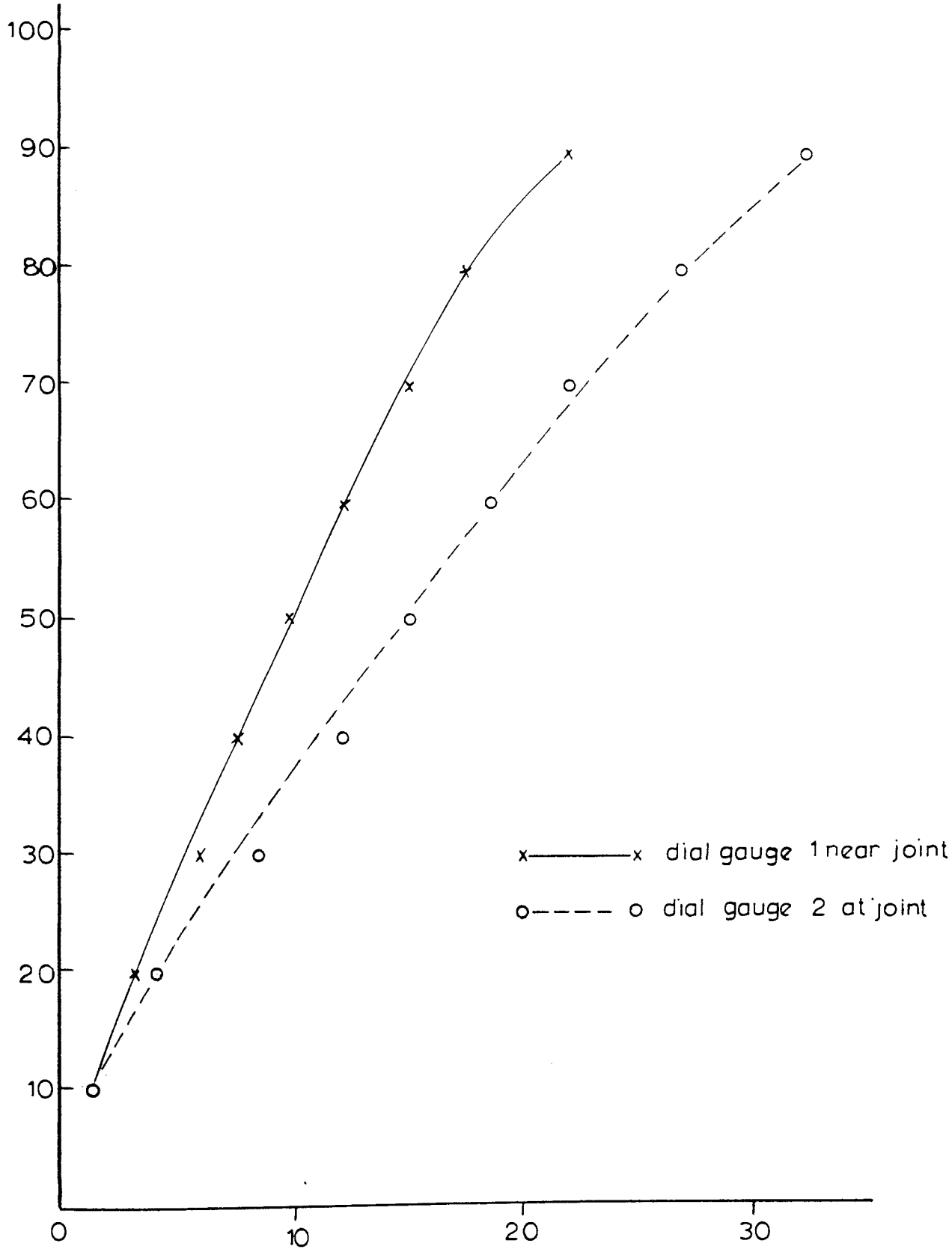

Fig. 3 31. Load versus deflection at and near joint beam C7

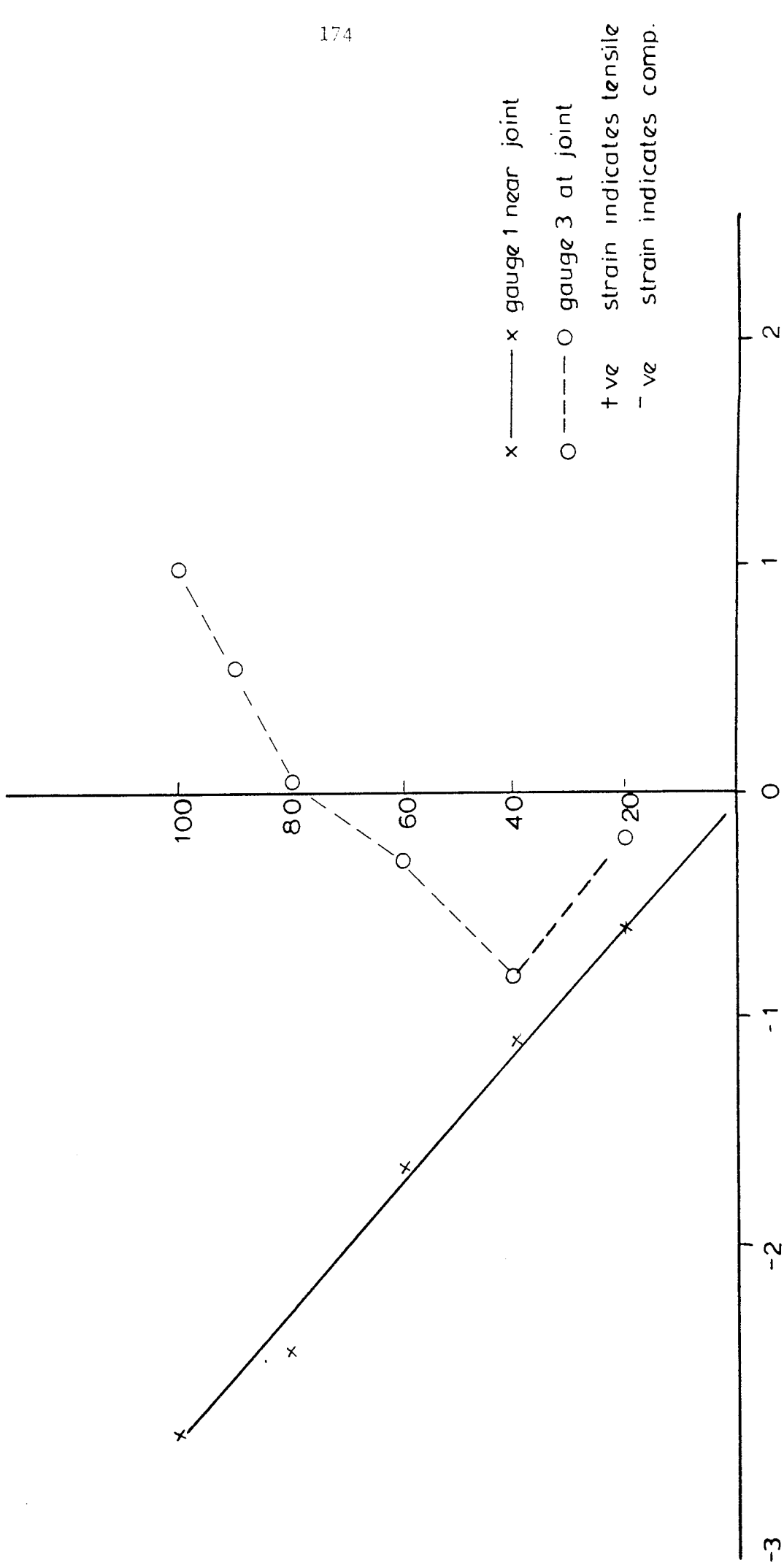

Fig. 3.32. Load versus strain at the compression flange at and near joint beam C_7

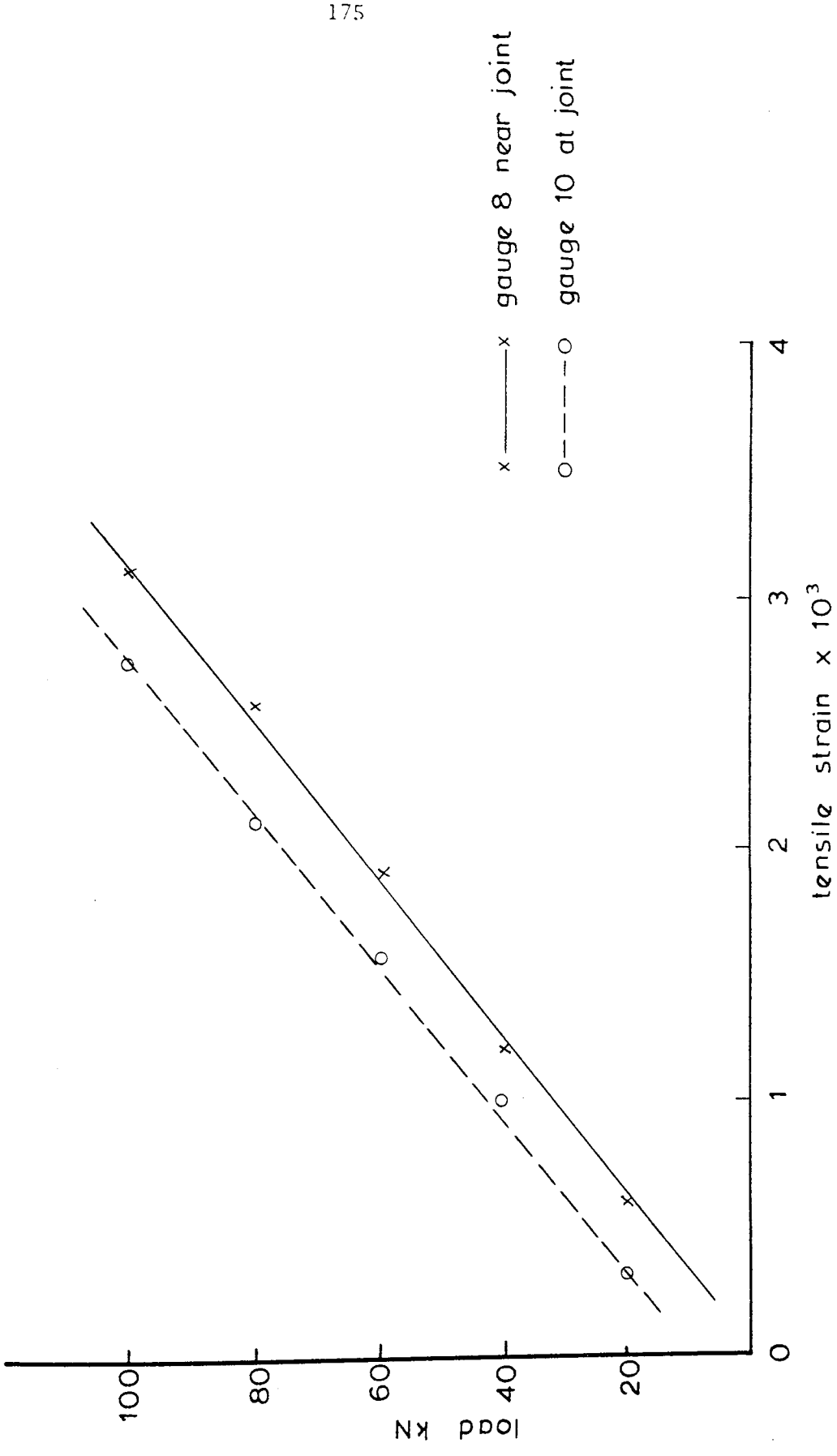

Fig. 3.33 Load versus strains on the tension flange at and near joint beam C_7

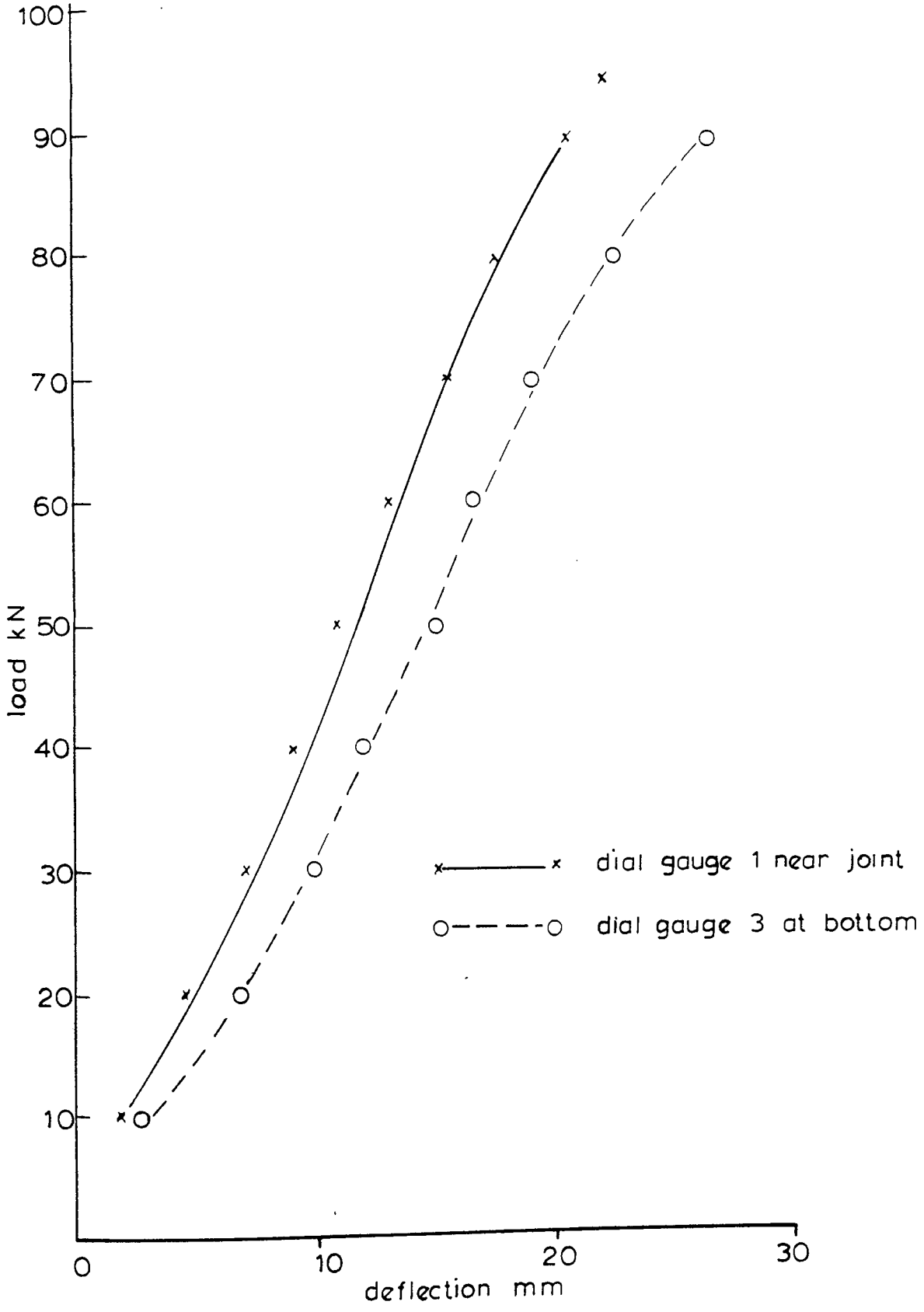

Fig. 3.34. Load versus deflection at and near joint beam C_8

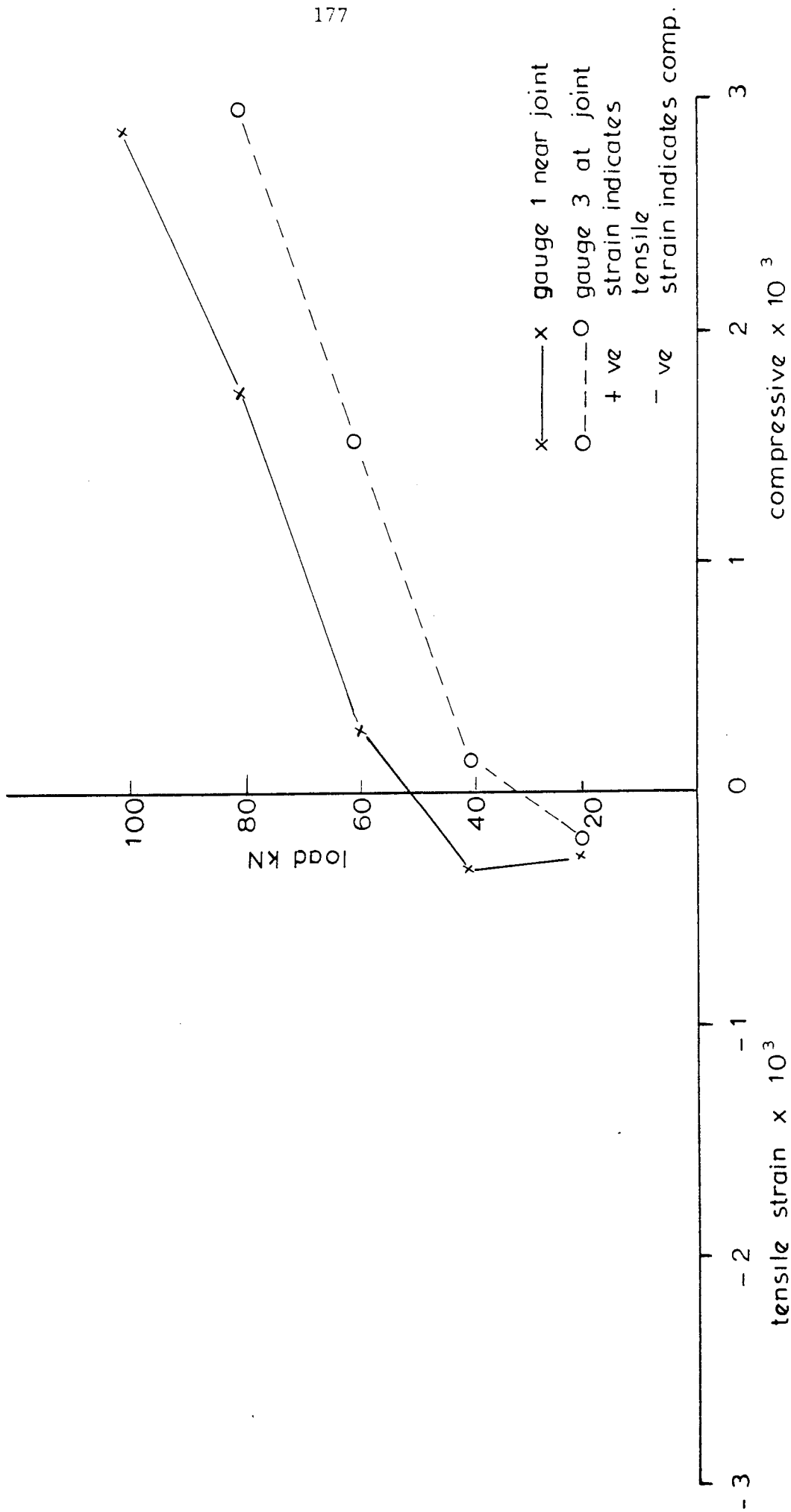

Fig. 3.35 Load versus strain on the compression flange at and near joint beam C_8

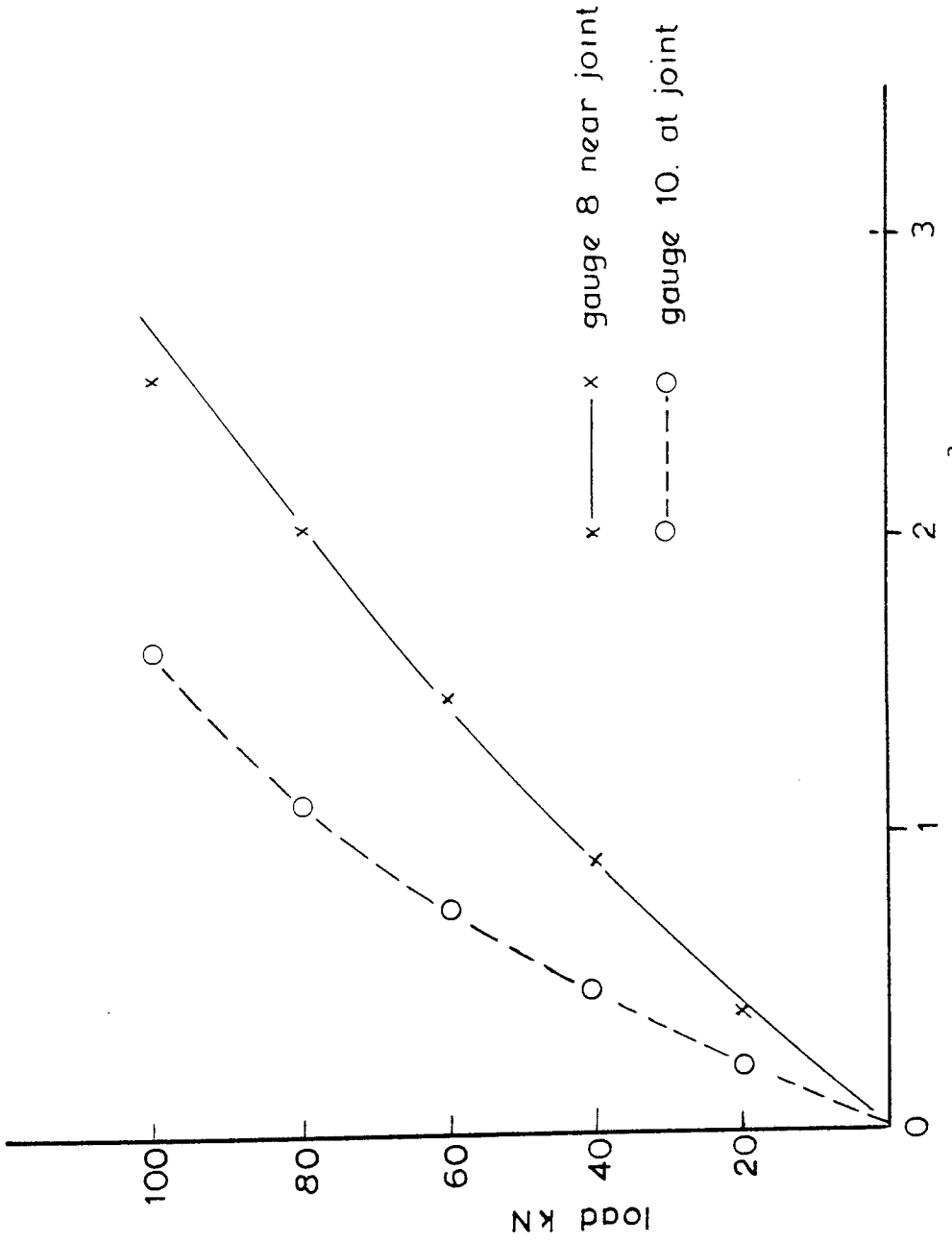

Fig. 3.36 Load versus strains on the tension flange at and near joint beam C_8

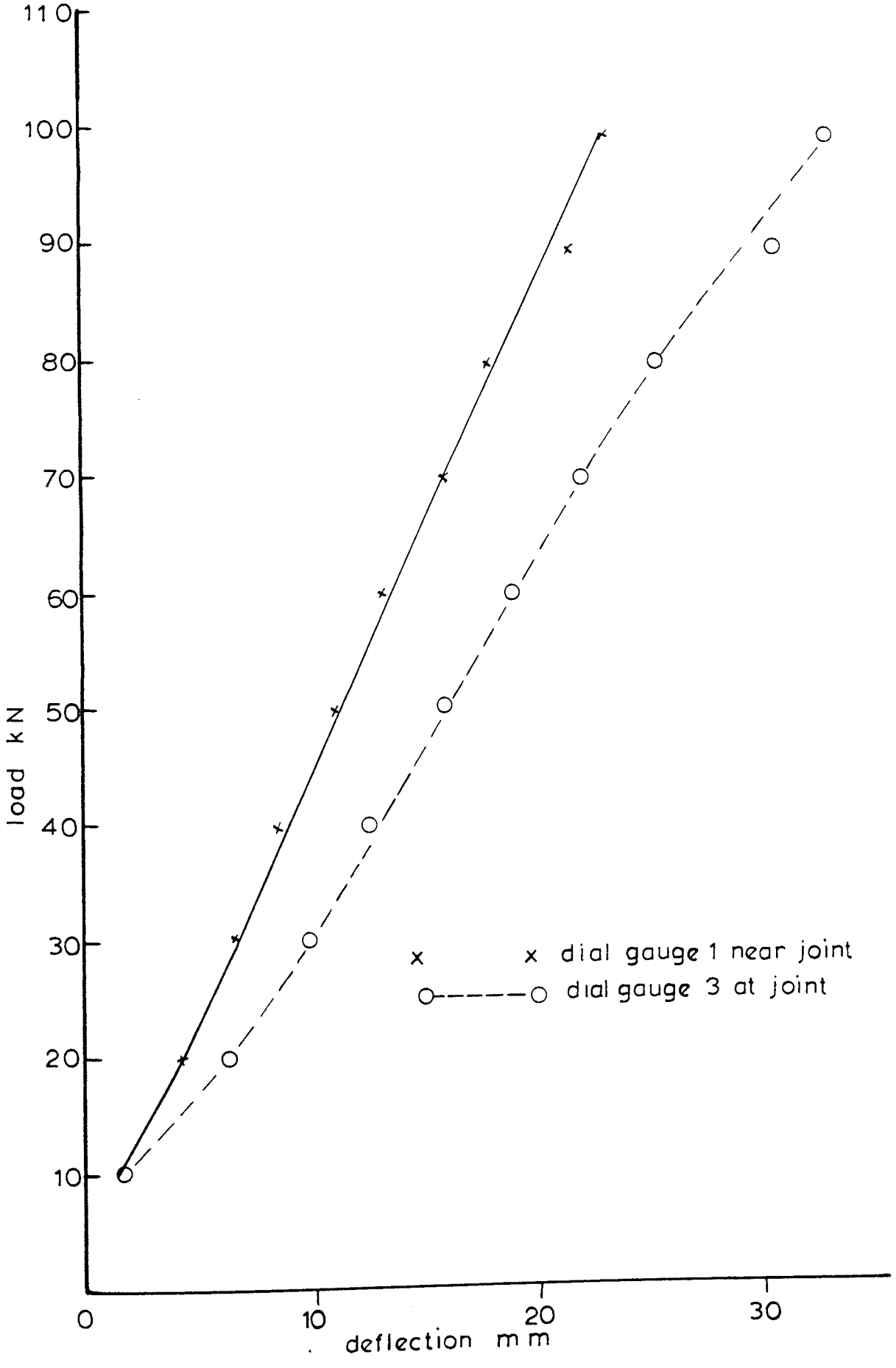

Fig. 3 37. Load versus deflection at and near joint beam C9

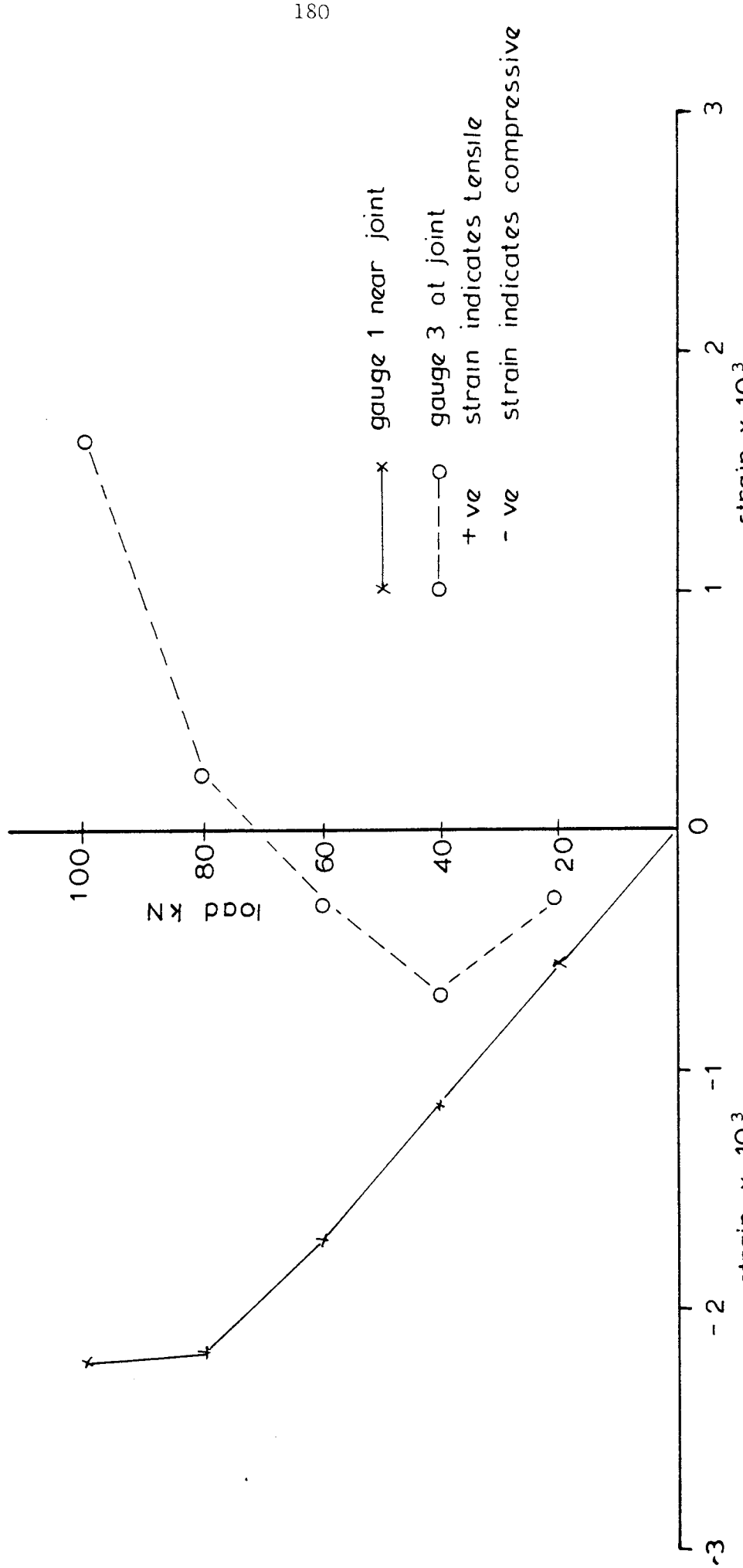

Fig. 3.38 Load versus strain at the compression flange at and near joint beam C_9

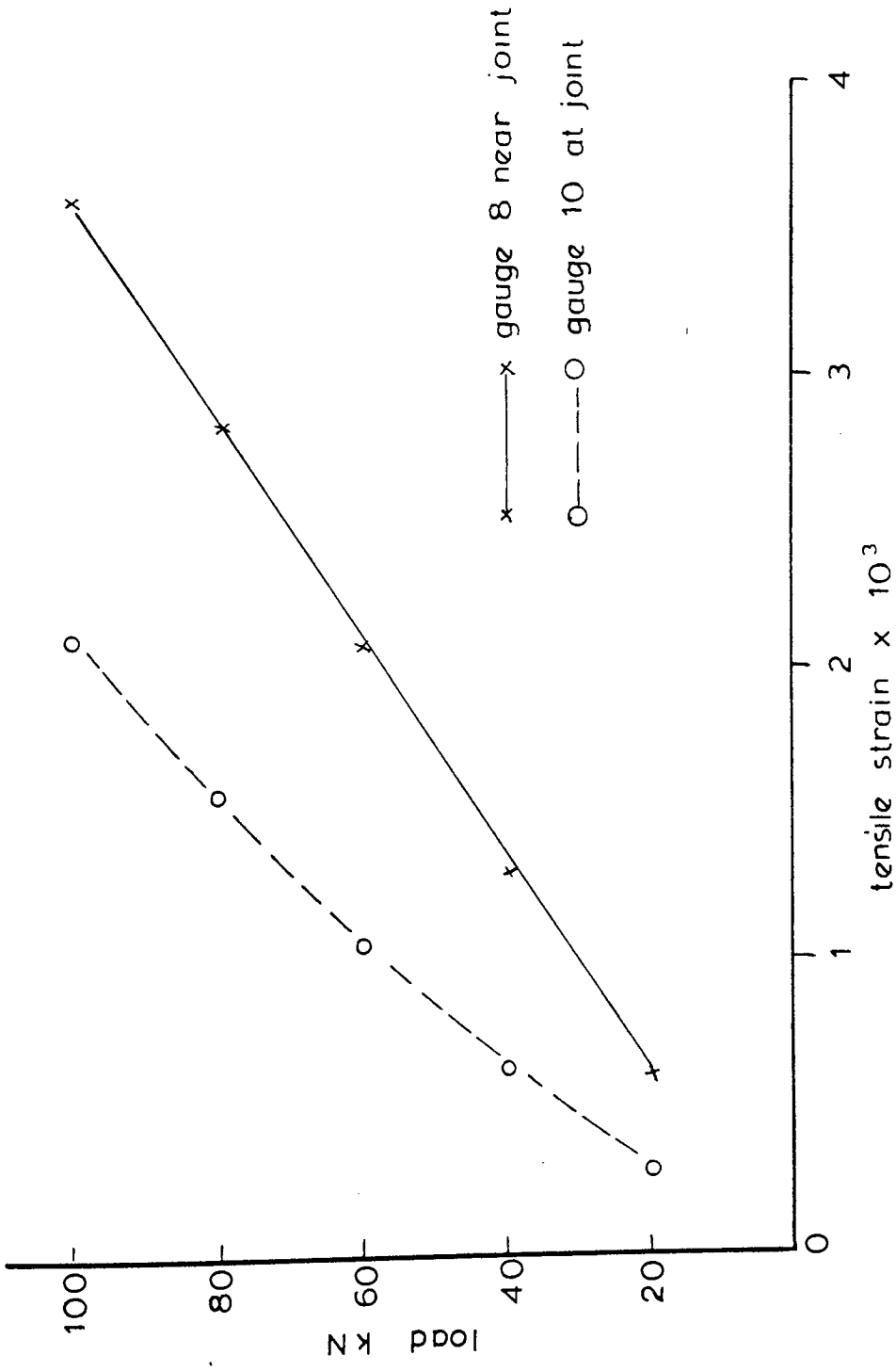

Fig. 3.39. Load versus strains on the tension flange at and near joint beam C_g.

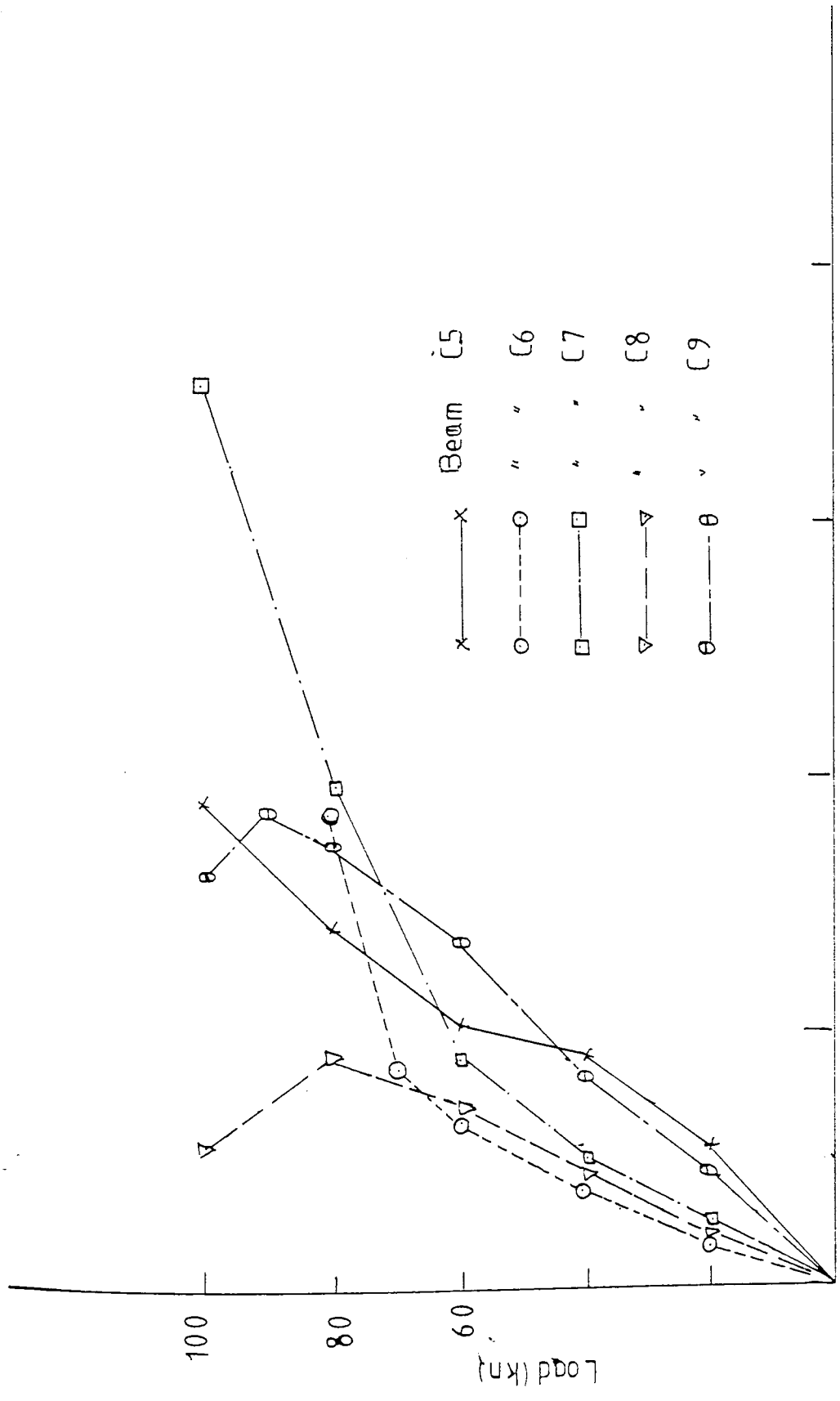

Fig 3.40 load versus shear strain at support beams type C4 – C9

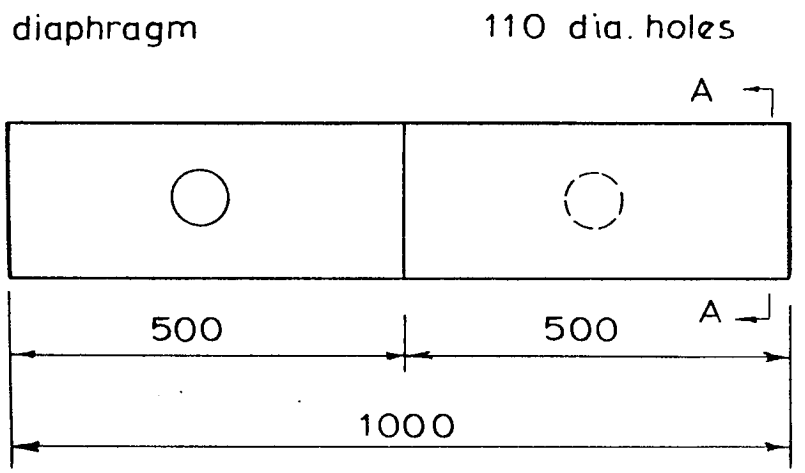

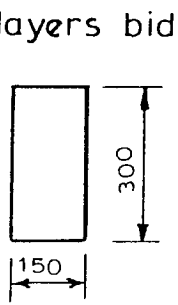

Section A A

Note – Special diaphragm support assembly fig 2 is included in the first and last beam units

Fig. 3.41 Detail of beam unit reference beam C_{10}

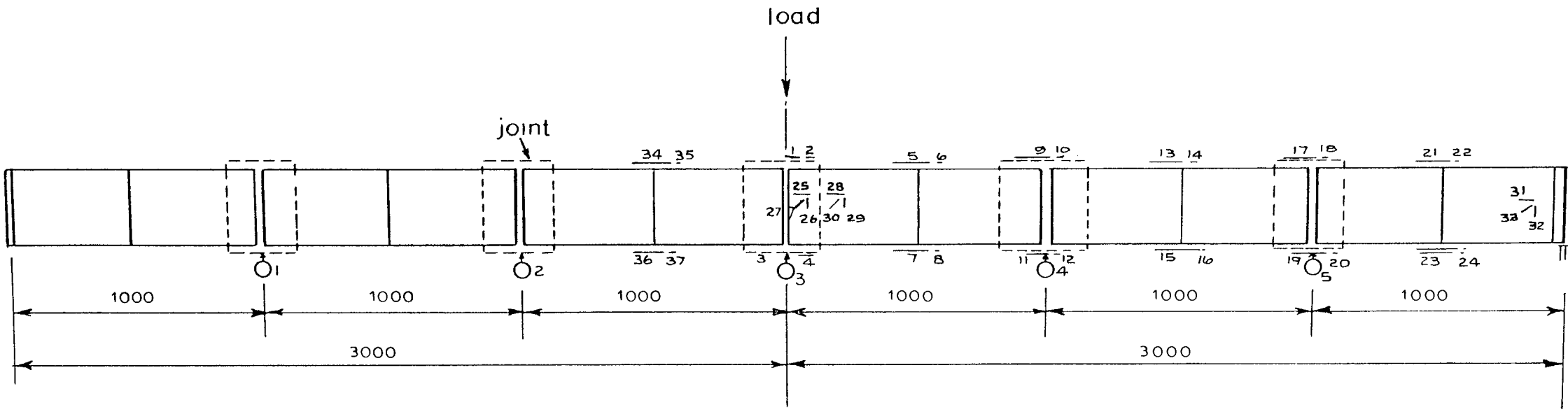

Note
- O Dial gauge
- — — Longitudinal and transverse strain gauges
- ⁻/1 Strain rosette

Dimensions in mm

Fig. 3.42 Beam C_{10} assembly and instrumentation

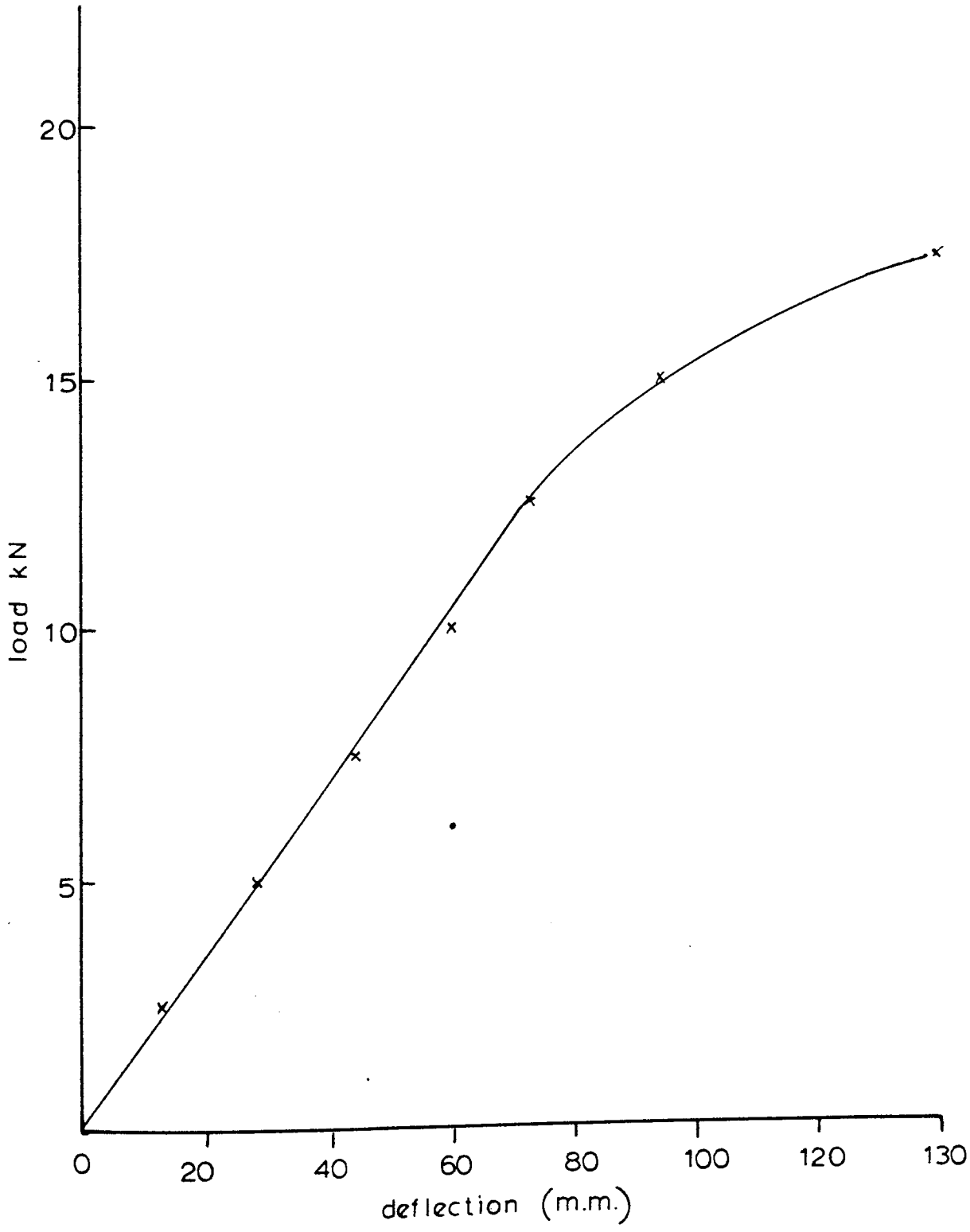

Fig. 3.43. Load versus mid span deflection beam C_{10}

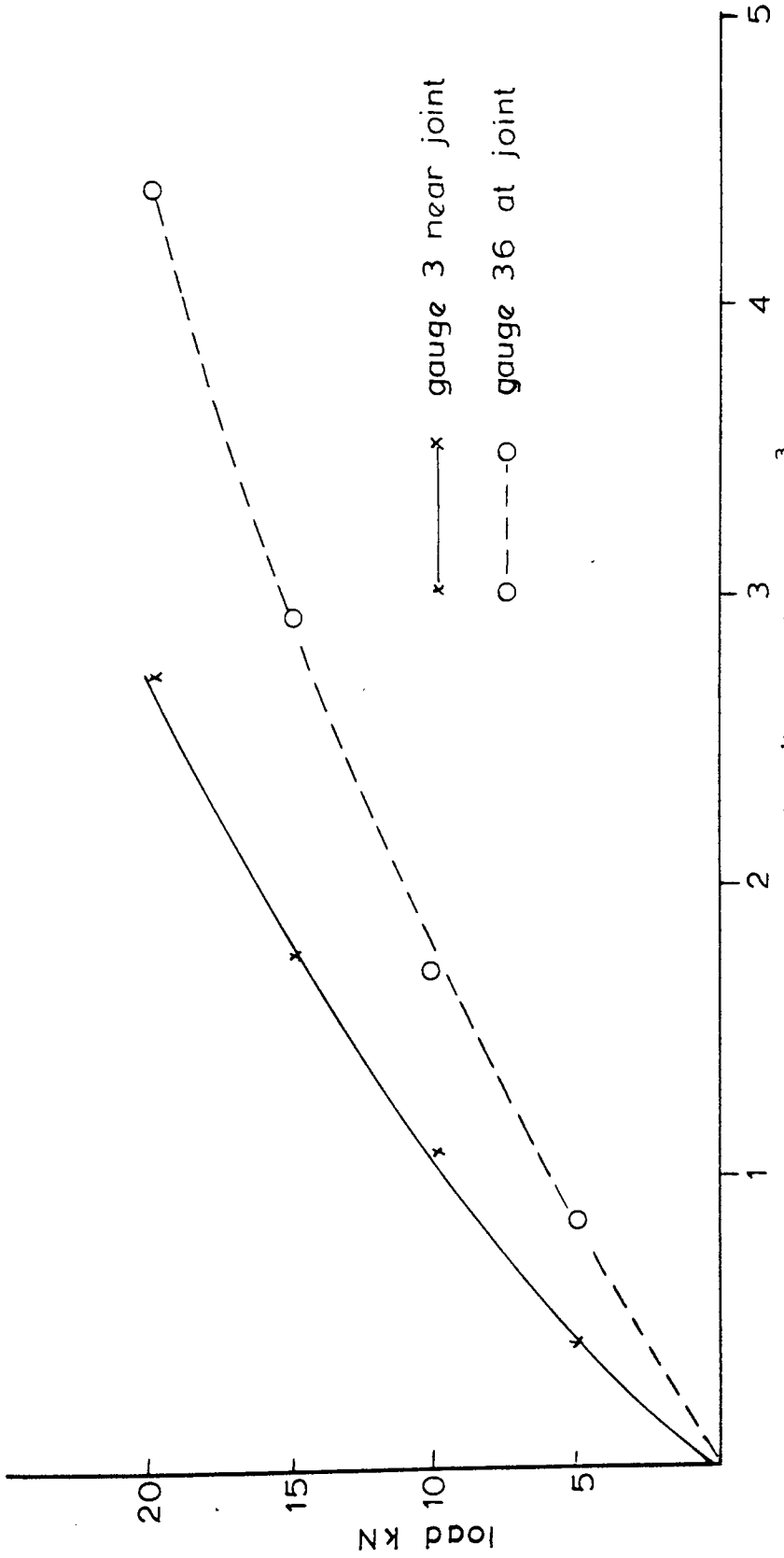

Fig. 3.44. Load versus strain in tension flange at and near joint beam C_{10}

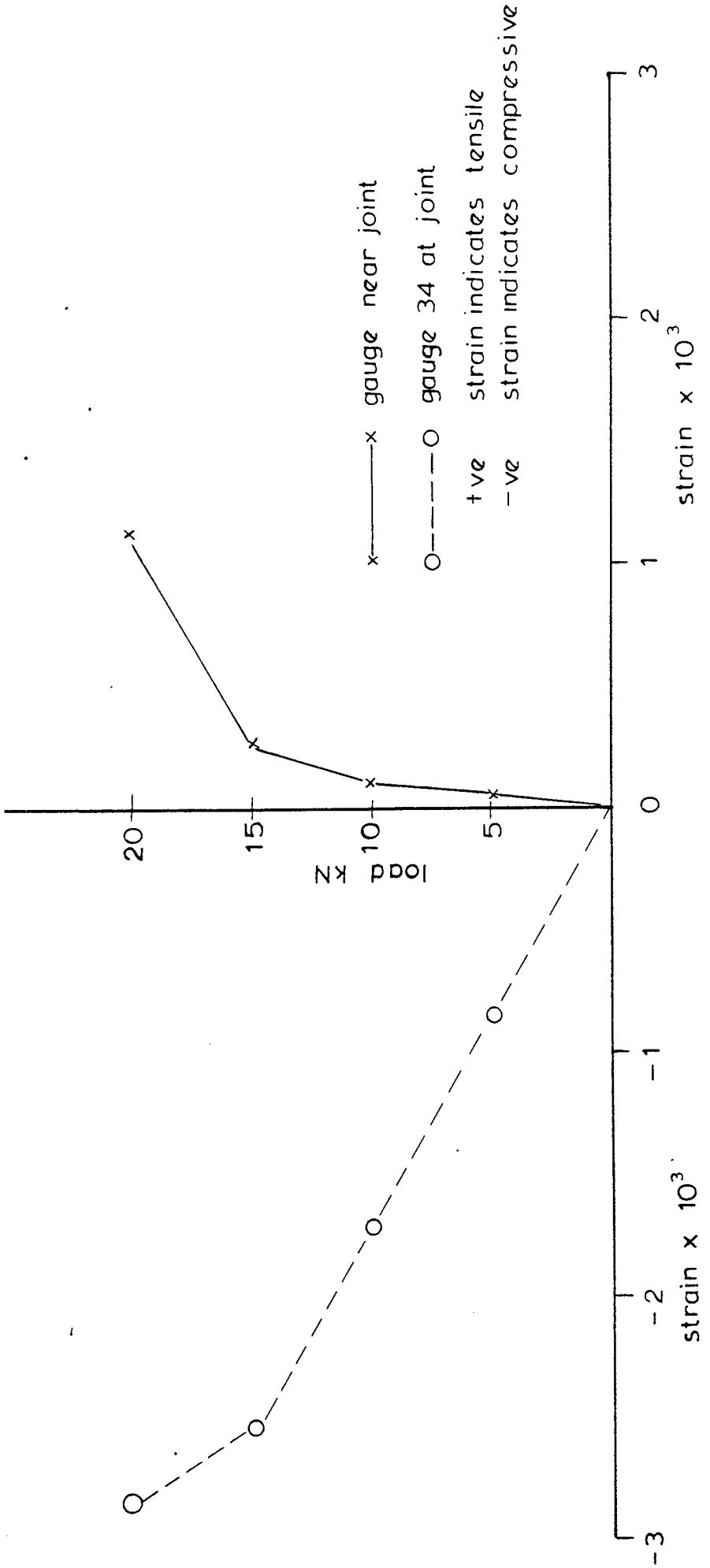

Fig. 3.45 Load versus strain in compression flange at and near joint beam C.10

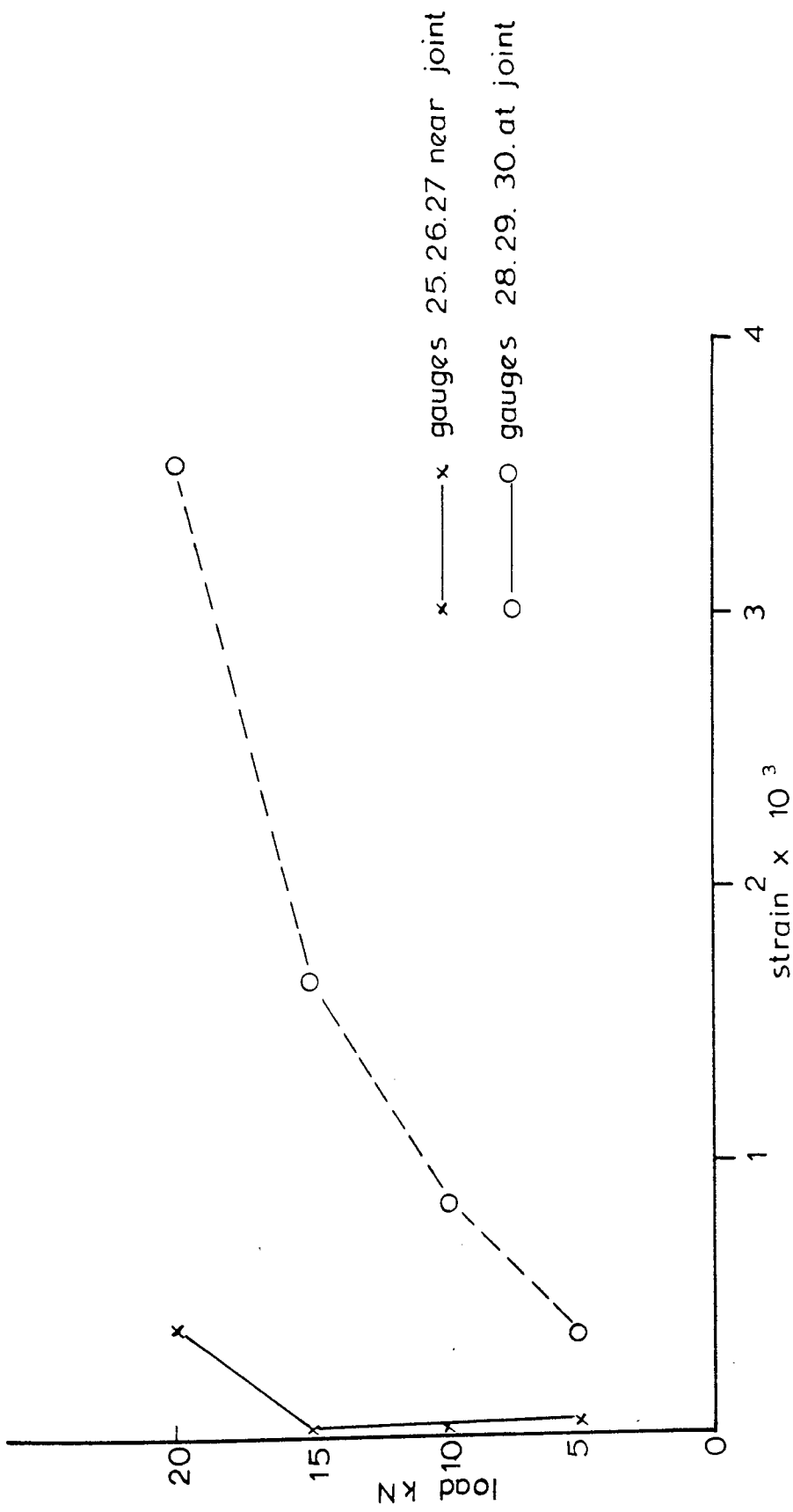

Fig 3.46 Load versus shear strain at and a way from joint beam C_{10}

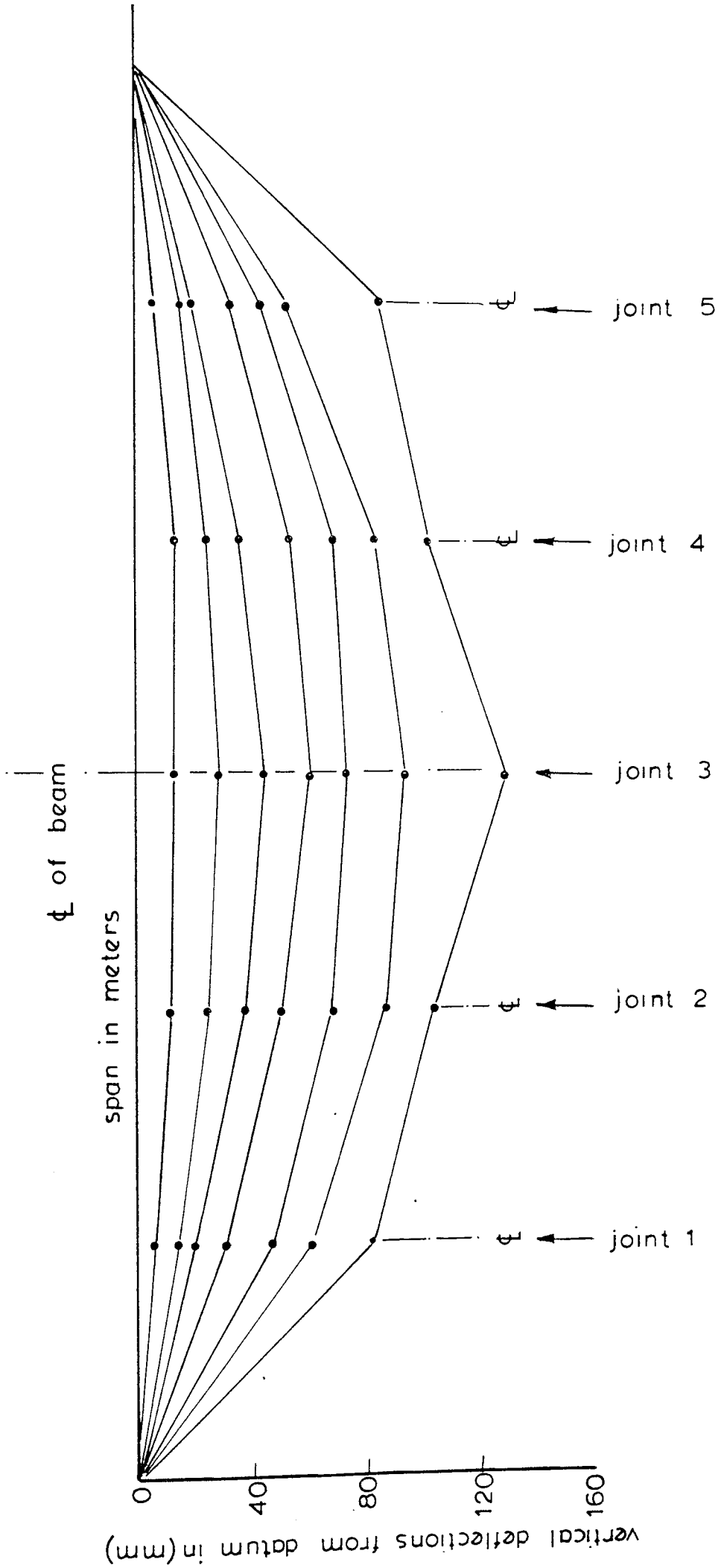

Fig. 3.47 Vertical profile along the span (beam type C_{10}) at loading increments

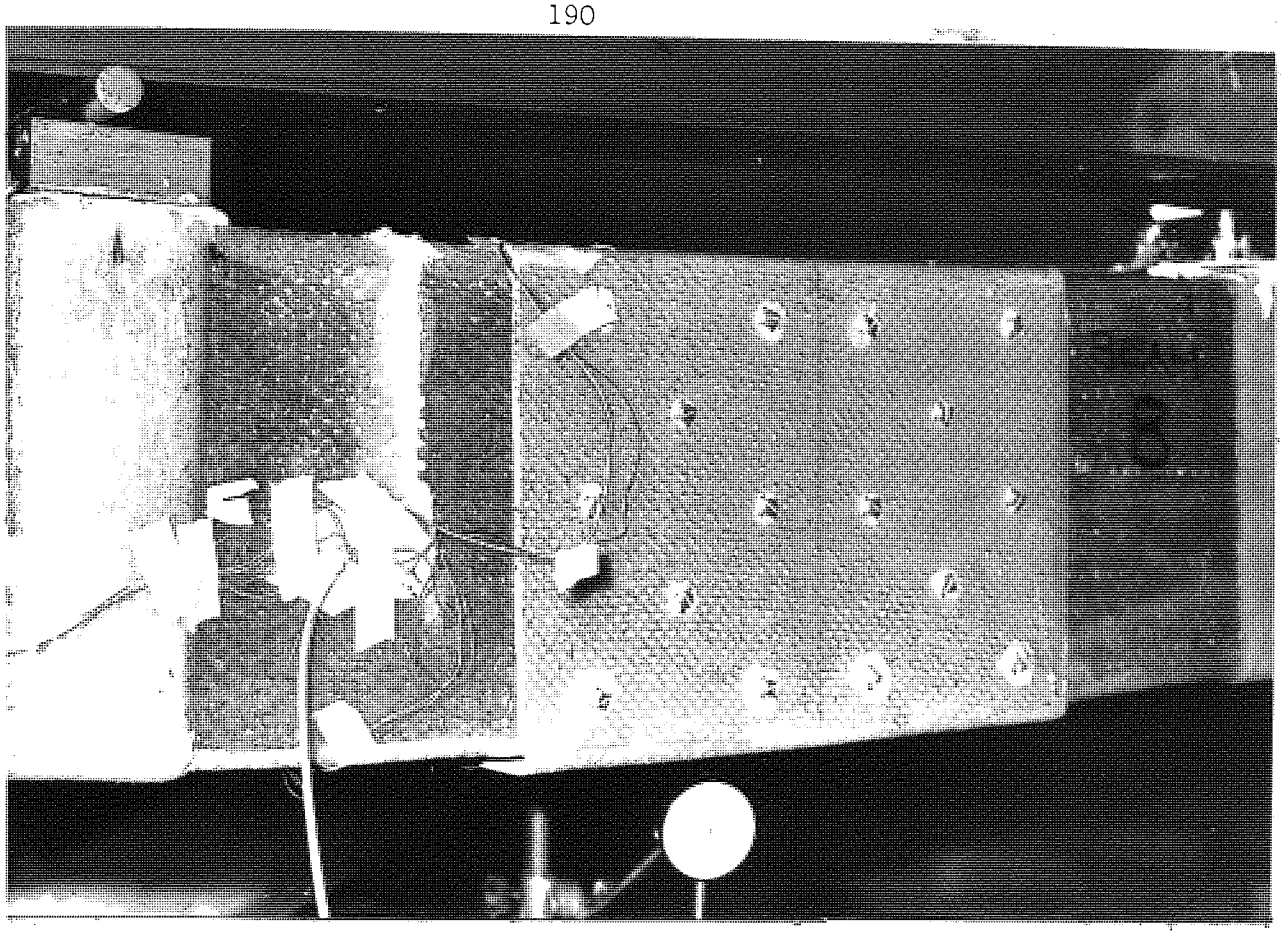

FIGURE 3.48 MODE OF FAILURE OF BEAM TYPE C3 SHOWING THE DELAMINATION OF MATERIAL AROUND SELF RAWL PLUGS

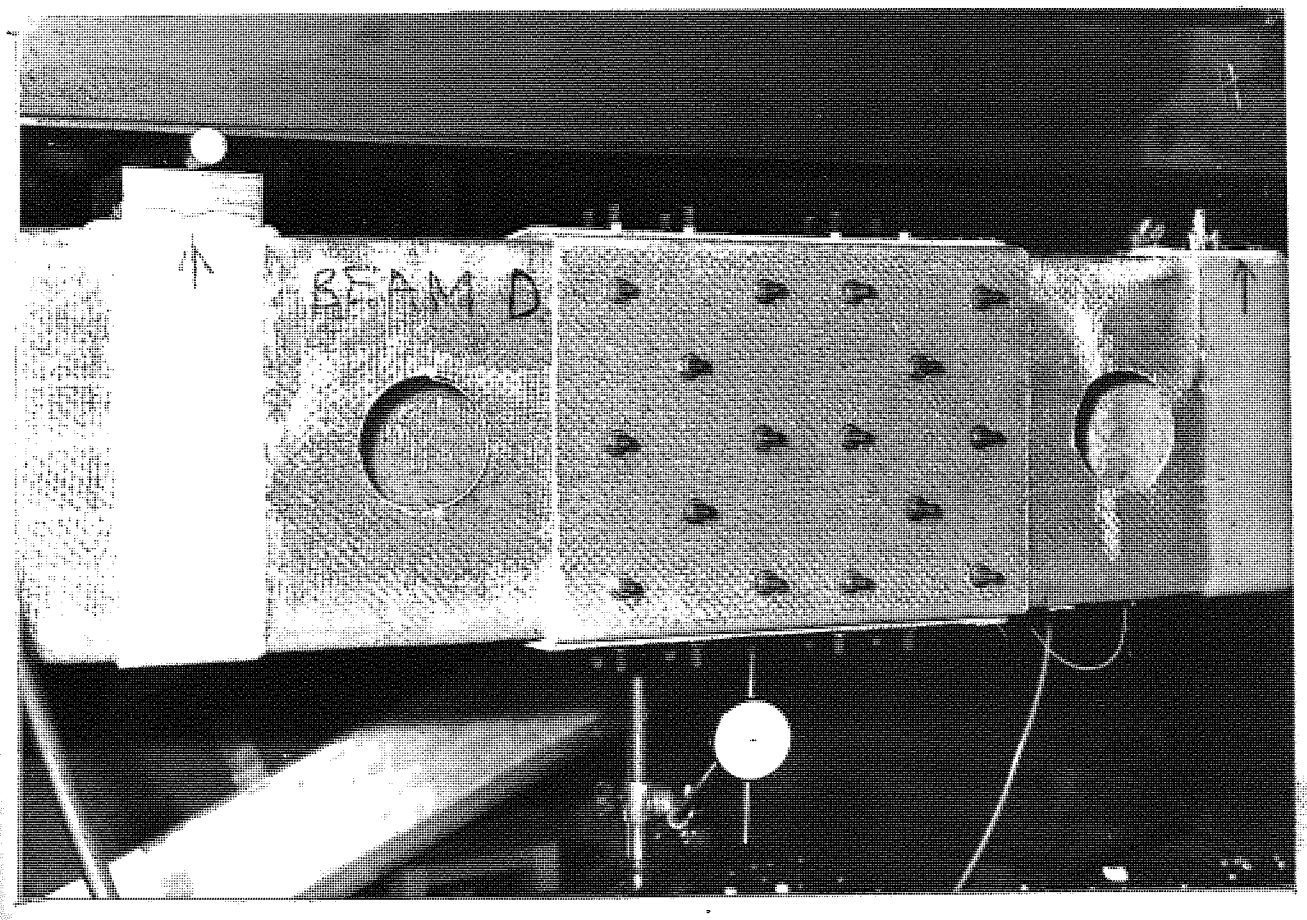

FIGURE 3.49 MODE OF FAILURE OF BEAM TYPE C4

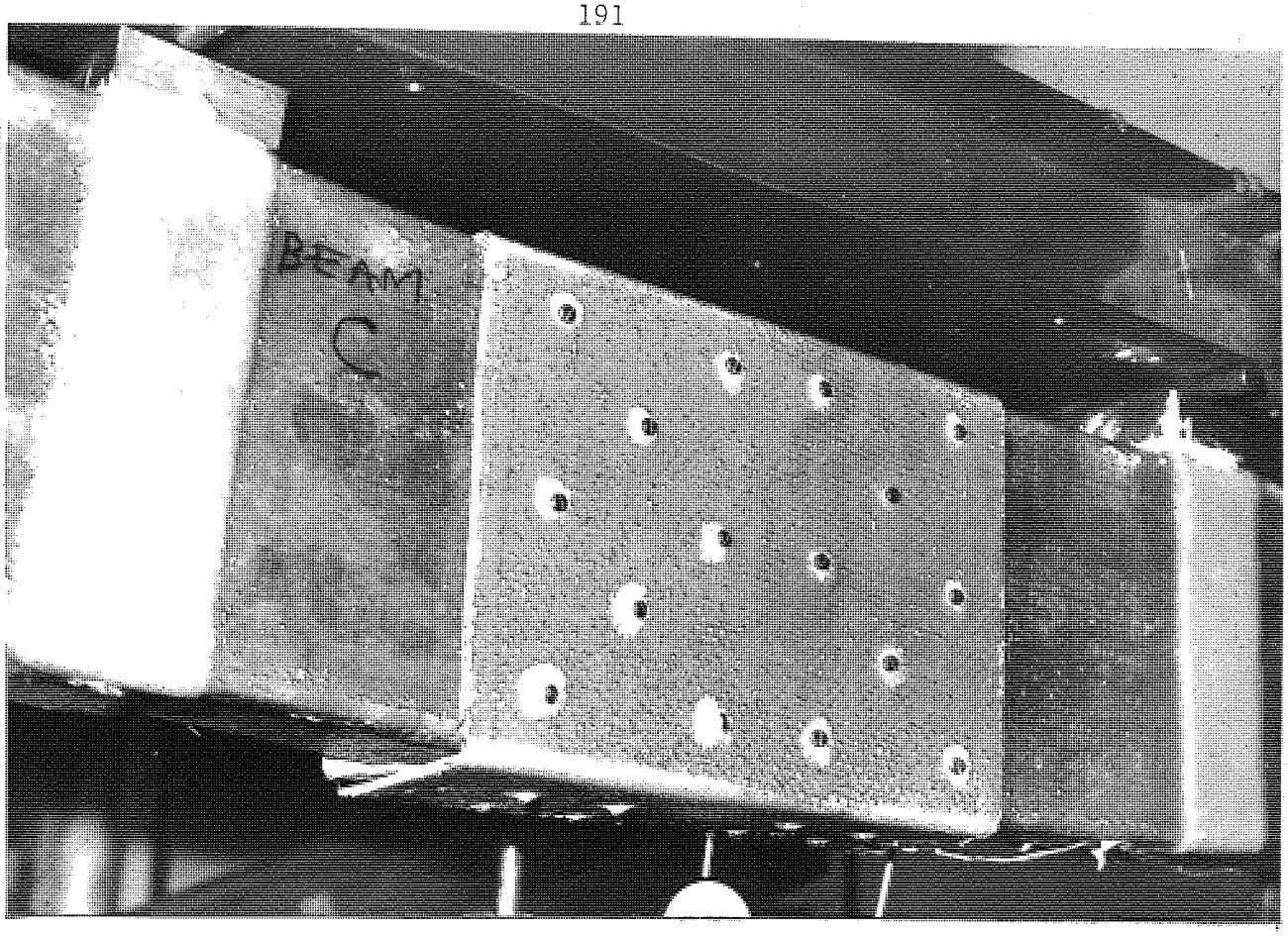

FIGURE 3.50 MODE OF FAILURE OF BEAM TYPE C2 SHOWING THE DELAMINATION OF MATERIAL AROUND SELF TAPPING SCREWS AND THE OPENING OF THE JOINT BELOW

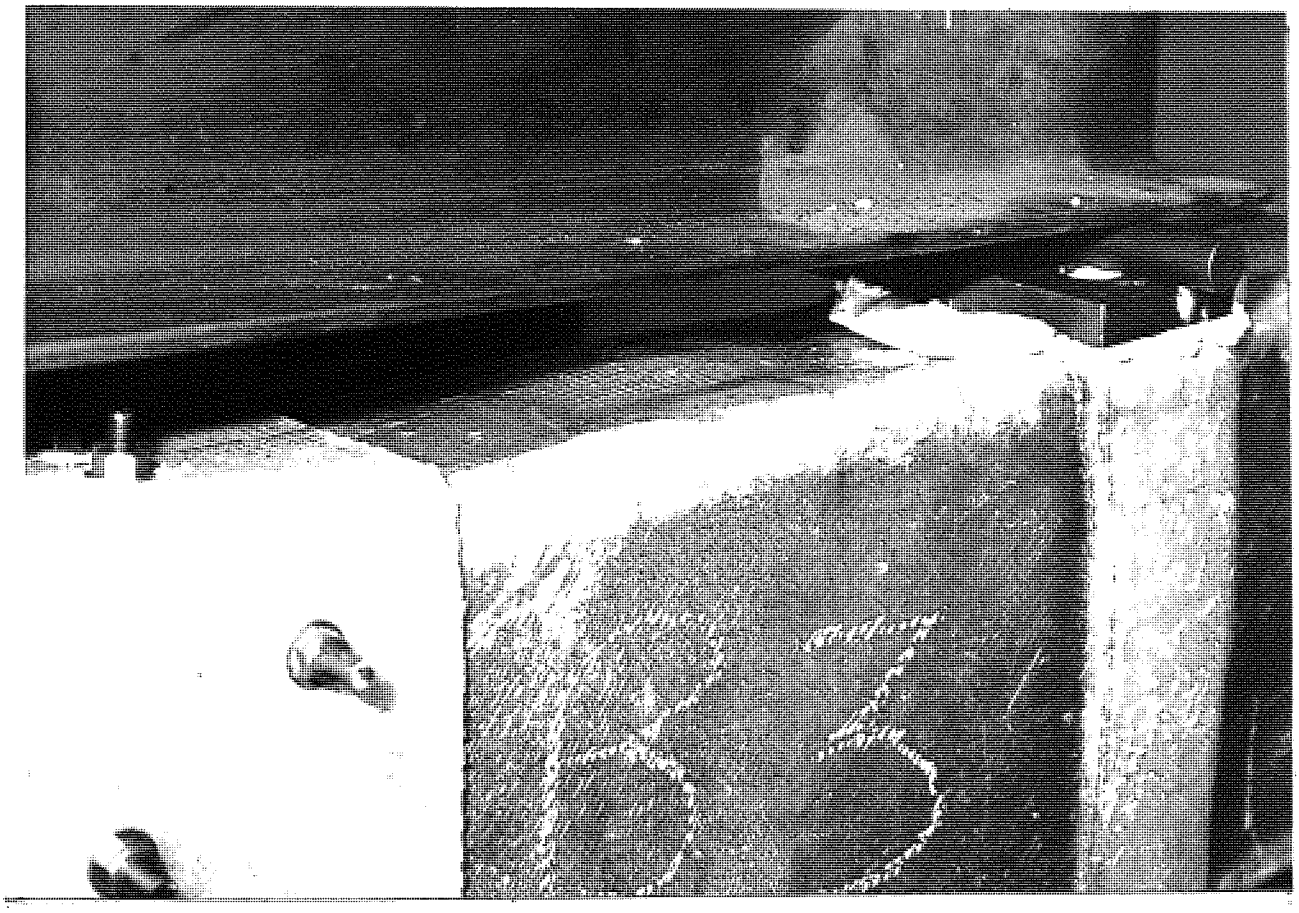

FIGURE 3.51 DEVELOPMENT OF LOCAL BUCKLING IN COMPRESSION FLANGE NEAR THE JOINT PRIOR TO FAILURE (BEAM TYPE C4)

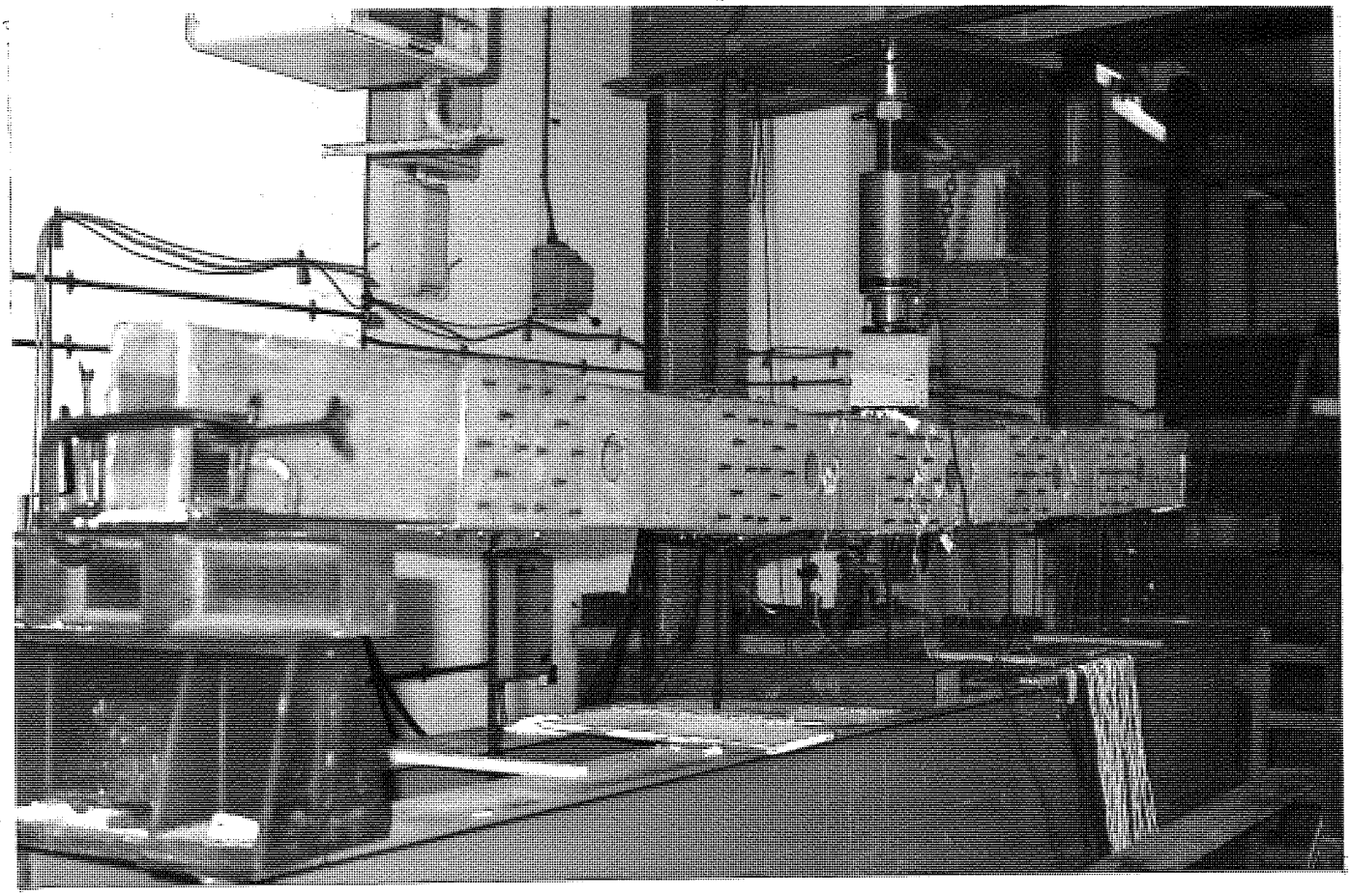

FIG 3.52 MULTIPLE JOINTED BEAM TYPE C10 AT THE BEGINNING OF TEST

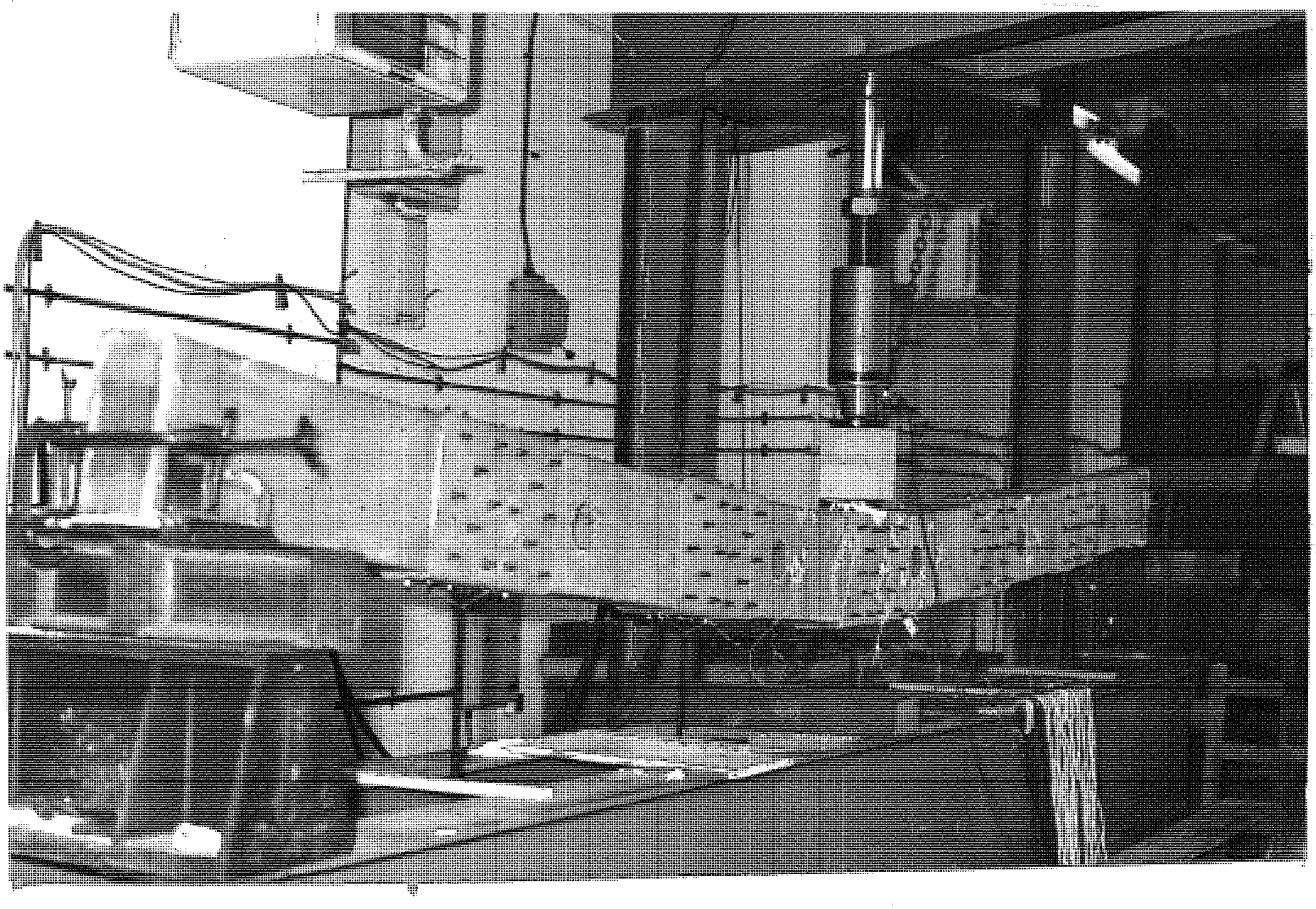

FIG 3.53 MULTIPLE JOINTED BEAM TUPE C10 MODE OF FAILURE

REFERENCES

3.1 A. RUFOLO "A Design Manual for joining of Glass Reinforced Structural Plastics" U.S. Naval Lab, Report Navship 250 - 634 - 1, August 1961.

3.2 H. A. PERRY, "Adhesive Bonding of Reinforced Plastics", McGraw-Hill 1959.

3.3 G. S. SMITH, "Structural Problems in the Design of G.R.P. Ships", Proc. of Sympos. on G.R.P. Ship Construction, RINA, London, October 1972.

3.4 F ERDOGAN and M RATWANI, Vol 5, J Composite Material, July 1971, page 378

3.5 P K SINHA and M N REDDY, "Fibre Science and Technology 9", Applied Science Publishers Limited, England, 1976.

3.6 L J HART SMITH, "Design and Analysis of Adhesive Bonded Joints", paper presented at Air Force Conference on Fibrous Components in Flight Vehicle, Design Dayton, Ohio, USA, September 26-28, 1972. Also Douglas paper No 6059 A, Douglas Aircraft Company, USA.

3.7 O, VOLKERSEN, Luftfahrtfarschung, 1938.

3.8 S, KELSEY and N. K, BENSON, Institute Fu Statik und Dynamik Technische, Hochschule, Stuttgart, 1966, 1SD Report No 10.

3.9 H. W, EICKNER, Basic Shear Strength Properties of Metal - bonding Adhesive as Determined by lap-joint Formulas of Volkersen and Goland and Reissner, 1955, US Dept. of Agriculture Forest Products Lab, F.P.L. Report No 1850.

3.10 M, GOLAND and REISSNER, Journal of Applied Mechanics 1944, 11, A17.

3.11 MINISTRY OF TECHNOLOGY, ADhesion, Fundamental and practise, A report of an International conference held at the University of Nottingham, England, 20-22 September 1966, MacLaren and Sons Limited, London.

3.12 GIBBS and COX INC., Marine Design Manual for Fiberglass Reinforced Plastics, McGraw-Hill Book Company.

3.13 C. M, WOODWARD and D. G, HALL, BSc Hons, dessertation May 1975, Dept of Civil Engineering, The University of Aston in Birmingham.

3.14 J. P, WASZCZAK and T. A, CRUSE, Journal of Composite Materials, Vol 5, July 1971, page 421.

3.15 ARBED - F and G, Technical Report, Force Transmitting Components, KE Units in Polyurethane fiber-mat Federal Republic of Germany.

CHAPTER 4

BOX BEAMS (COMBINED BENDING SHEAR AND TORSION)

4.1 INTRODUCTION

Following the investigation of G.R.P. box beams under the effect of combined bending and shear it was decided to extend the research programme to study the behaviour of G.R.P. box beams under combined bending, shear and torsion, as in practice beam elements are often subjected to a combination of such structural actions. Three 3 m beams series BT1, BT2, BT3 were selected for testing. The arrangement and fibre orientation of these beams was the same as beam series B5, B1 and B4 respectively used in the bending series (chapter 2).

4.2 BEAM INSTRUMENTATION

The manner of loading shown in fig (4.1) subjects the beam to a combination of a maximum bending, shear and torsion at the centre, while at the ends the beam is subjected to a combination of maximum shear and torsion only. Fig (4.2) shows the instrumentation of a typical beam in which the transverse strain gauges measure the transverse strains arising from torsion, whilst the longitudinal and rossette strain gauges measure the strains in longitudinal bending and shear.

Two dial gauges, set at the ℄ of the beam under each web, recorded vertical deflections, and the twist of the beam under torsion.

4.3 TEST RIG

A large portal testing rig was used to carry out the tests for all beams fig (4.3). The torsional load was applied by means of a

hydraulic jack with proving ring which transmitted the torque load to a specially designed torque frame fig (4.4) fixed at the centre of the beam. An anti-twist frame fig (4.5) was fixed at the end of the beam to achieve the desired boundary conditions.

4.4 BOUNDARY CONDITIONS

The test rig arrangement was meant to satisfy as closely as possible the following boundary conditions at the ends:-

(1) Twisting is restrained by the anti-twist frame fig (4.5).

(2) Simple support with regard to longitudinal bending.

(3) The ends of the beam are prevented from warping by the inclusion of end diaphragms.

(4) Rotation of the beam at midspan is allowed through pads of steel and a greezed needle bearing.

4.5 EXPERIMENTAL PROGRAMME

Three tests were carried out as detailed below.

(1) For beam series BT1, a constant concentrated load was applied (15 kN which is approximately $\frac{1}{4}$ of the ultimate load in the bending series tests) while varying torque load up to failure.

(2) For beam series BT2, a constant torsional load was applied ($\frac{1}{4}$ of the ultimate torque load determined from (1), whilst varying the concentrated load up to failure.

(3) For beam series BT3, the torque and concentrated loads were varied simultaneously up to failure.

4.6 TEST RESULTS

Experimental tensile, compressive, shear stresses and deflections arising from concentrated and torque loads were tabulated and compared with their corresponding theoretical predictions based on the analysis of simple bending and St Venant torsion (simple engineer's theory) are shown in Tables (4.4-4.15).

4.7 STRUCTURAL PROPERTIES

Coupons cast in the same manner as the beam series BT1, BT2 and BT3 were tested using the same methods described in chapter 2 for obtaining the structural properties. As the cross-section of the G.R.P. box beam elements have different structural properties depending on the axis considered, it was intended to use an equivalent section with a normalized structural property in the analysis when considering a particular structural action and a corresponding axis. For example when the section is analysed in longitudinal bending, one longitudinal modulus and a corresponding equivalent cross-section are used.

On the other hand, if the same section is analysed in torsion one shear modulus and a corresponding equivalent section are used. In each case the equivalent thickness of the beam element is found by relating its modulus to the modulus of the compression flange. In Tables (4.1-4.3), the structural properties, and the equivalent sections in bending and torsion are tabulated for use in the theoretical analysis.

4.8 THEORETICAL ANALYSIS - INTRODUCTION

Additional structural actions should be considered when a G.R.P. box beam is subjected to combined bending shear and torsion. Considering the testing arrangement fig (4.3) the stresses which may arise due to these structural actions are listed below. It is assumed that distortion of the beam's cross-section is prevented by the inclusion of end and intermediate diaphragms.

(A) Longitudinal stresses, these are due to

(i) Longitudinal bending

(ii) Torsional warping.

(B) Shear stresses due to

(i) Longitudinal bending

(ii) Due to St. Venant torsion

(iii) Torsional warping.

The term torsional warping shall be explained later. The analytical methods considered to deal with the stresses mentioned above are:-

(1) Analysis of simple bending and St. Venant torsion by simple engineer's theory.

(2) Analysis of torsional warping by Kollbrunner, Hajdin and Heilig [4.1, 2, 3].

4.9 RESOLUTION OF FORCES

For the purpose of analysis the torque load W_T is replaced by a statically equivalent combination of symmetric and antisymmetric loading. These are further represented by a combination of symmetric and antisymmetric loading systems acting on the webs fig (4.6).

4.10 ANALYSIS OF SIMPLE BENDING AND ST VENANT TORSION (Simple Engineer's theory)

Using the engineer's theory of bending in which plane cross-sections are assumed to remain plane, the longitudinal compressive, tensile and shear stresses due to vertical loads may be computed from the formulae (2.10 and 2.11) described in chapter 2.

Deflections at mid span due to vertical load may be obtained from the formulae

$$d = \frac{WL^3}{48EI} \qquad (4.1)$$

in which

W = the total vertical load

E = the equivalent elastic modulus in bending

I = the 2nd moment of area for an equivalent section in bending.

For the St Venant torsion of thin walled beams of closed section, Kollbrunner and Basler [4.4] gave the following expression

$$V_{srt.}h = \frac{T_{svt}}{2\,A_{enc}} = \frac{T}{2\Omega} \qquad (4.2)$$

where $V_{SVT.}h$ = shear flow in St Venant torsion

V_{svt} = shear stress

h = thickness of the section

T_{svt} = Torsional moment at cross-section of beam

= $W_T\,(b_1 + \frac{b}{2})$ considering fig (4.6).

The St Venant shear stresses are usually taken as constant through the cross-sectional thickness of the closed box beam. The effect of diaphragms and local reinforcement inside the box beams are neglected in this analysis.

Compressive, tensile and shear stresses and deflections based on the foregoing theory are shown in Tables (4.4-4.15) for beam series BT1, BT2 and BT3.

4.11 BEHAVIOUR OF BOX BEAMS UNDER TORSIONAL LOAD

Consider a box beam whose cross-section cannot distort because of the existance of rigid transverse diaphragms all along the span. The diaphragms however, are assumed not to restrict longitudinal displacements. Fig (4.7a) shows how the cross-section of such a box beam twists under torsional loading. The chain dotted configuration in fig (4.7b) shows how this leads to out of plane (longitudinal) displacements of cross-sections except at midspan where by symmetry

the cross-section remains plane. These longitudinal displacements are called torsional warping displacements and are associated with shear deformations in the planes of the flanges and webs. The mid span vertical deflection of each web occurring in torsion without distortion is denoted by at fig (4.7a). The term warping torsion is also used to denote the state of loading and stresses associated with torsional warping displacements.

If the diaphragms are removed so that the cross-section can be distorted, then the cross-section will exhibit additional twisting under torsional loading causing a further deflection in the web fig (4.7a). This in turn increases the out of plane displacements of cross-sections as shown in fig (4.7b). Thus box beams with no diaphragms when subjected to torsional loading undergo warping displacements which are composed of two components VIZ torsional warping displacements and distortional warping displacements. Both these components give rise to longitudinal normal stresses (warping stresses) when the warping is constrained e.g. by symmetry at mid span or at a continuous or built up support or by end diaphragms. In these circumstances the significance of the warping stresses depend on the geometry of the beam cross-section as well as on the nature of the loading and support conditions. The warping stresses can form a significant addition to the ordinary bending stresses resulting from the symmetrical component of loading.

4.12 STRESS PATTERNS OF BOX BEAMS WITH DIAPHRAGMS UNDER TORSION

The theory of St Venant torsion is inadequate for the analysis of box beams unless the cross-section of the beam does not warp. Steinle [4.5] gave special geometrical proportions for which the cross-section does not warp in torsion, but these proportions are

unlikely to be realised in practise. When torsional warping arises the pattern of warping displacement is such that the (longitudinal) torsional warping stresses vary both around the cross-sectional perimeter as shown in fig (4.8b) and along the beam as shown in fig (4.8c). Hence longitudinal shear stresses arise and these cause complementary shear stresses to occur in the plane of the cross-section which are called warping shear stresses as in fig (4.8d). Thus the total internal resistive torsional moment for a box beam cross-section (without distortion) is made up of a combination of St Venant stresses fig (4.8c) and torsional warping shear stresses fig (4.8d). The way in which these two components of torsional moment are distributed along the length of a beam is shown in fig (4.8e) for the case of a concentrated torsional moment text applied at mid span.

4.13 BIMOMENT

Fig (4.8b) shows the distributions at a cross-section of (longitudinal) warping stress for the case of torsional warping. Similar figures may also be represented for distortional warping stresses. It has been shown in detailed analytical treatments [4.1,6] that each of these stress distributions has zero longitudinal force resultant and zero moment resultant. They may therefore each be represented by a statically equivalent warping force group as shown in fig (4.10a) where all the four forces are equal in magnitude. This group generates a warping displacement pattern and is the force system naturally associated with warping. Instead of working with a group of four forces it is usual to represent them by a pair of equal and opposite moments in parallel planes as shown in fig (4.10b) where the moments are taken about a horizontal axis or in fig (4.10c)

where the axis of the moments is taken as vertical. Such a pair of moments is called a bimoment and has zero force resultant and zero moment resultant. A positive bimoment is shown in fig (4.10b) in which each component moment acts clock-wise when viewed from the plane of the other and the moments act about horizontal axis but it can also be as shown in fig (4.10c).

The idea of representing a warping stress system by a pair of equal and opposite moments in parallel planes was developed by Vlasov [4.7] The magnitude of the bimoment is equal to the moment multiplied by the distance between the planes. This gives dimensions of (force x length^2). A bimoment is the simplest possible physical representation of the longitudinal normal stress system associated with warping. It satisfies the following conditions which arose in Vlasov's analysis of thin walled beams.

(1) There must be zero force resultant and zero moment resultant of the longitudinal normal stress system which is therefore self-equilibrating at a cross-section.

(2) In general there must exist longitudinal displacements of cross-section varying around the perimeter.

(3) The quantity which enters into the analysis must be of dimension (Force x length^2).

4.14 ANALYSIS OF TORSIONAL WARPING BY THE METHOD OF KOLLBRUNNER, HAJDIN AND HEILIG [4.1,2,3]

The analysis considers only the torsional loading system of fig (4.6) and it is assumed that there is no distortion of cross-sections.

4.14.1 Summary of Procedure for Analysis

Valsov [4.7] Kollbrunner and Hajdin [4.1, 4.2] have developed the theory of warping torsion of thin walled box beams of closed or open-closed cross-section. The torsional warping (longitudinal) stresses f_{twr} and torsional warping shear stresses V_{twr} are obtained in terms of the applied Text, the bimoment B_{twr} and section properties known as sectorial co-ordinate W_{twr} and the torsional warping moment of inertia C_{twr} as shown later.

4.14.2 Bimoment B_{twr}, Sectorial Co-ordinate W_{twr} and Torsional Warping Moment of Inertia C_{twr}

For the purpose of numerical calculation, quantitative definitions are given to the above mentioned terms.

The torsional warping bimoment B_{twr} is defined as

$$B_{twr} = \int f_{twr} \, w_{twr} \, dA \qquad (4.3)$$

where

A = total area of cross-section

f_{twr} = torsional warping stress

W_{twr} = sectorial co-ordinate in torsional warping referred to the shear centre (see below).

To find the sectorial co-ordinate W_{twr} it is necessary to compute the position of the shear centre of the section. Khan and Stafford Smith [4.8] adopted the following procedure to compute the position of shear centre of a closed section and hence the sectorial co-ordinate W_{twr}.

(a) Select an arbitrary pole. It is advantageous to place this on a line of symmetry.

(b) Reduce the sectorial area diagram drawn from the arbitrary pole using the formula

$$\bar{w}' = w_b - P\bar{S} \tag{4.4}$$

where $\bar{w}'$ is reduced sectorial area

w_b sectorial area referred to the temporary pole.

$$P = \text{average radius} = \int_0^s \frac{2A_{enc}}{ds/h} \tag{4.5}$$

$$S = \text{reduced length along the profile} = \int_0^s \frac{ds}{h} \tag{4.6}$$

A_{enc} and h as defined in equation (4.2).

(c) Compute the area moment of the $\bar{w}'$ diagram $\bar{w}'$ y dA about the axis of symmetry say x.

(d) Divide the area moment from step (c) by the moment of inertia of the section about the axis of symmetry Ix. This gives the distance of the shear centre $\pm \alpha x$ from the arbitrary pole.

(e) The next step is to modify the $\bar{w}'$ diagram to account for the new shear centre and to obtain the W_{twr} diagram by the formula

$$W_{twr} = \bar{w}' \pm \alpha x \, y \tag{4.7}$$

The torsional warping moment of inertia of the cross-section is defined as

$$C_{twr} = \int_A w_{twr}^2 \, d\,A \qquad dA = t\,ds \tag{4.8}$$

This quantity is of dimension (length^6)

4.14.3 Relationship between Applied Load, Internal Stress-Resultants and Twist

Kollbrunner and Hajdin [4.1] and Heilig [4.3] gave the following

expressions for the torsional warping of a single-span, thin-walled beam of closed or open-closed cross-section. Torsionally restrained at each end but without warping restraint at the ends, and subject to a mid span concentrated torsional moment Text as shown in fig (4.1).

$0 < Z < \ell/2$

$$B_{twr}(Z) = \frac{Text}{2K_2 K_3} \frac{\sinh K_2 Z}{\cosh \frac{K_2 \ell}{2}} \tag{4.9}$$

$$T_{svt}(Z) = \frac{Text}{2}\left(1 - \frac{\cosh K_2 Z}{K_3 \cosh \frac{K_2 \ell}{2}}\right. \tag{4.10}$$

$$T_{twr}(Z) = \frac{Text}{2 K_3} \frac{\cosh K_2 Z}{\cosh \frac{K_2 \ell}{2}} \tag{4.11}$$

$$\theta_z(Z) = \frac{Text}{2G\, C_{svt}\, K_2 K_3}\left(K_2 K_3 Z - \frac{\sinh K_2 Z}{\cosh \frac{K_2 \ell}{2}}\right. \tag{4.12}$$

$\ell/2 < Z < \ell$:

$$B_{twr}(Z) = \frac{Text \sinh K_2 (\ell - Z)}{\cosh \frac{K_2 \ell}{2}} \tag{4.13}$$

$$T_{svt}(Z) = \frac{Text}{2}\left(-1 + \frac{\cosh K_2 (\ell - Z)}{K_3 \cosh \frac{K_2 \ell}{2}}\right. \tag{4.14}$$

$$T_{twr}(Z) = -\frac{Text \cosh K_2 (\ell - Z)}{\cosh \frac{K_2 \ell}{2}} \tag{4.15}$$

$$\theta_z(Z) = \frac{Text}{2G\, C_{svt} K_2 K_3} K_2 K_3 (\ell - Z) - \frac{\sinh K_2 (\ell - Z)}{\cosh \frac{K_2 \ell}{2}} \tag{4.16}$$

where $B_{twr}(z)$ = bimoment of torsional warping at section z.

$T_{svt}(z)$ = torsional moment due to St Venant shear stresses at section z.

$T_{twr}(z)$ = torsional moment due to the torsional warping shear stresses at section z.

$\theta_z(z)$ = twist about shear axis at section z.

$$K_2 = \frac{GC_{svt}}{E\,\bar{C}_{twr}} \tag{4.17}$$

$$K_3 = \frac{C_{cen}}{C_{cen} - C_{svt}} \tag{4.18}$$

$$\bar{C}_{twr} = K_e\, C_{twr} \tag{4.19}$$

C_{cen} = central torsional moment of inertia of cross-section = $\int_A a_1^2\, dA$ (4.20)

C_{svt} = Torsional moment of inertia of cross-section in St Venant torsion

$$= \frac{4A_{enc}^2}{\frac{ds\ per}{h}} \tag{4.21}$$

and

$$\frac{ds\ per}{h} = \frac{b}{h_{top}} + \frac{b}{h_{bot}} + \frac{2d}{h_{web}} \tag{4.22}$$

b = breadth between mid lines of webs fig (4.11)

d = depth between mid lines of compression and tension flanges fig (4.11)

h_{top} = thickness of compression flange

h_{bot} = thickness of tension flange

h_{web} = thickness of web

A_{enc} = enclosed area = bd

h = thickness of section

S_{per} = the peripheral co-ordinate along the mid line of the cross section.

Note that $(T_{svt} + T_{twr})$ equals $\frac{1}{2}$ Text in magnitude for all sections Z as is required for equilibrium fig (4.8e.

4.14.4 Torsional Warping Stresses f_{twr}

The following expression gives the torsional warping stress f_{twr}

$$f_{twr} = \frac{B_{twr} W_{twr}}{C_{twr}} \qquad (4.23)$$

The form of this expression is the same as the expression

$$f_x = \frac{M_x y}{Ix} \qquad (4.24)$$

used to obtain longitudinal stresses since M_x and B_{twr} are all stress resultants at section Z; Y and W_{twr} are co-ordinates of the point considered on the cross-section; and Ix and C_{twr} are all geometrical properties of the entire cross-section.

Under eccentric loading the longitudinal stress f_x and f_{twr} of equation (4.23) are superimposed with due regard to sign.

4.14.5 Torsional Warping Shear Stresses V_{twr}

These are given by the following expression

$$V_{twr} = T_{twr} \frac{\frac{dw_{twr}}{d\ S\ per}}{C_{cen} - C_{svt}} \qquad (4.25)$$

where

$$\frac{d\ W_{twr}}{d\ S\ per} = a_1 - \frac{C_{svt}}{2\ A_{enc}\ h} \qquad (4.26)$$

The method of evaluating the derivative of W_{twr} is shown in detail in the example given.

4.14.6 St Venant Shear Stresses V_{svt}

Knowing T_{svt} from equations (4.10 and 4.14) V_{svt} is obtained using equation (4.2).

4.14.6 Numerical Example

To compute the stresses mentioned in sections 4.14.3, 4.14.4 and 4.14.6 in terms of the external applied torque Text, beam type BT1 is considered.

The equivalent section in torsion for beam BT1 obtained from Table 4.1 is shown in fig (4.11). Let x by the axis of symmetry. An arbitrary pole A is chosen as shown in fig (4.12).

$$Ixx = 295.17 \times 3.90 \times 75^2 \times 2 + \frac{3.9^3}{12} \times 295.11$$

$$+ \frac{154.82^3}{12} \times 5.3 + \frac{154.82^3}{12} \times 4.35$$

$$= 15,937,695 \text{ mm}^4$$

From equation (4.6)

$$So = \frac{300 \times 2}{3.90} + \frac{150}{5.30} + \frac{150}{4.3}$$

$$= 216.62$$

From equation (4.5)

$$P = \frac{2 \times 300 \times 150}{50}$$

$$= 415.47$$

and hence

$$P\,\bar{S} = 415.47 \quad \frac{s}{t}$$

and from equation (4.4)

$$\bar{w}' = wb - P\bar{S}$$

wb, $P\bar{S}$ and $\bar{w}'$ diagrams may therefore be drawn (see figures 4.12, 4.13 and 4.14).

Now compute the area moment of the $\bar{w}'$ diagram $\int \bar{w}'\, y\, d\, A$ about the axis of symmetry. Referring to fig (4.14) $\int \bar{w}'\, y\, d\, A = \bar{w}'\, s\, h\, b$ along depth $+ \frac{w\, s^2\, h}{3}$ along width.

$$= \left(\frac{\bar{w}'_1 + \bar{w}'_2}{2}\right) \frac{bd}{2} \times 2\, h + \left(\frac{b}{2}\right)^2 \times \frac{1}{3} \times (\bar{w}'_1 + \bar{w}'_2) \times 2\, (h_{top} + h_{bot})$$

$$= \left(\frac{5879.2 + 15338.4}{2}\right) \times \frac{150 \times 300}{2} \times 2 \times 3.90$$

$$+ \left(\frac{150}{2}\right)^2 \times \frac{1}{3} (1533505 + 5875.8) \times 2 \times (5.30 + 4.35)$$

$$= 2{,}629{,}412{,}034 \text{ mm}^3$$

from step d in section 4.14.2

$$\alpha x = 164.98 \text{ mm}$$

Fig 4.15 shows the W_{twr} diagram computed from equation (4.7). To find the torsional warping moment of inertia C_{twr}, the Simpson integration method is used to evaluate the integral in equation (4.8) thus

$$C_{twr} = \frac{150}{6} \times 5.30\, [2 \times 6494^2] + \frac{150 \times 4.35}{6}\, [2 \times 5211.9^2]$$

$$+ \frac{2 \times 300 \times 3.9}{6}\, [(6.494)^2 + 4\, \frac{(-6494 + 5211.9)^2}{2}$$

$$+ (5211.9)^2]$$

$$= 4.54069006 \times 10^{10} \text{ mm}^6$$

Evaluation of B_{twr} at mid span

In equation (4.20)

$$C_{cen} = \int_A a_1^2 \, d\,A$$

$$= 150 \times 5.3 \times 164.98^2 + 2 \times 300 \times 3.9 \times 75^2 + 150 \times 3.90 \times 135.02^2$$

$$= 45,465,912 \text{ mm}^4$$

and from equation (4.21)

$$C_{svt} = \frac{4 \times (150 \times 300)^2}{\frac{150}{5.30} + \frac{150}{4.30} + \frac{300 \times 2}{3.9}}$$

$$= 37.322 \times 10^6 \text{ mm}^4$$

In equation (4.18)

$$K_3 = \frac{45,465912}{45465912 - 37322000}$$

$$= 5.583$$

In equation (4.19)

$$\overline{C}_{twr} = 5.583 \times 4.54069 \times 10^{10} = 25.35067 \times 10^{10}$$

In equation (4.17) with average Poisson's ratio taken as 0.13

and $\frac{G}{E} = 0.269629$

hence $K_2 = \frac{0.269629 \times 37.322 \times 10^6}{25.3506}$

$$= 630 \times 10^{-3} \text{ mm}^{-1}$$

From equation (4.9) at mid span

$$B_{twr} = \frac{Text \tan h\ 1}{2 \times 7.97 \times 10^{-3} \times 5.583}$$

$$= 10.825\ Text.\ Nmm^2$$

Evaluation of T_{svt} at mid span

In equation (4.10) at $z = \frac{\ell}{2}$ i.e. just to the left of mid span

$$T_{svt} = \frac{Text}{2}\left(1 - \frac{1}{5.583}\right)$$

$$= 0.4104\ Text\ \ Nmm$$

Evaluation of T_{twr} at mid span

In equation (4.11) at $z = \frac{\ell}{2}$

$$T_{twr} = 2 \times \frac{Text}{5.583}$$

$$= 0.08955\ Text\ Nmm$$

The angle of twist θ may be computed from equation (4.12) which results in

$$\theta = Text\ \frac{(6.30 \times 10^{-3} \times 5.583 \times 1500 - 0.7615)}{2 \times 3.64 \times 37.322 \times 10^{6} \times 6.30 \times 10^{-3} \times 5.583}$$

$$= 5.4410 \times 10^{-6}\ Text\ radians$$

Accordingly the vertical deflection under the web at mid span

$$= \theta \times 300$$

$$= 1.632 \times 10^{-3}\ Text\ mm$$

Evaluation of torsional warping stresses f_{twr} at mid span

In equation (4.23)

$$f_{twr} = \frac{B_{twr}\ W_{twr}}{C_{twr}}$$

Referring to fig (4.15)

At B $\quad f_{twr} = \dfrac{\text{Text} \times 10.825 \times 6494}{25.35 \times 10^{10}}$

$$= 2.773 \times 10^{-7}\ \text{Text} \qquad N/mm^2$$

and at C $\quad = \dfrac{\text{Text} \times 10.82 \times 5208}{25.35 \times 10^{10}}$

$$= 2.223 \times 10^{-7}\ \text{Text} \qquad N/mm^2$$

Evaluation of torsional warping shear stresses V_{twr} at mid span

In equation (4.25)

$$V_{twr} = T_{twr} \frac{\dfrac{dw_{twr}}{ds\ per}}{C_{cen} - C_{svt}}$$

after substituting the values of T_{twr}, C_{cen} and C_{svt}; the following is obtained

$$V_{twr} = 0.01098 \times 10^{-6}\ \text{text} \times \frac{dw_{twr}}{ds\ per}$$

The term $\dfrac{dw_{tvr}}{ds\ per}$ is equal to the slope of the w_{twr} diagram fig (4.5).

Hence at B $\quad \dfrac{dw_{twr}}{ds\ per} = \dfrac{6494}{75} = 86.58$

at C $\quad \dfrac{dw_{twr}}{ds\ per} = -\dfrac{(+5208.55 - 6494)}{300}$

$$= 4.284$$

Hence for V_{twr};

at segment AB

$$V_{twr} = 0.95064 \times 10^{-6} T_{ext} \text{ N/mm}^2$$

at segment BC

$$V_{twr} = -0.04703 \times 10^{-6} T_{ext} \text{ N/mm}^2$$

Evaluation of St Venant shear stress

From equation (4.2)

$$V_{svt} = \frac{T_{svt}}{2 A_{enc} h}$$

and on substituting values of T_{svt}, A_{enc} and H,

at segment AB $V_{svt} = 8.6037 \times 10^{-7}$ Text

and at segment BC, $V_{svt} = 1.16923 \times 10^{-6}$ Text

4.15 CONCLUSION

Compressive and Tensile Stresses

From Tables (4.4-4.6) the experimental tensile and compressive stresses were generally lower than the predicted theoretical results, however in beam type BT2, the experimental tensile stresses exhibited a better correlation with the theory. A common phenomenon was that the experimental tensile and compressive stresses were shown to be greater than the corresponding theoretical stresses due to concentrated load by a margin which may be comparable to that produced by the vertical component of the torque load, Table (4.4).

Shear Stresses

Apart from beam type BT3, shear stresses at mid span due to vertical load in the webs were higher than the corresponding total theoretical shear stress, Tables (4.10-4.12). This may be due to

the complexity of stresses at mid span. Shear stresses due to St Venant torsion showed a close correlation with the theory.

Deflection

The experimental deflections due to vertical loads were comparable with the theoretical deflections, Table (4.13-4.15). The maximum rotation exhibited by the web was 0.06626 radians (3^{o}-47') indicating that a G.R.P. box beam can sustain a considerable twist under torsional loading.

Fibre Orientation

As fibre orientation in bending and shear series (chapter 2) was found to be of little significance and because of the variation in the manner of loading in the beams tested for combined bending, shear and torsion, it is not possible to make a direct comparison between the three beams, BT1, BT2 and BT3. However, a comparison may be made between beam type BT1 and BT3 where in both cases the torque was applied up to failure. From such a comparison it may be concluded that the fibre arrangement (bidirectional) in beam type BT1 has attained the maximum ultimate torque load.

Mode of Failure

All beams failed at the mid span region where the maximum stresses were induced. The warping of the section became more apparent with the increase of the torque load, especially at the webs, which eventually ended in a crack propagation. Also it was observed that near the point of application the concentrated load, local buckling developed in the compression flange.

Structural Property	Webs	Comp flange	Tension flange
Average thickness	4.10	5.30	4.20
Longitudinal modulus E_L kN/mm^2	14.10	13.50	13.80
Transverse modulus E_T kN/mm^2	14.00	13.40	13.50
Shear modulus G kN/mm^2	3.46	3.64	3.51
Longitudinal Poisson's ratio ν_{LT}	0.13	0.13	0.13
Transverse Poisson's ratio ν_{TL}	0.13	0.13	0.13
Modulus at 45^o E_{45} kN/mm^2	9.68	9.90	9.70
Equivalent longitudinal modulus kN/mm^2	13.50	13.50	13.50
Equivalent thickness in bending section mm	3.92	5.30	4.11
Equivalent shear modulus kN/mm^2	3.64	3.64	3.64
Equivalent thickness in torsion section mm	3.90	5.30	4.35
Average Poisson's ratio in bending	0.13	0.13	0.13
Average Poisson's ratio in torsion	0.13	0.13	0.13

TABLE 4.1

STRUCTURAL PROPERTIES OF BEAM TYPE BT1

Structural Property	Webs	Comp flange	Tension flange
Average thickness	4.30	5.35	4.28
Longitudinal modulus E_L kN/mm^2	16.80	17.80	17.70
Transverse modulus E_T KN/mm^2	9.65	6.20	7.26
Shear modulus G kN/mm^2	5.34	4.52	4.46
Longitudinal Poisson's ratio ν_{LT}	0.32	0.27	0.19
Transverse Poisson's ratio ν_{TL}	0.18	0.08	0.10
Modulus at 45^o E_{45} kN/mm^2	12.81	9.27	10.20
Equivalent longitudinal modulus kN/mm^2	17.80	17.80	17.80
Equivalent thickness in bending section mm	4.06	5.35	4.26
Equivalent shear modulus kN/mm^2	4.52	4.52	4.52
Equivalent thickness in torsion section mm	5.08	5.32	4.22
Average Poisson's ratio in bending	0.26	0.26	0.26
Average Poisson's ratio in torsion	0.12	0.12	0.12

TABLE 4.2

STRUCTURAL PROPERTIES OF BEAM TYPE BT2

Structural Porperty	Webs	Comp. flange	Tension flange
Average thickness	5.50	5.40	4.20
Longitudinal modulus E_L kN/mm^2	15.10	17.60	17.80
Transverse modulus E_t kN/mm^2	7.34	5.01	7.20
Shear modulus G kN/mm^2	6.49	4.62	4.20
Longitudinal Poisson's ratio $_{LT}$	0.25	0.27	0.22
Transverse Poisson's ratio $_{TL}$	0.12	0.08	0.11
Modulus at 45^o E_{45} kN/mm^2	12.37	9.04	9.80
Equivalent longitudinal modulus kN/mm^2	17.60	17.60	17.60
Equivalent thickness in bending section mm	4.72	5.42	4.25
Equivalent shear modulus kN/mm^2	4.62	4.62	4.62
Equivalent thickness in torsion section mm	7.72	5.40	3.82
Average Poisson's ratio in bending	0.25	0.25	0.25
Average Poisson's ratio in torsion	0.10	0.10	0.10

TABLE 4.3

STRUCTURAL PROPERTIES OF BEAM TYPE BT3

Conc. load kN	Torque kN/m	Comp. stress Experimental N/mm^2	Comp. stress theory		Comp. stress Theory total N/mm^2
			Due to conc. load N/mm^2	Due to vertical component of torque load N/mm^2	
15	0	37.82	36.6	0	36.60
15	0.90	39.00	36.60	4.88	41.48
15	1.80	41.75	36.60	9.76	46.36
15	2.70	44.37	36.60	14.64	51.24
15	3.60	47.20	36.60	19.52	56.12
15	4.50	51.98	36.60	24.40	61.00
15	5.40	53.30	36.60	29.28	65.88
15	6.30	57.53	36.60	34.16	70.76
15	7.20	60.61	36.60	39.04	75.64

TABLE 4.4

EXPERIMENTAL AND THEORETICAL COMPRESSIVE STRESSES AT MID SPAN FOR BEAM TYPE BT1

Conc. load kN	Torque kN/m	Comp. stress Experimental N/mm^2	Comp. stress theory		Comp. stress Theory total N/mm^2
			Due to conc. load N/mm^2	Due to vertical component of torque load N/mm^2	
0	2.138	4.27	0	10.23	10.23
1	2.183	5.61	2.15	10.23	12.38
2	2.138	6.87	4.31	10.23	14.54
3	2.138	10.66	6.46	10.23	16.23
4	2.138	12.58	8.61	10.23	18.84
5	2.138	15.11	10.77	10.23	21.00
6	2.138	17.52	12.92	10.23	23.15
7	2.138	20.06	15.07	10.23	25.30
8	2.138	22.92	17.23	10.23	27.46
9	2.138	24.37	19.38	10.23	29.61
10	2.138	26.93	21.54	10.23	31.77

TABLE 4.5

EXPERIMENTAL AND THEORETICAL COMPRESSIVE STRESSES AT MID SPAN FOR BEAM TYPE BT2

Conc. load kN	Torque kN/m	Comp. stress Experimental N/mm^2	Comp. stress theory		Comp. stress Theory total N/mm^2
			Due to conc. load N/mm^2	Due to vertical component of torque load N/mm^2	
0	0	0	0	0	
1	0.45	11.51	2.05	2.05	4.1
2	0.90	13.17	4.10	4.11	8.2
3	1.35	14.75	6.16	6.16	12.32
4	1.80	16.48	8.21	8.21	16.42
5	2.25	17.87	10.27	10.27	20.54
6	2.70	19.63	12.32	12.32	24.64
7	3.15	21.69	14.37	14.37	28.74
8	3.60	24.00	16.42	16.42	32.84
9	4.05	27.32	18.48	18.48	36.96
10	4.5	31.49	20.53	20.53	41.06
11	4.95	36.63	22.58	22.58	45.16

TABLE 4.6

EXPERIMENTAL AND THEORETICAL COMPRESSIVE STRESSES AT MID SPAN FOR BEAM TYPE BT3

Conc. load kN	Torque kN/m	Tensile stress Experimental N/mm^2	Tensile stress theory		Tensile stress theory total N/mm^2
			Due to conc. load N/mm^2	Due to vertical component of torque load N/mm^2	
15	0	32.50	33.47	0	33.47
15	0.90	34.30	33.47	4.46	37.93
15	1.80	39.09	33.47	8.92	42.39
15	2.7	44.21	33.47	13.39	46.86
15	3.60	48.30	33.47	17.85	51.32
15	4.50	53.58	33.47	22.31	55.78
15	5.40	57.71	33.47	26.78	60.20
15	6.30	60.03	33.47	31.24	64.70
15	7.2	63.42	33.47	35.70	69.17
15	8.1	66.39	33.47	40.16	73.63

TABLE 4.7

EXPERIMENTAL AND THEORETICAL TENSILE STRESSES
AT MID SPAN FOR BEAM TYPE BT1

Conc. load kN	Torque kN/m	Tensile stress Experimental N/mm^2	Tensile stress theory		Tensile stress theory total N/mm^2
			Due to conc. load N/mm^2	Due to vertical component of torque load N/mm^2	
0	2.138	4.89	0	11.02	
1	2.138	5.30	2.32	11.02	13.34
2	2.138	7.08	4.64	11.02	15.66
3	2.138	8.63	6.96	11.02	17.98
4	2.138	13.61	9.28	11.02	20.30
5	2.138	16.05	11.60	11.02	22.62
6	2.138	19.08	13.92	11.02	24.94
7	2.138	20.06	16.24	11.02	27.26
8	2.138	26.45	18.56	11.02	29.58
9	2.138	29.03	20.88	11.02	31.90
10	2.138	32.60	23.20	11.02	34.22

TABLE 4.8

EXPERIMENTAL AND THEORETICAL TENSILE STRESSES
AT MID SPAN FOR BEAM TYPE BT2

Conc. load kN	Torque kN/m^2	Tensile stress Experimental N/mm^2	Tensile stress theory		Tensile stress theory total n/mm^2
			Due to conc. load N/mm^2	Due to vertical component of torque load N/mm^2	
0	0	0	0		0
1	0.45	12.53	2.21	2.21	4.42
2	0.90	14.84	4.42	4.42	8.84
3	1.35	17.23	6.64	6.64	12.28
4	1.80	19.31	8.85	8.85	17.70
5	2.25	20.52	11.07	11.07	22.14
6	2.70	23.52	13.28	13.28	26.56
7	3.15	26.10	15.49	15.49	30.98
8	3.60	28.22	17.71	17.71	35.42
9	4.05	30.49	19.93	19.93	39.84
10	4.50	33.55	22.14	22.14	44.28
11	4.95	35.87	24.35	24.35	48.70

TABLE 4.9

EXPERIMENTAL AND THEORETICAL TENSILE STRESSES
AT MID SPAN FOR BEAM TYPE BT3

Conc load (P)	Torque kN/m	Shear stress at web due to vertical Load Experimental	Shear stress at web theory		Shear stress at web theory total N/mm^2	Shear stress at comp. flange due to St Venant torsion	
			due to conc. load N/mm^2	due to vertical component of torque load N/mm^2		Experimental N/mm^2	Theory N/mm^2
15	0	0	3.77	0	3.77	0	0
15	0.90	0.42	3.77	0.50	4.27	5.40	2.29
15	1.80	1.21	3.77	1.00	4.77	8.25	4.58
15	2.70	4.60	3.77	1.51	5.28	12.10	6.88
15	3.60	6.42	3.77	2.01	5.78	14.20	9.17
15	4.50	8.13	3.77	2.51	6.28	16.38	11.47
15	5.40	11.76	3.77	3.02	6.79	18.45	13.76
15	6.30	13.84	3.77	3.52	7.29	21.59	16.06
15	7.20	14.19	3.77	4.02	7.79	24.00	18.35
15	8.10	14.36	3.77	4.52	8.29	25.12	20.64

Table 4.10

Experimental and theoretical shear stresses at mid span due to vertical loading and St Venant torsion for beam type BT1

Conc load	Torque kN/m	Shear stress at web due to vertical load Experimental N/mm^2	Shear stress at web theory		Shear stress at web theory total N/mm^2	Shear stress at comp. flange due to St Venant torsion	
			due to conc. load N/mm^2	due to vertical component of torque load N/mm^2		Experimental N/mm^2	Theory N/mm^2
0	2.138	1.24	0	1.15	1.15	5.31	4.82
1	2.138	1.23	0.24	1.15	1.39	5.56	4.82
2	2.138	1.22	0.48	1.15	1.63	6.21	4.82
3	2.138	1.92	0.72	1.15	1.87	4.93	4.82
4	2.138	2.17	0.96	1.15	2.11	5.89	4.82
5	2.138	2.54	1.21	1.15	2.36	5.75	4.82
6	2.138	2.98	1.45	1.15	2.60	6.89	4.82
7	2.138	3.43	1.69	1.15	2.84	7.33	4.82
8	2.138	3.88	1.93	1.15	2.08	6.72	4.82
9	2.138	4.74	2.17	1.15	3.32	5.89	4.82
10	2.138	5.01	2.41	1.15	3.56	5.90	4.82

Table 4.11

Experimental and theoretical shear stresses at mid span due to vertical loading and St Venant torsion for beam type BT2

Conc load	Torque kN/m	Shear stress at web due to vertical load Experimental N/mm^2	Shear stress at web theory		Shear stress at web theory total N/mm^2	Shear stress at comp. flange due to St Venant torsion	
			due to conc. load N/mm^2	due to vertical component of torque load N/mm^2		Experimental N/mm^2	Theory N/mm^2
0	0	0	0	0	0	0	0
1	0.45	0.19	0.21	0.21	0.42	0.46	0.811
2	0.90	0.51	0.42	0.42	0.84	1.01	1.62
3	1.35	0.44	0.64	0.64	1.28	1.59	2.43
4	1.80	0.89	0.85	0.85	1.70	2.20	3.24
5	2.25	1.07	1.06	1.06	2.12	2.73	4.05
6	2.70	1.19	1.27	1.27	2.54	3.32	4.86
7	3.15	1.65	1.48	1.48	2.96	3.95	5.68
8	3.60	2.19	1.69	1.69	3.38	4.53	6.49
9	4.05	2.54	1.91	1.91	3.82	5.18	7.30
10	4.5	2.73	2.12	2.12	4.24	5.93	8.11
11	4.95	2.91	2.33	2.33	4.66	3.15	8.92

Table 4.12

Experimental and theoretical shear stresses at mid span due to vertical loading and St Venant torsion for beam type BT3

Conc kN	Torque k Nm	Rotation Experimental x 10^3 Radians	Vertical deflection under webs		Average deflection due to vertical load	
			mm	mm	Experimental mm	Theory mm
15	0	0			18.24	12.79
15	0.90	11.06	20.00	18.34	19.17	14.50
15	1.80	23.60	23.11	19.57	21.34	16.20
15	2.70	38.00	25.29	19.59	22.44	17.91
15	3.60	44.26	26.44	19.90	23.22	19.61
15	4.50	50.66	27.62	20.02	23.82	21.31
15	5.40	54.80	28.73	20.51	24.62	23.02
15	6.30	58.00	29.47	20.77	25.12	24.72
15	7.20	61.33	30.00	20.80	25.40	26.43
15	8.1	66.26	30.69	20.75	25.72	28.13

Table 4.13

Experimental and Theoretical Deflections at mid span for beam type BT1

Conc load kN	Torque k Nm	Rotation Experimental x 10^3 Radians	Vertical deflection under webs		Average deflection due to vertical load	
			mm	mm	Experimental mm	Theory mm
0	2.138		0	0	0.89	2.94
1	2.138	18.80	3.30	0.48	1.89	3.56
2	2.138	14.80	4.32	2.10	3.21	4.79
3	2.138	12.93	4.71	2.77	3.74	5.41
4	2.138	16.40	6.94	4.48	5.71	5.88
5	2.138	18.26	8.54	5.80	7.17	6.65
6	2.138	22.26	9.86	6.52	8.19	7.27
7	2.138	17.30	10.05	7.45	8.75	7.89
8	2.138	23.06	10.60	7.76	9.18	8.51
9	2.138	18.93	12.25	8.65	10.45	9.31
10	2.138	24.00	13.27	10.07	11.67	9.75

Table 4.14

Experimental and Theoretical Deflections at mid span for beam type BT2

Conc load kN	Torque k Nm	Rotation Experimental x 10^3 Radians	Vertical deflection under webs		Average deflection due to vertical load	
			mm	mm	Experimental mm	Theory mm
0	0	0	0	0	0	0
1	0.45	6.67	2.57	1.57	2.07	1.20
2	0.90	10.67	4.29	2.69	3.49	2.38
3	1.35	12.67	4.97	3.07	4.02	3.58
4	1.80	18.00	5.90	3.20	4.55	4.78
5	2.25	19.87	7.34	4.36	5.85	5.96
6	2.70	32.80	8.56	3.64	6.10	7.16
7	3.15	45.46	9.67	2.85	6.26	8.36
8	3.60	48.93	11.42	4.08	7.75	9.84
9	4.05	51.07	12.55	4.89	8.72	10.74
10	4.50	55.07	13.06	4.80	8.95	11.64
11	4.95	58.27	13.65	4.91	9.28	13.12

Table 4.15

Experimental and Theoretical Deflections at mid span for beam type BT3

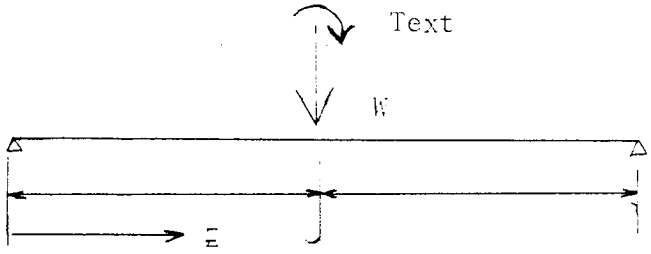

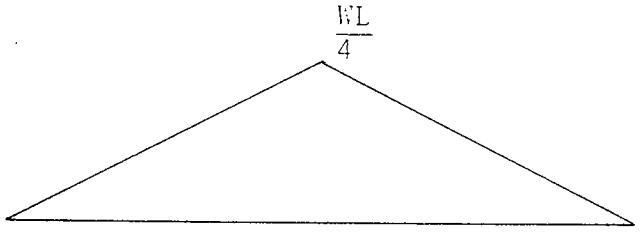

B. M. diagram

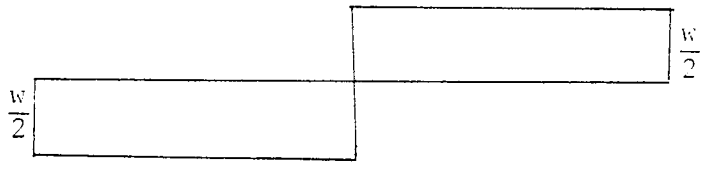

Shear diagram

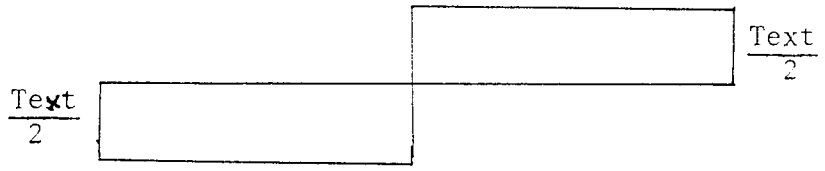

Torque diagram

FIGURE 4.1 APPLIED MOMENT DIAGRAMS

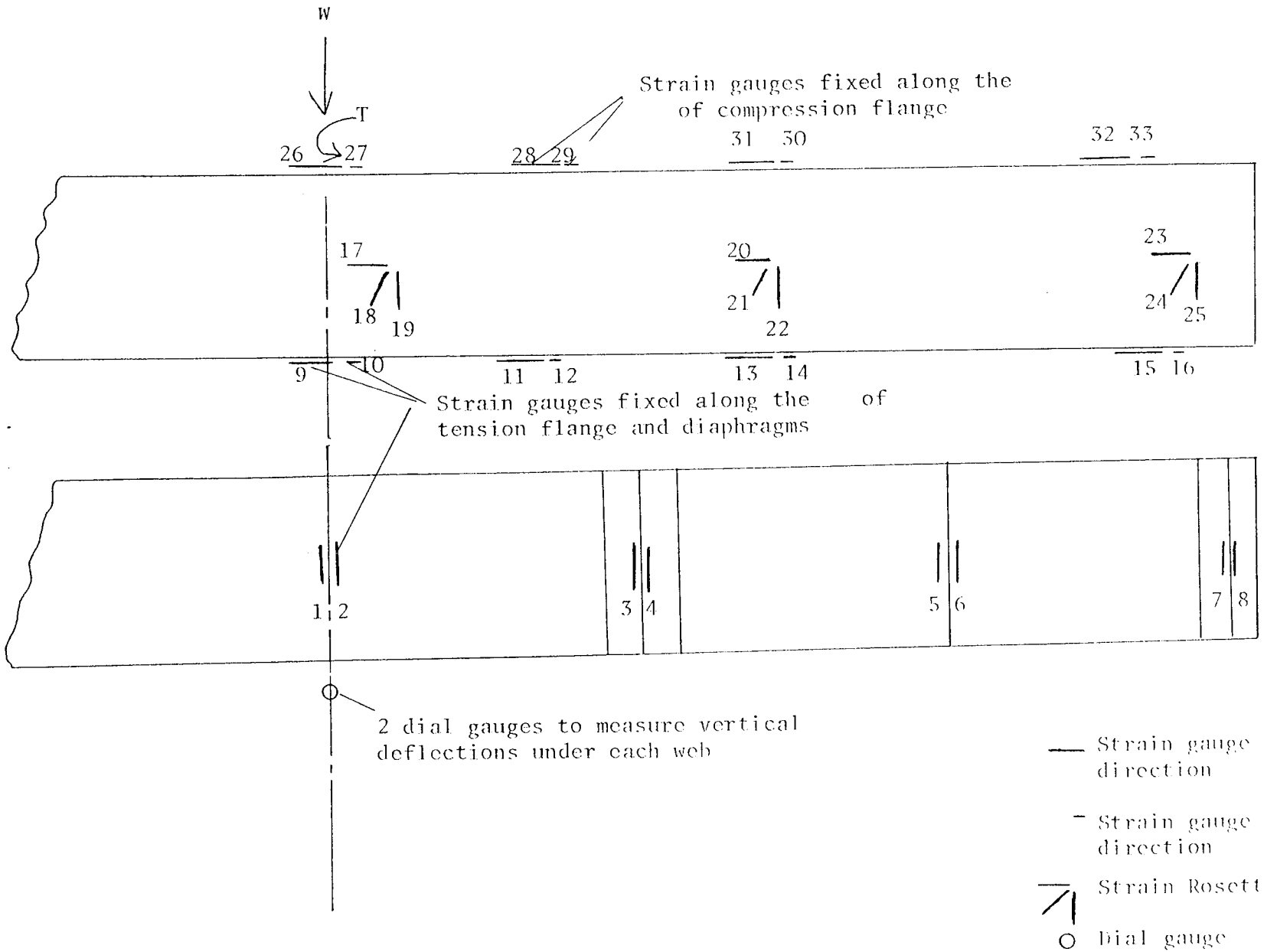

FIGURE 4.2 BEAM INSTRUMENTATION

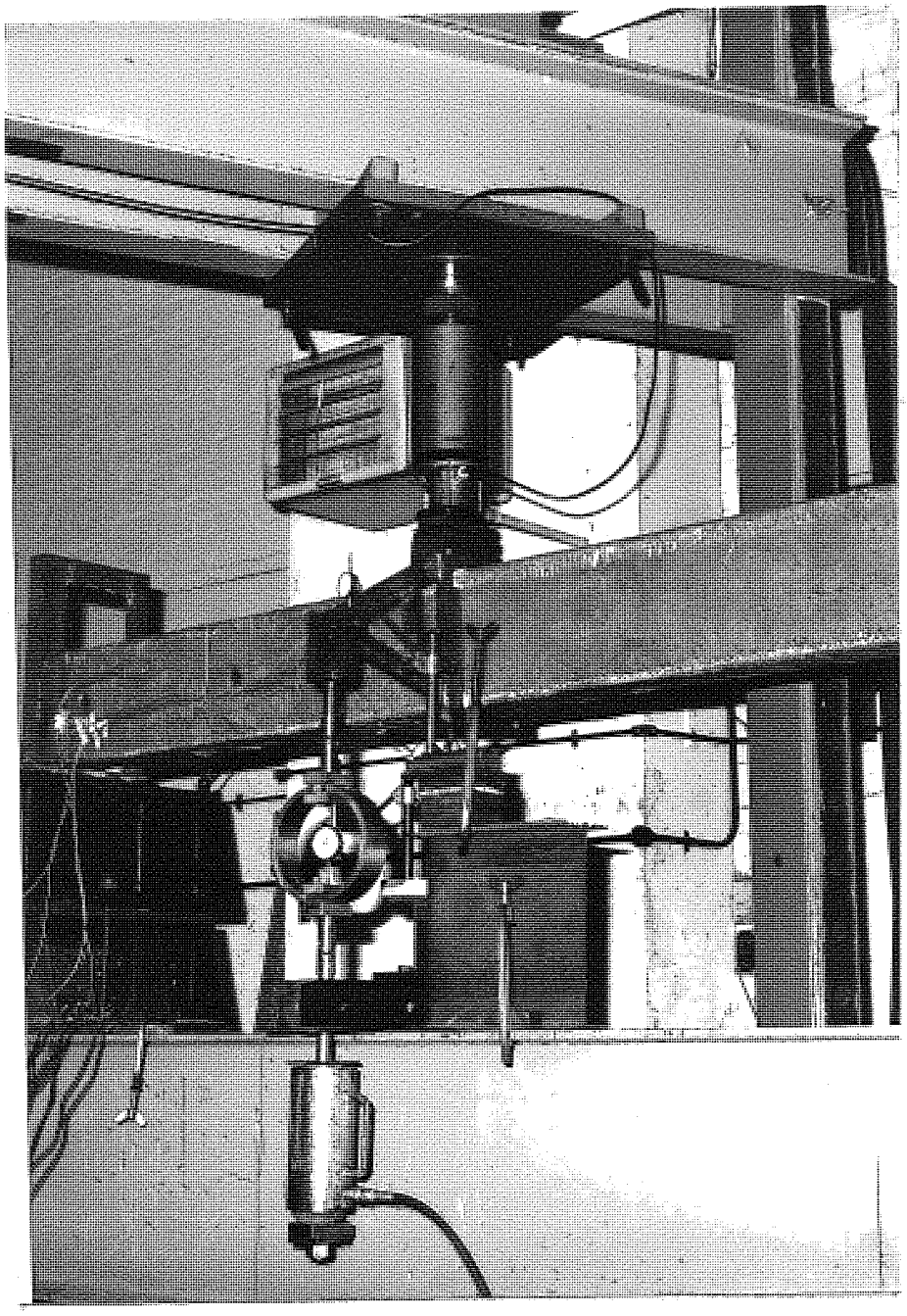

FIGURE 4.3 TEST SET UP FOR COMBINED BENDING AND TORSION

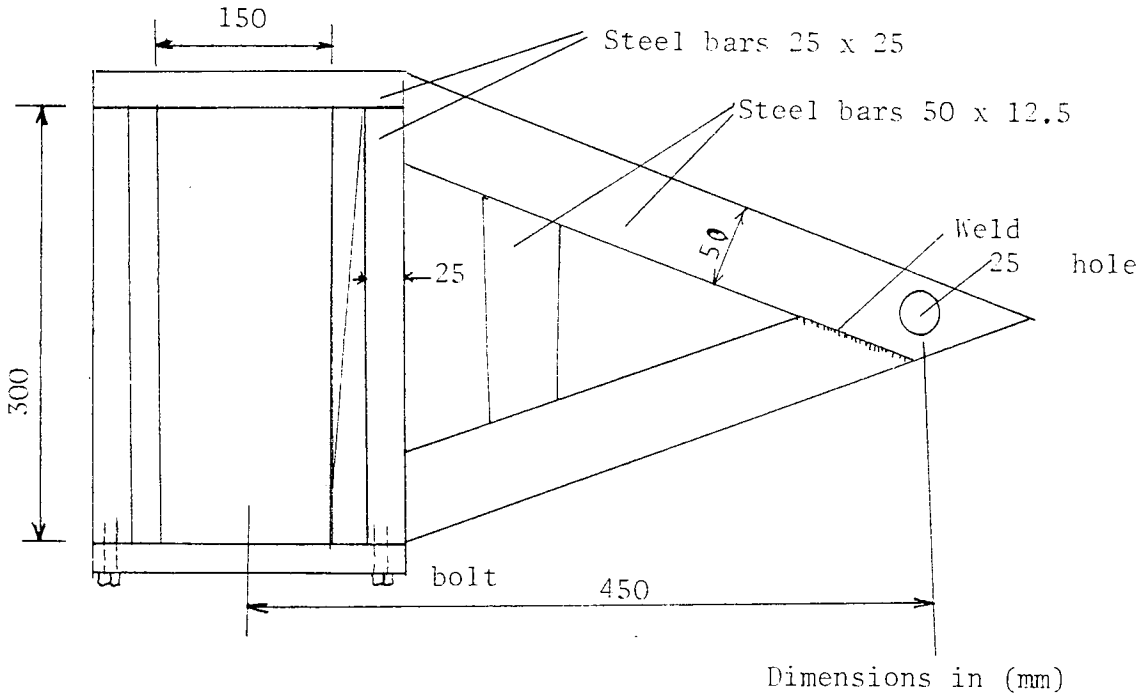

FIGURE 4.4 TORSIONAL LOADING FRAME

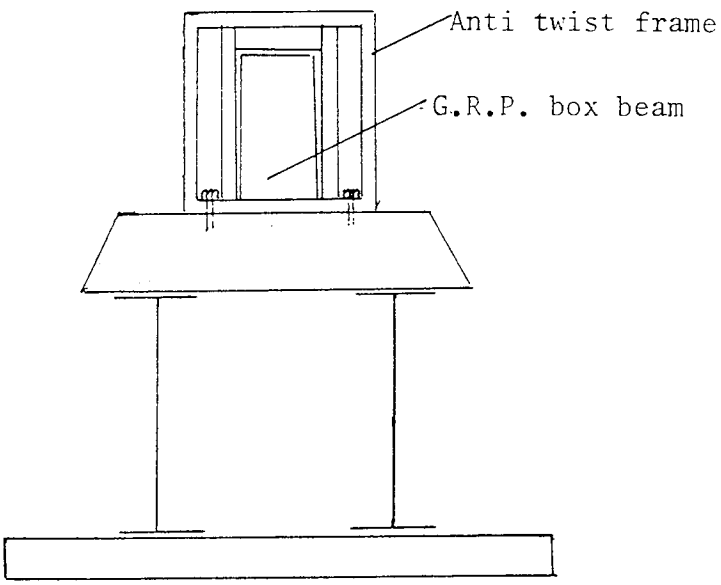

FIGURE 4.5 ANTI TWIST FRAME AT SUPPORTS

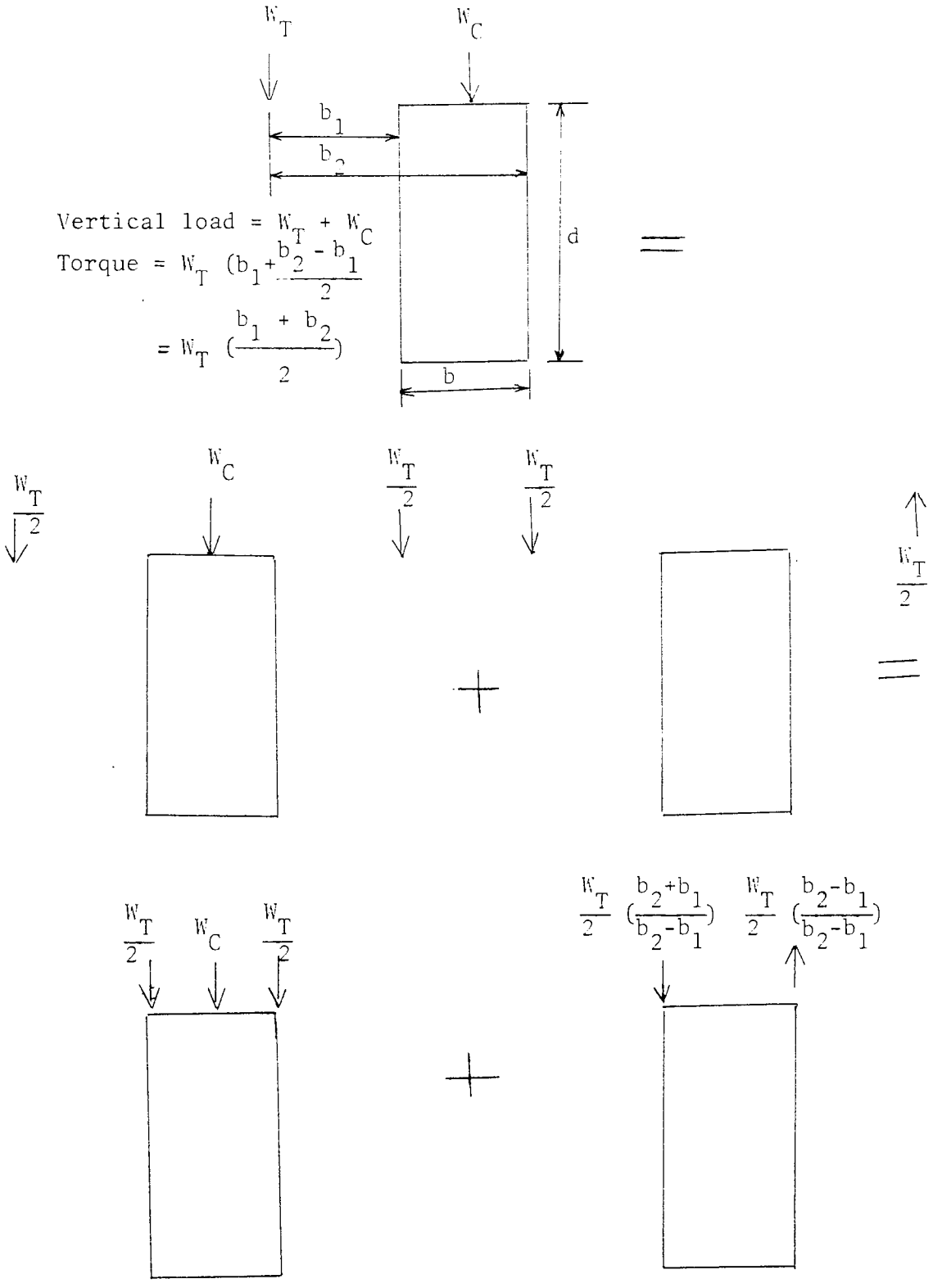

Vertical load system
Total vertical load = $W_C + W_T$

Torsional system

$$\text{Torque} = \frac{W_T}{2}\left(\frac{b_2+b_1}{b_2-b_1}\right)(b_2-b_1)$$

$$= W_T\left(\frac{b_2+b_1}{2}\right)$$

FIGURE 4.6 RESOLUTION OF LOADING

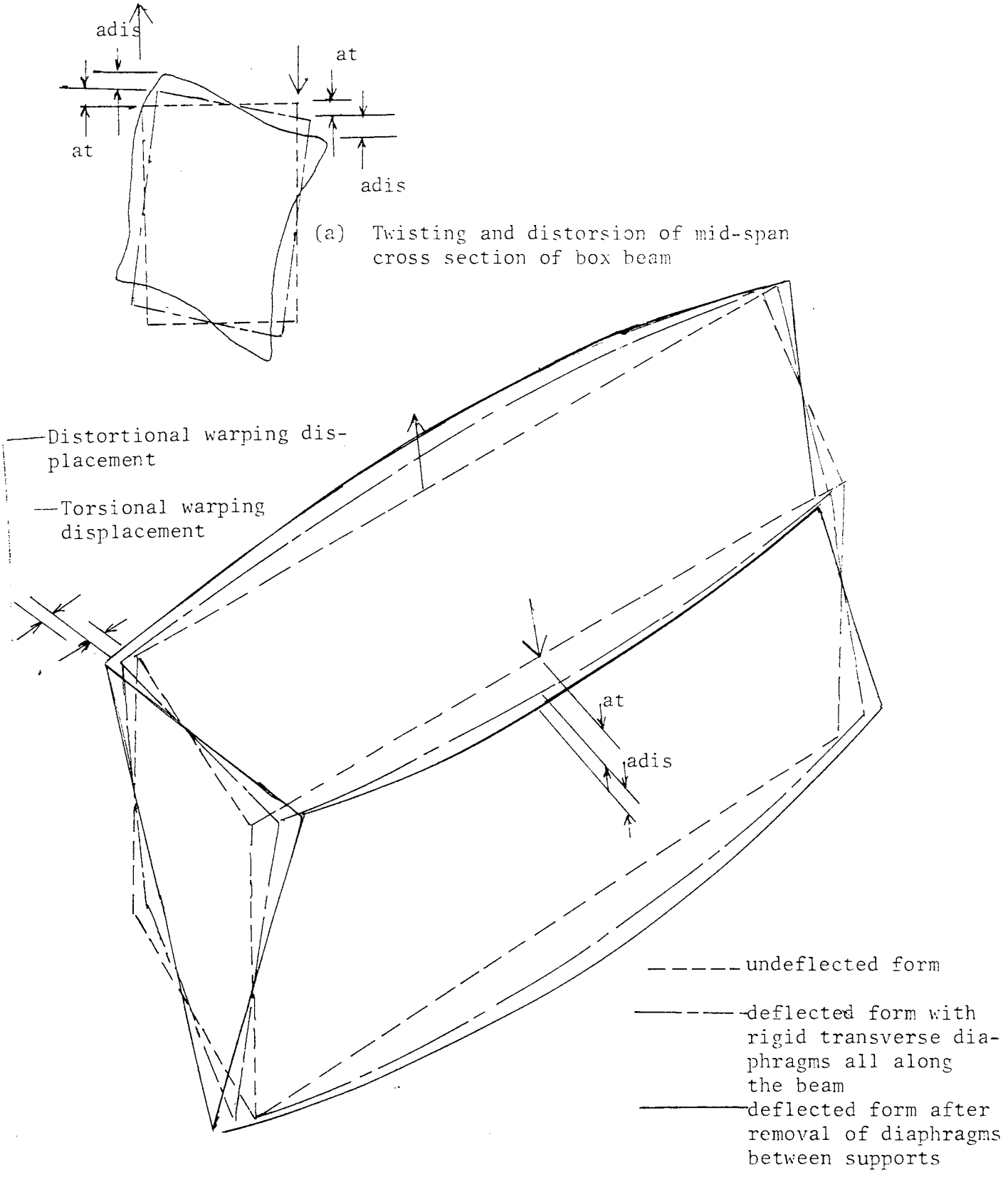

FIGURE 4.7 BEHAVIOUR OF BOX BEAM UNDER TORSIONAL LOADING

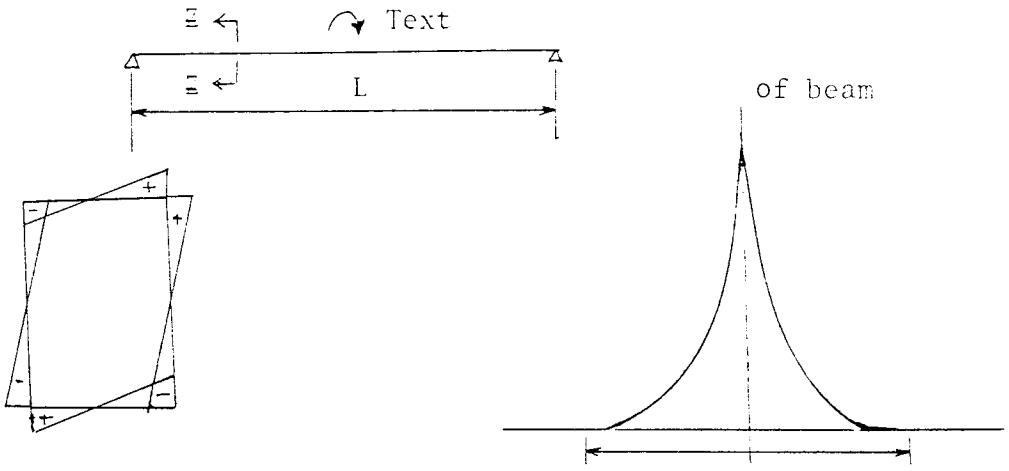

(b) Diagram of torsional warping stress at section Z Z

(c) Variation of torsional warping stress along beam

(c) Diagram of torsional shear stress (St Venant) at section ZZ

(d) Diagram of torsional warping shear stress at Section ZZ

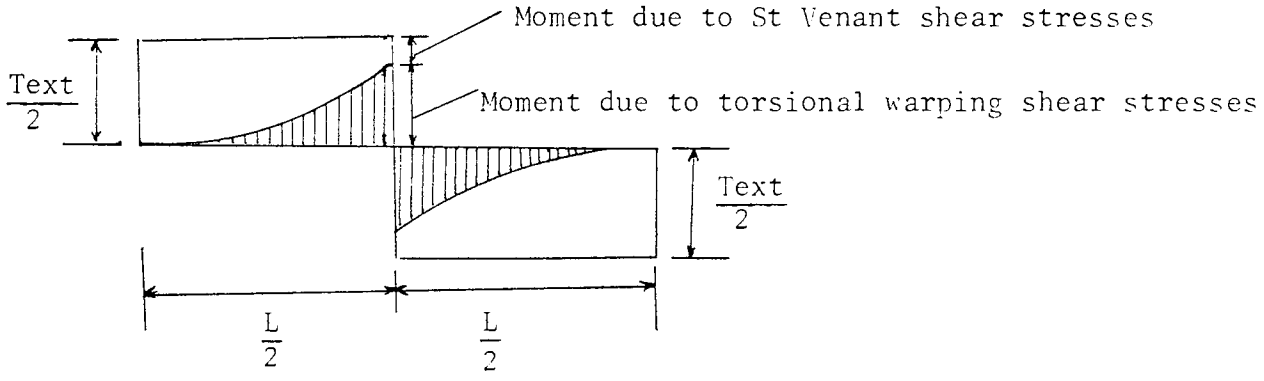

(e) Variation of component internal torsional moments along beam

FIGURE 4.8 STRESS PATTERNS IN BOX BEAM UNDER TORSION

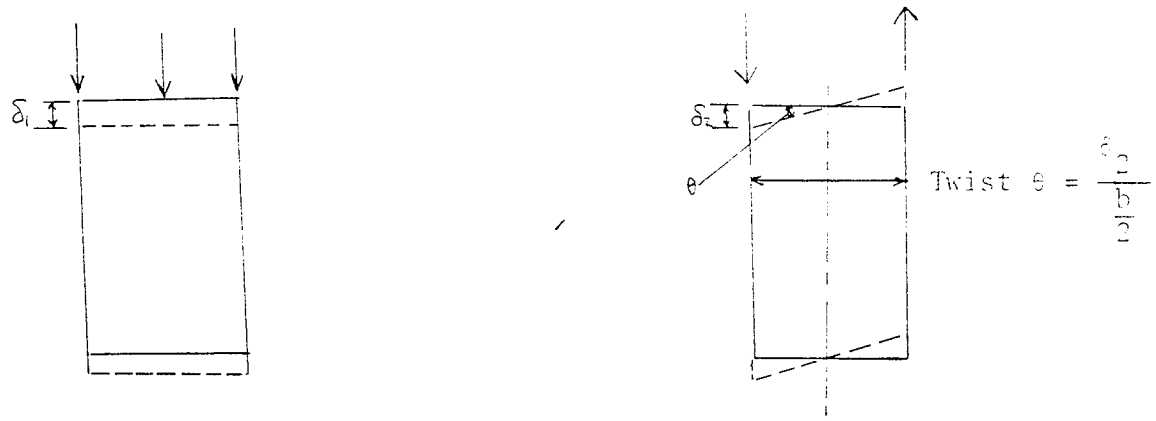

(a) Bending deflection due to symmetric loading

(b) Torsion deflection due to anti summetric loading

FIGURE 4.9 COMPONENTS OF VERTICAL DEFLECTION UNDER WEB

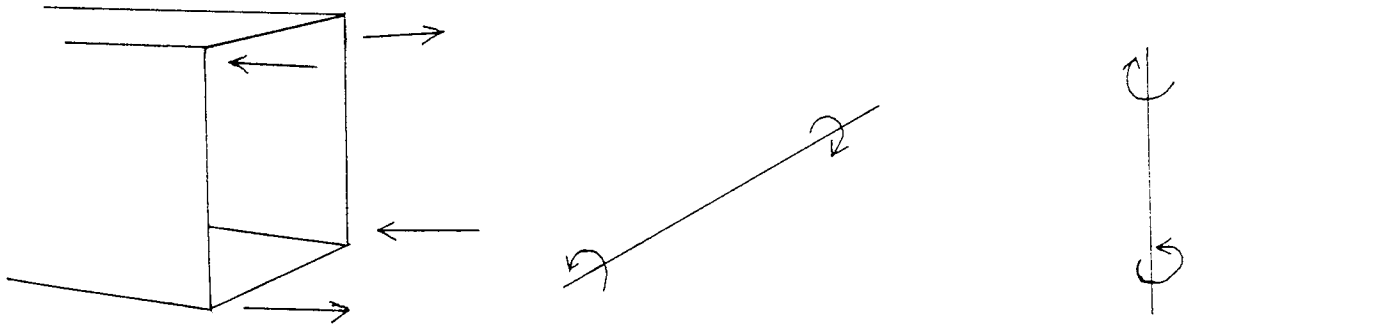

(a) Warping force group Four forces equal in magnitude

(b) Positive bimoment shown using horizontal axis

(c) Positive bi-moment, shown using vertical axis

FIGURE 4.10 WARPING FORCE GROUP AND BIMOMENT

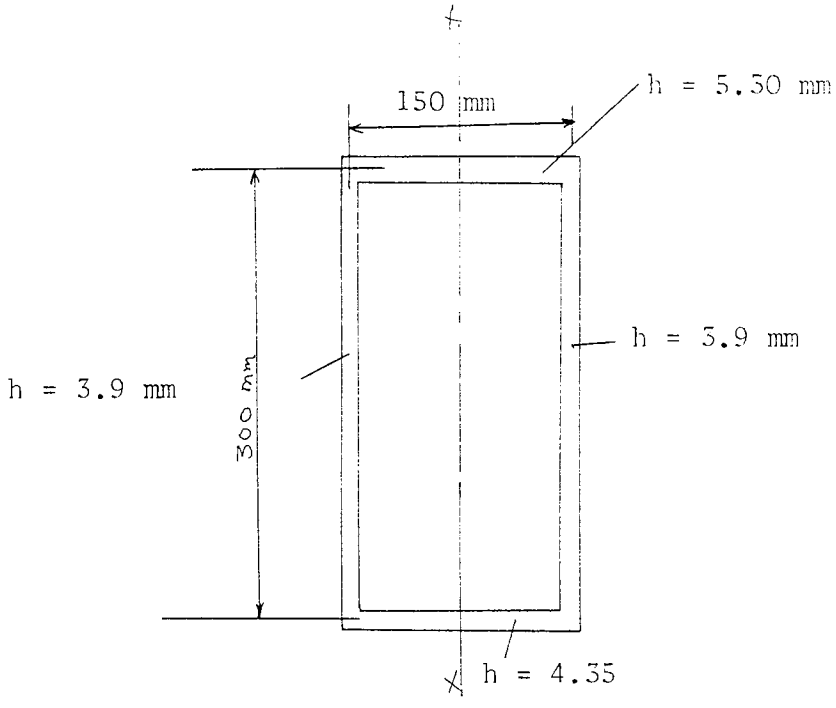

FIGURE 4.11 EQUIVALENT SECTION IN TORSION
BEAM TYPE BT1

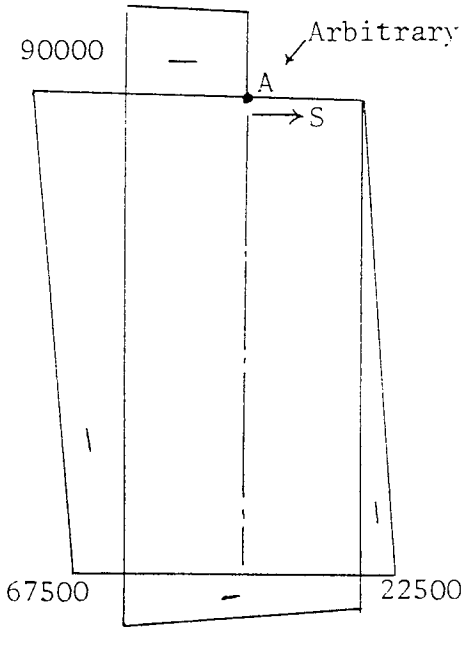

FIGURE 4.12 wb DIAGRAM

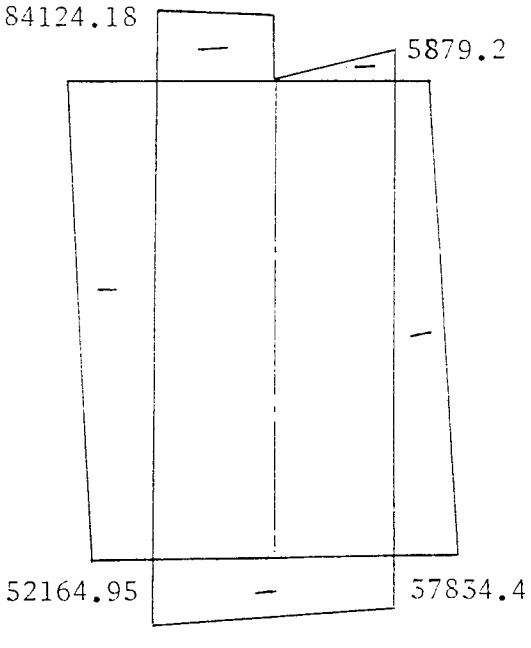

FIGURE 4.13 $P\bar{S}$ DIAGRAM

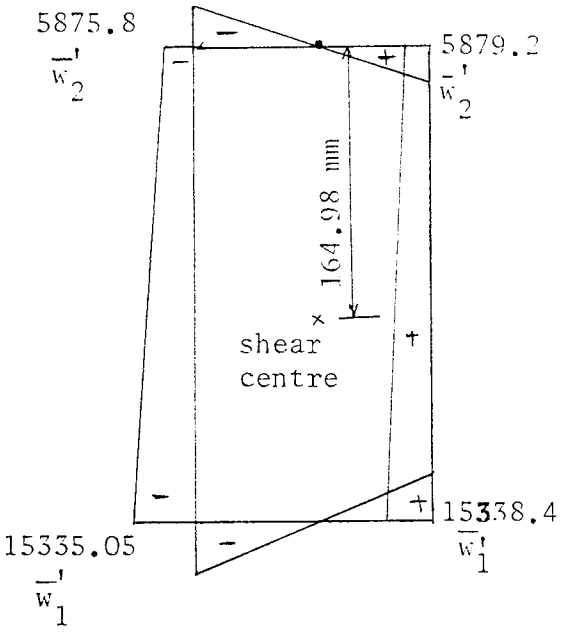

FIGURE 4.14 $\bar{w}'$ DIAGRAM

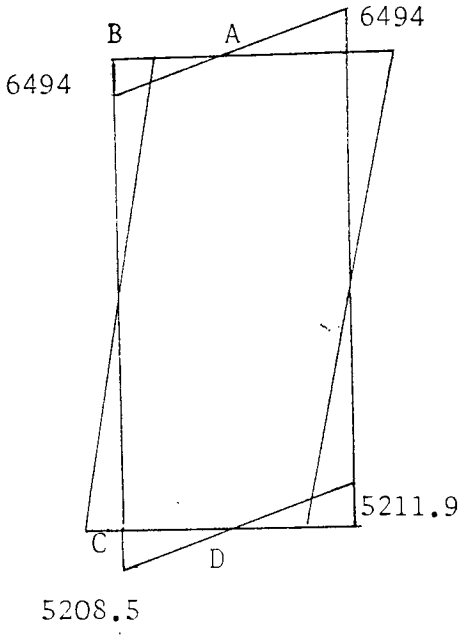

FIGURE 4.15 W_{twr} DIAGRAM

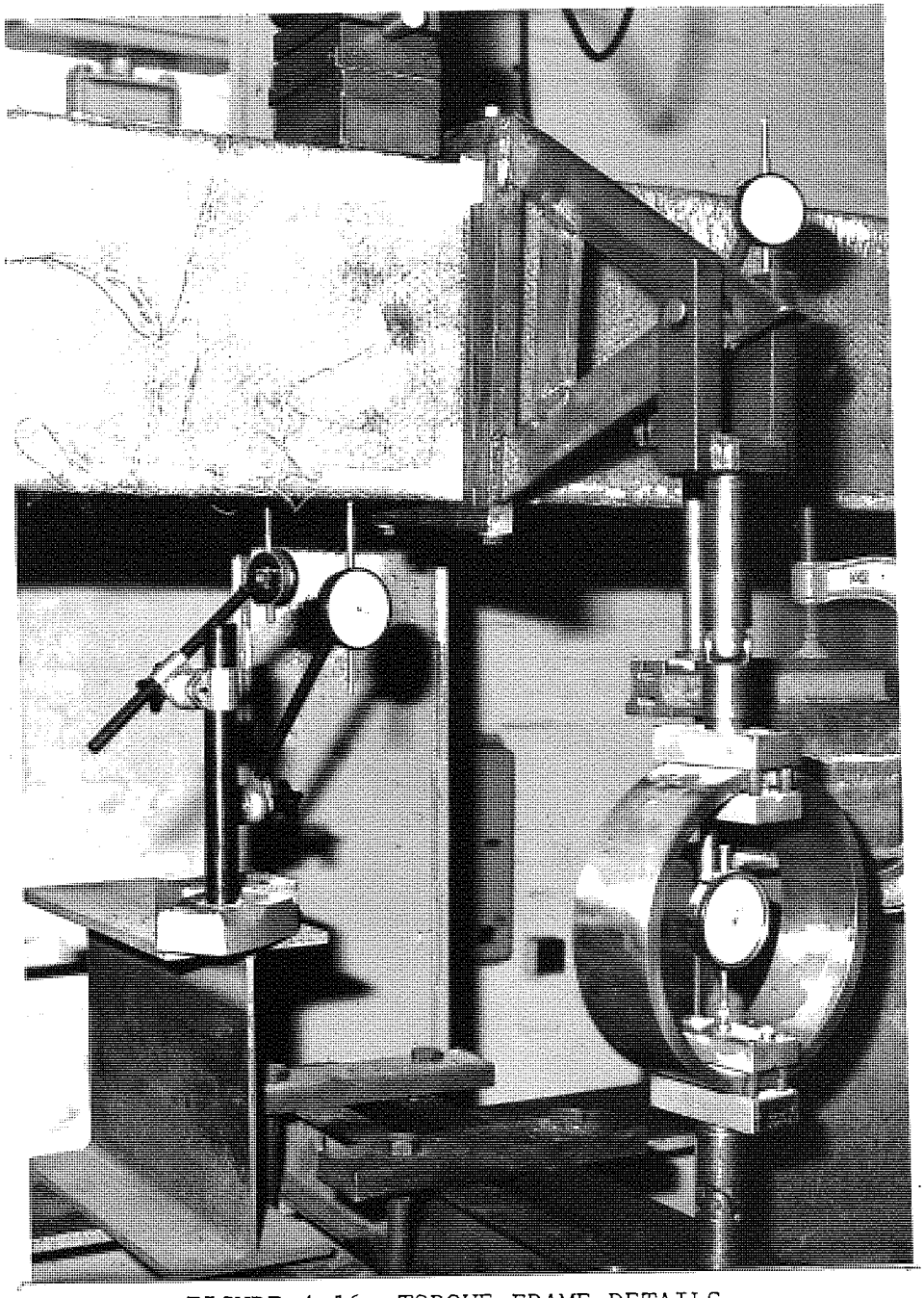

FIGURE 4.16 TORQUE FRAME DETAILS

REFERENCES

4.1 KOLLBRUNNER, C F, and HAJDIN, N, "Warping Torsion of Thin-walled Beams of Closed Section. Mittechungen der Technischen Kommission, Heft 32, 1966. Schweizer Stahlban Vereinigung, Zurich.

4.2 KOLLBRUNNER, C F and HAJDIN, N, "Wolbkrafttorsion Dunnwandiger Stabe Mitoffenem Profile". (Warping Torsion of Thin-walled Beams of Open Section). Teil 1, Mitteilungen der Technischen Kommission Heft 29. Verlag Schweizer Stahlban - Vereinigung, Zurich, October 1964.

4.3 HEILIG, R, A Contribution to the Theory of Box-Girders of Arbitrary Cross-sectional Shape. Cement and Concrete Association 1971. Translation No 145.

4.4 KOLLBRUNNER, C F and BASLER, K. Sektorielle Grossen und spannungen bei affenen, dunnwandigen Querschnitten. (Sectorial Quantities and Stresses in Open Thin-Walled Cross-Sections). Mitteilungen der Technischen Kommission, Heft 28. Schweizer Stahlban-Vereinigung, Zurich. January 1964.

4.5 STEINLE, A, "Torsion und Profilverformungbeim einzelligen Kastentrager. (Torsion and Cross-sectional Distortion of the Single-Cell Box Beam). Beton - und Stahlbetonbau, September 1970, pp 215-222.

4.6 STEINLE, A, Torsion und Profilverformung. (Torsion and Cross-Sectional Distortion). Dissertation Universitat ITechnische Hochschule) Suttgart, 1967.

4.7 VLASOV, V Z, "Thin-walled Elastic Beams" National Science Foundation, 1961.

4.8 KHAN and STAFFORD SMITH, "Bracing in Thin Walled Open Section Beams". Proceedings of the Institution of Civil Engineers Part 2, 1975, 59 Mar. 79-89.

CHAPTER 5

CREEP BEHAVIOUR OF BOX BEAMS

5.1 INTRODUCTION

Creep is a time-dependant strain in a material resulting from a constant load . In the case of reinforced plastics creep is greatly influenced by the creep characteristics of the reinforcing material. The reinforcing material may consist of glass, mats or flakes of natural or synthetic polymeric material. In a reinforced plastic the chief function of the plastic resin is to bind the reinforcing fibres together making it possible for the reinforced plastic to function as a unit rather than as an agglomeration of individual fibres. Thus the resin must serve to distribute the stresses amongst the individual fibres. In so doing the plastic resin is itself subjected to stress and therefore may creep. The following actions are probably involved in creep of reinforced plastics:-

(a) Creep of the reinforcement.

(b) Gradual straightening of segments of reinforcing fibres. Such straightening requires simultaneous creep of the resin which is tending to restrain the fibres in their initial configuration.

(c) Creep of the resin in regions in which it is highly stressed in transferring stress from fibre to fibre.

(d) Gradual rupture of the bond between resin and fibres with attendant slip of the released portion of fibres relative to the resin and other fibres.

(e) At later stages, periodic, random rupture occurring at an increasing rate of those individual fibres which becomes subjected to a higher stress due to the effects (a) to (d) above than they are able to accommodate.

In this chapter creep behaviour of glass reinforced plastics will be examined in an attempt to understand creep behaviour in complete G.R.P. structural elements. Little work has been carried out to date on creep of G.R.P. structural elements and the little which does exist is conflicting [5.1 - 5.6]. It was, therefore, decided to cast three box beams to make a preliminary study of creep behaviour. It was also decided to subject two of these beams to imposed loads of the same magnitude which was to be applied as a permanent load to one beam but as an alternating load to the other. After suitable period of alternating load application the second beam load was also applied as a permanent load. The third beam was to be subjected to its own self weight only.

5.2 BEAM SELECTION

It was decided to adopt the same cross section (150 mm x 300 mm) as that used for the bending and torsion series B1-B5 and BT1-BT3.

An increased span of 6 m was adopted which in conjunction with an imposed load of 1 ton (1000 kg) corresponds to a loading of $\frac{1}{3}$ ultimate load which was considered reasonable for the study of creep behaviour.

5.3 DIAPHRAGM SPACING

To increase the stiffness of the 6 m span beam, a spacing of 500 mm between diaphragm was adopted along the full length of the span as it proved to be effective in the bending series beams B1-B5. However bearing in mind the recommendations of previous research workers in box beams, [2.2, 2.5 and 2.6], the 500 mm spacing was checked against the Kristick formulae [2.5] and found to be less than the minimum required spacing.

5.4 BEAM REINFORCEMENT

A bidirectional reinforcement (commercial name Y103) was chosen to reinforce the beam components for the following reasons:-

(1) The bidirectional beam series B5 tested in bending attained the maximum ultimate capacity in compression.

(2) It obviates the use of chopped mat along the corners of the box beam as a bidirectional material can control any stress concentrations due to its orthotropic nature.

(3) Previous tests of box beams in bending and shear (Chapter 2) have shown that the main failure mechanism was local buckling. A bidirectional material will resist local buckling in all directions in contrast to unidirectional material which resists local buckling in the single fibre direction only.

(4) Bidirectional material is easier to handle and thus considerable time is saved compared to the use of unidirectional material. The arrangement of reinforcement adopted for the beam fig (5.1) is similar to that of beam B5 in the bending series B1-B5, i.e. four layers in the webs, tension flange and diaphragms and six layers in the compression flange.

5.5 BEAM CASTING

The same mould was used to obtain two 3 m length beams each with two reinforcement layers only including diaphragms. The two-two layered beams were then brought together and three layers (300 mm wide) of chopped mat were used to bond them after checking the alignment of the newly formed 6 m length beam. A further two layers (1000 mm wide) of bidirectional material were then applied at the joint. The rest of the reinforcement for the beam was then applied continuously along the full length of the 6 m beam.

5.6 BEARING AND SUPPORT DESIGN

The same special support and bearing arrangements were used as in the bending and torsion series B1-B5 and BT1-BT3. 100 x 50 mm timber pads were placed at the support points of the steel frame testing rig for compatibility.

5.7 BEAM LOADING

Loads were applied at $\frac{1}{3}$ span points to give a central constant moment zone and eliminate possible local deformation which might have occurred under a single central point load. Fig (5.2) shows the general arrangement of the test rig and load application making use of available scrap material. The scrap material was placed into metal containers so as to give 28 kg per containers. The metal containers were then laid carefully on the supporting frame in a symmetrical arrangement so that the supporting frame was not tilted. The total applied including the supporting frame was 1 ton (1000 kg).

5.8 TEST RIG

The test rig shown in fig (5.2) and (5.3) was used. It comprised of two triangular steel frames which were designed to accommodate two beams with their imposed loads - care was taken that no interference occurred while loading and unloading operations were carried out on the beam under alternating load.

5.9 BEAM INSTRUMENTATION AND MEASUREMENTS TAKEN

A typical beam instrumentation is shown in fig (5.4). Deflections and strains were recorded for a total period of approximately 20 months which was considered to be suitable for extrapolation for longer periods. Demec gauges were chosen for measuring the strain rather than electrical strain gauges as the latter are more influenced by humidity and other environmental factors.

Readings were taken at increasing intervals up to a month and thereafter every month. A suitable programme for taking records was selected and is described below:-

Beam R1 was subjected to a permanent imposed load of 1000 kg. Readings were taken at the following intervals after loading:-

1 hr, 5 hr, 1 d, 2d, 4d, 7d, 15d, 30d, 60d 90d, ... etc after loading.

Beam R2 was subjected to an alternating load of 1000 kg for a period of three months and afterwards the load was applied permanently. Readings were recorded at the following intervals of time starting from initial loading:-

0 Load 1d unload 2d load 4d unload 7d load 15d

unload 30d load 60d unload 90d load permanently applied.

i.e. after 90 days the load was permanently applied and readings were taken every 30 days.

Beam R3 was subjected to its own self weight and readings taken as for beam R1.

NB. hr = hour

d = day

5.10 CONTROL OF ENVIRONMENTAL FACTORS

The creep tests were carried out in the lower basement of the university where humidity temperature variations are expected to be minimum.

5.11 PREVIOUS RESEARCH

Static, fatigue and creep tests of a glass fabric laminated with a polyster resin [5.1] revealed that fatigue strength at 10^7 completely reversed cycles decreased from 86.2 N/mm^2 at 77^o to

24.14 N/mm^2 at 300°F. Creep strength at 100 hrs decreased from 219.3 N/mm^2 at 77°F to 173.1 N/mm^2 at 400°F. At 400°F substantial shrinkage was observed together with an increase in modulus with time and temperature. The rate of increase in creep strain "creepocity" during a creep test at 77° from 20 seconds to 40 hours was about 10.6%. At 400°F creepocity varied from 20.7 to 49.3%.

Boller [5.2] describes test on fatigue properties under various conditions. Moisture was found to affect fatigue strength only slightly, at 10^7 cycles the drop in fatigue strength due to the presence of moisture was only 2% of the static tensile strength.

The effect of stress concentrations on average fatigue strength for notched polyester/glass material at room temperature after 10^7 cycles at zero mean stress was about 23% of ultimate tensile strength. Average difference between notched and unnotched material was about 4.5% of ultimate tensile strength. At high temperatures e.g. 500°F, the difference decreases.

Regarding the effect of elevated temperature, a typical result for polyester/glass laminates at 500°F was a reduction in fatigue strength at 10^7 cycles of between 7% and 18% of static tensile strength value at room temperature.

The following conclusions were drawn from [5.3] which dealt with the effect of time, temperature and environment on the mechanical properties of glass reinforced plastics.

1 - All laminates lose strength when test temperature is increased.

2 - Flexural strengths of laminates are reduced by the presence of water.

3 - Short-time mechanical properties determined in air at room temperature are of limited value. They do not necessarily measure

the ability of a material to support sustained loading in a normal environment.

4 - Laminating resins, reinforcements and interface reagents differ significantly in structural performance.

5 - Goldfein [5.4] claimed that creep properties of glass reinforced plastics may be calculated from modulus of elasticity data at high temperature using the parameter K = T(20 + logt). Results were accurate to within 10% for periods of time from 0.1 to 10000 hours.

On the effect of long term loading on glass reinforced plastic laminates K. H Boller [5.5] concluded that:

(a) Glass mat laminate data show a considerable amount of scatter. Glass cloth laminates are more consistant.

(b) 181 glass cloth/polyester laminate at 60% of short time strength had endured 10000 hours loading without failure.

(c) In water for 10000 hours the stress level sustained is only 35% of short time strength.

(d) Ratio of strain at failure to strain at zero-hours decreases with increase in stress.

(e) Tensile strains appear to conform to the relationship

$$E = E_o(1 + t^n) \text{ where}$$

E = total strain in inches per inch of a material under constant stress.

E_o = Some initial strain marking the begining of this function.

t = time in hours

n = an exponent, dimensionless.

J. Kabelka [5.6] carried out investigations into the long term

strength properties of G.R.P. and he concluded that the measurements of long term deformations revealed that the effect of compressive and shearing stresses on the strain of the structure is considerable. In the case of creep under tensile stress he expressed the strain as a function of temperature and time with the following equation.

$$\Sigma(t,T,\sigma) = \sigma A(T) \left(\frac{t}{t_o}\right)^{BT}$$

in which A(T) and B(T) are functions of temperature only and t > 1 minute.

For creep in compression, he found that the relationship between strain and time on the logarithmic scale can be considered linear only within a relatively low stress range.

In the case of creep in shear, he established a relationship between the relative displacement, stress and time which can be expressed in the following equation

$$\gamma = \sinh \frac{T}{\tau_o} [a + bt - t_*{}^{m}] \quad \text{for } t > t_*$$

where τ, τ_o = shear stresses at t time and initial time.

a, b are constants

m exponent

5.12 TEST RESULTS

For beams R1, R2 and R3 creep behaviour in terms of deflection, tensile compressive and shear strains was plotted against time in hours fig (5.5-5.8). In the case of deflection tensile and compressive strains mid span dial gauge No 2, Demec gauges No 18 and 8 were chosen for the plot, Demec gauges No 9, 10 and 11 see fig (5.4)

were also chosen for the study of creep shear strain at the support.

Creep deflections, compressive, tensile and shear strains, were also plotted against log time fig (5.9-5.12). Further graphs of log - log plots of deflections, tensile compressive creep strains are also shown in fig (5.13-5.16).

In the case of beam R2 deflections, tensile, compressive and shear total (Elastic + creep) strains were plotted against durations of loading and unloading fig (5.21-5.24) Table (5.1) shows the initial values for deflection tensile, compressive and shear strains immediately after the begining of the test.

5.13 DISCUSSION

5.13.1 Deflection Behaviour

Beam R2 exhibited a slightly higher, but similar, creep deflection curve than beam R1 though the same 1000 kg load was imposed on each of them.

At the first 500 hour beam R1 and beam R2 achieved 65.7% and 69.3% of their ultimate creep at 15000 hours, and at the first 1000 hours the corresponding creep values were 74.2% and 70.6%. From the shape of the curves fig (5.5) it can be seen that these are steep during the first 4000 hours and that they tend to the horizontal after that point.

For beam R3 creep deflection seems to increase steadily with time but with rather scattered data. From fig (5.5), the rate of creep, and percentage of creep against time were determined and are shown in Table (5.2). The values obtained indicate clearly that the rate of creep is maximum at small values of time and decreases with large values of time, and this is the expected result from the known creep behaviour of G.R.P. material.

The maximum creep deflections after 15000 hours for beam R1 and R2 were 35 and 37.5 mm and these represent 108.66% and 113.36% of their initial deflection at 0 hour with imposed load. These deflections also correspond to $\frac{1}{171}$ and $\frac{1}{160}$ of their spans (6 m).

5.13.2 Tensile Creep

Again beams R1 and R2 exhibited similar sets of curves fig (5.6). However, the curves were not as steep in the first 2000 hour as they were for deflection behaviour.

Fig (5.6) shows that 38% and 37% of their ultimate creep was attained at 15000 hours. For beam R3 tensile creep showed an increase with time at a gradual rate.

5.13.3 Compressive Creep

Data of compressive creep for beam R1 and R2 were scattered, however a set of curves was selected to describe creep behaviour fig (5.7). Creep strain appears to increase steadily between 6000 and 8000 hours and then tend to decrease. This was not the case for beam R3 where a rather consistant set of data was obtained. Two explanations may be put forward for the data inconsistency of beam R1 and R2.

The first is that a creep recovery might have gradually started to take place during the period of the tests.

The second reason is that from previous tests on box beams under the same loading system, it is known that local buckling in the compression flange occurred prior to failure.

In the case of beam R1 and R2 the imposed load represents $\frac{1}{3}$ of its expected ultimate load, and though buckling of the compression flange was not usually obvious it could have taken place and hence lead to inconsistant data due to different modes of buckling being formed.

5.13.4 Shear Creep

Shear creep strain against time curves fig (5.8) showed somewhat more consistancy than the compressive creep strains. Curves were steep up to the first 6000 hours and after that tend to become steady for about 2000 hours after which time creep rises again. The scattered data could be the result of some form of local buckling in the web. Creep percentage achieved during the first 500 hours for beam R1 and R2 was only 20% and 23.7% of their ultimate creep at 15000 hours.

Beam R3 showed that creep strain increased steadily up to 5000 hours the rate of increase then slowed down, finally creep strain was decreasing with time.

5.14 PREDICTION OF CREEP BEHAVIOUR

To examine the creep behaviour in deflection tension compression and shear strain further plots fig (5.9-5.12) were made of creep behaviour of those properties against time to a log scale. Further plots (5.13-5.16) were also made for the log of these properties in creep against log time.

As a result of these plots three equations were derived to describe creep behaviour namely:-

$$\varepsilon = \varepsilon_o + m(t/t_o)^n \qquad (5.1)$$

$$\varepsilon = \varepsilon_o + A \log_e t \qquad (5.2)$$

$$\varepsilon = \varepsilon_o + B\log_e t + C_t \qquad (5.3)$$

where

ε represents the total deformation or tensile compressive or shear strain at time t.

ε_o represents the initial deformation or tensile compressive or shear strain immediately after start of creep test.

t_o is a constant taken equal to unity and having the dimension of time.

m, n, A, B and C are constants which depends on the stress, material and temperature.

The test data for creep properties for beam R1 are compared with the above three equations plotted for the first 2000 hours in fig (5.17-5.20). Accordingly the values of the constants, m, n, A, B and C are established in Table (5.5).

Comparing the theoretical and experimental plots the following conclusions were drawn.

(a) Equations 5.2 yields the best prediction of long time creep deformation.

(b) Equation 5.1 yields the best prediction of long time creep in tensile strain. From equation (5.1) it may be shown that log $(\varepsilon - \varepsilon_o)$ is a linear function of log t with a slope of n. Thus creep data plotted as log $(\varepsilon - \varepsilon_o)$ versus log t should describe a straight line, the plot of fig (5.14) shows that this is in fact the case.

(c) None of the predictive equations show good agreement with the compressive creep test data.

(d) Up to a period of 5000 hours equation (5.3) describes with reasonable accuracy creep behaviour in shear. Fig (5.20).

5.15 CREEP BEHAVIOUR UNDER ULTERNATING LOAD

Generally creep deformation, tensile compressive and shear strains tend to increase during periods of imposed loading fig (5.21-5.24). During periods unloaded creep recovery was observed to be greater during the first 200 hours and after at a slower rate.

5.16 CONCLUSIONS

(1) The rate of creep (creepocity) whether in tensile compressive,

shear strain or in deflection depends on the load imposed, the higher the load the greater creepocity.

(2) Creep rate appears to be influenced by environmental temperature for G.R.P. beams loaded under their own weight. Creep test data for beam R3 exhibited scattering and it is suggested that these variations were due to temperature and humidity variations. With imposed loads on the beam the factors of temperature and humidity became negligible.

(3) Glass reinforced plastic is more liable to creep than conventional structural materials and under conditions of continuous loading this may eventually lead to stress rupture.

(4) A factor of safety of at least six is strongly recommended where deflection characteristics are a significant criteria of design (e.g. for beam structures). Where the structural system chosen is one in which deflection are not critical in design (e.g. deep folded plate structures) a lower factor of safety may be adopted and in these circumstances three would be recommended.

Initial Reading at the begining of test	Beam R1	Beam R2	Beam R3
Deformation (mm)	32.13	33.08	2.57
Tensile strain	1.20×10^{-3}	1.4×10^{-3}	1.96×10^{-4}
Compressive strain	1.38×10^{-3}	1.42×10^{-3}	1.67×10^{-4}
Shear strain	1.19×10^{-3}	1.28×10^{-3}	2.09×10^{-4}

TABLE (5.1)

Initial readings taken at the begining of creep test for Beams R1, R2 and R3

	Creep of initial deflection at the begining of the test			Rate of Creep (Creepocity) mm x 10^{-3} per hour		
Time hour	Beam R1	Beam R2	Beam R3	Beam R1	Beam R2	Beam R3
0						
500	77.61	78.59	1.17	50	52	.06
1000	80.72	84.64	1.94	2	4	.04
2000	88.48	92.80	3.89	2.5	2.7	.05
3000	93.91	98.24	6.61	1.75	1.8	.07
4000	99.34	101.87	9.72	1.75	1.2	.08
5000	100.90	104.89	13.62	0.5	1	.10
6000	103.22	107.01	16.34	0.75	0.7	.07
7000	104.31	107.92	17.89	0.35	0.3	.04
8000	105.55	108.82	19.45	0.40	0.3	.04
9000	106.17	110.33	20.62	0.2	0.5	.03
10000	106.79	110.64	21.40	0.2	0.1	.02
11000	107.11	110.94	23.34	0.1	0.1	.05
12000	107.42	111.85	25.29	0.1	0.3	.05
13000	107.73	112.45	29.18	0.1	0.2	0.1
14000	108.66	113.36	35.02	0.3	0.3	.15

TABLE (5.2)

Deformation expressed as a percentage of the initial deformation taken at the begining of the test and the corresponding creepocity up to 14000 hours.

	Creep of initial strain at the begining of the test			Rate of Creep (Creepocity) Strain $\times 10^{-8}$ per hour		
Time hour	Beam R1	Beam R2	Beam R3	Beam R1	Beam R2	Beam R3
0						
500	13.33	13.57	30.61	32	38	12
1000	20.00	20.00	51.02	16	18	8
2000	32.50	30.00	81.63	15	14	6
3000	41.66	37.86	112.24	11	11	6
4000	50.00	44.28	132.65	10	9	4
5000	56.66	50.71	153.06	8	9	4
6000	62.5	56.43	168.36	7	8	3
7000	67.50	60.71	178.57	6	6	2
8000	71.66	65	188.77	5	6	2
9000	75.83	68.57	193.87	5	5	1
10000	78.33	72.86	204.08	3	6	2
11000	82.5	75.71	206.63	5	4	0.5
12000	85	77.86	214.28	3	3	1.50
13000	88.33	80.71	219.39	4	4	1
14000	90.83	82.86	224.49	3	3	1

TABLE (5.3)

Tensile creep expressed as a percentage of the initial strain taken at the begining of the test and the corresponding creepocity up to 1400 hours.

	Creep of initial strain at the begining of the test			Rate of Creep (Creepocity) Strain x 10^{-8} per hour		
Time hour	Beam R1	Beam R2	Beam R3	Beam R1	Beam R2	Beam R3
0						
500	10.14	18.31	35.93	28	52	12
1000	14.49	23.94	41.92	12	16	2
2000	21.74	30.98	49.10	10	10	1.2
3000	29.98	36.62	59.88	10	8	2.8
4000	34.78	40.84	65.86	8	6	1
5000	39.13	43.66	77.84	6	4	2
6000	42.02	45.07	83.83	4	2	1
7000	44.20	45.77	95.80	3	1	2
8000	44.20	45.07	107.78	0	-1	2
9000	44.02	43.66	119.76	-0.25	-2	2
10000	42.75	40.14	131.73	-1.25	-5	2
11000	42.02	36.62	149.70	-1.50	-5	3
12000	36.23	30.28	155.68	-8	-9	1
13000	31.88	23.24	155.68	-6	-10	0
14000	25.36	15.49	15.68	-9	-11	0

TABLE (5.4)

Compressive creep expressed as a percentage of the initial strain taken at the begining of the test and the corresponding creepocity up to 1400 hours.

	Creep of initial strain at the begining of the test			Rate of Creep (Creepocity) Strain x 10^{-8} per hour		
Time hour	Beam R1	Beam R2	Beam R3	Beam R1	Beam R2	Beam R3
0						
500	46.22	33.59	19.14	110	86	8
1000	71.42	50.78	95.69	60	44	32
2000	108.40	75.78	167.4	44	32	15
3000	132.77	93.75	215.3	29	23	10
4000	147.05	107.03	263.1	17	17	10
5000	157.98	114.84	287.08	13	10	5
6000	163.86	122.65	406.69	7	10	25
7000	169.74	126.56	320.57	7	5	-18
8000	172.26	126.56	315.78	3	0	-1
9000	176.47	121.09	315.78	5	-7	0
10000	182.35	117.96	311.00	7	-4	-1
11000	189.07	117.18	296.65	8	-1	-3
12000	197.47	119.53	296.65	10	3	0
13000	205.8	125.00	282.29	10	7	-3
14000	219.32	132.81	267.94	16	10	-3

TABLE (5.5)

Shear creep strain expressed as a percentage of the initial strain taken at the begining of the test and the corresponding creepocity up to 14000 hours.

Type of Creep behaviour	Equation No	Constant	Value
Deformation	1	m	1
	1	n	.483
	2	A	4
	3	B	4
	3	C	6×10^{-3}
Tensile strain	1	m	1×10^{-5}
	1	n	0.496
	2	A	5.15×10^{-5}
	3	B	1.885×10^{-5}
	3	C	1.5×10^{-7}
Compressive strain	1	m	1×10^{-5}
	1	n	0.410
	2	A	2.461×10^{-5}
	3	B	1.609×10^{-5}
	3	C	5.88×10^{-8}
Shear strain	1	m	1×10^{-5}
	1	n	0.658
	2	A	1.375×10^{-4}
	3	B	1.0457×10^{-4}
	3	C	2.226×10^{-7}

TABLE (5.5)

Values of parameters for the prediction equations 5.1, 5.2 and 5.3 based on the best representation for the first 2000 hours.

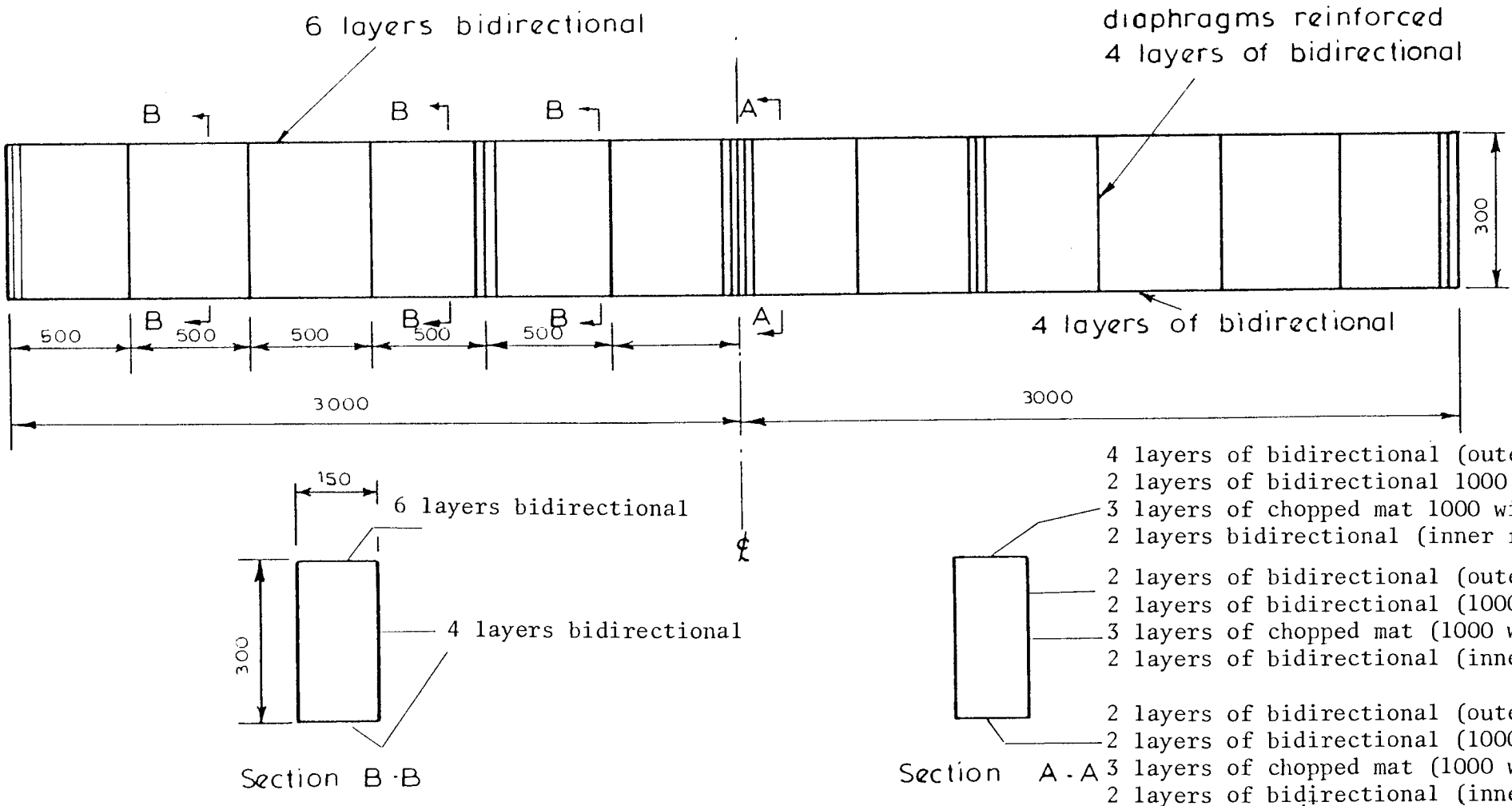

Fig. 5.1 Arrangement of reinforcement and diaphragms

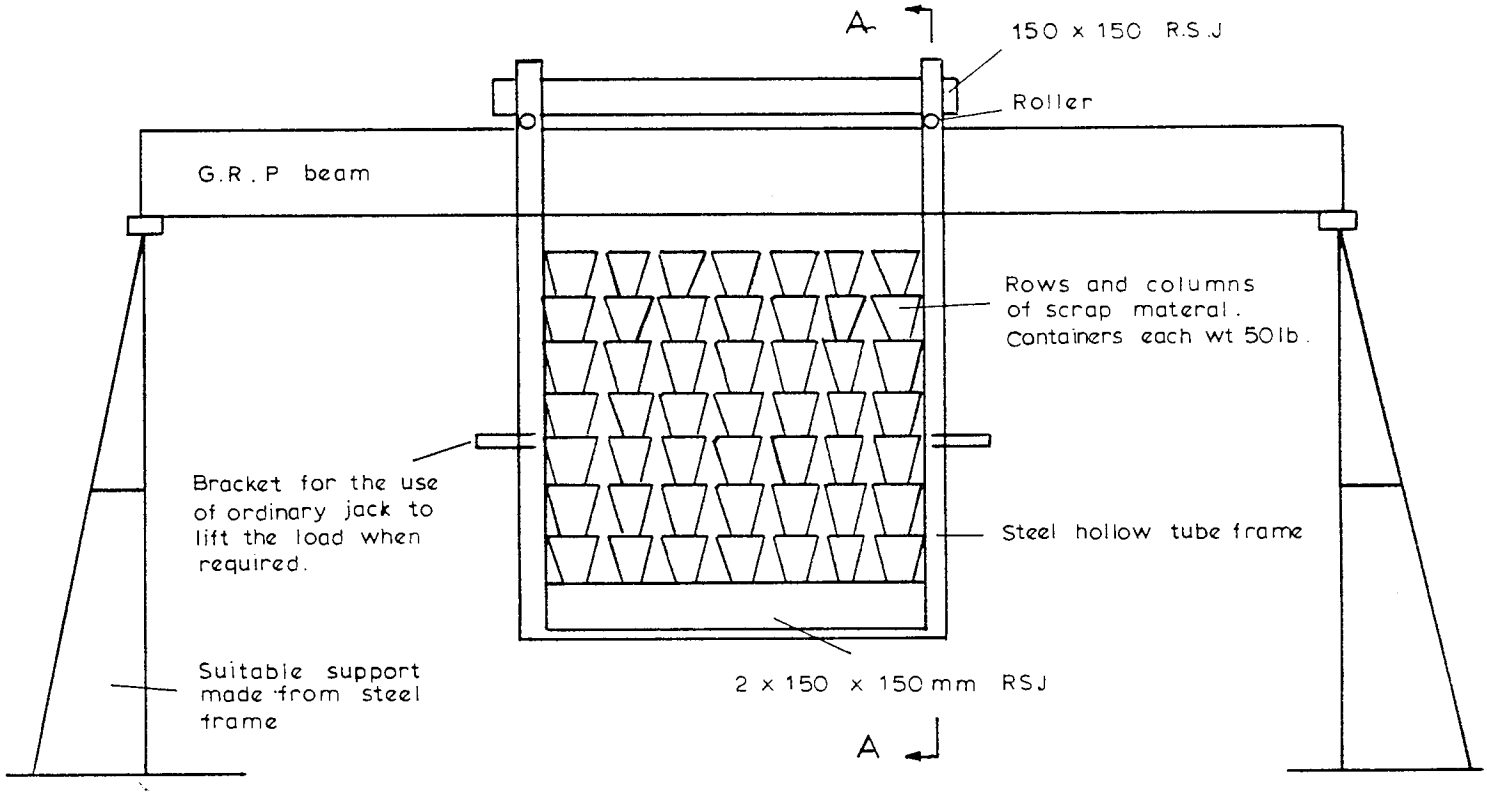

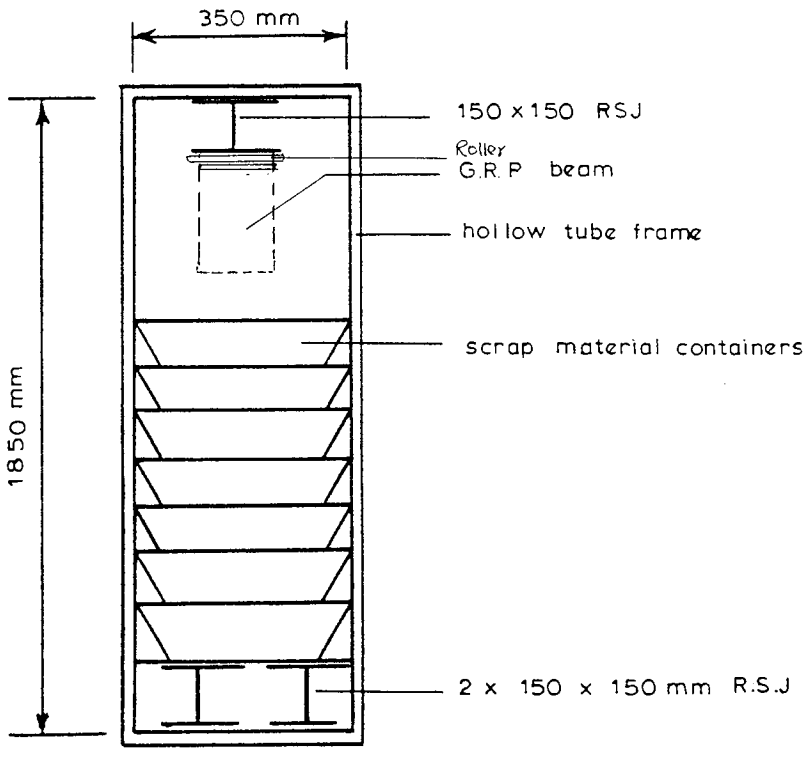

Section A-A

Fig. 5.2 Creep loading rig

FIGURE 5.3a CREEP RIG SET UP FOR BEAM TYPE R1 AND R2

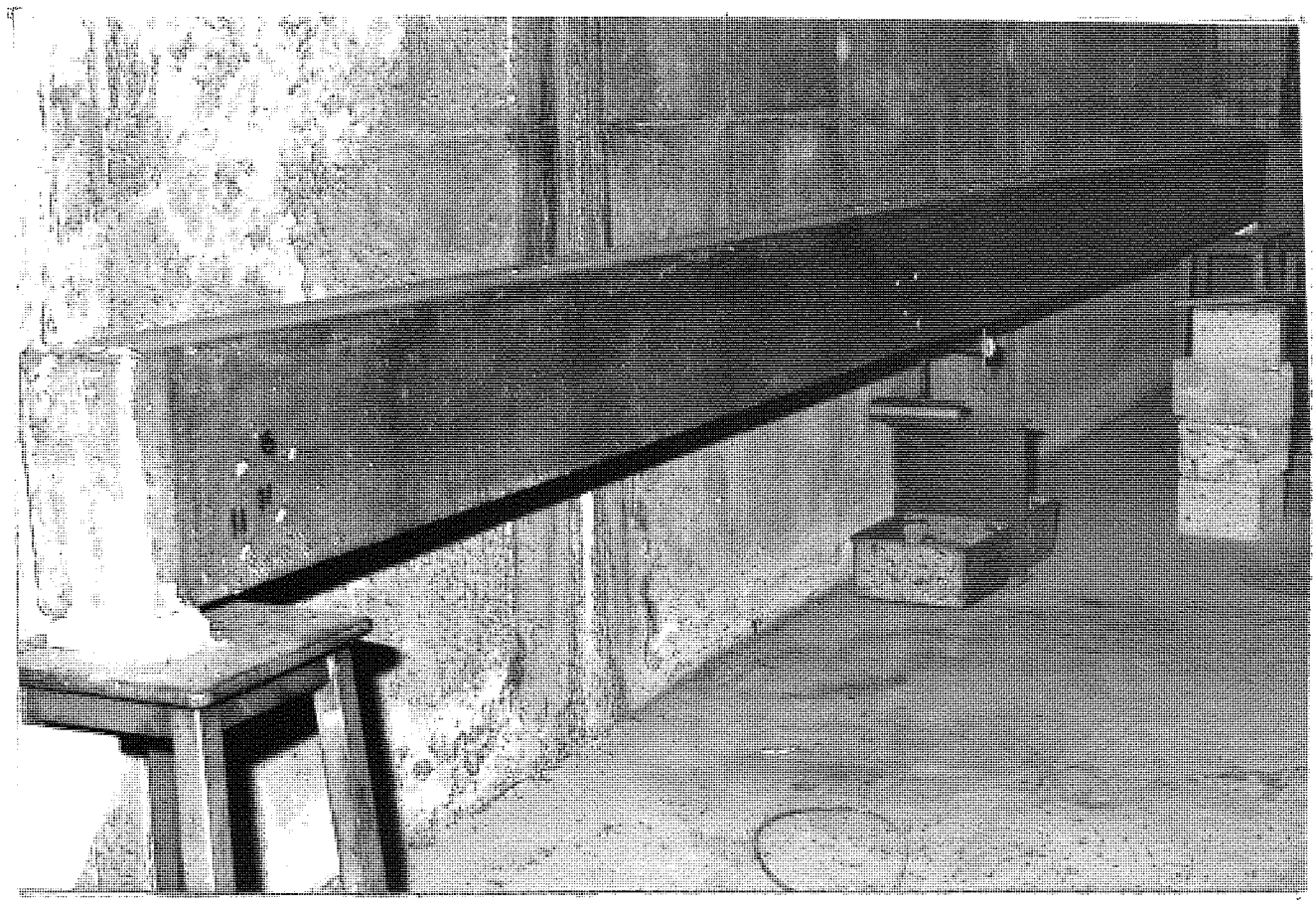

FIGURE 5.3b BEAM TYPE R3 LEFT UNDER SELF WEIGHT

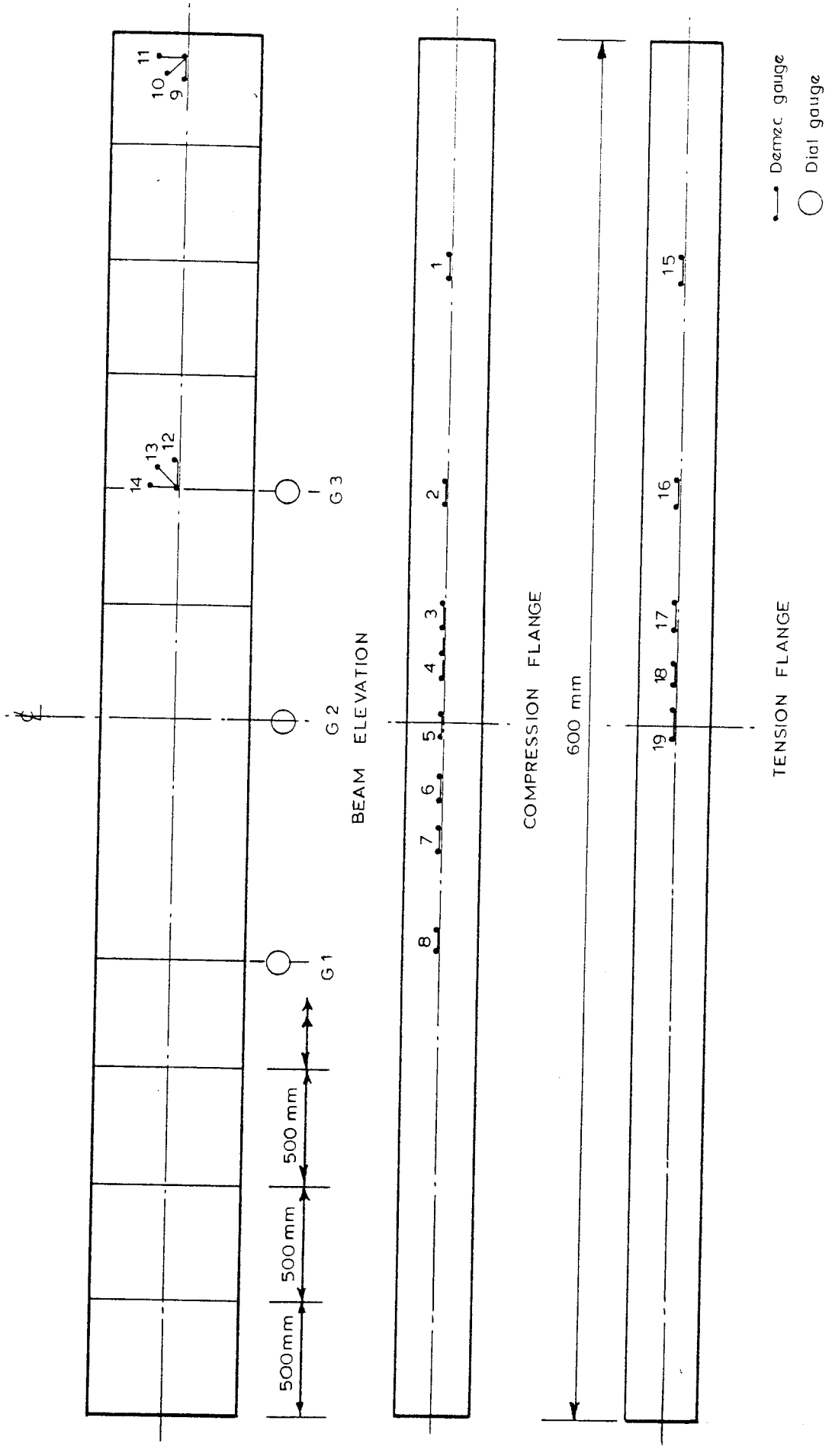

Fig. 5.4 Arrangement of demec and dial gauges.

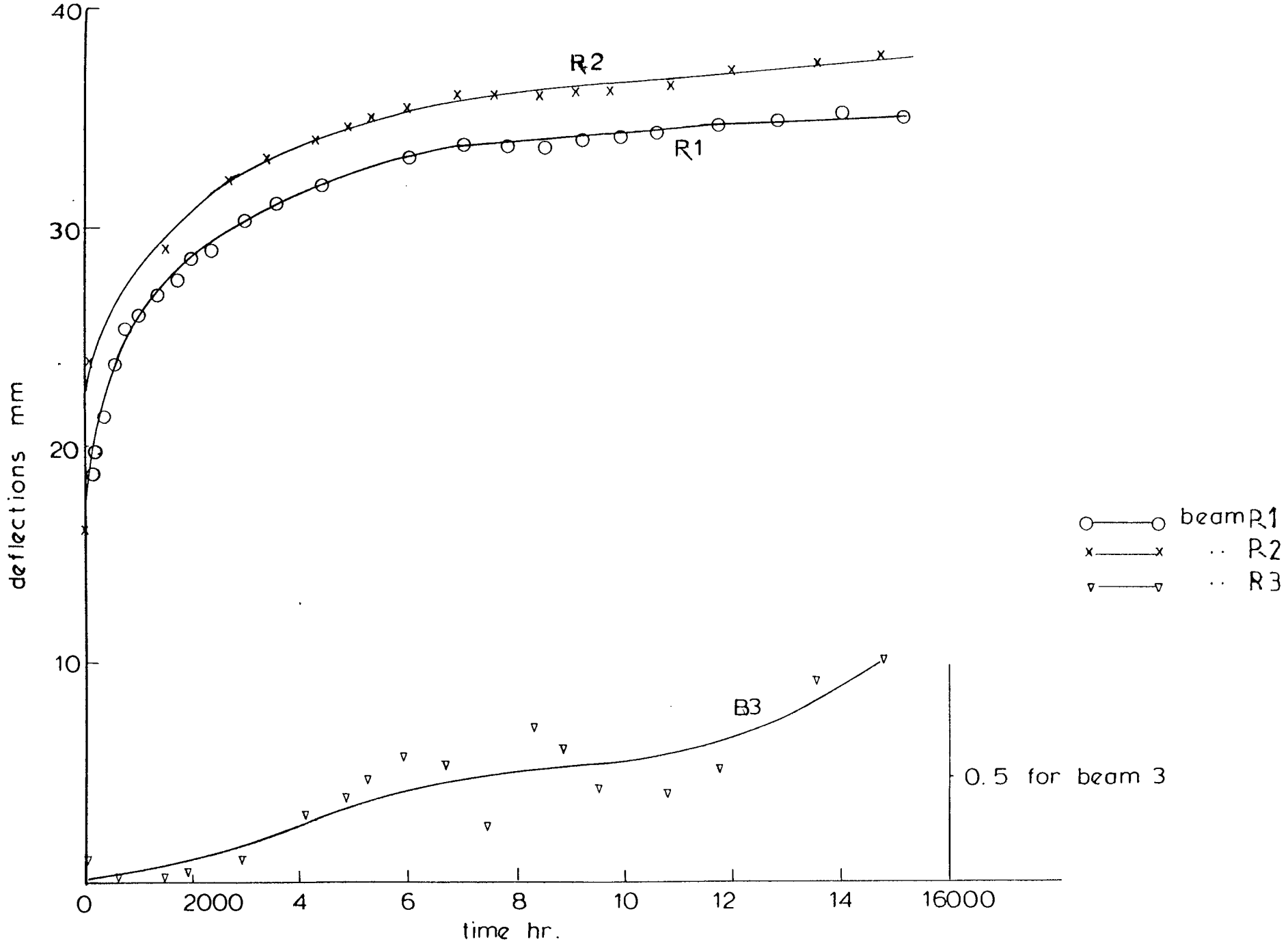

Fig. 5.5. Load versus deflection at mid span

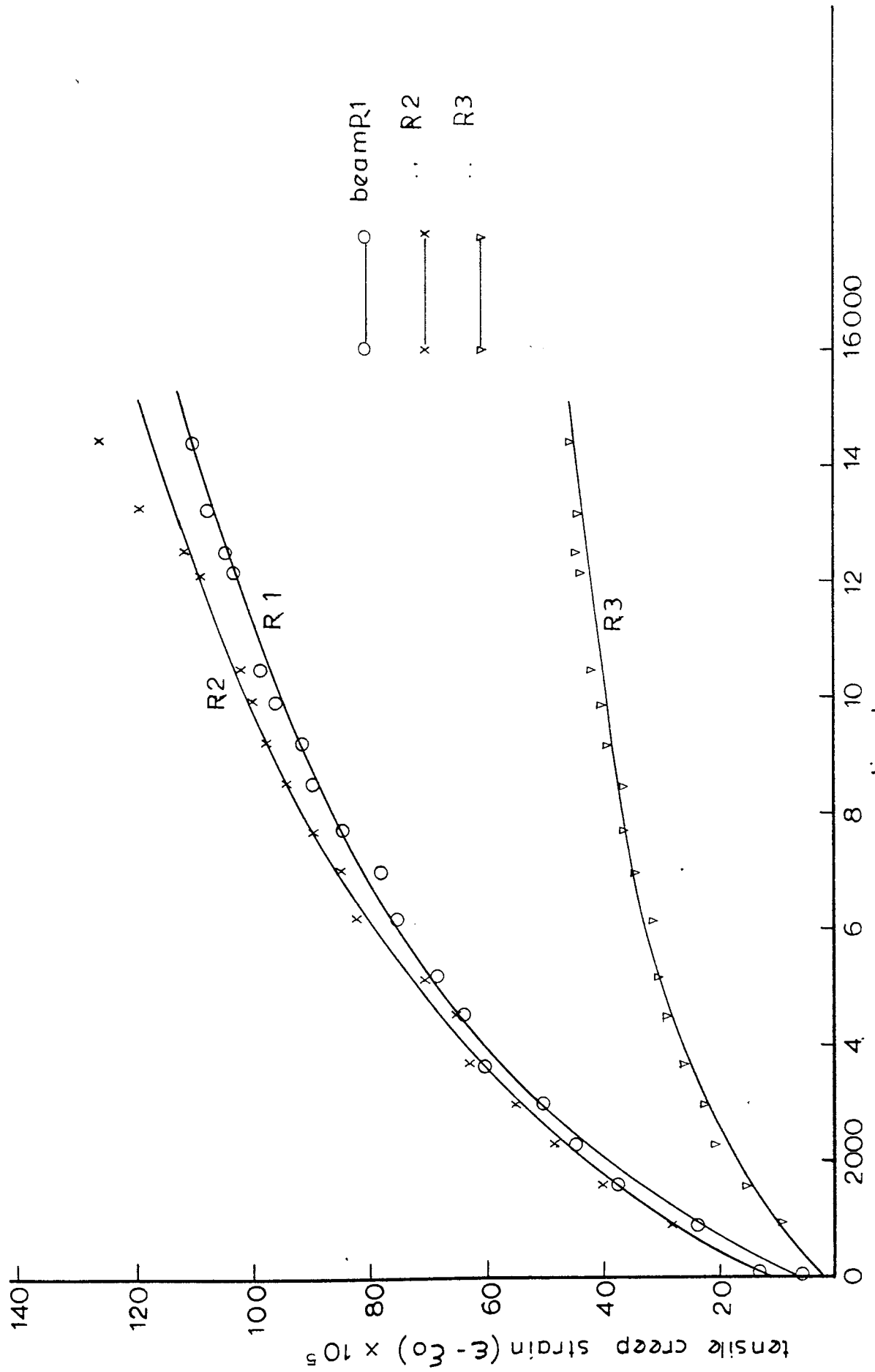

Fig. 5.6 Tensile creep strain versus time

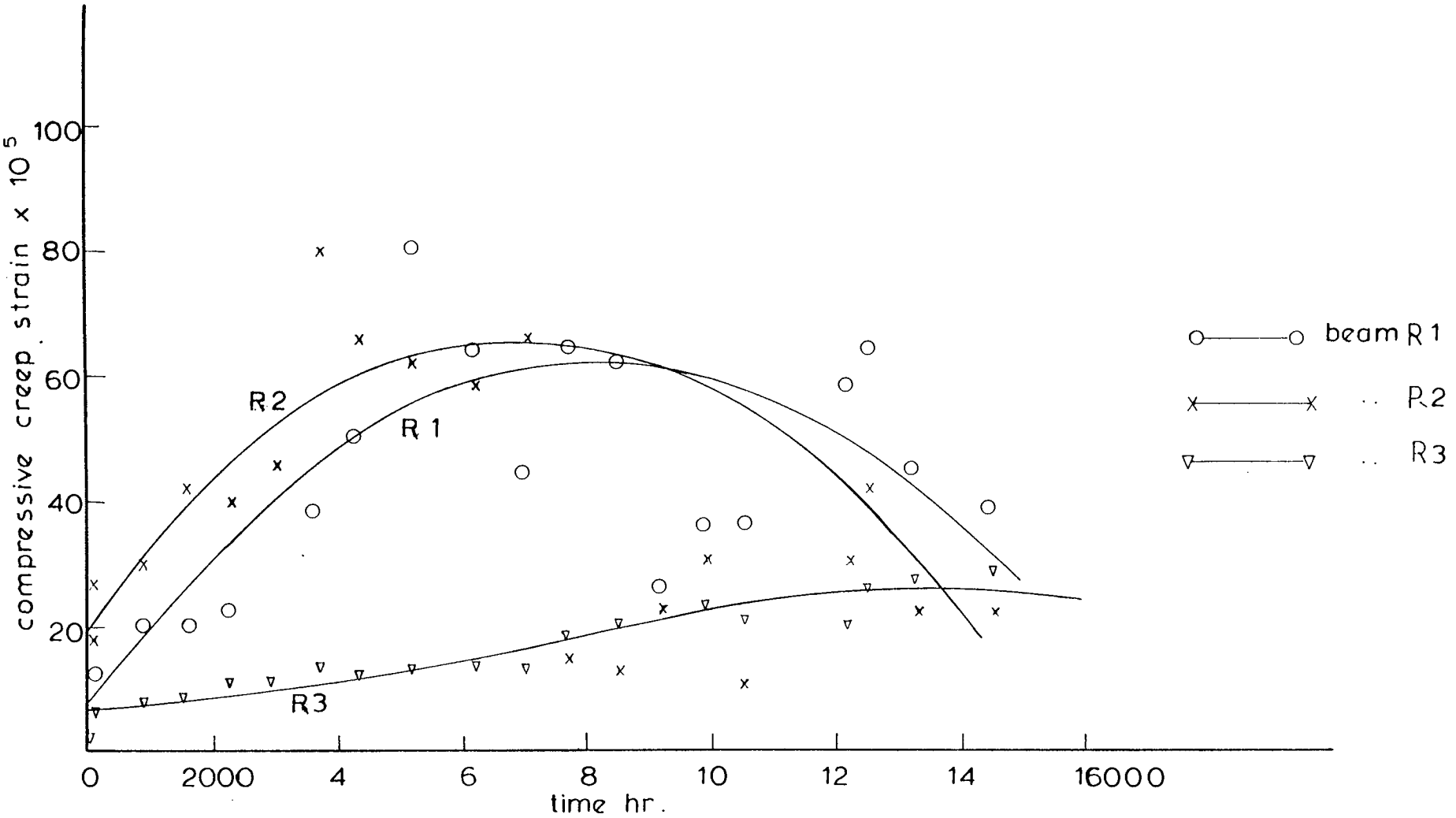

Fig. 5.7. Compressive creep strain versus time

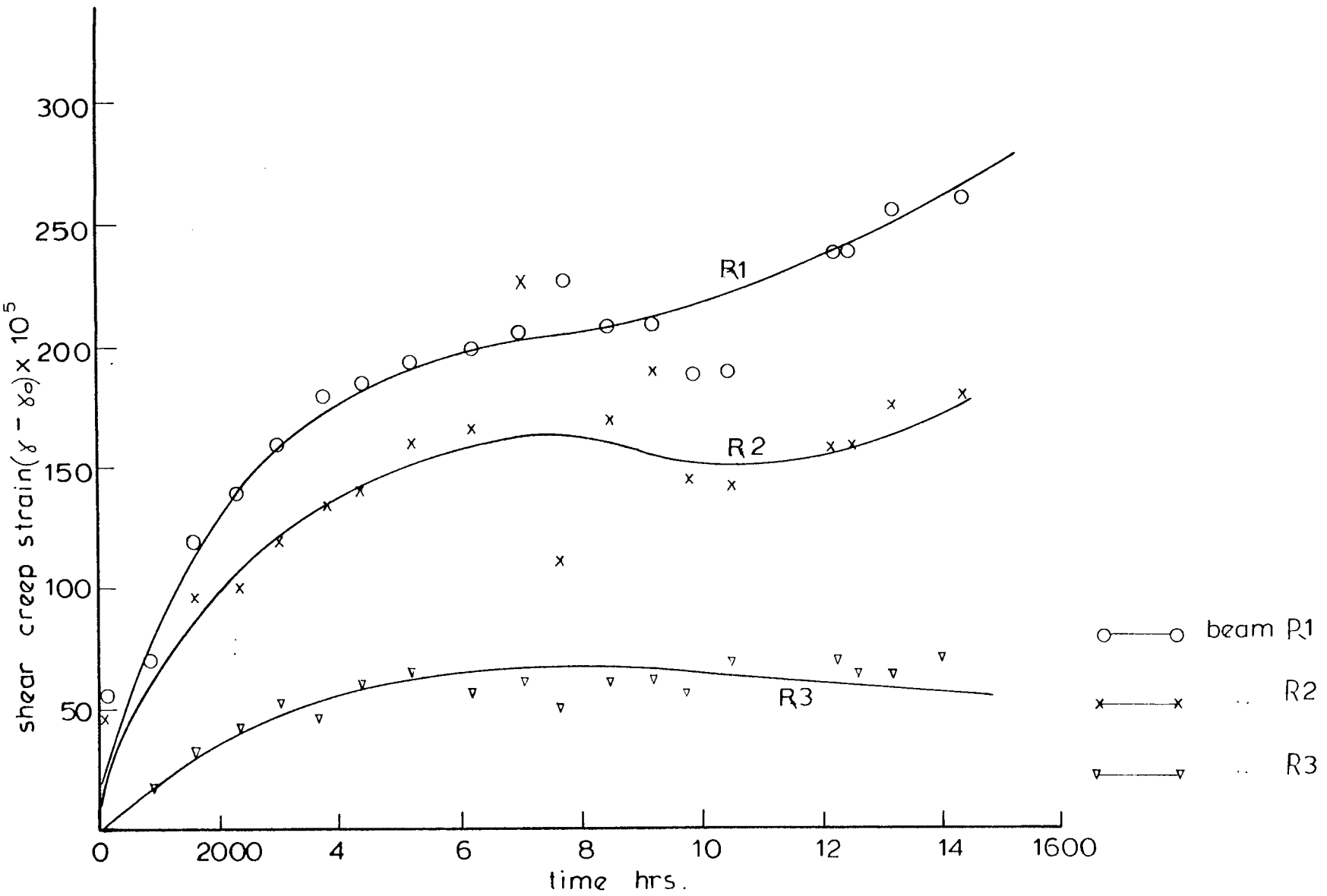

Fig. 5.8. Shear creep strain at support versus time

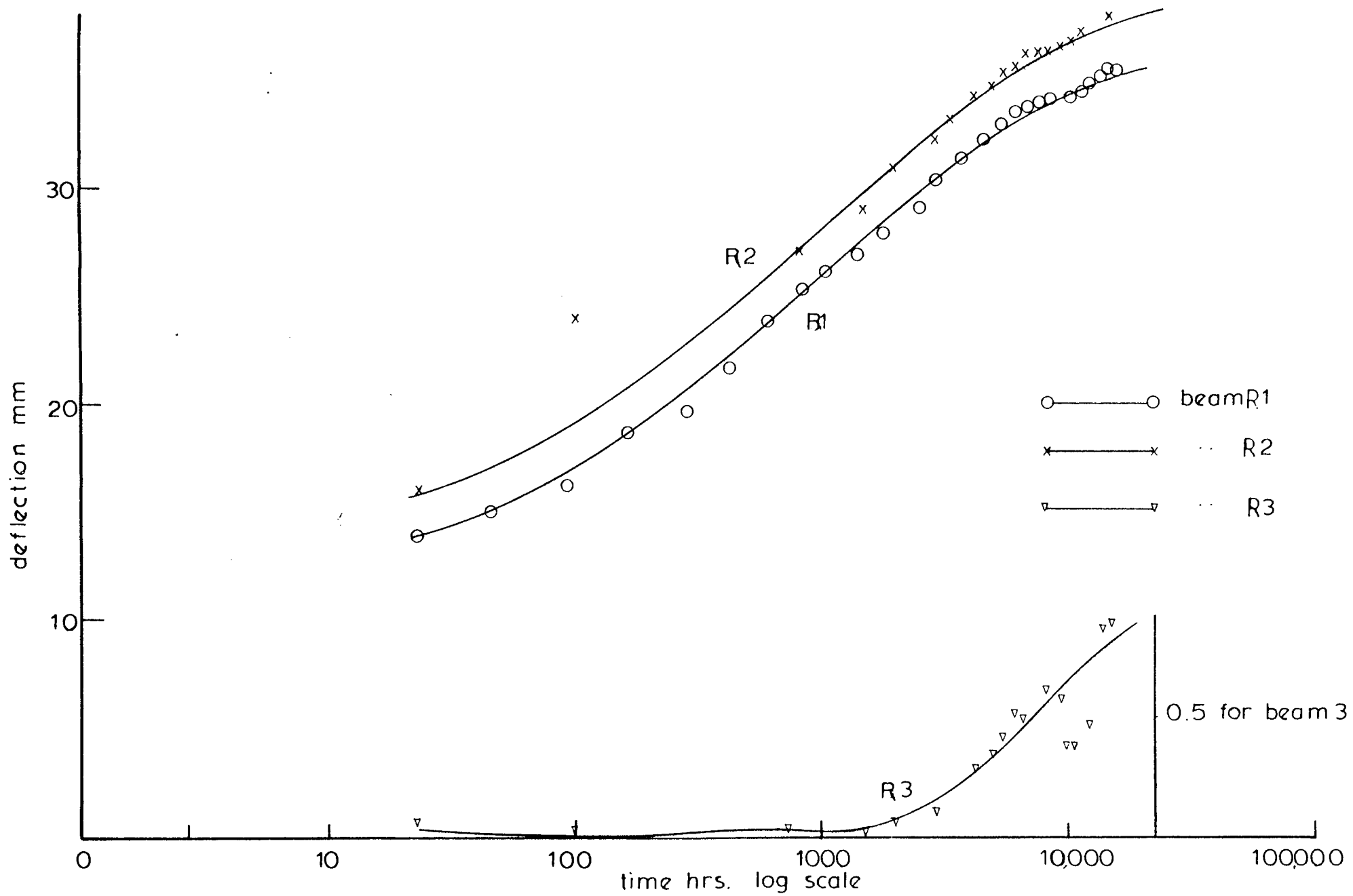

Fig. 5.9. Deflection versus time (log scale)

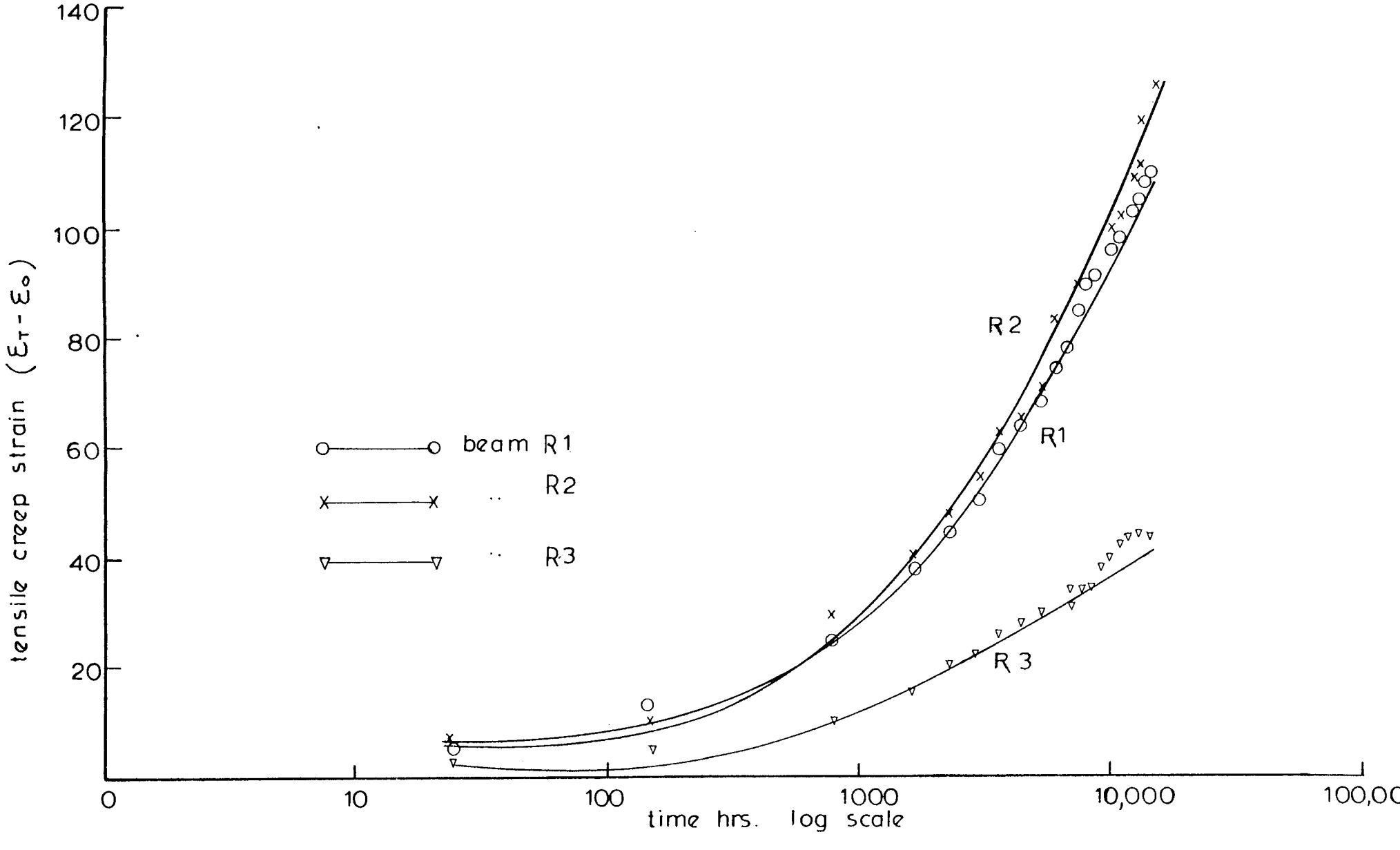

Fig.. 5 10. Tensile creep strain versus time in log scale

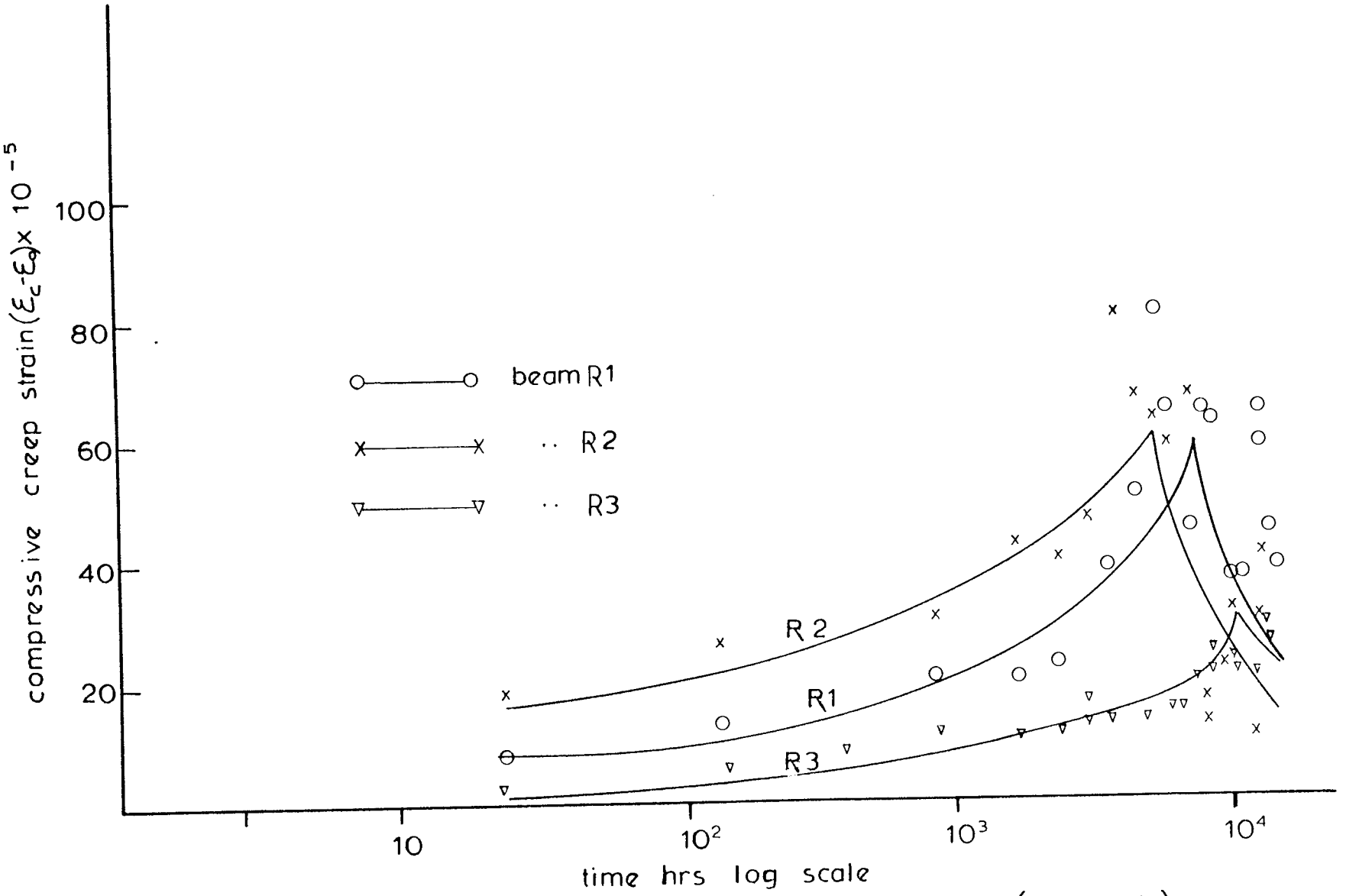

Fig. 5.1¹. Compressive creep strain versus time (log scale)

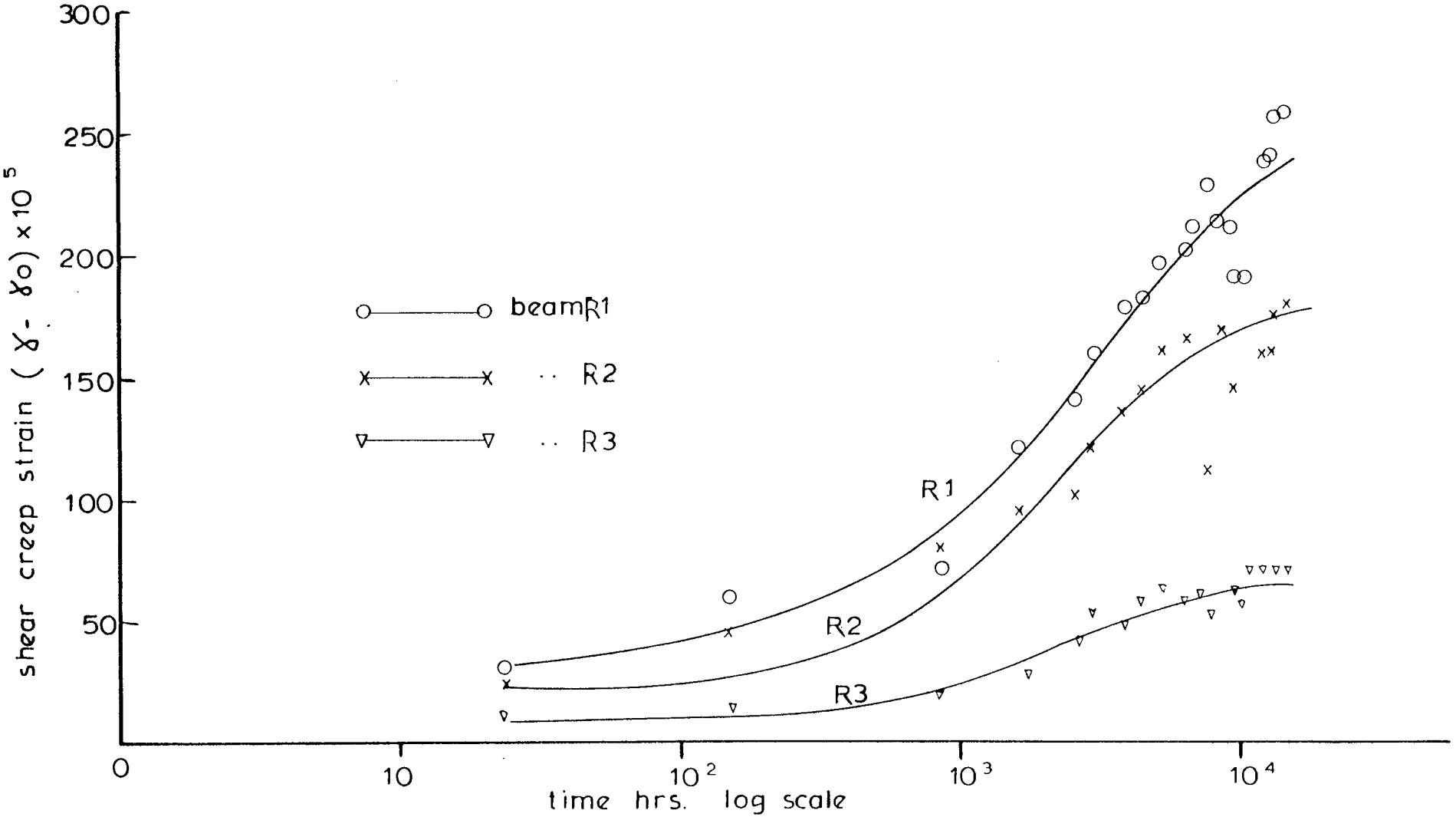

Fig. 5.12 Shear creep strain at support versus time (log scale)

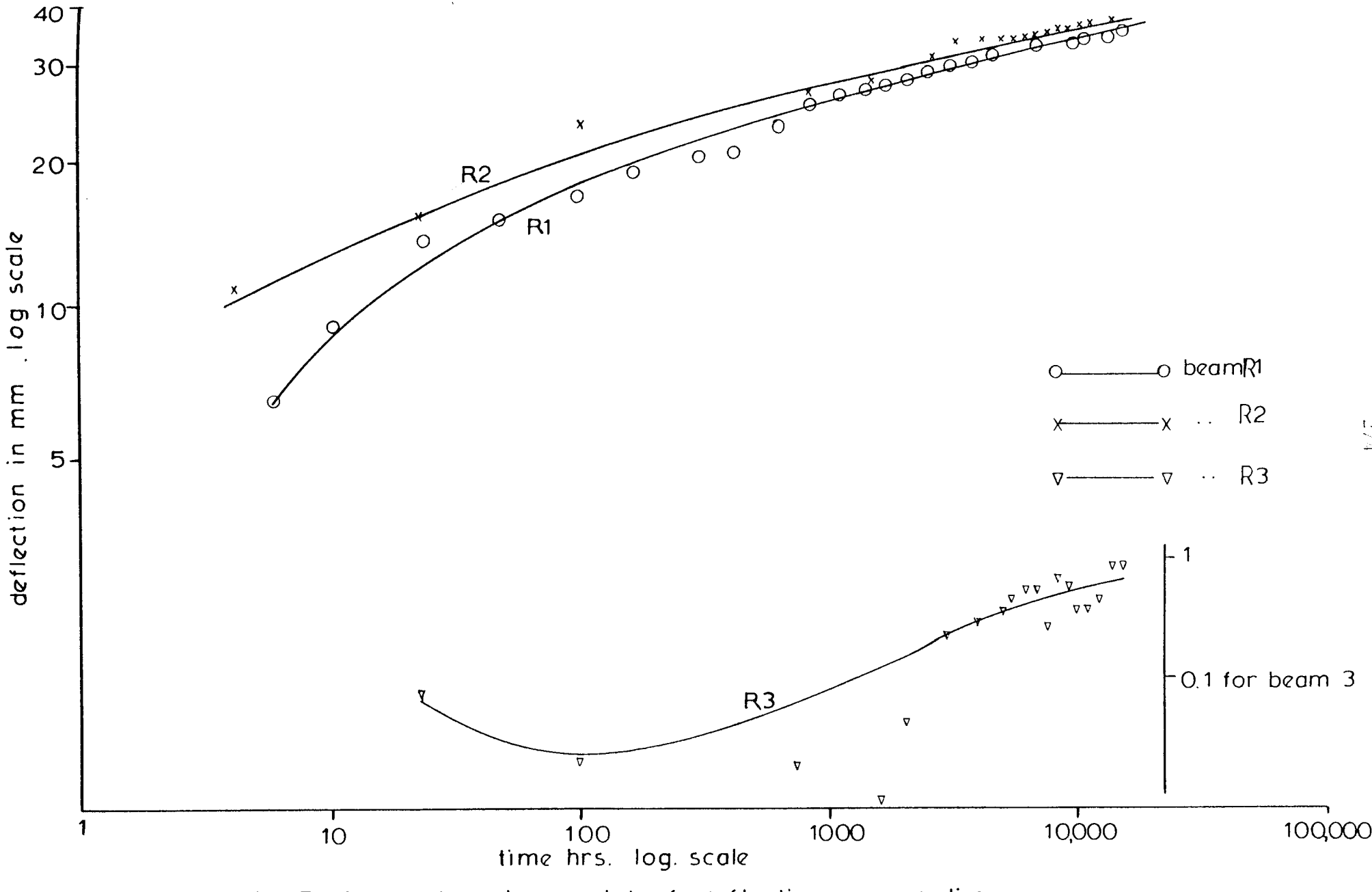

Fig. 5. 13. Log - Log plot of deflection versus time

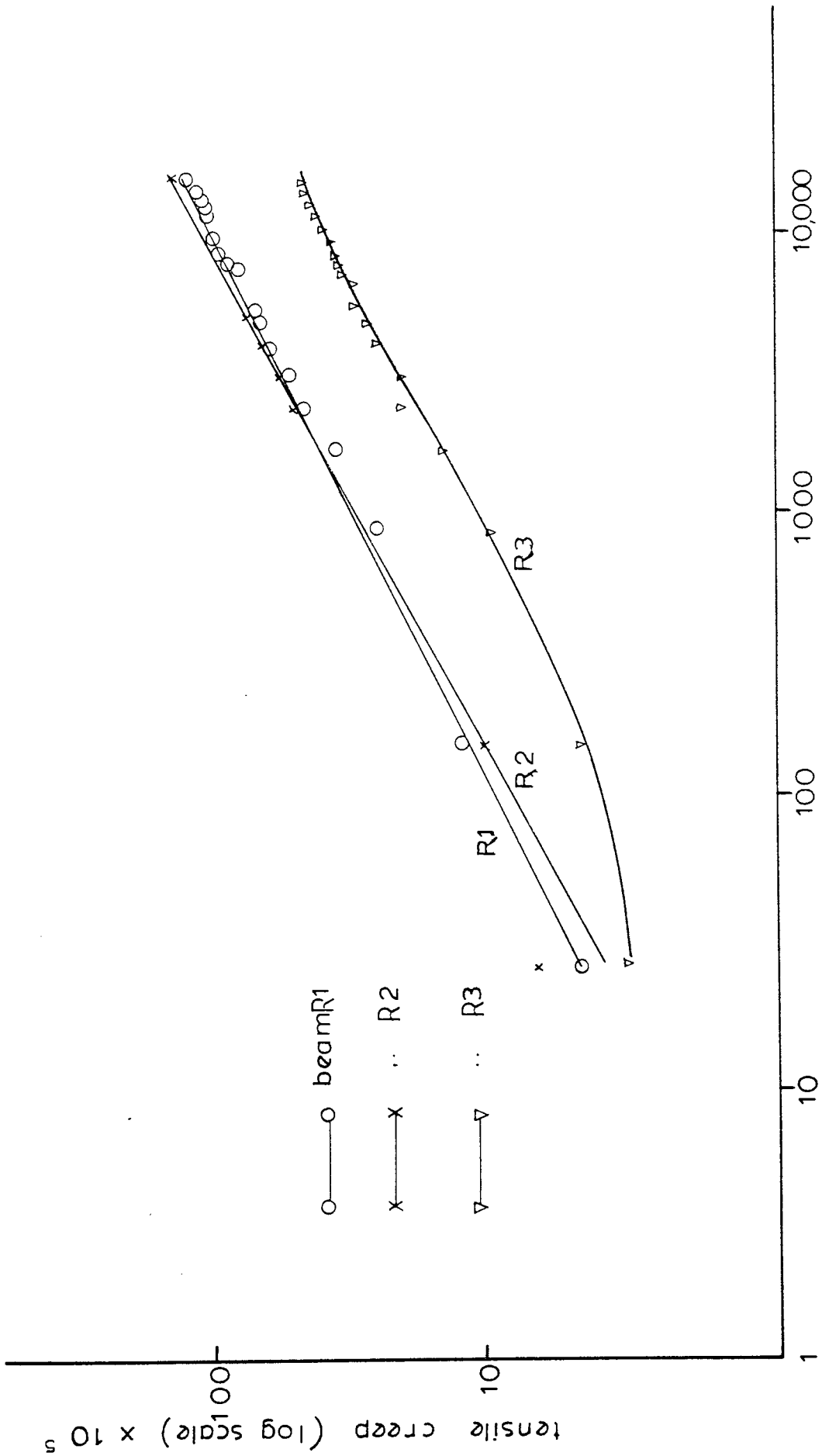

Fig 5.14 Log - Log plot of tensile creep strain versus time

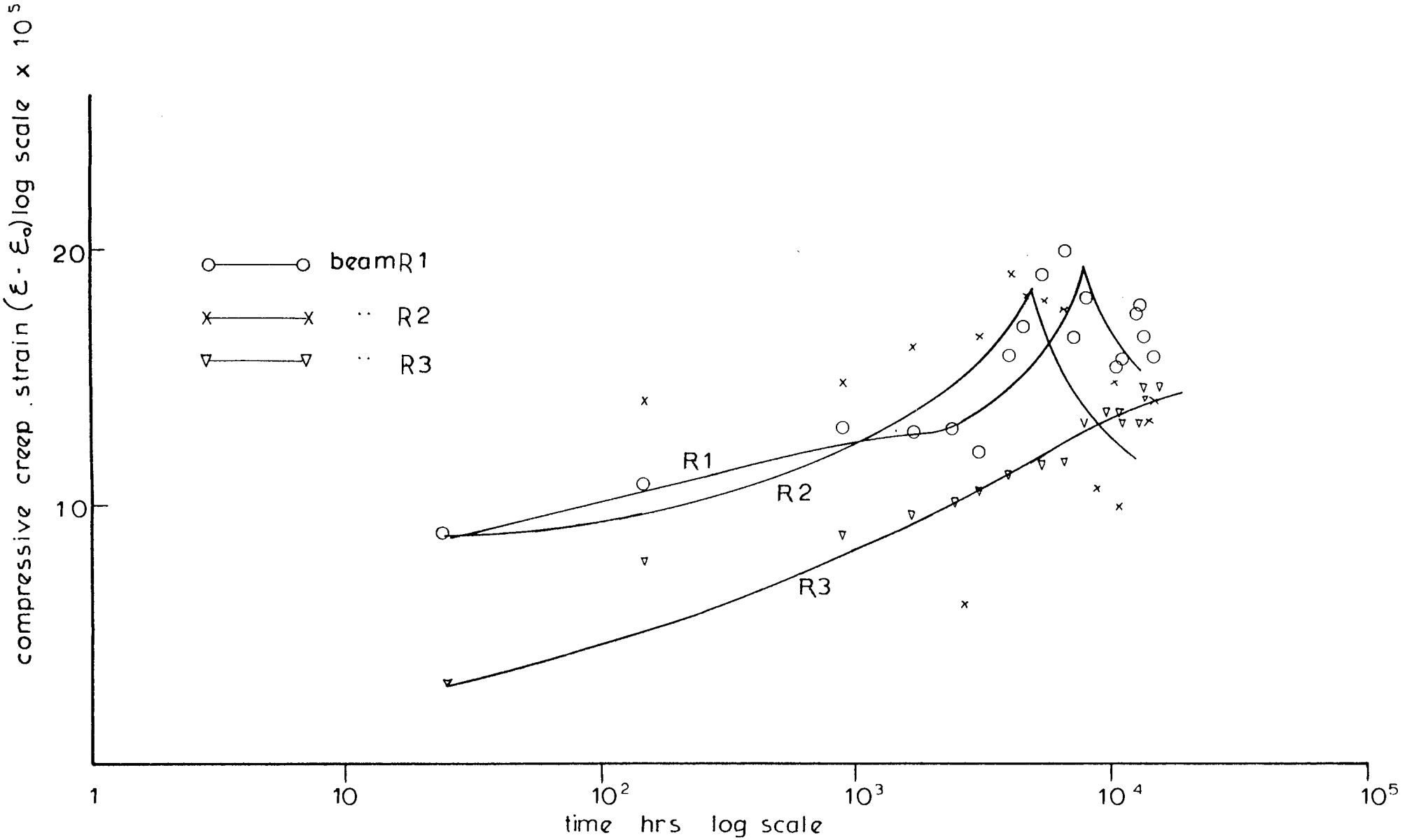

Fig. 5.15. Log - Log plot of compressive creep strain versus time

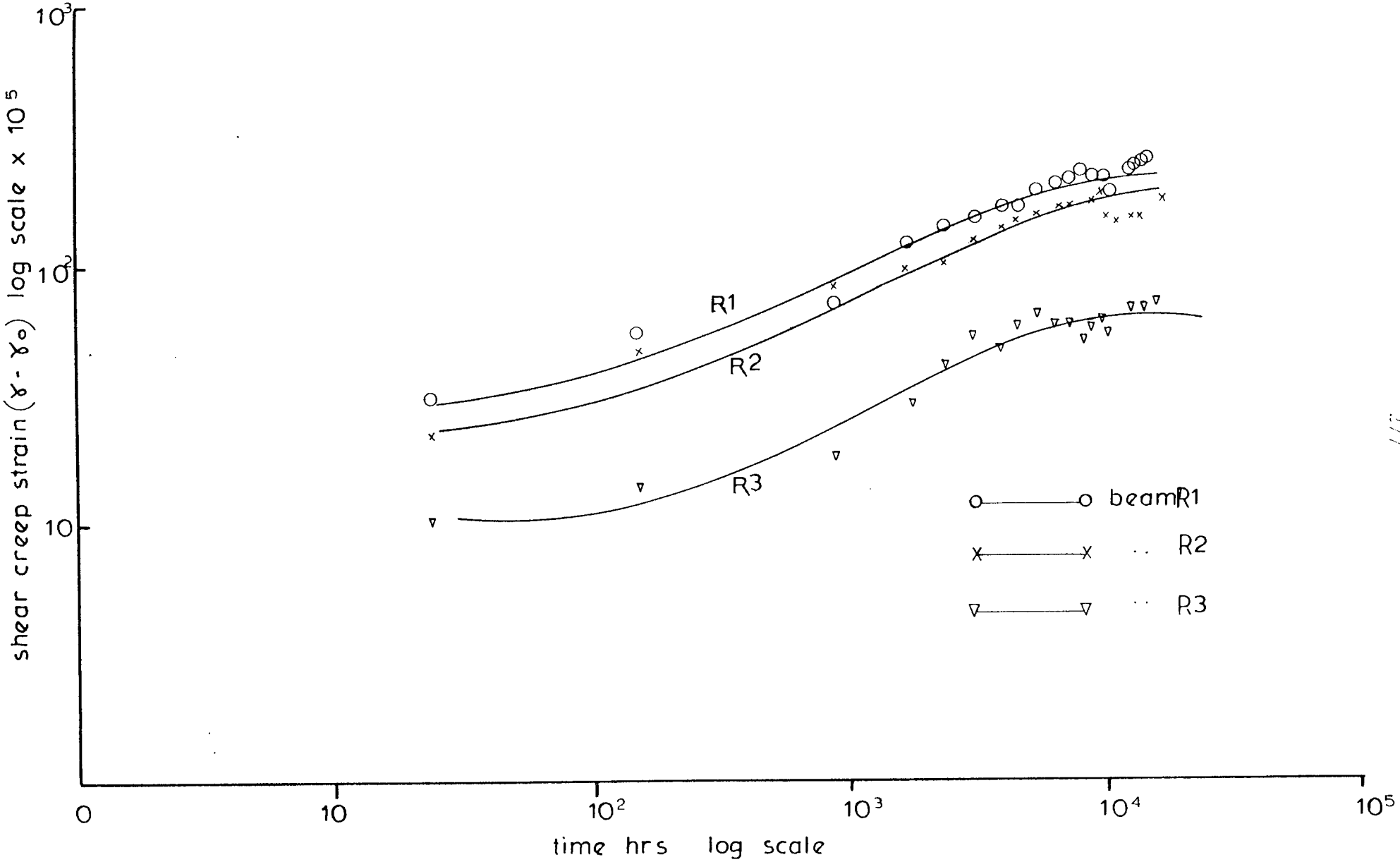

Fig. 5.16 Log - Log plot of shear creep strain at support versus time

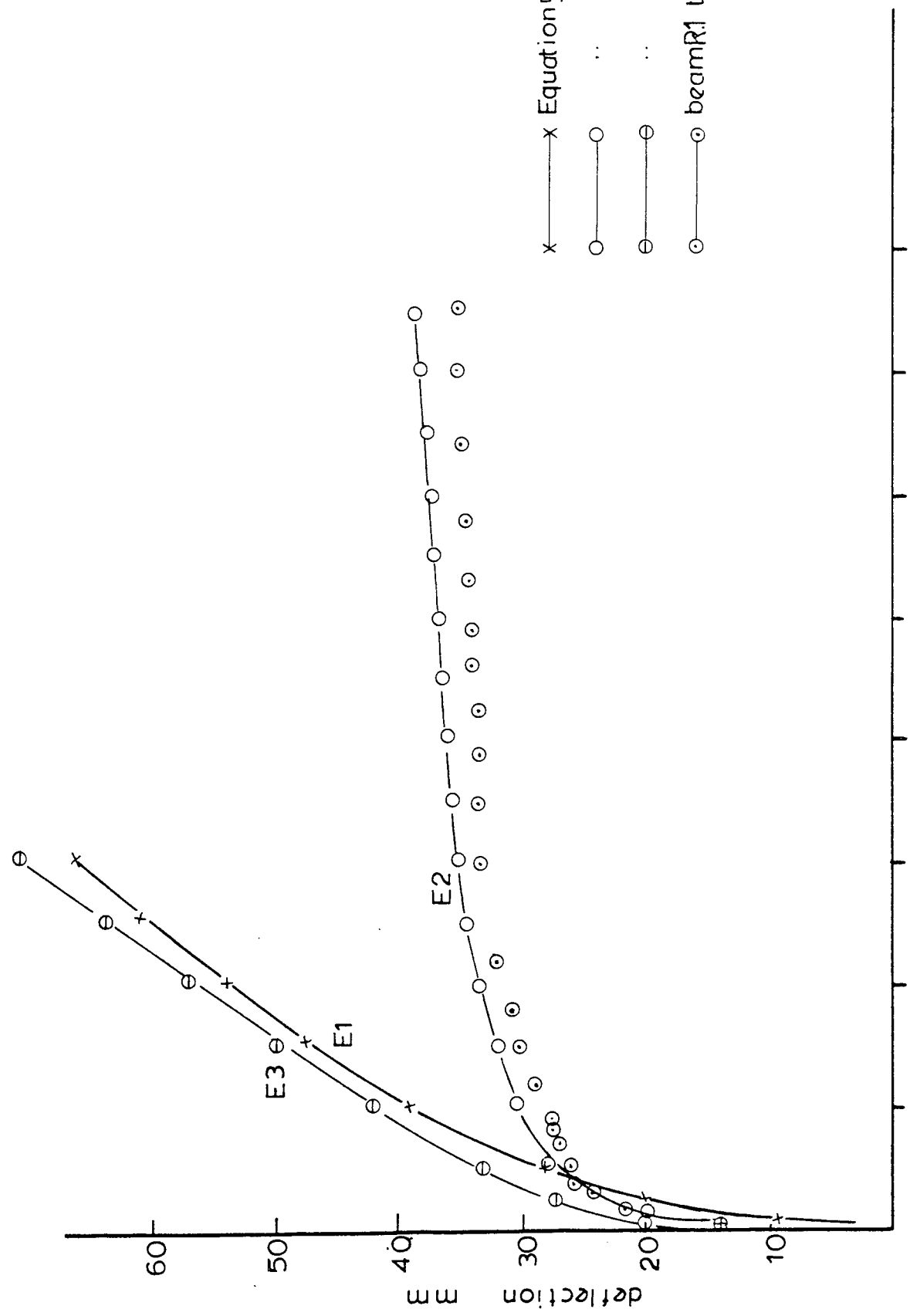

Fig . 5.17 Rect linear plot of creep deflection at mid span beam 1 compared with the prediction of equations 1,2 & 3.

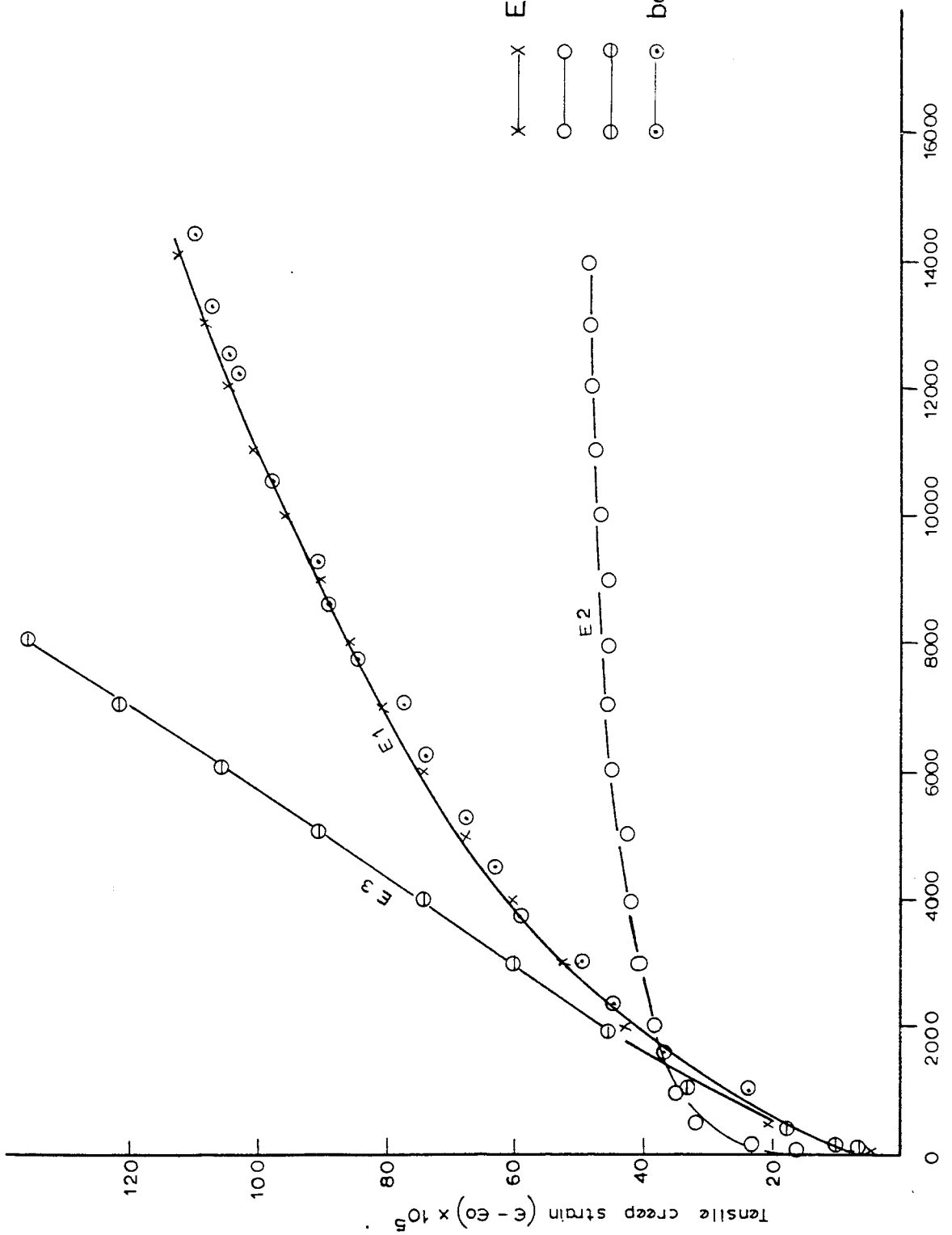

Fig. 5.18 Rectilinear plot of tensile creep strain at mid span beam 1 compared with the prediction of equations 1.2. and 3.

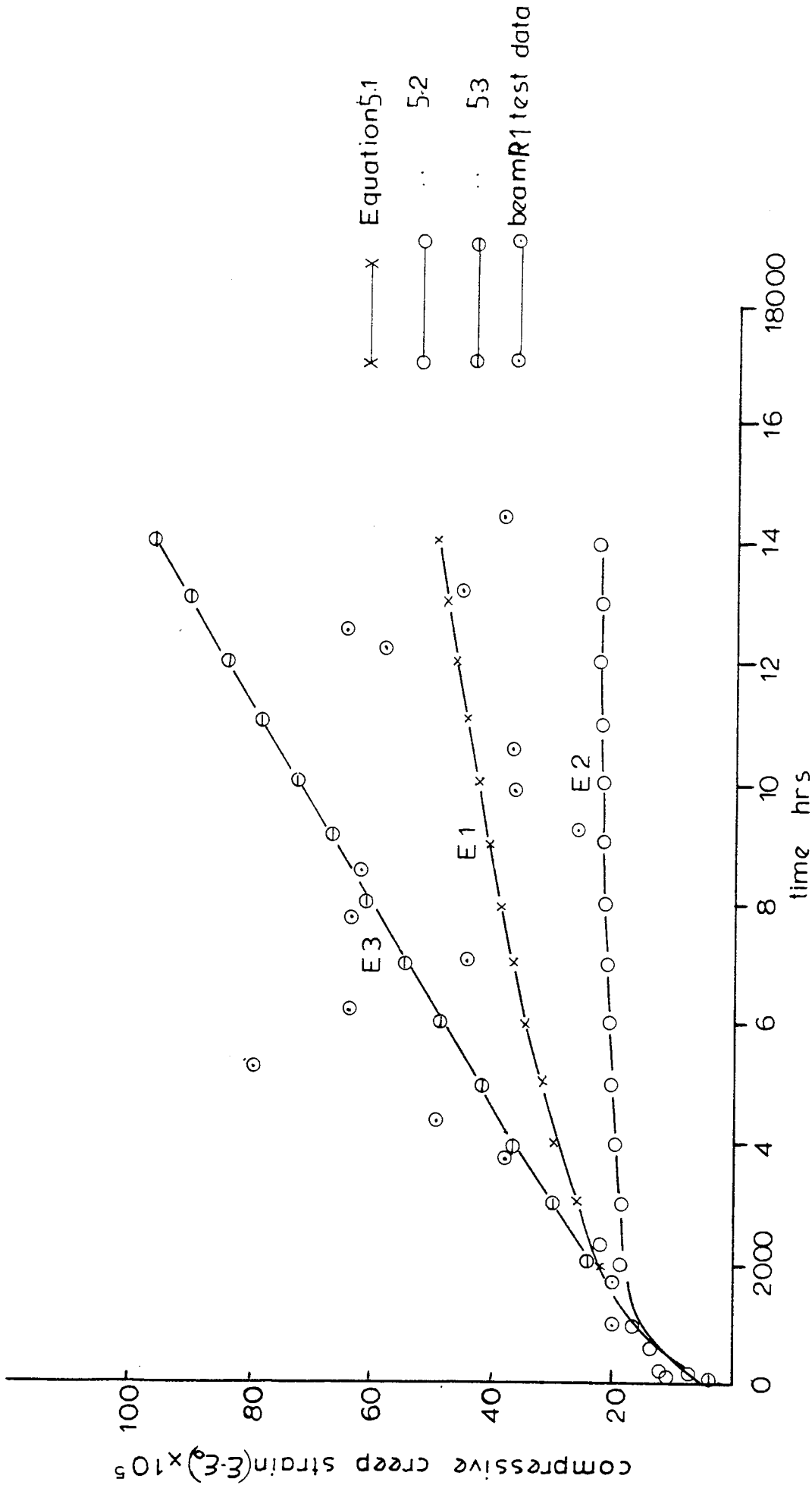

Fig. 5.19 Rectlinear plot of compressive creep strain at mid span beam 1 compared with the prediction of equations 1.2.&.3

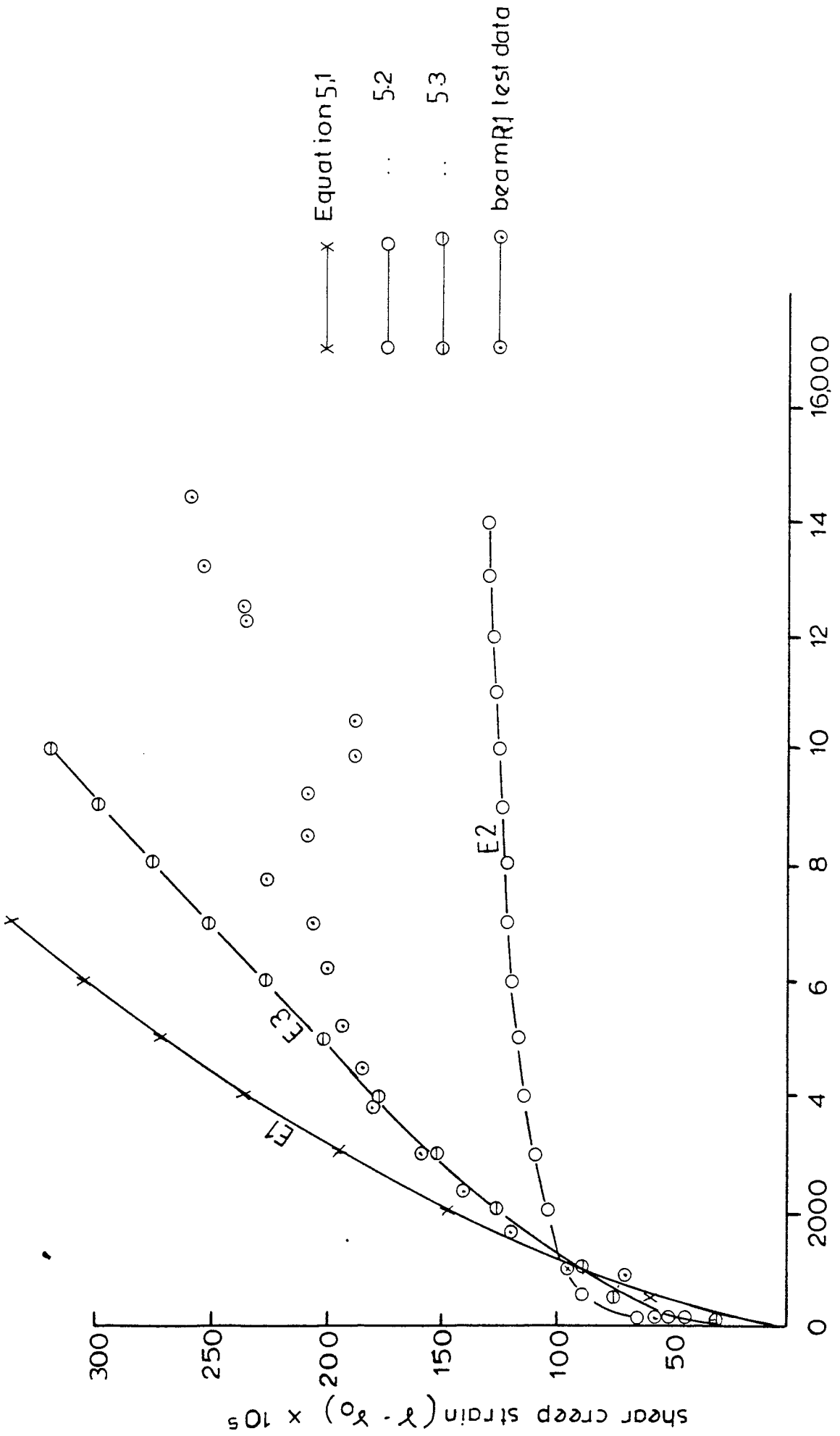

Fig. 5.20 Rectinear plot of shear creep strain at mid span beam 1 compared with the prediction of equation 1.2 & 3

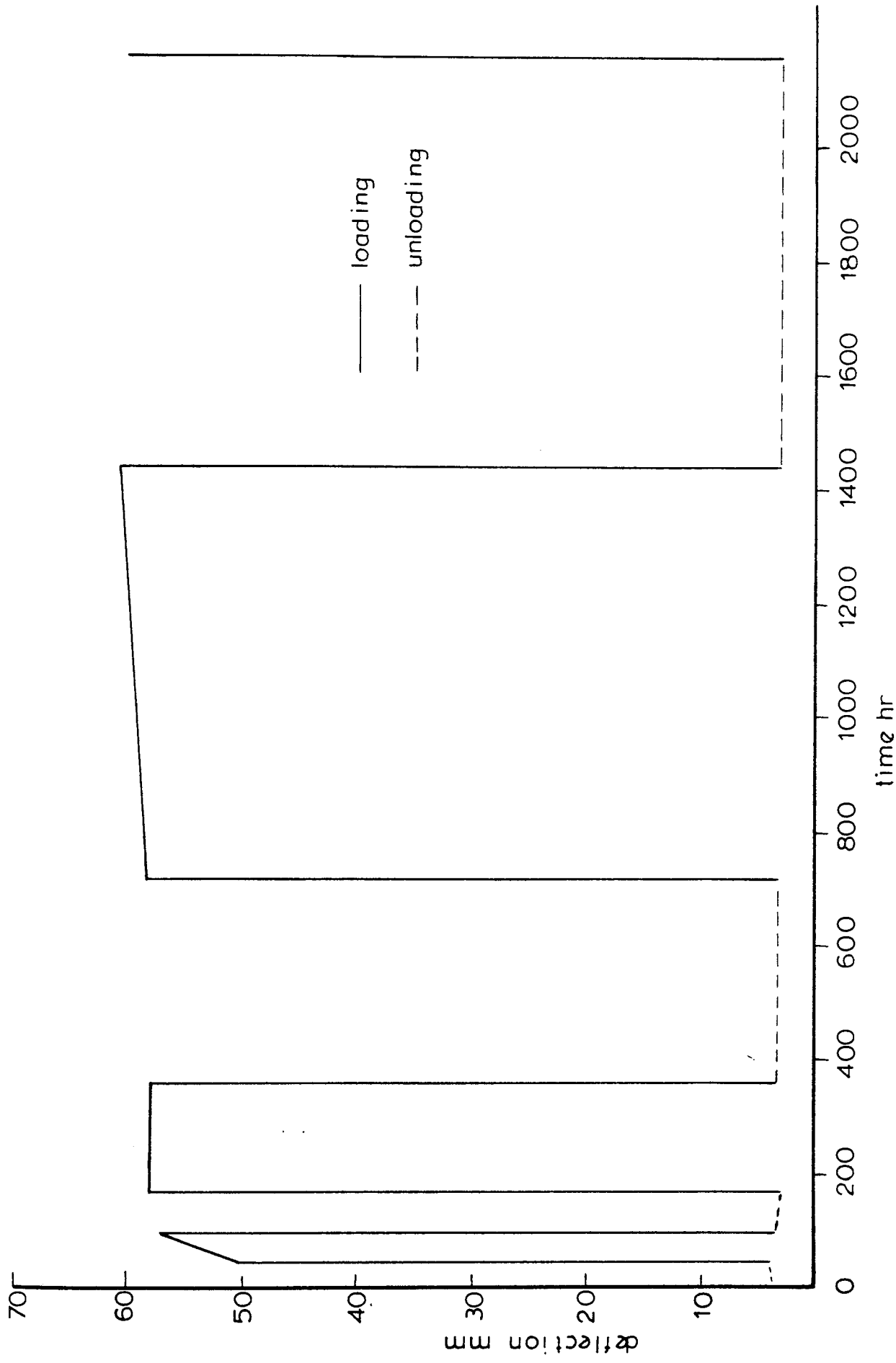

Fig. 5.21. Total deflection elastic + creep during loading and unloading versus time beam R2

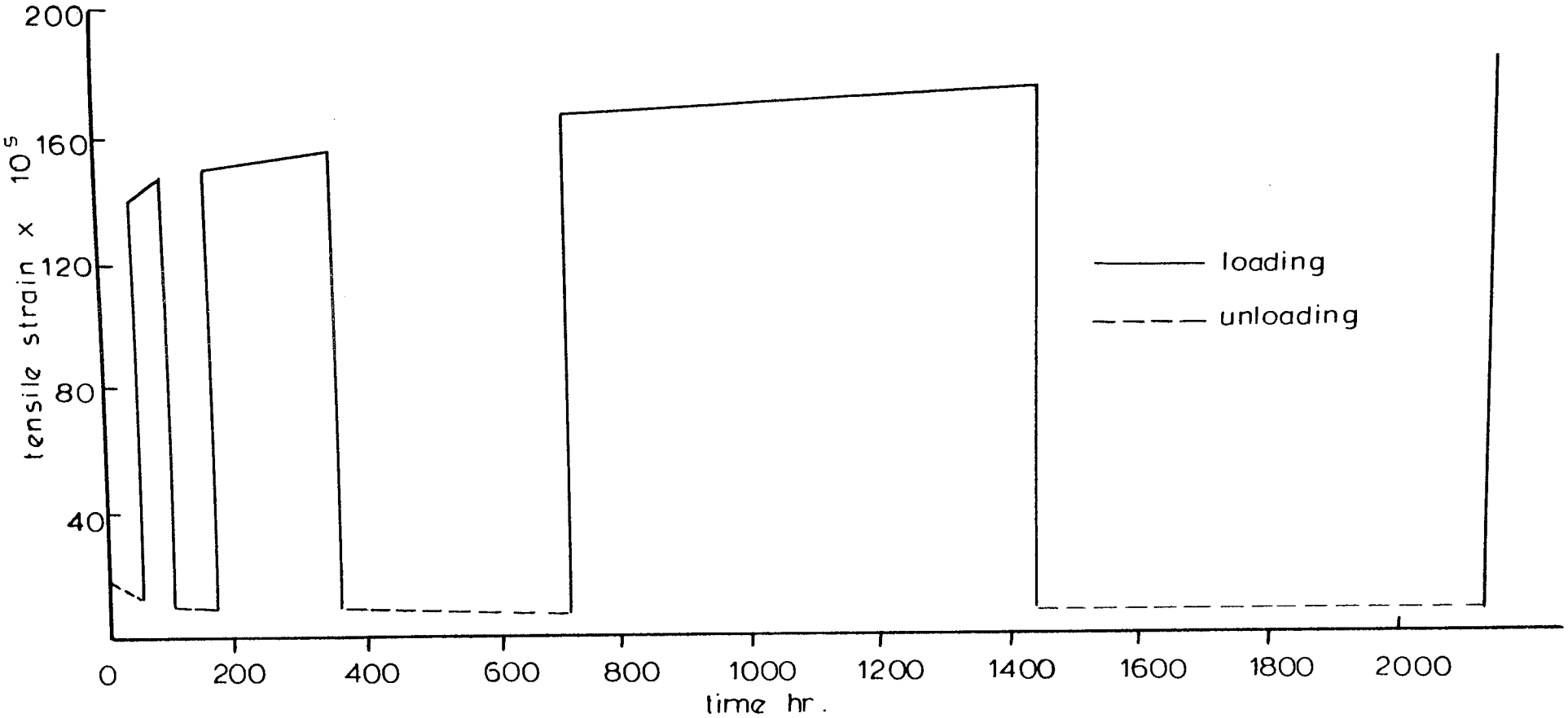

Fig. 5.22. Total tensile strain elastic + creep during loading versus time beam R2

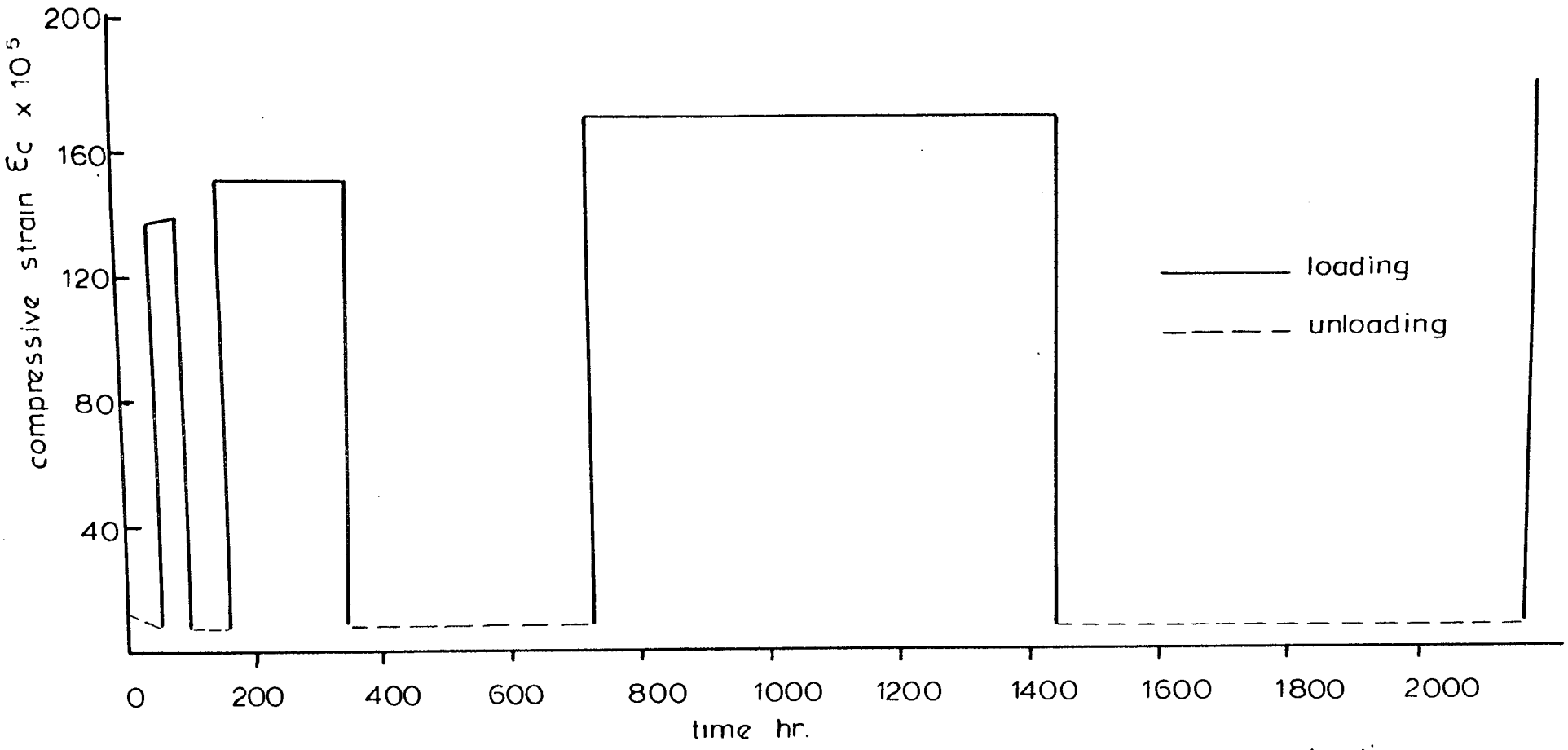

Fig. 5.23. Total compressive strain elastic + creep during loading and unloading versus time beam R2

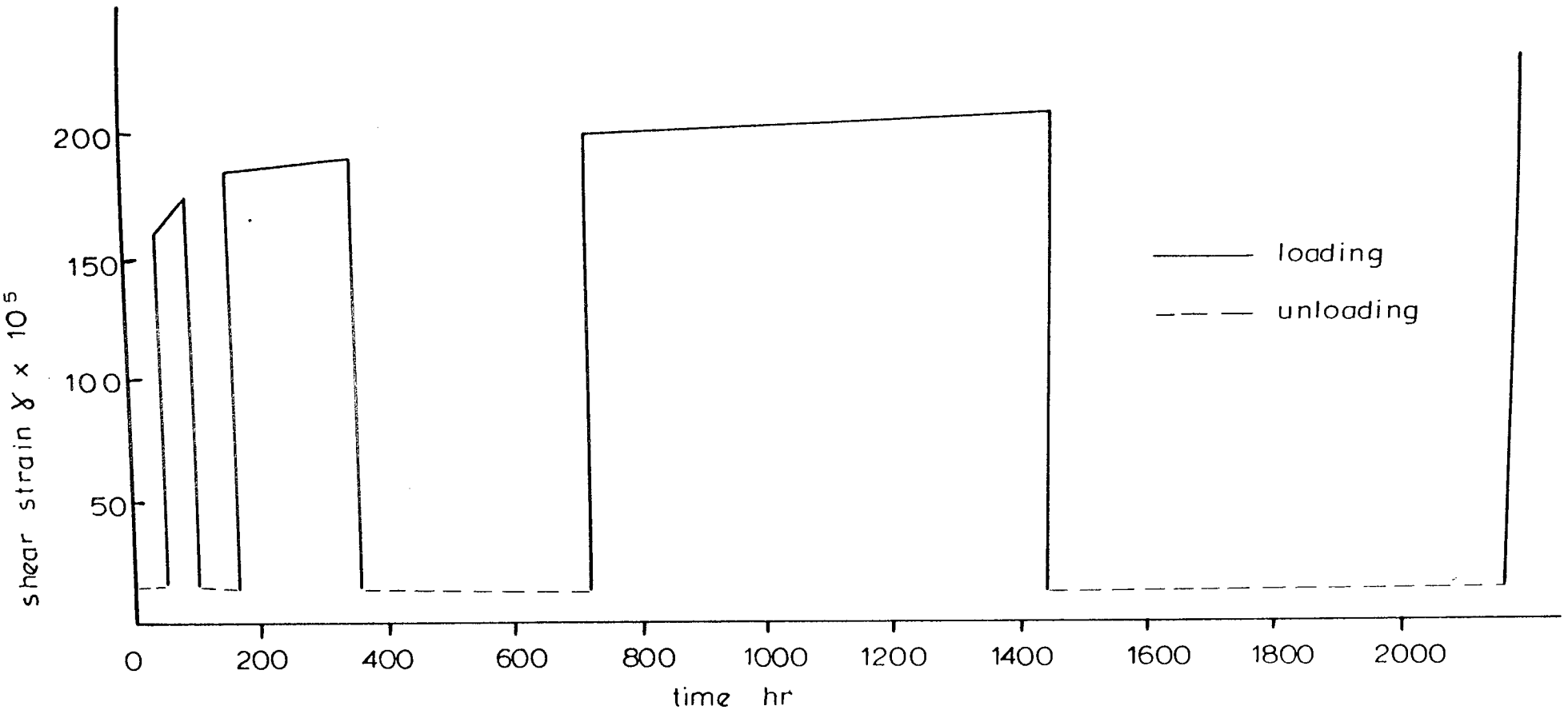

Fig. 5.24. Total shear strain elastic + creep during loading and unloading versus time beam R2

REFERENCES

5.1 WILLIAM N FINDLEY and WILL J WORLEY, "Some Static, Fatigue and Creep Test of a Glass Fabric Laminated with a Polyester Resin", Engineering Experimental Section, University of Illinois, AF, Technical Report No 6389, April 1951.

5.2 K H BOLLER, "Fatigue Properties of Fibrous Glass Reinforced Laminates Subjected to Various Conditions", Modern Plastics, June 1957.

5.3 B B PUSEY, "Effect of Time, Temperature and Environment on the Mechanical Properties of Glass Reinforced Plastics', Plastics Technolog, August 1956.

5.4 S GOLDFEIN, "Creep Properties of Glass Reinforced Plastics, A.S.T.M. Bulletin, October 1957, No 225.

5.5 K H BOLLER, "Effect of Long-term Loading on Glass Fibre Reinforced Plastic Laminates", Proceeding of 11th Annual Conference of S.P.I. Reinforced Plastic Division, February 1956, Section IB.

5.6 KABELKA J, "Long Term Strength Properties of G.R.P.", 5th International Plastic Conference, 1966.

CHAPTER 6

POST BUCKLING BEHAVIOUR

6.1 INTRODUCTION

The post-buckling behaviour of thin plates is an important topic in structural engineering since plates are possibly unique in their extensive use as load carrying structural components up to and into the post buckling range. Unlike one dimensional structural members such as columns stiffened compression elements will not necessarily collapse when the buckling stress is reached. In this chapter the elastic post-critical behaviour of individual G.R.P. plates is considered under uniaxial in-plane compression since this type of loading condition may arise in plate components of many thin walled structures.

6.2 TEST ARRANGEMENTS

The plates were subjected to compressive loads applied by a Dennison test machine with the edges of the plates being supported by an aluminium frame so as to simulate the boundary conditions assumed in the theory fig (6.1). The frame was adjustable to accommodate plates of different thickness. The load was read directly off the testing machine and lateral deflections were measured by dial gauges to an accuracy of 0.01 mm fig (6.1). Strain was measured by electrical strain gauges similar to those already described in chapters 2, 3 and 4.

6.3 TEST PROCEDURE

The plate was positioned in the loading machine in an accurate vertical position. Then the load was applied to the plate and

released repeatedly for two or three times until uniform and constant readings were obtained from the deflection gauges. The test was then run and lateral deflections and strain gauge readings were normally taken after every load increment. The loading was usually continued until a clear collapse pattern of the plate under test had developed. Test coupons were later extracted from the plate for modulus and strength determination according to the methods described in chapter 1.

6.4 THEORY

6.4.1 General Laminate Plate Formulation

The general differential equation describing the behaviour of anistropic plates subjected to an in-plane edge loading and neglecting any bending membrane coupling terms given by references [6.1,2]

$$D_{11}\frac{\partial^4 w}{\partial x^4} + 4D_{16}\frac{\partial^4 w}{\partial x^3 \partial y} + 2D_3\frac{\partial^4 w}{\partial x^2 \partial y^2} + 4D_{26}\frac{\partial^4 w}{\partial x \partial y^3}$$

$$+ D_{22}\frac{\partial^4 w}{\partial y^4} + N_x\frac{\partial^2 w}{\partial x^2} + 2N_{xy}\frac{\partial^2 w}{\partial x \partial y} + N_y\frac{\partial^2 w}{\partial y^2} = 0 \qquad (6.1)$$

where $D_3 = D_{12} + 2D_{66}$

and D_{11}, D_{22}, D_{26}, and D_3 are flexural stiffnesses.

N_x, N_y, N_{xy} the stress resultants as defined in section (1.13).

With plates laminated in a symmetrical arrangement about the mid plane so that the laminate principle axes coincide to those of the plate, the normal stress-twist curvature terms D_{16} and D_{26} will vanish from equation (6.1) yielding

$$D_{11}\frac{\partial^4 w}{\partial x^4} + 2D_3\frac{\partial^4 w}{\partial x^2 \partial y^2} + D_{22}\frac{\partial^4 w}{\partial y^4} + N_x\frac{\partial^2 w}{\partial x^2}$$

$$+ 2N_{xy} \frac{\partial^2 w}{\partial x \partial y} + N_y \frac{\partial^2 w}{\partial y^2} = 0 \qquad (6.2)$$

This type of plate is referred to as specially orthotropic plate. A detailed derivation of equation (6.2) may be found in reference 6.3

With isotropic plates $D_{11} = D_3 = D_{22} = D$ and equation (6.2) becomes

$$\frac{\partial^4 w}{\partial x^4} + \frac{2\partial^4 w}{\partial x^3 \partial y^2} + \frac{\partial^4 w}{\partial y^4} + \frac{N_x}{D} \frac{\partial^2 w}{\partial x^2} + 2N_{xy} \frac{\partial^2 w}{\partial xy} + N_y \frac{\partial^2 w}{\partial y^2} = 0 \qquad (6.3)$$

6.4.2 Post Buckling Behaviour of Plates

To understand why plates exhibit a post buckling strength a simply supported isotropic plate is considered as an example, fig (6.2a). The origin of the co-ordinates is located in the lower left hand corner of the plate. Since a finite deflection analysis involves deformations in the plane of the middle surface both in plane as well as transverse boundary conditions must be specified. The transverse boundary conditions corresponding to simply supported edges are

$$w = \frac{\partial^2 w}{\partial x^2} = 0 \quad \text{at } x = 0, b$$

$$w = \frac{\partial^2 w}{\partial y^2} = 0 \quad \text{at } y = 0, b,$$

With regard to the in plane boundary conditions the following assumptions are made.

(a) All edges remain straight and the plate retains its rectangular outline during bending as indicated by the dashed lines fig (6.2a).

(b) The shear forces N_{xy} vanish along the four edges of the plate.

(c) The edges y = 0, b are free to move in the y direction.

The restraint assumed to exist along the edges y = 0, b represents an intermediate condition between the case of total finity and the case of zero restraint. For total finity to exist there can be no movement (i.e. displacement v = 0) and for zero restraint there cannot be any stress (i.e. $N_y = 0$). In this intermediate case the edges are permitted to move provided that they remain straight. Thus only the average value of N_y and N_y itself must be equal to zero. For the loaded edges x = 0, b displacements U remain constant in the y direction. This condition is realized if the plate is compressed between parallel plattens.

For convenience the average value of the applied compressive stress is denoted by σ_{xb}.

Thus $$\sigma_{xb} = -\frac{1}{bh}\int_0^b N_x d_y \qquad (6.4)$$

where h = thickness of the plate.

The negative sign in equation (6.4) denotes compression. The following expression is assumed to describe the lateral deflection.

$$w = f\sin\frac{\pi x}{b}\sin\frac{\pi y}{b} \qquad (6.5)$$

substitution of equation (6.5) into the Von Karman compatability equation.

$$\frac{\partial^4}{\partial x^4} + \frac{2\partial^4 F}{\partial x \partial y^2} + \frac{\partial^4 F}{\partial y^4} = E\left[\left(\frac{\partial^2 w}{\partial x \partial y}\right)^2 - \frac{\partial^2 w}{\partial x^2}\frac{\partial^2 w}{\partial y^2}\right]$$

$$= f^2\frac{\pi E}{b^4}\left(\cos^2\frac{\pi x}{b}\cos^2\frac{\pi y}{b}\sin^2\frac{\pi x}{b}\sin^2\frac{\pi y}{b}\right) \qquad (6.6)$$

which in view of the identities

$$\cos^2\alpha = \frac{1}{2}(1 + \cos 2\alpha)$$

$$\sin^2\alpha = \frac{1}{2}(1 - \cos 2\alpha)$$

can be reduced to

$$\frac{\partial^4 F}{\partial x^4} + 2\frac{\partial^4 F}{\partial x^2 \partial y^2} + \frac{\partial^4 F}{\partial y^4} = f^2 \frac{E\pi^4}{2b^4}\left(\cos\frac{2\pi x}{b} + \cos\frac{2\pi y}{b}\right) \tag{6.7}$$

The solution of this equation consists of a complementary and a particular part that is

$$F = Fc + Fp \tag{6.8}$$

To obtain the complementary solution of equation (6.8) the right hand side of the equation is set equal to zero, which is equivalent to letting w = 0. Thus the complementary solution of equation (6.7) corresponds to the in-plane stress distribution that exists in the plate just prior to buckling. At that instant the in-plane stresses are known to consist of a uniform stress N_x and $N_y = N_{xy} = 0$. Hence a complementary solution may take the form

$$Fc = AY^2 \tag{6.9}$$

In view of the stress equation

$$\sigma_{xb} = -\frac{\partial^2 F}{\partial y^2} = -2A \tag{6.10}$$

Equation (6.9) can be rewritten as

$$Fc = -\frac{\sigma_{xb} y^2}{2} \tag{6.11}$$

Having established that the complementary solution represents the in-plane stress distribution that exists prior to buckling, it is

obvious that the particular solution corresponds to the changes in the plane stress distribution that result from buckling. Considering the form of the right hand side of equation (6.7), the particular solution can be written as

$$F_p = B\cos\frac{2\pi x}{b} + C\cos\frac{2\pi y}{b} \tag{6.12}$$

substituting this expression into equation (6.7) and equating coefficients of like terms one obtains

$$B = C = \frac{Ef^2}{32} \tag{6.13}$$

Thus

$$F_p = \frac{Ef^2}{32}\left(\cos\frac{2\pi x}{b} + \cos\frac{2\pi y}{b}\right) \tag{6.14}$$

and the complete solution of equation (6.7) is

$$F = \frac{Ef^2}{32}\left(\cos\frac{2\pi x}{b} + \cos\frac{2\pi y}{b}\right) - \frac{\sigma_{xb}y^2}{2} \tag{6.15}$$

To evaluate the coefficient f, the Galerkin method may be used, which takes the form

$$\int_0^b \int_0^b Q(f)\, g\,(x, y)\, d_x d_y = 0 \tag{6.16}$$

Detailed analysis involving the Galerkin equation (Appendix C) results in

$$\sigma_{xb} = \frac{4DH^2}{hb^2} + \frac{E\pi^2 f^2}{8b^2} \tag{6.17}$$

or

$$\sigma_{xb} = \sigma_{cr} + \frac{E\pi^2 f^2}{8b^2} \tag{6.18}$$

since $\frac{4D\pi^2}{hb^2}$ is the critical stress of the plate equation (6.18) gives

the relationship between the average applied stress σ_{xb} and the maximum lateral deflection f subsequent to the onset of buckling. A graphical representation of the relationship is shown in fig (6.2b), from which it can be seen that the plate begins to deflect laterally at the critical load and beyond that point as long as the lateral deflection is infinitesimally small, the stiffness of the plate is zero, that is the load deflection curve has a zero slope. However, as soon as the lateral deflection becomes finite, the stiffness starts to increase and continues to do so as the deflection grows. It is thus possible for the plate to resist axial loads in excess of the critical load subsequent to buckling.

To trace the stress distribution along the edges of the plate it may be noted that the longitudinal stress

$$\sigma_x = \frac{-\partial^2 F}{\partial y^2} = \frac{E\pi^2 f^2}{8b^2} \cos \frac{2y}{b} + \sigma_{xb} \tag{6.19}$$

and from equation (6.18)

$$f^2 = \frac{8b^2}{E\pi^2} (\sigma_{xb} - \sigma_{cr}) \tag{6.20}$$

$$\text{Thus } \sigma_x = \sigma_{xb} + (\sigma_{xb} - \sigma_{cr}) \cos \frac{2\pi y}{b} \tag{6.21}$$

Similarly the transverse stress σ_y may be found to be

$$\sigma_y = (\sigma_{xb} - \sigma_{cr}) \cos \frac{2\pi x}{b} \tag{6.22}$$

The stress distributions given in equations (6.21) and (6.22) are shown plotted in fig (6.2c). Comparing these stresses with the longitudinal and transverse stresses that existed prior to buckling, two essential differences are apparent. These are that the transverse stresses σ_y, present subsequent to buckling were non existant prior to buckling, and that the longitudinal stress σ_x which is constant

up to the onset of buckling varies along the edge after buckling has occurred.

The transverse stresses that are present in the post buckling range vary from a maximum compressive stress at the edges x = 0, b to a maximum tensile stress at the centre of the plate. Of these the tensile stress σ_y is by far the more important. Its presence tends to stiffen the plate against lateral deflection and to prevent collapse from occurring after the critical load has been reached. The post buckling strength exhibited by the plate can thus be attributed to the middle surface tensile stress σ_y that arises subsequent to the onset of buckling.

Prior to buckling all longitudinal fibres have the same stiffness and the applied stress is uniformly distributed across the width of the plate. However, in the deformed configuration subsequent to buckling, the fibres near the supported edges have a greater resistance to lateral deflection than those in the centre of the plate. The longitudinal stresses in the post buckling range are therefore distributed across the width of the plate as indicated in fig (6.2c). They vary from a maximum at the edges y = 0, b to a minimum at the centre of the plate. A major portion of the increased load carrying capacity that takes place subsequent to buckling is thus resisted by the relatively stiff portion of the plate adjacent to the longitudinal edges.

Equation (6.17) may be applied also to a rectangular plate since it includes the general term

$$\sigma_{cr} = \frac{KD}{b^2}^2 \qquad (6.23)$$

where

$$K = \left(\frac{mb}{a} + \frac{n^2}{m}\frac{a}{b}\right)^2 \qquad (6.24)$$

The derivation of the above equations may be found in reference 6.8

The factor K depends on the aspect ratio a/b (length/width) and on m and n the number of half-waves that the plate buckles into. Since the critical value of P_{cr} is the smallest value in equation (6.23), the values of m and n that minimize it must be determined. It is obvious that σ_{cr} increases as n increases and that n = 1 results in the minimum value of σ_{cr} along the length a that corresponds to a minimum value of K and hence σ_{cr}.

Minimizing K gives

$$\frac{K}{m} = \left(\frac{mb}{a} + \frac{a}{mb}\right)\left(\frac{b}{a} - \frac{a}{bm^2}\right) = 0 \qquad (6.25)$$

from which $m = \frac{a}{b}$

Substituting m in equation (6.24) results in K = 4 and equation (6.23) becomes

$$\sigma_{cr} = \frac{4D^2}{b^2} \qquad (6.26)$$

In the case of orthotropic plates further modification is applied to equation (6.17), and this is effected by substituting $\sqrt{D_1 D_2}$ for D and $\sqrt{E_1 E_2}$ for E where D_1, D_2 are the flexural rigidities in the lateral and longitudinal directions.

E_1, E_2 are the elastic modulu in the lateral and longitudinal directions.

Hence equation (6.17) becomes

$$\sigma_{xb} = \frac{4\sqrt{D_1 D_2}}{hb^2}\pi^2 + \frac{\sqrt{E_1 E_2}}{8b^2}\pi^2 f^2 \qquad (6.27)$$

6.4.3 Prediction of the Post Buckling Load

The post buckling behaviour of an isotropic plate can be analysed using large deflection theory (section 6.4.2). The following differential equation for large deflection buckling of a plate was introduced by Von Karman [6.4]

$$\frac{\partial^4 w}{\partial x^4} + \frac{2\partial^4 w}{\partial x^2 \partial y^2} + \frac{\partial^4 w}{\partial y^4} =$$

$$\frac{t}{D}\left(\frac{\partial^2 F}{\partial y^2}\frac{\partial^2 w}{\partial x^2} - \frac{2\partial^2 F}{\partial x \partial y}\frac{\partial^2 w}{\partial x \partial y} + \frac{\partial^2 F}{\partial x^2}\frac{\partial^2 w}{\partial y^2}\right) \qquad (6.28)$$

where F is a stress function defining the median fibre stress of the plate and

$$\sigma_x = \frac{\partial^2 F}{\partial y^2} \qquad (6.29)$$

$$\sigma_y = \frac{\partial^2 F}{\partial x^2} \qquad (6.30)$$

$$\tau_{xy} = \frac{-\partial^2 F}{\partial x \partial y} \qquad (3.31)$$

It has been found that the solution of the differential equation for large deflection theory has little application in practical design because of its complexity. For this reason a concept of "effective width" was introduced by Von Karman [6.4] in 1932. The concept is related to the stress distribution along the loaded end of the plate. Considering fig (6.2a), the stress distribution is uniform prior to buckling as shown in fig (6.3a). After buckling a portion of the pre-buckling load of the centre strip transfers to the edge portion of the plate. As a result the non-uniform stress distribution is

developed as shown in fig (6.3b). The redistribution of stress continues until the stress at the edge reaches the yield point of the material and then the plate begins to fail plastically fig (6.3c).

In the "effective width" concept instead of considering the non-uniform distribution of stress over the entire width of the plate w, it is assumed that the total load is carried by a fictitious effective width b subjected to a uniformly distributed stress equal to the edge stress σ_{max} as shown, fig (6.4). The width b is selected so that the area under the curve of the actual non-uniform stress distribution is equal to the sum of the two parts of the equivalent rectangular shaded area with a total width b and an intensity of stress equal to the edge stress σ_{max}, that is

$$\int_0^w \sigma \, dx = b\sigma_{max} \tag{6.32}$$

It may also be considered that the effective width b_c represents a particular width of the plate which just buckles when the compressive stress reaches the yield point of the material. Therefore, for a long plate the theoretical value of b may be determined as follows:

$$\sigma_{cr} = F_y = \frac{\pi^2 E}{3(1-\nu^2)\,(b/t^2)^2} \tag{6.33}$$

where

$$b = Ct\sqrt{\frac{E}{F_y}} \tag{6.34}$$

$$C = \frac{\pi}{\sqrt{3(1-\nu^2)}} \tag{6.35}$$

E = the modulus of the material

F_y = the yielding strength of the material

ν = Poisson's ratio of the material

whenever w > b

$$\sigma_{cr} = \frac{\pi^2 E}{3(1-\nu^2)} \tag{6.36}$$

$$w = Ct\sqrt{\frac{E}{\sigma_{cr}}} \tag{6.37}$$

From equations (6.34) and (6.37) the following relationship between b and w may be obtained

$$\frac{b}{w} = \sqrt{\frac{\sigma_{cr}}{F_y}} \tag{6.38}$$

Based on his extensive investigation on light gauge, cold-formed steel sections, Winter [6.5] indicated that equation (6.37) is equally applicable to the element in which the stress is below the yield point and therefore equation (6.37) can then be rewritten as

$$b = Ct\sqrt{\frac{E}{\sigma_{max}}} \tag{6.39}$$

where σ_{max} is the maximum edge stress, which may be less than the yield stress. Test results previously obtained by Schler and Winter indicate that the term C used in equation (6.39) depends primarily on the non-dimensional parameter $\sqrt{\frac{E}{\sigma_{max}}}\left(\frac{t}{w}\right)$

6.4.4 Prediction of the buckling load (Orthotropic Plates)

An approximate solution for orthotropic plates with both unloaded edges fixed was given in References (6.6 and 6.7), from which the buckling load may be predicted by the following.

$$N_{xcr} = \frac{\pi^2\sqrt{D_1 D_2}}{b^2}\left[\frac{D_1}{D_2}\left(\frac{m'}{\phi}\right) + \frac{8}{3}\frac{n'^2 D_3}{\sqrt{D_1 D_2}} + \frac{16n'^4}{3}\frac{\sqrt{D_2}}{\sqrt{D_2}}\left(\frac{\phi}{m'}\right)^2\right] \tag{6.40}$$

where $\phi = \frac{a}{b}$ is the aspect ratio of the plate.

$$D_1 = \frac{Ext^3}{12(1-\nu_x\nu_y)} \text{ in the longitudinal direction}$$

$$D_2 = \frac{Ext^3}{12(1-\nu_x\nu_y)} \text{ in the transverse direction}$$

and $D_3 = \frac{1}{2}(\nu_x D_y + \nu_y D_x) + 2(GI)_{xy}$

where $2(GI)_{xy} = 2\frac{Gt^3}{12}$ is the average torsional rigidity and m is an integer.

The smallest value of $N_x cr$ occurs for n' = 1 consequently the critical load will be determined from

$$N_x(cr) = \frac{\pi^2\sqrt{D_1D_2}}{b^2}\left[\frac{D_1}{D_2}\left(\frac{m}{\phi}\right)^2 + \frac{2.67D_3}{\sqrt{D_1D_2}}\right.$$

$$\left. + 5.33\ \frac{D_2}{D_1}\left(\frac{\phi}{m}\right)^2\right] \qquad (6.41)$$

Reference [6.6] gives the boundary conditions for the m from the following.

if $0 < \phi < 0.931\ 4\ \frac{D_1}{D_2}$ then m = 1

if $0.931\ \frac{D_1}{D_2} < \phi < 1.61\ 4\ \frac{D_1}{D_2}$ then m = 2

if $1.61\ 4\ \frac{D_1}{D_2} < \phi < 2.28\ 4\ \frac{D_1}{D_2}$ then m = 3

For plates with a higher aspect ratio than those given by equation (6.41) the critical buckling load may be obtained from the equation.

$$N_x cr = \frac{\pi^2\sqrt{D_1D_2}}{b^2}\ K_{bmin} \qquad (6.42)$$

where $K_{bmin} = 2.67\ (1.73 + \frac{D_3}{\sqrt{D_1D_2}})$ (6.43)

6.5 TEST RESULTS

Experimental lateral deflections and strains at the centre of the plates were plotted against load up to the collapse state fig (6.5-6.8).

6.6 DISCUSSION

From experimental plots (axial deflections and strains versus load figs (6.5-6.8), it was possible to trace the initiation of the post buckling region. In all cases load versus deflection behaviour was linear up to the critical load value after which the behaviour tended to be non-linear. The values of the initial critical loads traced from the experimental plots fig (6.5-6.8) are shown and compared with theoretical equations, (6.61, 6.27) in Table 6.3. The comparison shows that the theoretical results are higher than the experimental.

Load versus lateral deflection was also plotted using test data and equation (6.27 and 6.41) and this comparison is shown in figs (6.9-6.16). Although equation (6.27) results in higher values than test data, it exhibits a similar load-deflection relationship in the post buckling range.

The values of initial critical loads derived from equations (6.41 and 6.42) were shown to be higher than those derived from either equation (6.27) or the test data (see Table 6.3).

The ultimate post buckling loads derived from equation (6.33 and 6.39) were greater than the experimental ultimate loads (Table 6.4). Plate type P_4 attained the maximum ultimate load (Table 6.3) and this is due to the multidirectional fibre orientation and the increased thickness of the plate compared with other types of plates. On examining the plates after collapse, it was noticed that the material

around the edge nearer to the corners of the plate were more delaminated than material around the central region.

This confirms the pattern of stress distribution for the post buckling region fig (6.2c) and the analysis carried out in section 6.4.3.

The variation between theoretical and experimental results in fig (6.9-6.17) and Tables 6.3 and 6.4, may be attributed to the following factors:-

(1) The theory described in section (6.4.2) is based on an approximate analysis and therefore, contains some minor inaccuracies, for example a precise analysis would indicate that in-plane shear stresses exist in addition to transverse tensile stresses after buckling has began.

A more precise analysis would also show variations in σx and σy across the thickness of the plate that the simplified analysis was not able to detect.

(2) All plates do have geometrical imperfections and the general theory of elastic stability demonstrates that such imperfections will have a profound effect upon the stability behaviour of any structure. Geometric imperfections in the shape of the natural buckling modes and inclusion of voids and non uniform thickness may have a marked effect upon the post buckling structural strength.

(3) In testing plates of this nature, it is virtually impossible to eliminate completely the misalignment factor which again has a considerable effect on the result.

Plate No	Plate type	Fibre arrangement	f_{max} N/mm^2	Post buckling load kN	
				Theory 6.33 Eqn. 6.39	Experimental
1	P_1	Angle ply +45,-45,-45,+45	120	10.946	2.750
2	P_1	Angle ply +45,-45,-45,+45	120	11.206	2.750
3	P_2	Cross ply 4[0/90]	180	15.303	1.750
4	P_2	Cross ply 4[0/90]	180	14.891	2.225
5	P_3	Unidirectional 0,0,0,0	190	16.421	2.00
6	P_3	Unidirectional 0,0,0,0	190	16.439	2.125
7	P_4	Multidirectional 0,+45,-45,-45,+45,0	140	16.694	2.750
8	P_4	Multidirectional 0,+45,-45,-45,+45,0	140	17.334	2.87

TABLE 6.4

EXPERIMENTAL AND THEORETICAL POST BUCKLING LOADS

Plate No	Plate Type	Fibre arrangement	Initial buckling load kN		
			Theory Eqn. 6.41	Theory Eqn. 6.27	Experimental
1	P_1	Angle ply 45,-45,-45,45	10.10	4.664	2.12
2	P_1	Angle ply 45,-45,-45,45	10.22	4.657	2.00
3	P_2	Cross ply 4[0/90]	14.730	9.343	2.17
4	P_2	Cross ply 4[0/90]	14.166	8.88	1.85
5	P_3	Unidirectional 0,0,0,0	7.827	6.509	1.40
6	P_3	Unidirectional 0,0,0,0	7.780	6.530	1.50
7	P_4	Multidirectional 0,+45,-45,-45,+45,0	14.14	8.756	2.00
8	P_4	Multidirectional 0,+45,-45,-45,+45,0	15.110	9.283	2.37

TABLE 6.3

EXPERIMENTAL AND THEORETICAL INITIAL BUCKLING LOADS

Plate No	Plate No	Longitudinal Modulus E_L (N/mm^2)	Transverse Modulus E_T (N/mm^2)	Shear Modulus$_2$ G_{LT} (N/mm^2)	Longitudinal Poisson's Ratio ν_{LT}	Transverse Poisson's ratio ν_{TL}
1	P_1	5750	5750	6800	0.51	0.51
2	P_1	5712	5712	6700	0.50	0.50
3	P_2	12930	12930	3250	0.167	0.167
4	P_2	12860	12860	3250	0.167	0.167
5	P_3	21350	4710	1980	0.310	0.070
6	P_3	21400	4750	2030	0.300	0.065
7	P_4	19500	6450	7050	0.480	0.160
8	P_4	19450	6500	6900	0.460	0.155

TABLE 6.2

ELASTIC PROPERTIES OF PLATES

Plate No	Plate Type	Material	Type and Fibre Arrangement	Dimensions mm
1	P_1	G.R.P.	Angle ply +45,-45,-45,+45	420 x 176 x 3.18
2	P_1	G.R.P.	Angle ply +45,-45,-45,+45	420 x 176 x 3.20
3	P_2	G.R.P.	Cross ply 4[0/90]	420 x 176 x 3.35
4	P_2	G.R.P.	Cross ply 4[0/90]	420 x 176 x 3.30
5	P_3	G.R.P.	Unidirectional 0,0,0,0	420 x 176 x 3.24
6	P_3	G.R.P.	Unidirectional 0,0,0,0	420 x 176 x 3.24
7	P_4	G.R.P.	Multidirectional 0,+45,-45,-45,+45,0	420 x 176 x 3.38
8	P_4	G.R.P.	Multidirectional 0,+45,-45,-45,+45,0	420 x 176 x 3.45

TABLE 6.1

PLATES CONFIGURATION

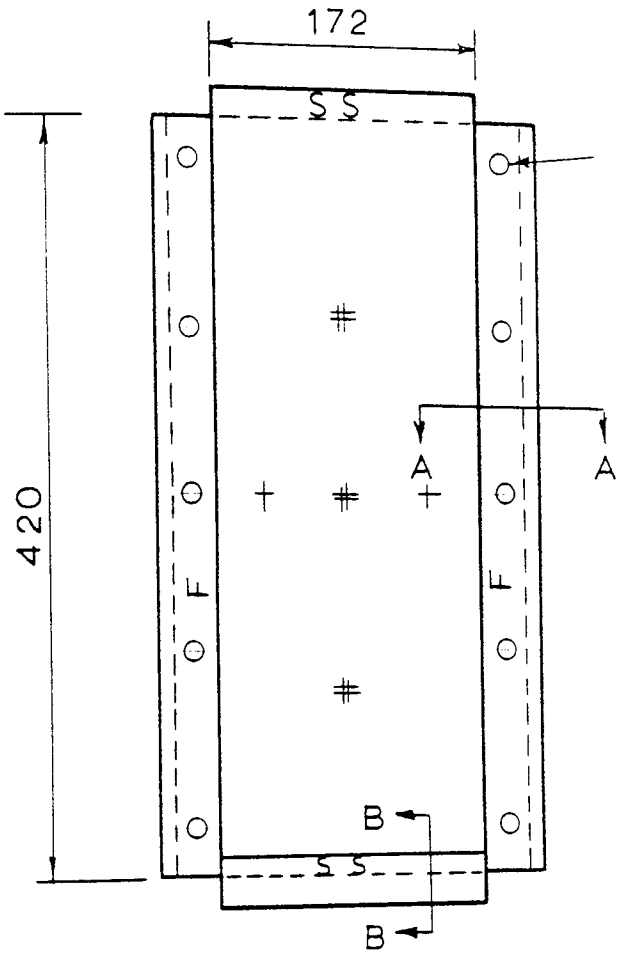

General set up

dial and strain gauge positions

\+ strain gauge position

F Fixed boundary

S S Simply supported

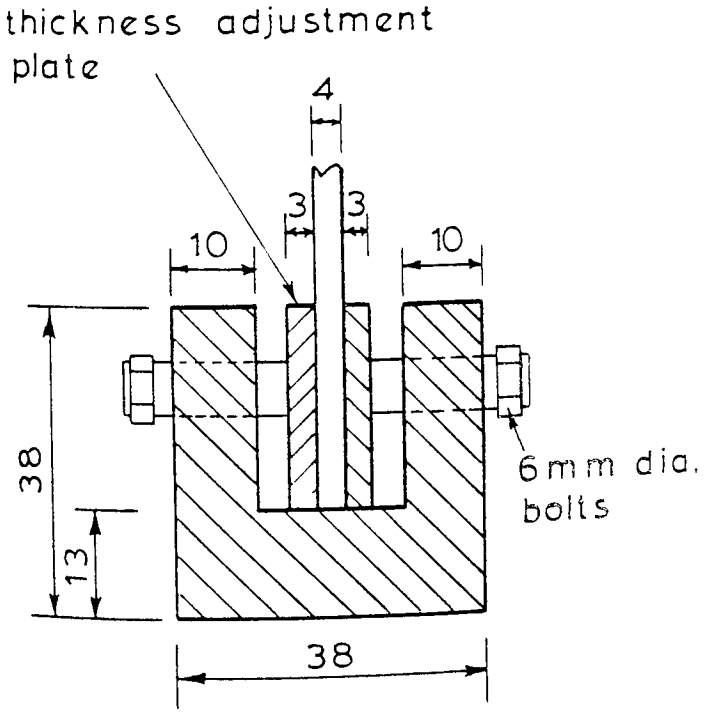

Section A · A

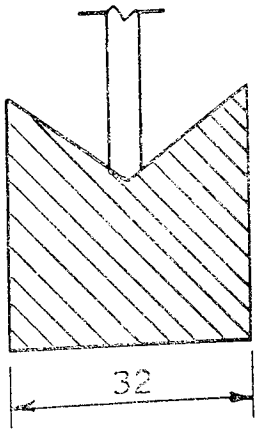

Section B · B

all dimensions in m.m.

Fig 6.1 boundary coditions for tests

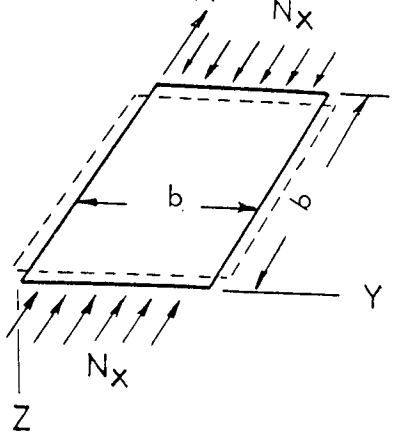

Fig. 6.2.a Simply supported plate compressed in X direction

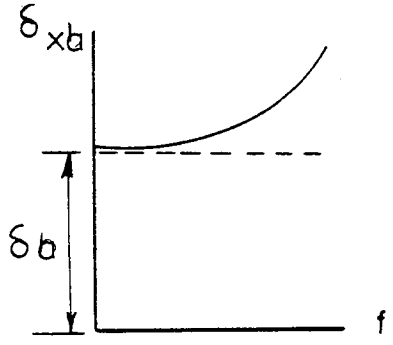

Fig. 6.2 b. Typical load deflection curve for post buckling region

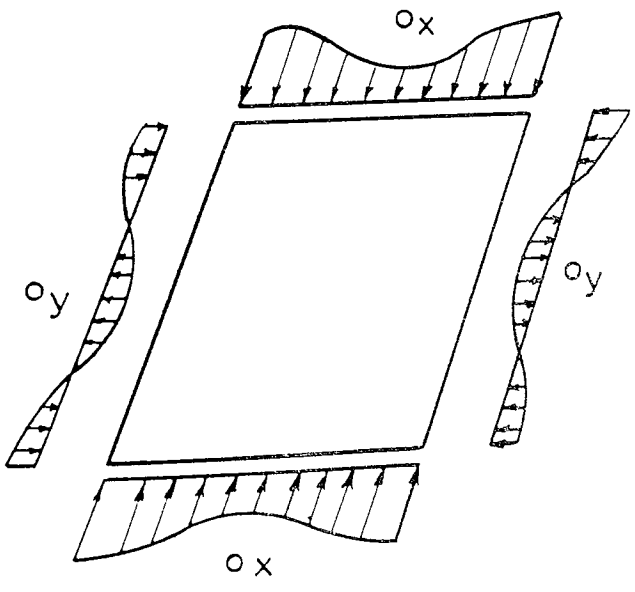

Fig. 6.2.c. Stress distribution in post buckling range.

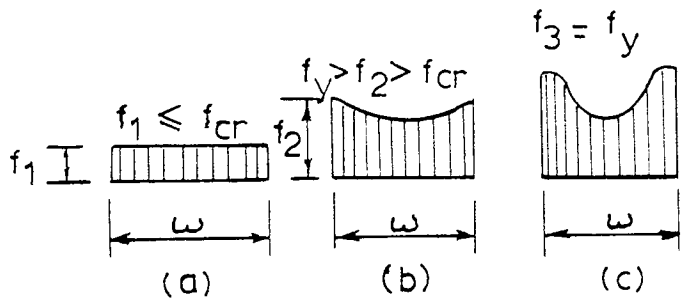

Fig. 6.3 Consecutive stages of stress distribution in stiffened compression elements

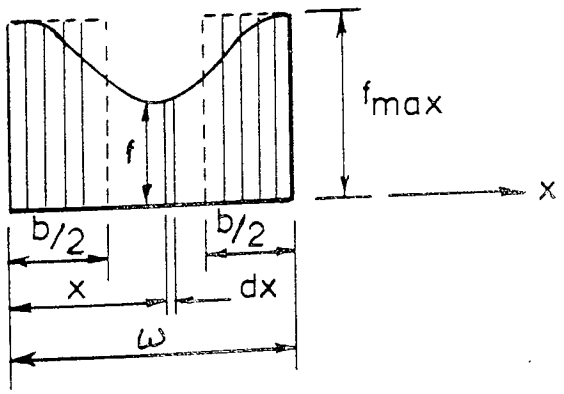

Fig. 6.4 Effective width of a stiffened compression element.

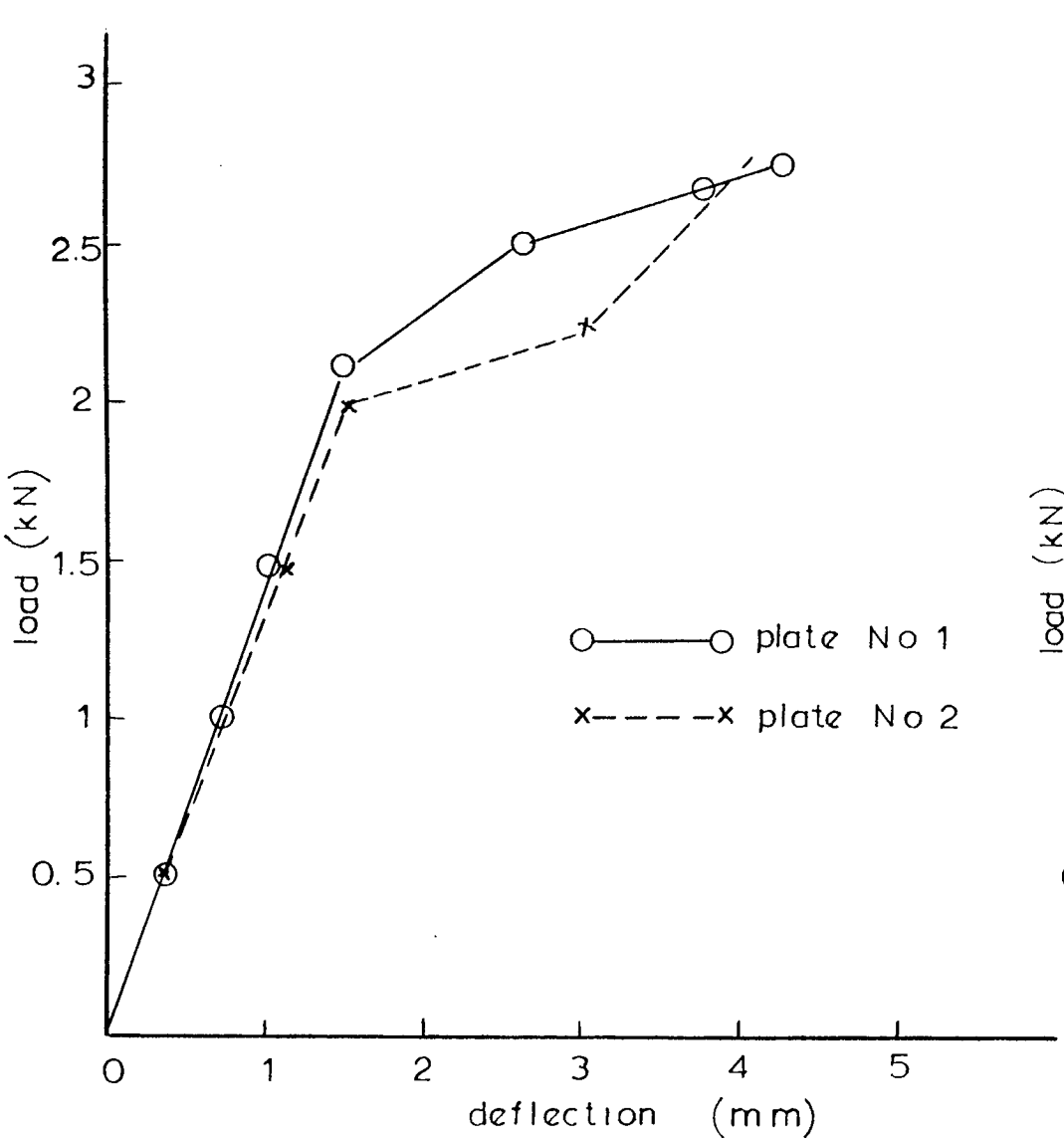

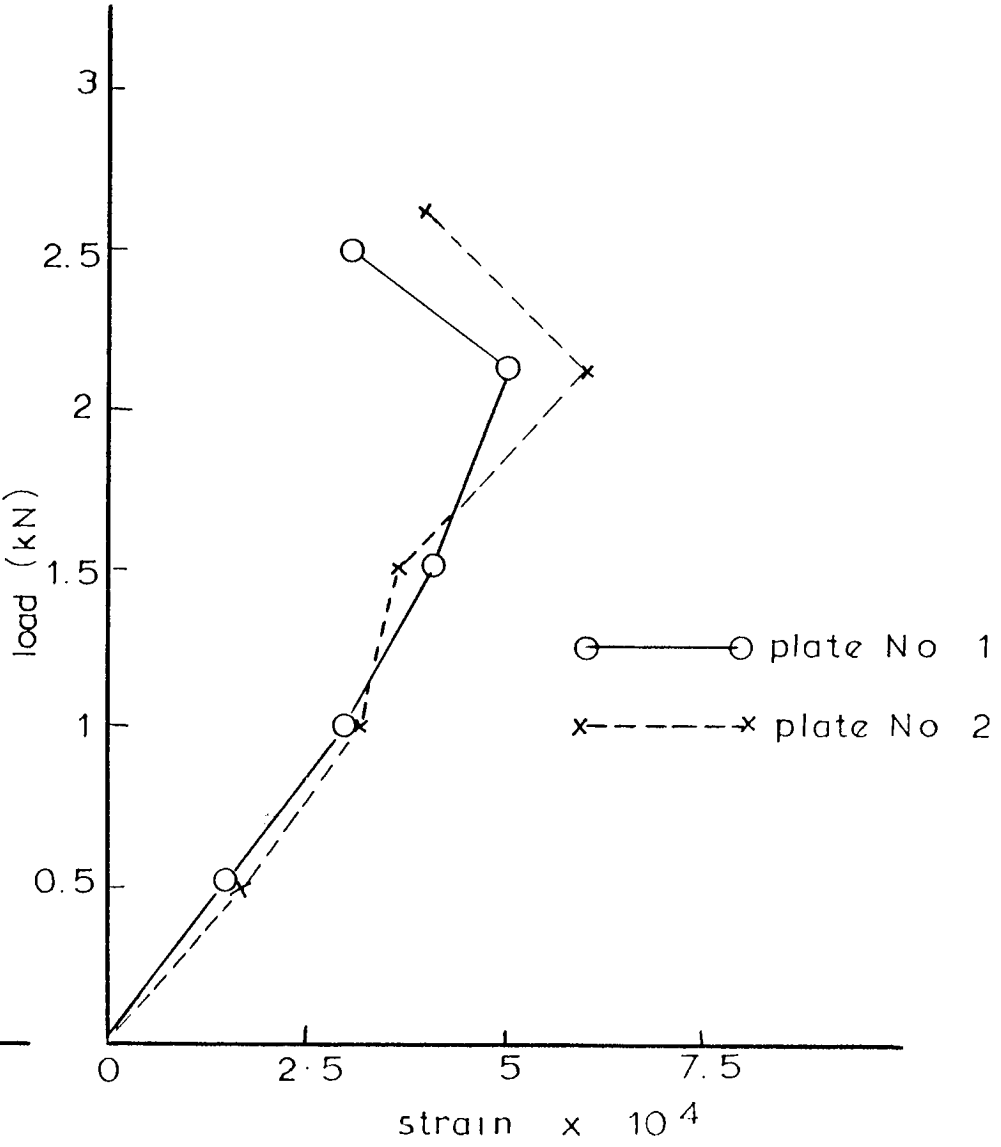

Fig.. 6.5 Plates type P1. Load versus axial deflection.

Load versus strain.

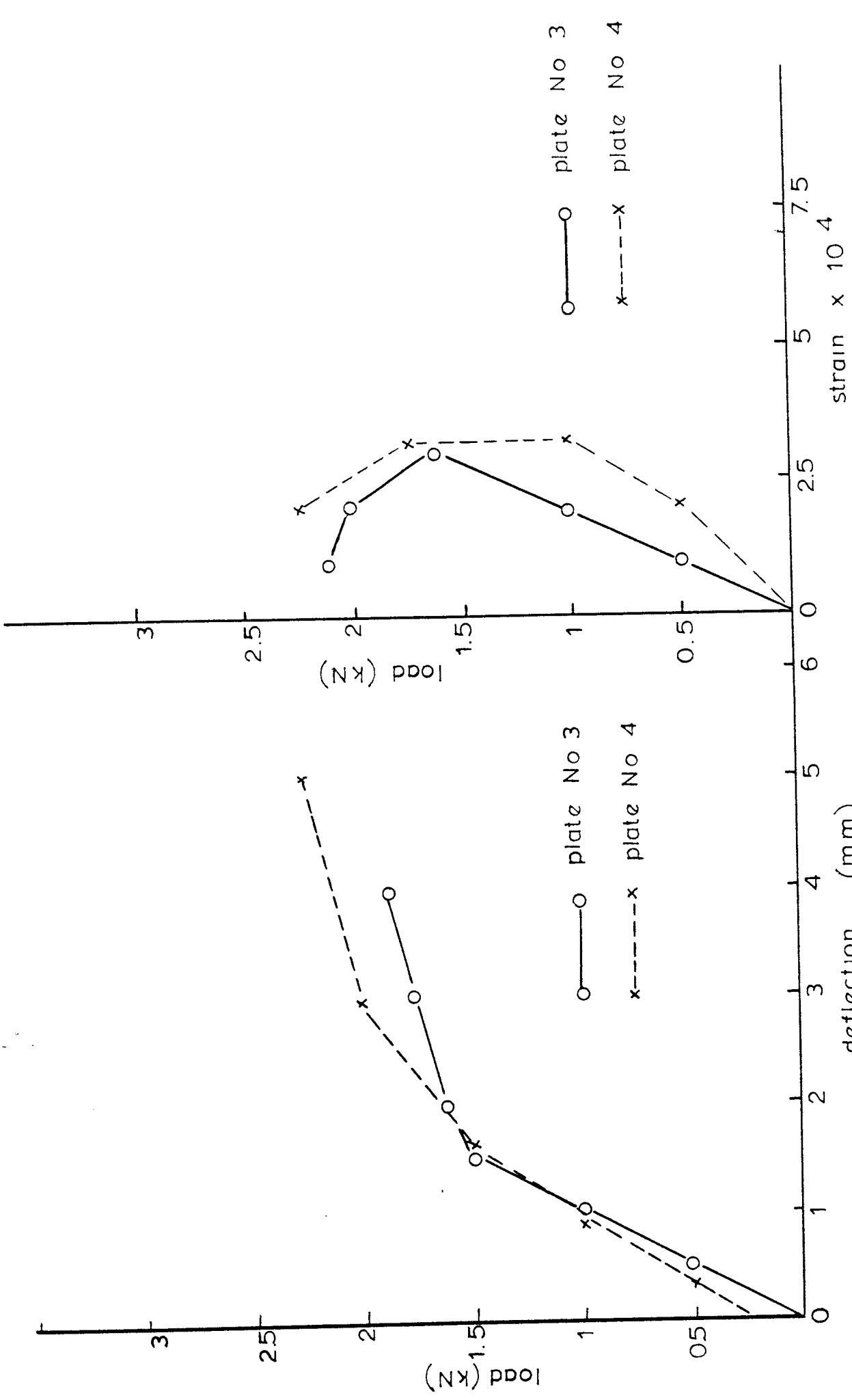

Fig. 6.6. Plates type P2. Load versus axial deflection.

Load versus strain

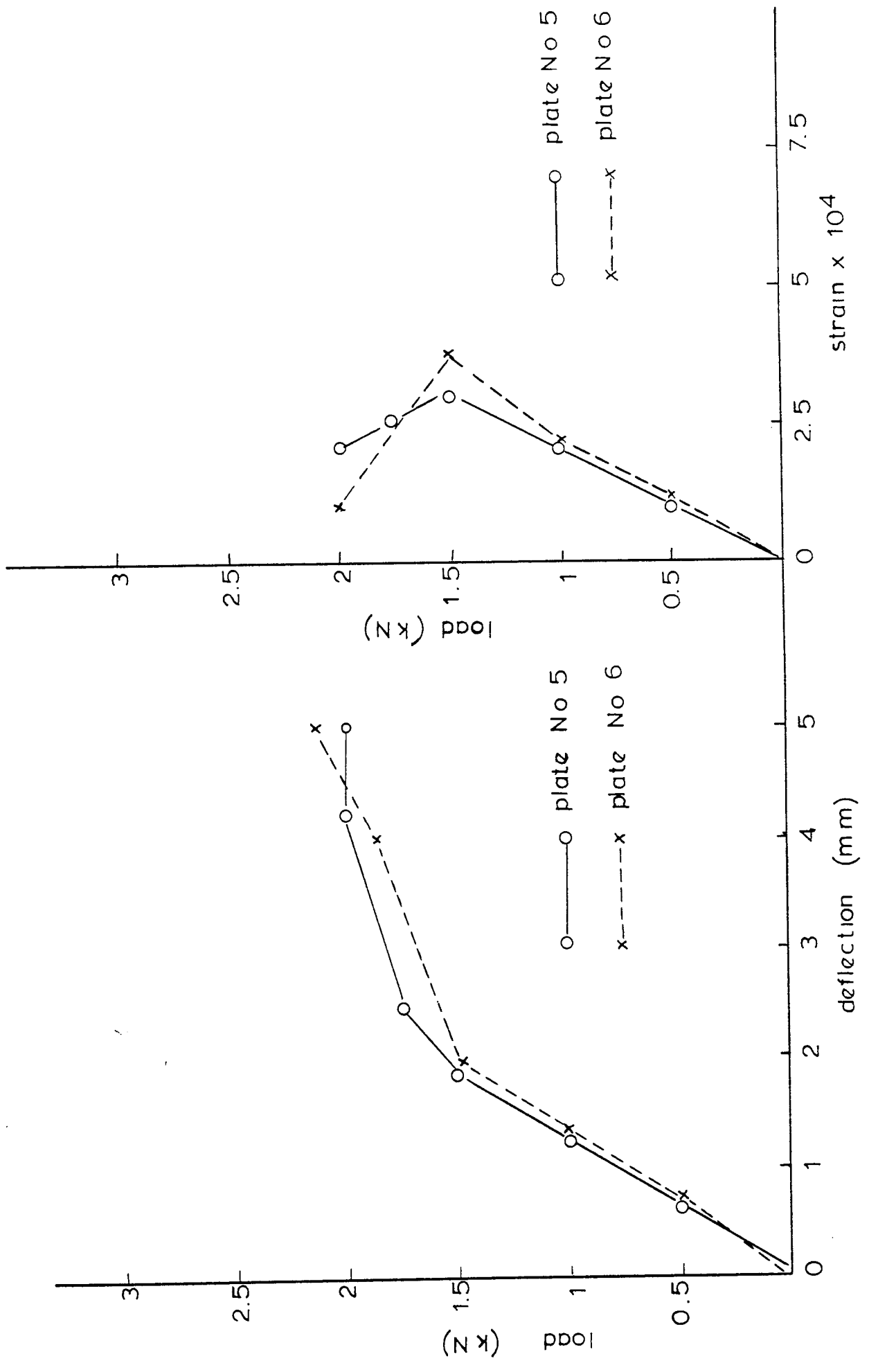

Fig. 6.7 Plates type P3. Load versus axial deflection. Load versus strain.

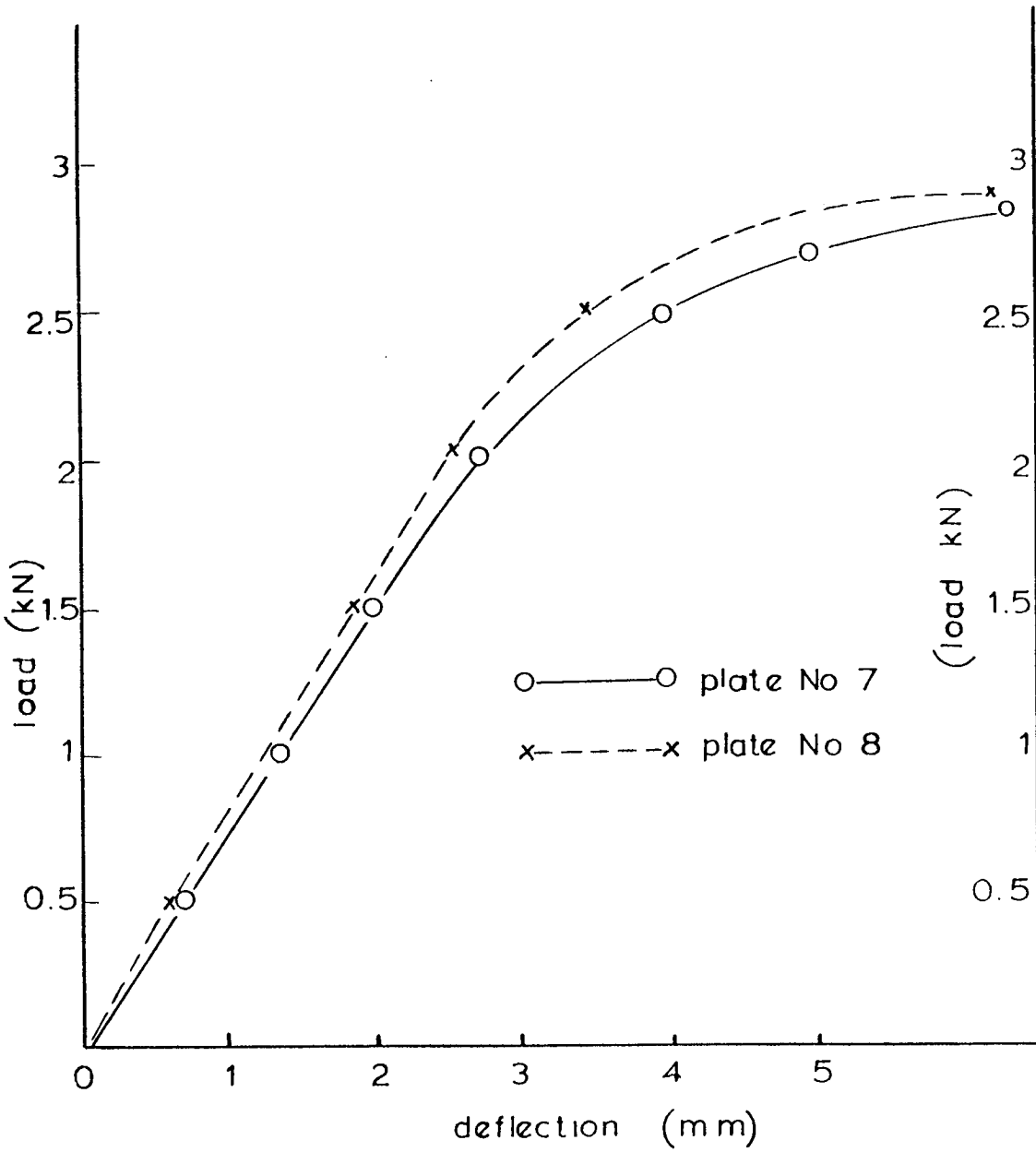

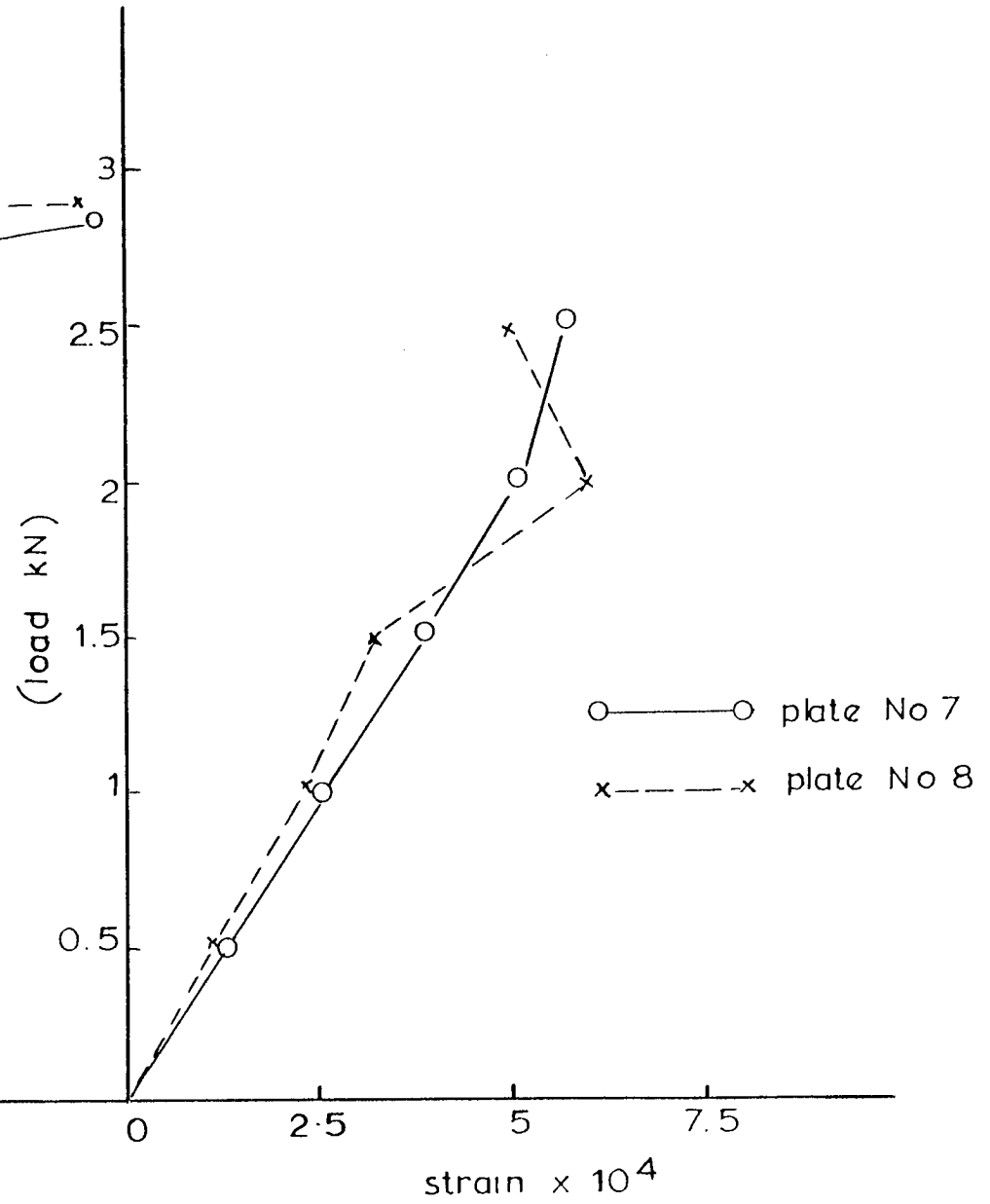

Fig. 6.8 Plates type P4. Load versus axial deflection. Load versus strain

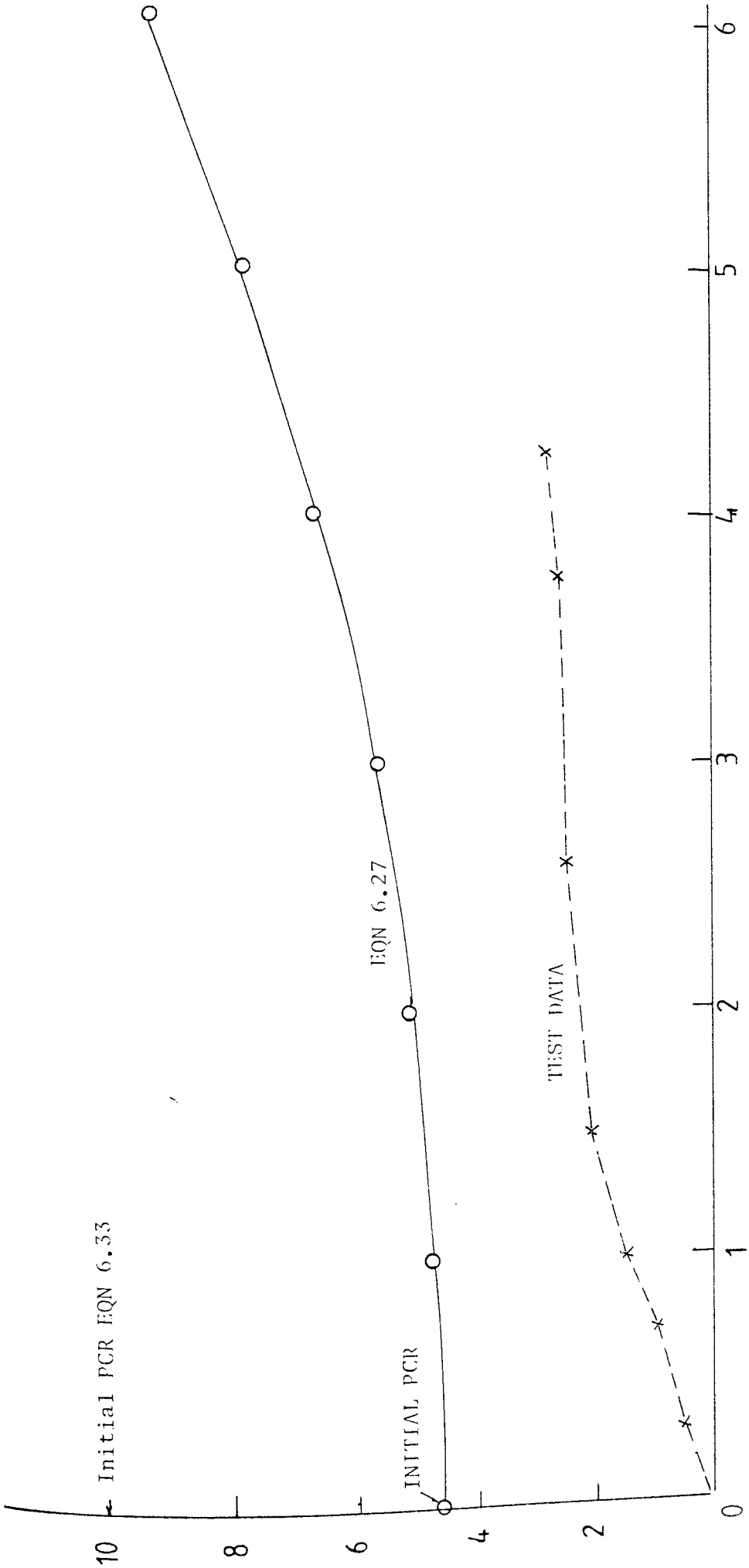

FIGURE 6.9 PLATE TYPE P_1 (No 1)

LOAD VERSUS LATERAL DEFLECTION FOR POST BUCKLING REGION

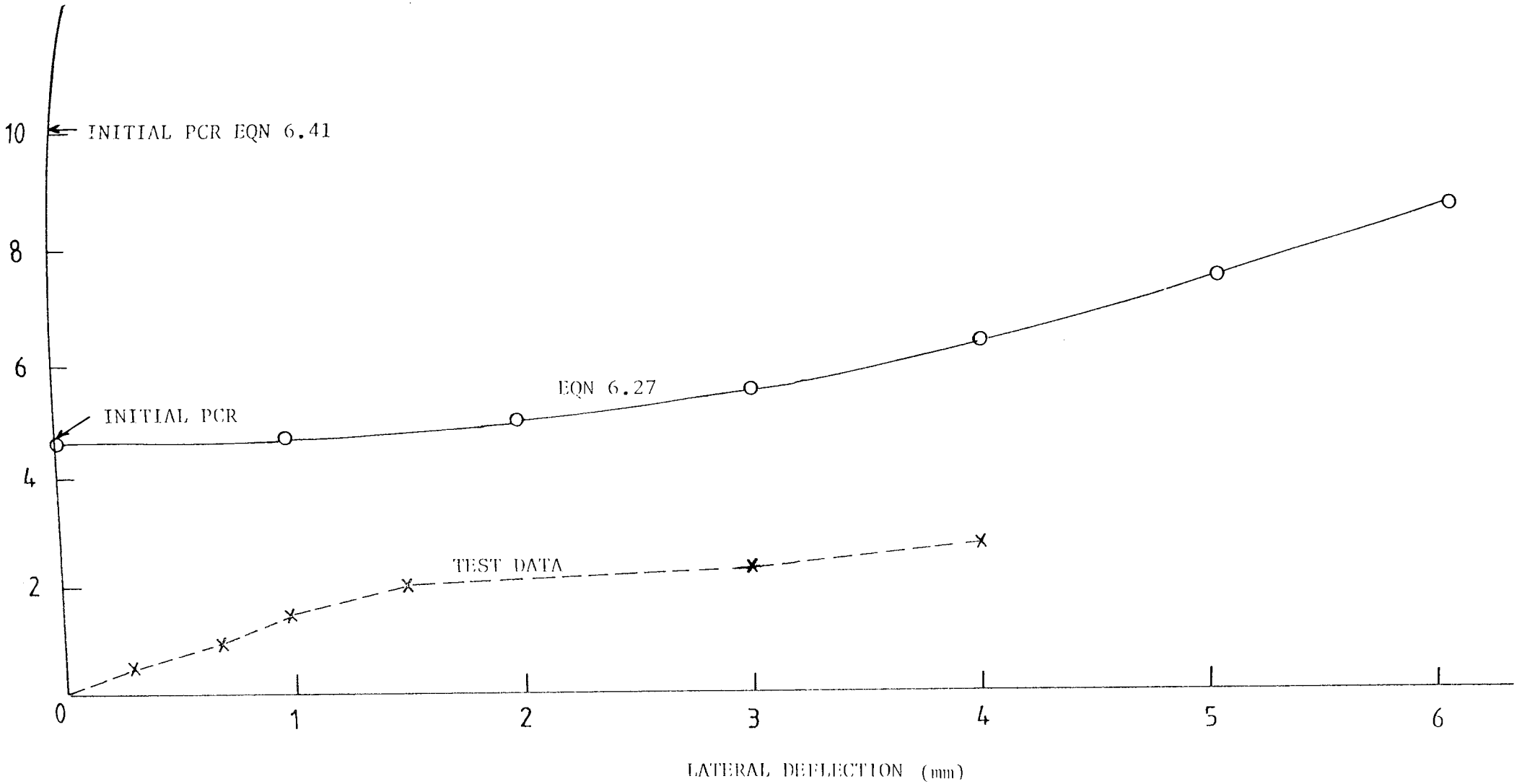

FIGURE 6.10 PLATE TYPE P_1 (No 2)

LOAD VERSUS LATERAL DEFLECTION FOR POST BUCKLING REGION

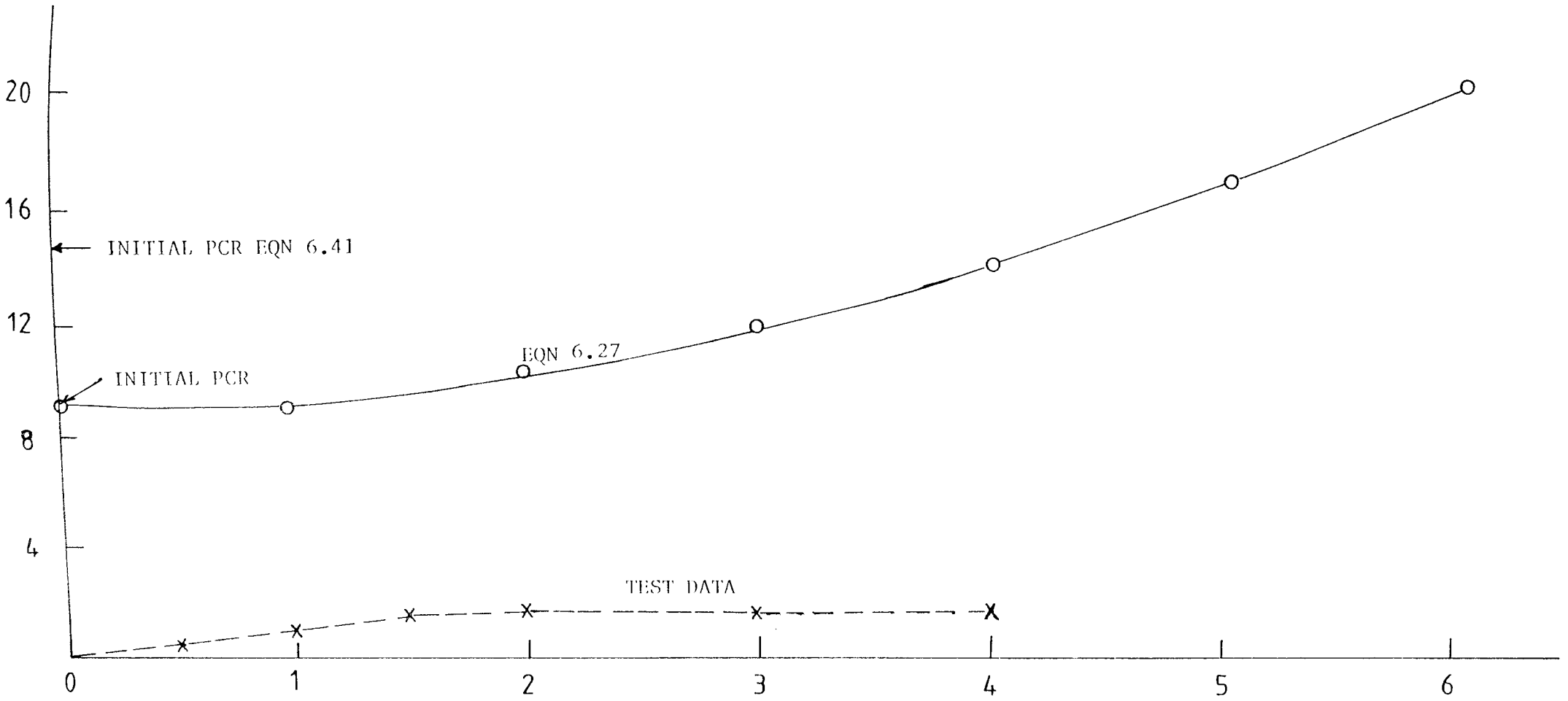

FIGURE 6.11 PLATE TYPE P_2 (No 3)

LOAD VERSUS LATERAL DEFLECTION FOR POST BUCKLING REGION

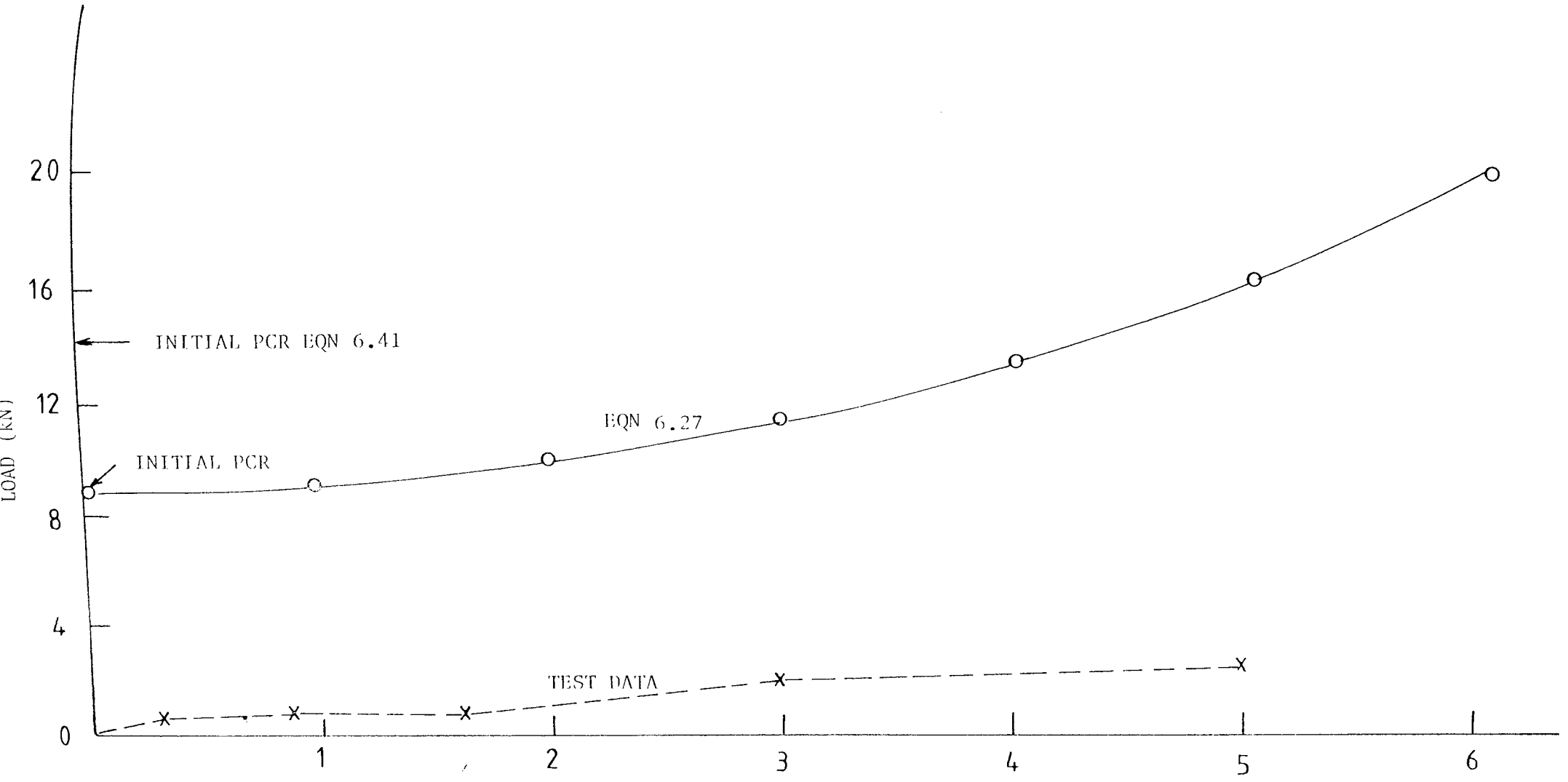

FIGURE 6.12 PLATE TYPE P_2 (No 4)

LOAD VERSUS LATERAL DEFLECTION FOR POST BUCKLING REGION

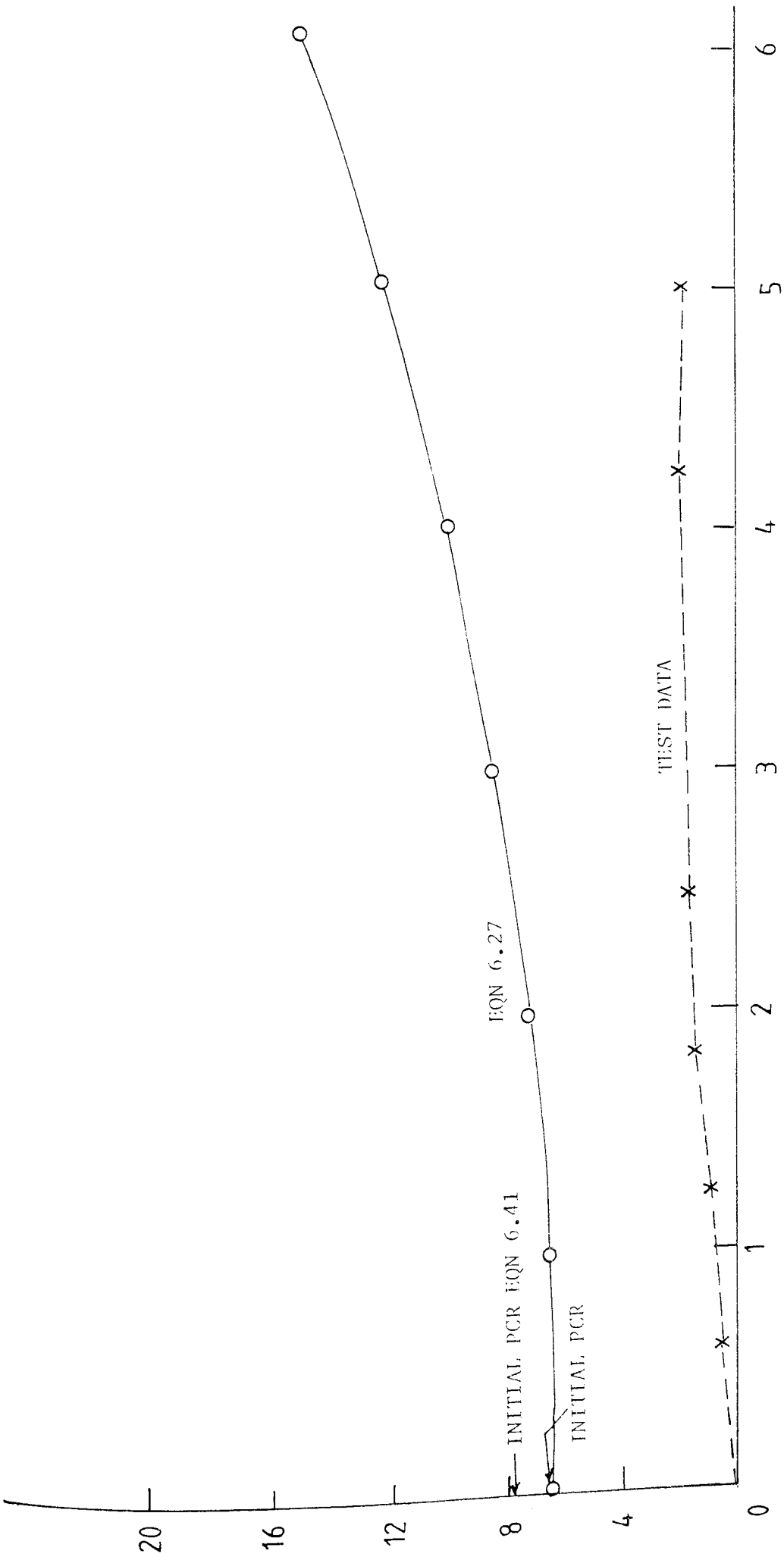

FIGURE 6.13 PLATE TYPE P_3 (NO 5)

LOAD VERSUS LATERAL DEFLECTION FOR POST BUCKLING REGION

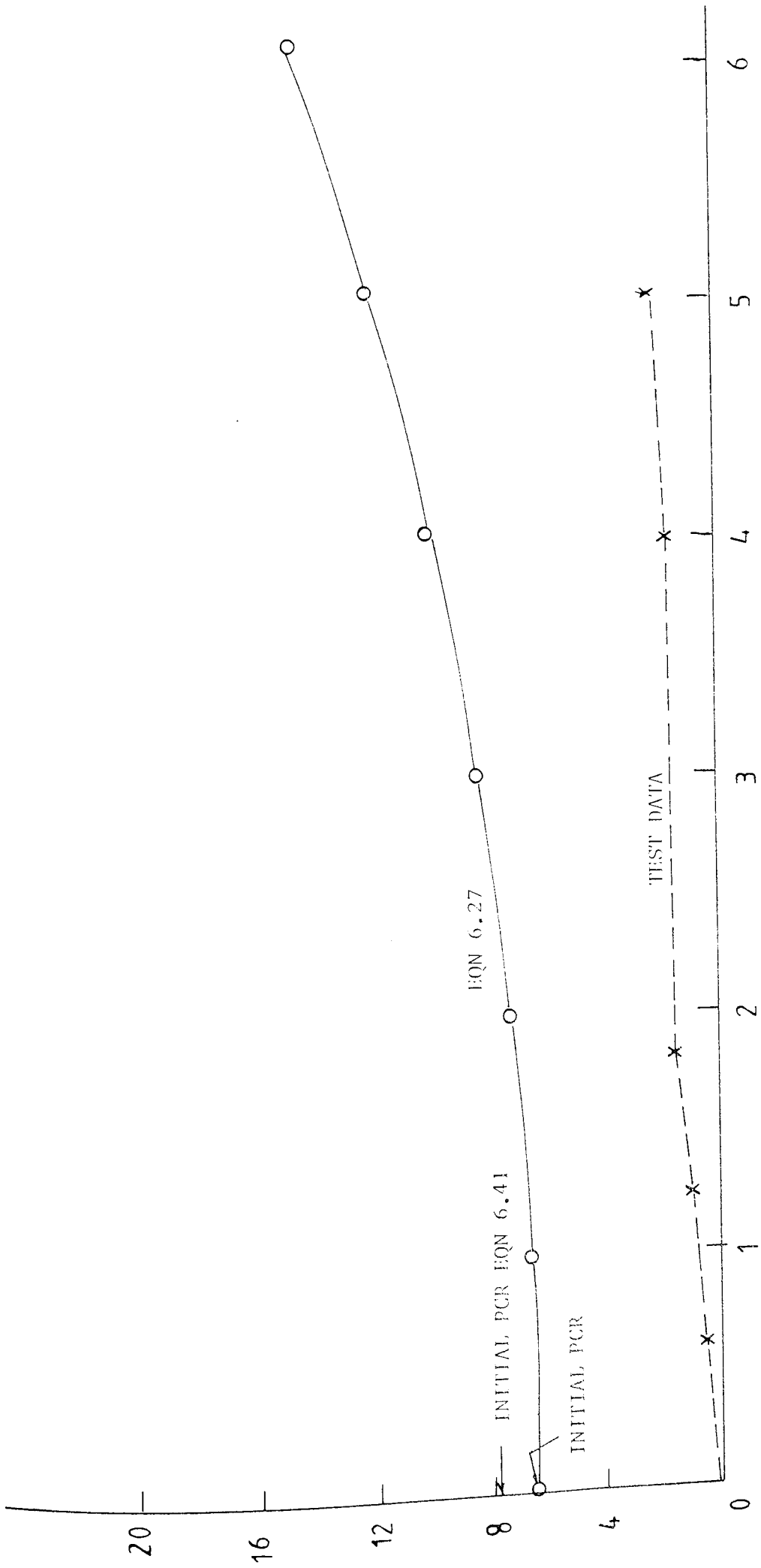

FIGURE 6.14 PLATE TYPE P_3 (No 6)

LOAD VERSUS LATERAL DEFLECTION FOR POST BUCKLING REGION

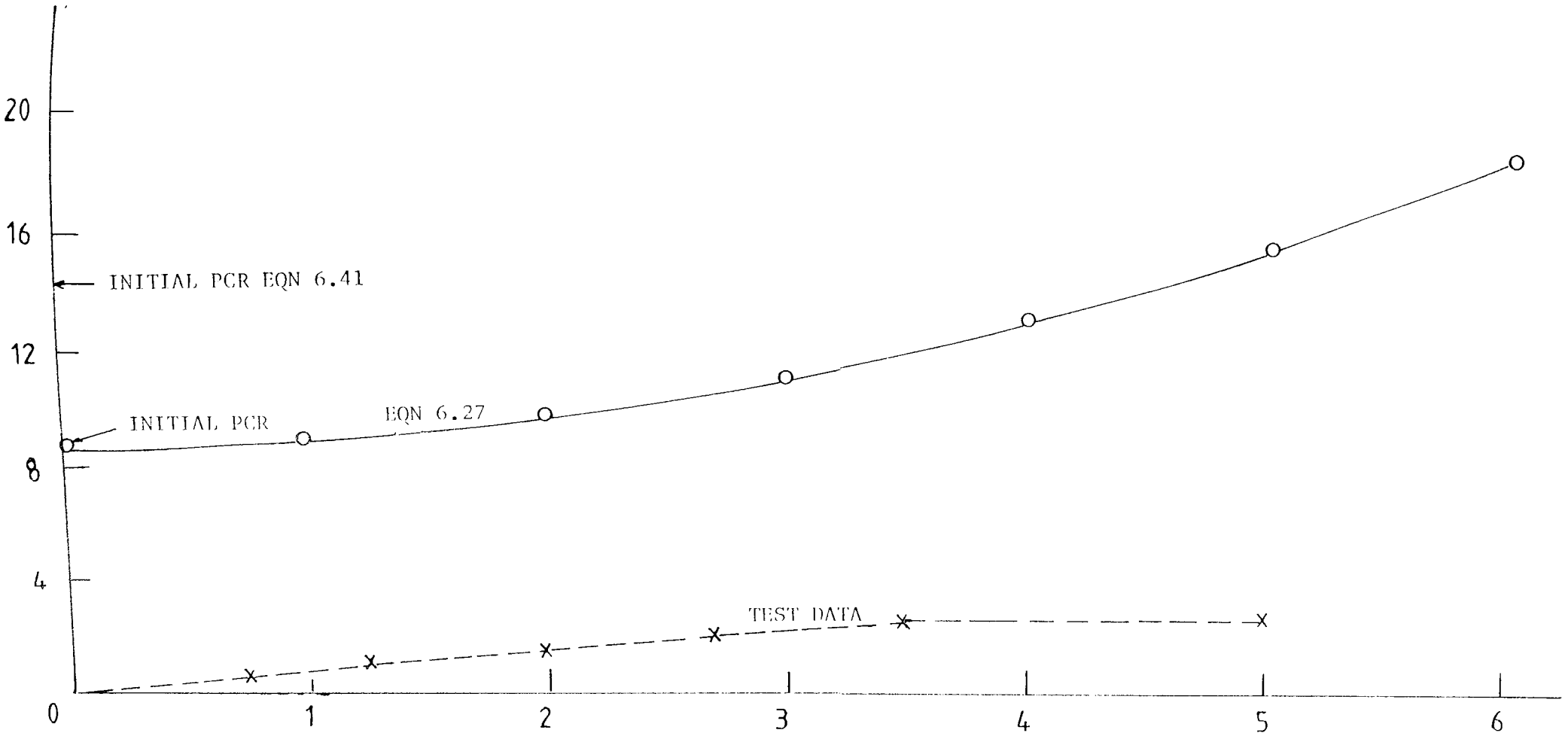

FIGURE 6.15 PLATE TYPE P_4 (No 7)

LOAD VERSUS LATERAL DEFLECTION FOR POST BUCKLING REGION

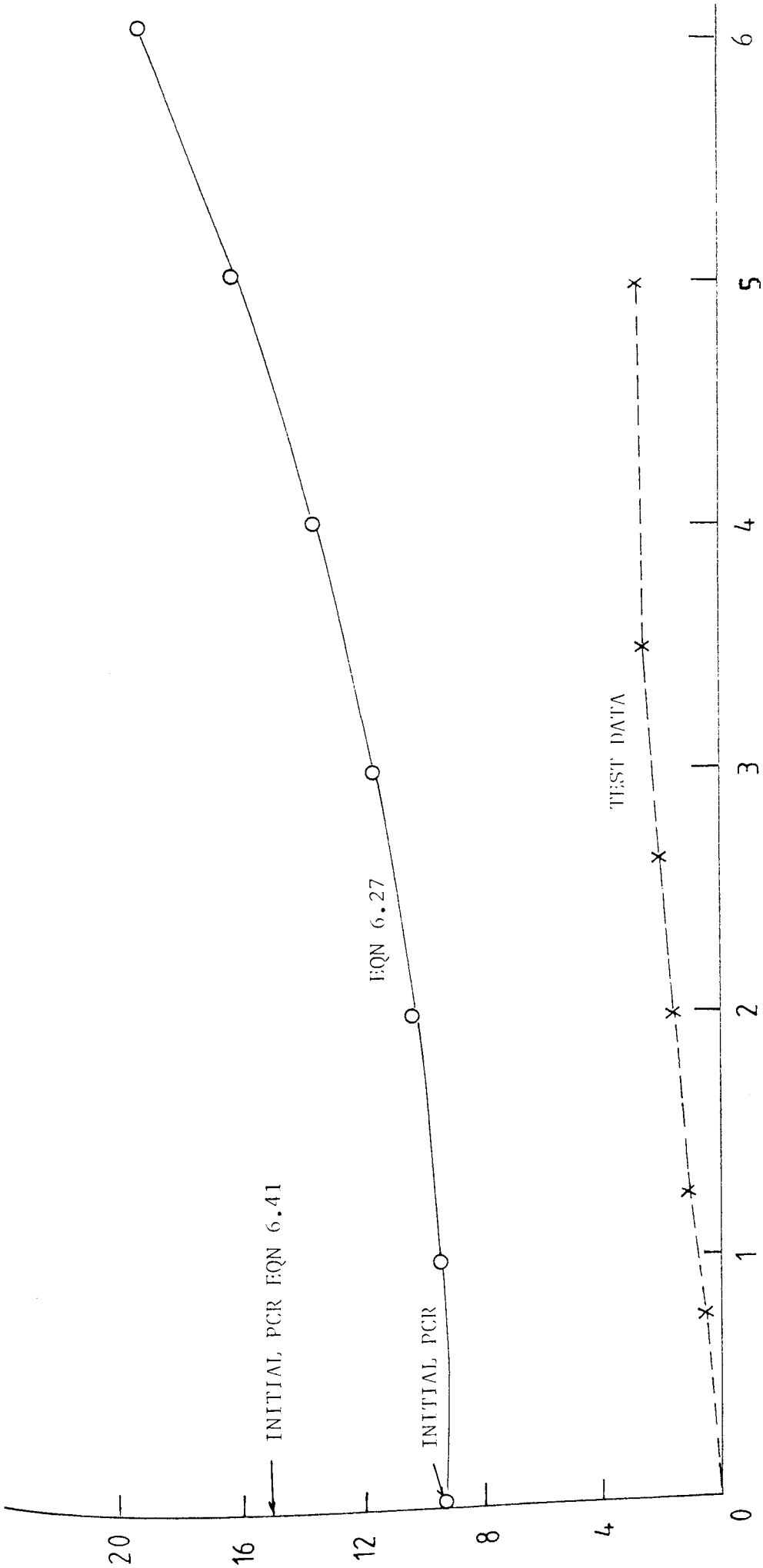

FIGURE 6.16 PLATE TYPE P_4 (No 8)

LOAD VERSUS LATERAL DEFLECTION FOR POST BUCKLING REGION

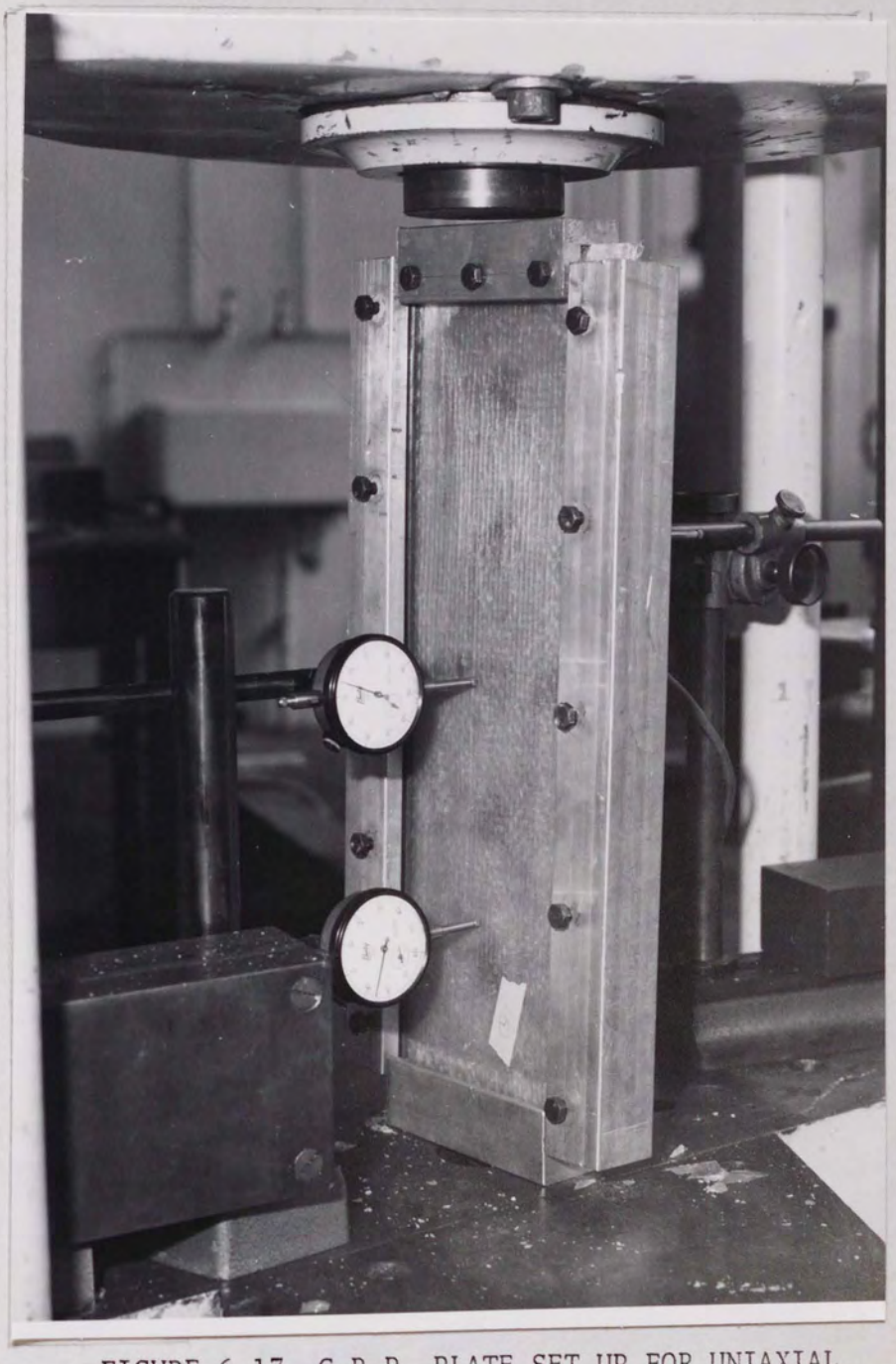

FIGURE 6.17 G.R.P. PLATE SET UP FOR UNIAXIAL COMPRESSION TEST

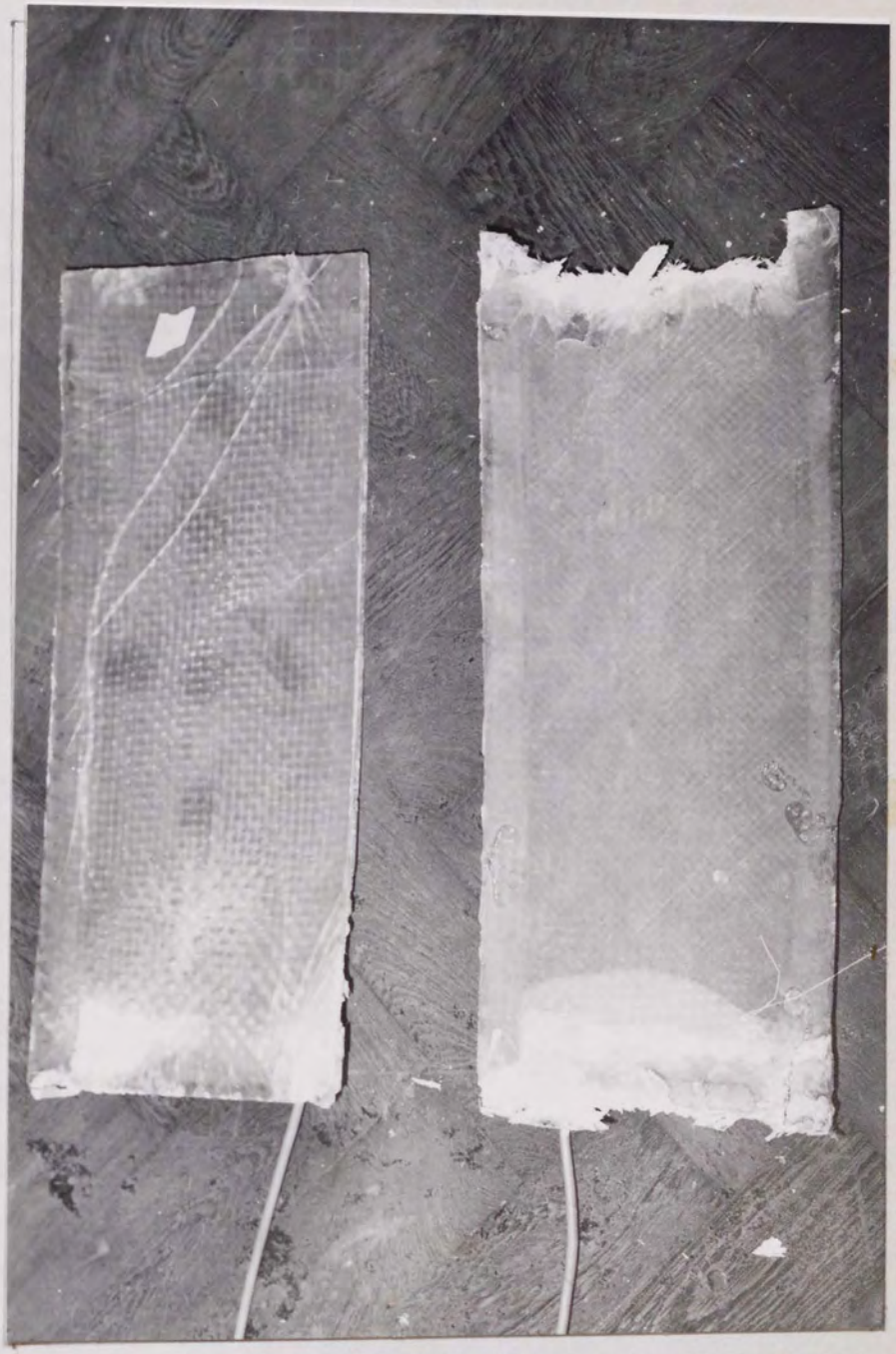

FIGURE 6.18 TYPICAL MODE OF FAILURE OF G.R.P. PLATES AFTER COLLAPSE, SHOWING THE STRESSED AREA AROUND THE EDGES

REFERENCES

6.1 HEARMON, R F S, "An Introduction to Applied Elasticity," Oxford University Press, London 1961.

6.2 LEKHNITSKI, S G, "Anisotropic Plates," Translated from the second Russian edition by S W Tsai and T Cheron, Gordon and Breach, 1968.

6.3 ASHTON, J E and WHITNEY, J M, "Theory of Laminated Plates," Technomic Publishing Co, Inc. 1970.

6.4 VON KARMAN, T, SECHLER, E E and DONNELL, L H "The Strength of Thin Plates in Compression", Transactions ASME, Vol 54, APM, 54-5, 1932.

6.5 WINTER, G, "Strength of Thin Steel Compression Flanges", with Appendix) Bulletin No 35/3. Cornell University Engineering Experiment Station, Ithaca, NY, 1947.

6.6 LEKHNITSKI, S G "Anisotropic Plates", Translated from the second Russian edition by S W Tsia and T Cheron, Gordon and Breach, 1968.

6.7 THIELEMANN, W, "Contribution to the Problems of Buckling of Orthotropic Plates", with special reference to plywood. NACA Tech, Memo, 1263, August 1950.

6.8 TIMOSHENKO and WOINOWSKY-KRIEGER, "Theory of Plates and Shells." Second edition, McGraw Hill Book Company.

6.9 CLIVE L DYM "Stability Theory and its Applications to Structural Mechanics". Noordhoff International Publishing.

CHAPTER 7

CONCLUSIONS AND RECOMMENDATIONS FOR FURTHER WORK

7.1 GENERAL CONCLUSION

For the purpose of civil engineering construction, the hand lay technique is considered to be suitable in the preparation of G.R.P. structural members, since this method offers a low capital investment and limited skill.

In comparison with conventional materials such as timber, concrete and steel, G.R.P. may be expensive, but if used in an intelligent way in shapes appropriate to its unique properties such as light weight high strength, translucency and low maintenance may lead to highly efficient and economical solutions to structural problems may result.

One of the restraining factors on the wider use of G.R.P. is the lack of information on its structural behaviour. A Code of Practice cannot be written until practice itself is established, but continuous research and experimentation with G.R.P. structures should lead eventually to the acceptance of G.R.P. as a structural material in its own right and the formulation of an appropriate Code of Practice.

G.R.P. structural elements exhibit large deformations without necessarily producing adverse effects on structural safety. This leads to the necessity of accepting additional deformations beyond those set in the Standard Code of Practice for other materials e.g. concrete, steel etc. However, in accepting large deformations architectural appearances should be considered. Thin walled structural members in the form of closed sections or open sections

stiffened by intermediate diaphragms appear to be the basic forms to adopt when designing structures in G.R.P. Apart from the normal stresses due to bending and shear, additional stresses due to torsional warping of the section, and buckling of the individual elements of the structure must be considered. The simple bending theory based on equivalent sections proved to be satisfactory in predicting the stresses and deflections of G.R.P. beams provided the cross-section does not warp.

G.R.P. structural elements can be connected with G.R.P. joints. Multiple joints are feasible but they tend to result in larger deformations.

G.R.P. structural elements are susceptible to creep and this is considered to be an important factor in designing G.R.P. structural members for both short and long term loading.

G.R.P. plates exhibits a post buckling range which indicates that a margin of safety exists if plates are designed on the basis of the initial buckling stress alone, however theoretical predictions for post buckling behaviour are not reliable.

7.2 RECOMMENDATIONS FOR FUTURE RESEARCH

Future research to further develop the research described in this thesis, is described below:-

(1) The design and manufacture of G.R.P. structural members to overcome the problem of large deformation and buckling. This may lead to the inclusion of different materials e.g. steel wires or sheets or to the introduction of corrugated stiffeners within the member.

(2) Development of provisional standard designs backed by thorough test data for different types of G.R.P. structural joints and the

adequacy of corresponding fastner dimensions, spacings and head or washer sizes.

(3) Creep behaviour for connected beams under a similar range of loading investigated in this research.

(4) Post buckling behaviour of G.R.P. plates in shear.

APPENDIX A

ANALYSIS OF SECTORIAL PROPERTIES FOR A CLOSED SECTION

With reference to Khan and Stafford procedure described in section 4.14.2 consider a rectangular box section a x b, with a constant thickness t.

$$S_o = \int \frac{ds}{t} = \frac{2a + 2b}{t} \tag{A1}$$

$$P = \text{average radius} = \frac{\Omega}{\int ds/t} = \frac{2ab}{\frac{2a}{t} + \frac{2b}{t}} = \frac{ab}{a + b}\, t \tag{A2}$$

$$P\bar{s} = \frac{abt}{a + b} \Sigma \frac{s}{t} = \frac{ab}{a + b}\, s \tag{A3}$$

w_b and $P\bar{s}$ diagrams are plotted accordingly (see fig A1a and A1b). Reduced sectorial diagram $\bar{w}' = w_b$ diagram - $P\bar{s}$ diagram, is also plotted in fig A1c.

The position of the shear centre of the section

$$\alpha x = \frac{\int \omega' y dA}{Ixx} \tag{A4}$$

Now $\int \bar{w}' y dA$ = msat along width + $\frac{ms^2 t}{3}$ along length (A5)

$$= \frac{(m_1+m_2)}{2} \frac{ba}{2} \times 2t + m_1 (\frac{b}{2})^2 \times \frac{1}{3} \times 2t +$$

$$+ m_2 (\frac{b}{2})^2 \times 2t$$

$$= \frac{ab}{2} (m_1 + m_2) + \frac{b^2}{6} (m_1 + m_2)t$$

$$= (\frac{b^2}{6} + \frac{ab}{2}) (m_1 + m_2)$$

$$= \frac{b(b+3a)}{6} (m_1 + m_2)t$$

$$Ixx = \frac{tb^2}{6}(3a + b) \text{ neglecting higher order of equation (2.3)} \quad \text{(A6)}$$

$$\alpha_x = \frac{\int \bar{w} y dA}{I_{xx}} = \frac{m_1 + m_2}{b} = \frac{ab^2 + a^2 b}{2(a + b)b} \quad \text{(A7)}$$

$$= \frac{ab(a + b)}{2b(a + b)} = \frac{a}{2} \text{ i.e. the position of the shear centre}$$

coincides with the centre of gravity fig (A1d).

The final sectorial diagram $\bar{w} = \bar{w}'$ diagram - αxy diagram.

From the $\bar{w}'$ diagram and αxy diagram it is clearly seen that the final sectorial diagram shall reduce to zero if

$$\frac{a^2 b}{2(a + b)} - \frac{ab}{4} = 0$$

$$\frac{a}{a + b} - \frac{1}{2} = 0$$

or a = b i.e. the section is a square.

The bimoment stresses are generally

$$w = \frac{B.\bar{w}}{I\bar{w}} \quad \text{(A8)}$$

where B = bimoment

$\bar{w}$ = sectional property

$I\bar{w}$ = sectorial moment of inertia.

As $\bar{w} = 0$ in case of square sections then Iw = 0 and hence bimoment stresses shall reduce to zero.

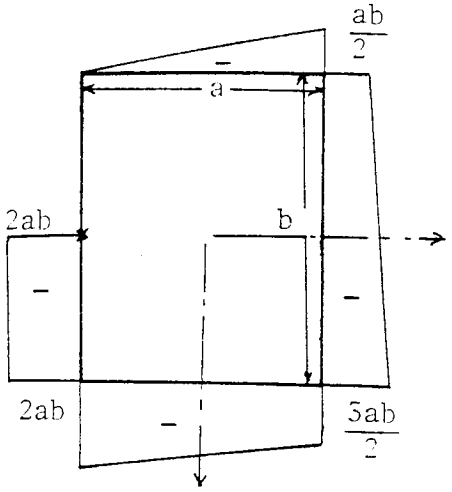

(a) wb diagram

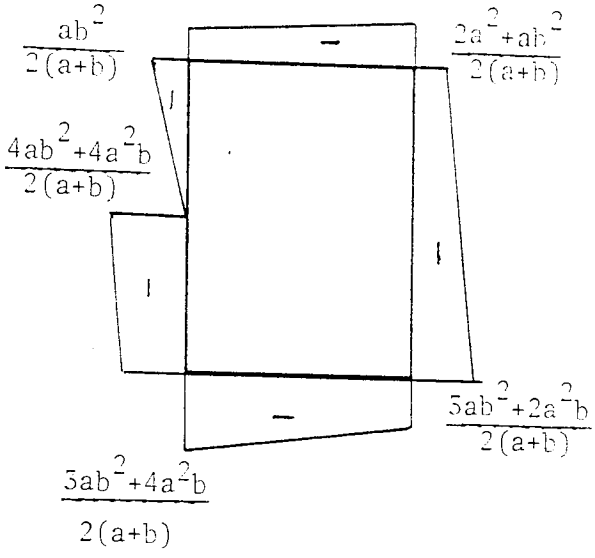

(b) $P\bar{S}$ diagram

Thickness constant = t

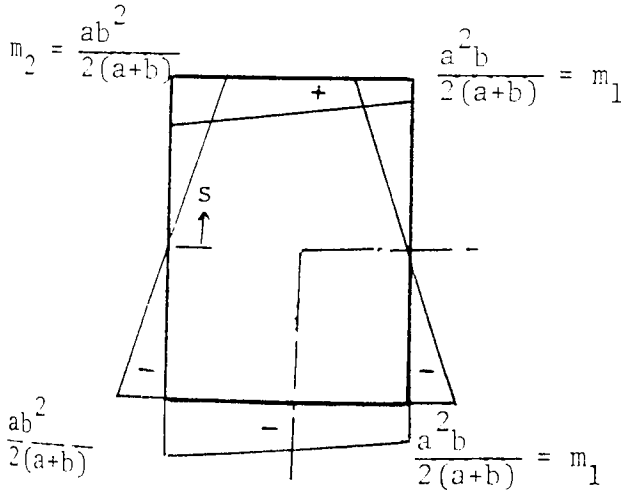

(c) $\bar{w}$ diagram

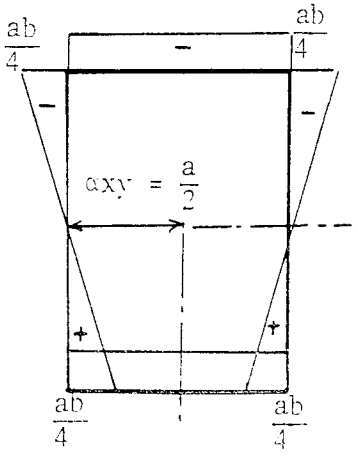

(d) σxy diagram

FIGURE A1 SECTORIAL DIAGRAMS FOR A RECTANGULAR SECTION

APPENDIX B

EVALUATION OF SECTION PROPERTIES BEAM B1

Diaphragms and local reinforcement are taken into consideration in the following manner.

Diaphragms

Total number of diaphragms including additional stiffeners at the support and at load application assemblies

$$= 15 + 4 \times \frac{4}{3} = \frac{61}{3}$$ (fig B.1)

Cross sectional area of each diaphragm = 295 x 145 mm^2. The total equivalent thickness of diaphragms

$$= \frac{61}{3} \times 4.22 \text{ mm}$$ (see Table 2.3)

Total length of the beam = 3000 mm

The average equivalent cross-sectional area of the diaphragms per mm may be represented by

$$= \frac{61}{3} \times \frac{4.22}{3000} \times 295 \times 145$$

$$= 1223.46 \text{ mm}^2$$

Local reinforcement

Area of local reinforcement for one diaphragm

$$= 2(295 \times 25 + 145 \times 25 + 14.50 \times 25) = 29250 \text{ mm}^2$$

The total equivalent thickness of local reinforcement

$$= \frac{61}{3} \times 2.81 \text{ mm}$$

The average equivalent cross sectional area of local reinforcement

$$= \frac{61}{3} \times \frac{2.81 \times 29250}{3000}$$

$$= 557.08 \text{ mm}^2$$

∴ Total equivalent corss sectional area for the diaphragms plus local reinforcement = 1223.46 + 557.08

$$= 1780.54 \text{ mm}^2$$

This is represented in the equivalent cross-section of the beam by a strip along the of the beam section having 295 mm depth and a width of $\frac{1780.54}{295} = 6.04$ mm (included as element 5 in the computational table of the moment of inertia).

Section properties

Referring to the computational table B1, the distance d, of the neutral axis from x - x.

$$d_1 = \frac{\Sigma M}{\Sigma A} = \frac{875906}{5577.04} = 157.06 \text{ mm}$$

The moment of interia of the section

$$Ix = kx' - Ad1^2$$

$$= 199402411 - 5577.04 \times 157.06^2$$

$$= 61828860 \text{ mm}^4$$

$$Zt = \frac{Ix}{d_1} = 393663 \text{ mm}^3$$

$$Zc = \frac{Ix}{304.27 - d_1}$$

$$= 420.004 \text{ mm}^3$$

The tensile and compressive stresses are calculated from the corresponding relationships, $\frac{M}{Z_T}$ and $\frac{M.}{Z_c}$

To calculate the maximum shear stress from equation (2.11)

$$\tau = \frac{VAY}{Ib}$$

It is necessary to compute the equivalent area above or below

the neutral axis and its new neutral axis N'A' distance y from the new neutral axis N.A. (Table B1).

The thickness b is equal to thickness of the webs plus the fixtious thickness of diaphragms and local reinforcement.

Element	Area mm^3	6 mm	h_1 mm	h mm	h_1^2 mm^2	h^2	$\frac{b}{2}(h_1^2-h^2)$ mm^3	h_1^3 mm^3	h^3 mm^3	$\frac{b}{3}(h_1^3-h^3)$ mm^4
①	1188.85	4.03	298.97	3.97	89.383	15.7	180075	26722854	62.5	35897612
②	1188.85	4.03	298.97	3.97	89.383	15.7	180075	26722854	62.5	35897612
③	607.60	153.06	3.97	0	15.70	0	1201	62.5	0	3188
④	811.2	153.06	304.27	298.27	92580	89383	244666	28169387	26722854	73802113
⑤	1780.54	6.04	298.97	3.97	89383	15.7	269889	26722854	62.5	53801886
$\Sigma A = 5577.04$					$\Sigma M = 875906$			$\Sigma I'x = 199402411$		

b = width of element
h = nearest distance of element to x-x
h_1 = furtherest distance of element from x -x

TABLE B1
COMPUTATION TABLE FOR THE MOMENT OF INERTIA AND CENTROIDAL DISTANCE OF THE EQUIVALENT SECTION OF BEAM B1

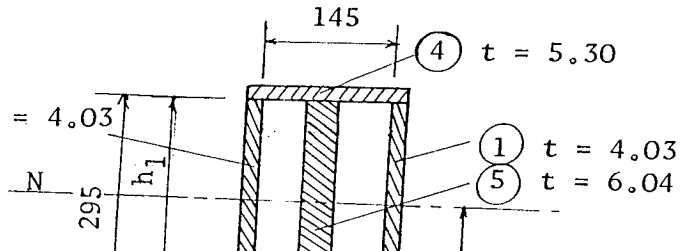

Dimens. in mm
Thickness t in mm

Element	Area mm^2	b mm	h_1 mm	h mm	h_1^3 mm^3	h^2 mm^2	$\frac{b}{2}(h_1^2-h^2)$ mm^3
①	571.89	4.03	141.91	0	20138	0	40579
②	571.89	4.03	141.91	0	20138	0	40579
③	811.2	153.06	147.21	0	21671	0	1172.70
④	890.27	6.04	141.91	0	20138	0	60817
	$\Sigma A' = 2845.25$				$\Sigma M' = 2592.45$		

TABLE B2

COMPUTATION TABLE FOR THE NEW CENTROIDAL DISTANCE Y FOR THE UPPER HALF OF THE BEAM TYPE B1 SECTION FROM THE NEUTRAL AXIS N.A.

Note:-

b, h, h_1 as defined in Table 1

$Y = \frac{\Sigma M'}{\Sigma A'}$

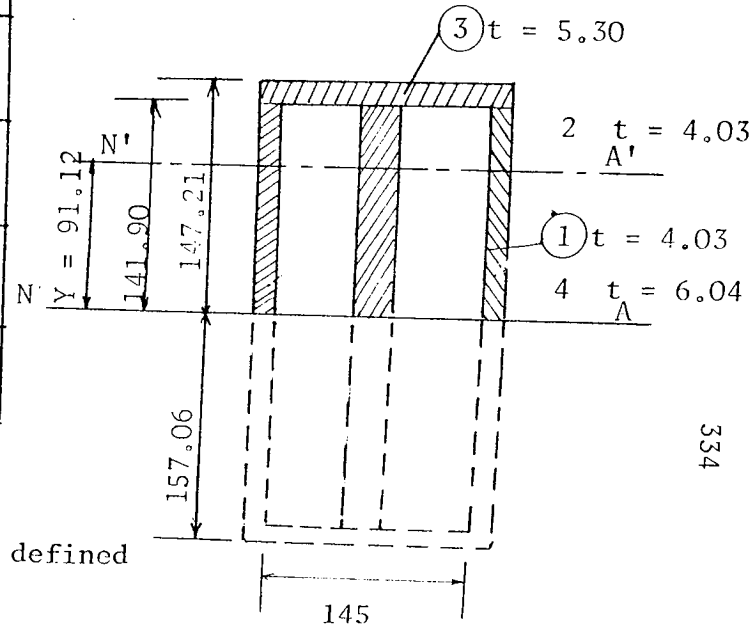

Thickness t in mm

FIG B1 Dimens. in mm

APPENDIX C

The Von Karman compatibility equations describing the finite-deflection behaviour of plates subjected to in plane forces are

$$\frac{\partial^4 F}{\partial x^4} + \frac{2\partial^4 F}{\partial x^2 \partial y^2} + \frac{\partial^4 F}{\partial y^4} = E\left[\left(\frac{\partial w}{\partial x}\right)^2 - \frac{\partial^2 w}{\partial x^2}\frac{\partial^2 w}{\partial y^2}\right] \qquad C.1$$

and

$$D\left(\frac{\partial^4 w}{\partial x^4} + \frac{2\partial^4 w}{\partial x^2 \partial y^2} + \frac{\partial^4 w}{\partial y^4}\right) - h\left(\frac{\partial^2 F}{\partial y^2}\frac{\partial^2 w}{\partial x^2} + \frac{\partial^2 F}{\partial x^2}\frac{\partial^2 w}{\partial y^2}\right.$$

$$\left. - \frac{2\partial^2 F}{\partial x \partial y} \cdot \frac{\partial^2 w}{\partial x \partial y}\right) = 0 \qquad C.2$$

where F is the stress function defining the median fibre stress of the plate.

E, D, h and w as defined in Chapter 6. Full derivation of the above equations may be obtained from Reference (6.9).

With respect to Galerkin equation

$$\int_0^a \int_0^a Q(f)\ g\ (x,y)\ dxdy = 0 \qquad C.3$$

Q(f) is the left hand side of equation C.2 and g (x,y) is the variable part of w. Substituting equation 6.5 for w and equation 6.15 for F

$$Q(f) = \frac{2f\pi^4}{a^4} \sin\frac{\pi y}{a} \sin\frac{\pi x}{a} + 2f\frac{\pi^4}{a^4} \sin\frac{\pi x}{a} \sin\frac{\pi y}{a}$$

$$-h\left[\frac{Ef^2}{32}\right]\left[\left(\frac{2\pi^2}{a^2} + x_a\right)\left(f\frac{\pi^2}{a^2} \sin\frac{\pi x}{a} \sin\frac{\pi y}{a}\right)\right.$$

$$\left. + \frac{2\pi^2}{a^2} \sin\frac{2\pi x}{a} \cdot \frac{f\pi^2}{a^2} \sin\frac{\pi x}{a} \sin\frac{\pi y}{a}\right] \qquad C.4$$

and Q(f) can be written as

$$Q(f) = [4fD\frac{\pi^4}{a^4} - \frac{Ehf^3\pi^4}{8a^4}(\cos\frac{2\pi x}{a} + \cos\frac{2\pi y}{a})$$

$$- x\ h\ f\frac{\pi^2}{a^2}]\sin\frac{\pi x}{a}\sin\frac{\pi y}{a} \qquad C.5$$

and the Calerkin equation takes the form

$$\int_0^a\int_0^a [(\frac{4fD\pi^4}{a^4} - xa\ hf\frac{\pi^2}{a^2})(\sin\frac{2\pi x}{a}\sin\frac{2\pi y}{a})$$

$$- \frac{Ehf^3\pi^4}{8a^4}(\cos\frac{2\pi x}{a}\sin\frac{2\pi x}{a}\sin\frac{2\pi y}{a}$$

$$+ \cos\frac{2\pi y}{a}\sin\frac{2\pi x}{a}\sin\frac{2\pi y}{a})]\,dxdy = 0 \qquad C.6$$

Making use of the definite integral

$$\int_0^a \sin\frac{2\pi x}{a}\,dx = \frac{a}{2} \qquad C.7$$

Equation A.6 can be reduced to

$$(\frac{4fD}{a^4}\pi^4 - xah\ f\frac{\pi^2}{a^2})\frac{a^2}{4} - \frac{Ehf^2\pi^4}{8a^4}\frac{a}{2}(\int_0^a \cos\frac{2\pi x}{a}\sin\frac{2\pi x}{a}\,dx$$

$$+ \int_0^a \cos\frac{2\pi y}{a}\sin\frac{2\pi y}{a}\,dy) = 0 \qquad C.8$$

Using the identity

$$\cos\frac{2\pi x}{a}\sin\frac{2\pi x}{a} = \frac{1}{2}(\cos\frac{2\pi x}{a} - \cos^2\frac{2\pi x}{a} \qquad C.9$$

and the definite integrals

$$\int_0^a \cos^2 \frac{2\pi x}{a}\, dx = \frac{a}{2} \qquad \text{C.10}$$

$$\int_0^a \cos \frac{2\pi x}{a}\, dx = 0 \qquad \text{C.11}$$

Equation A.8 reduces to

$$F\frac{D\pi^4}{a^2} - xa\, hf\frac{\pi^2}{4} + \frac{Ehf^3\pi^4}{32a^2} = 0$$

i.e.

$$xa = \frac{4D\pi 2}{ha^2} + \frac{E\pi^2 f^2}{8a^2}$$